Three-Phase UHV AC Transmission Research

EL-823
Research Project 68-2

Final Report, July 1978

Work Completed, December 1976

Prepared by

GENERAL ELECTRIC COMPANY
100 Woodlawn Avenue
Pittsfield, Massachusetts 01201

950 3392

Project Manager
Luciano E. Zaffanella

Principal Investigators
Michael G. Comber
Herman M. Schneider
Richard J. Nigbor

Prepared for

Electric Power Research Institute
3412 Hillview Avenue
Palo Alto, California 94304

EPRI Project Managers
F. S. Young
E. J. Ballard
Electrical Systems Division

DISTRIBUTION OF THIS DOCUMENT IS UNLIMITED

DISCLAIMER

This report was prepared as an account of work sponsored by an agency of the United States Government. Neither the United States Government nor any agency thereof, nor any of their employees, makes any warranty, express or implied, or assumes any legal liability or responsibility for the accuracy, completeness, or usefulness of any information, apparatus, product, or process disclosed, or represents that its use would not infringe privately owned rights. Reference herein to any specific commercial product, process, or service by trade name, trademark, manufacturer, or otherwise does not necessarily constitute or imply its endorsement, recommendation, or favoring by the United States Government or any agency thereof. The views and opinions of authors expressed herein do not necessarily state or reflect those of the United States Government or any agency thereof.

DISCLAIMER

Portions of this document may be illegible in electronic image products. Images are produced from the best available original document.

LEGAL NOTICE

This report was prepared by General Electric Company as an account of work sponsored by the Electric Power Research Institute, Inc. (EPRI). Neither EPRI, members of EPRI, General Electric Company, nor any person acting on their behalf: (a) makes any warranty or representation, express or implied, with respect to the accuracy, completeness, or usefulness of the information contained in this report, or that the use of any information, apparatus, method, or process disclosed in this report may not infringe privately owned rights; or (b) assumes any liabilities with respect to the use of, or for damages resulting from the use of, any information, apparatus, method or process disclosed in this report.

ABSTRACT

This report presents the results of the work performed at EPRI's Project UHV from Jaunary 1974 to December 1976. During this period, a three-phase ac test line with line voltages up to 1500 kV was constructed and operated.

The feasibility of UHV transmission has been demonstrated and the most important problems impacting on cost and performance have been identified. Design data on the corona performance of conductor and line configurations and on the dielectric strength of the external insulation of UHV transmission systems have been provided.

The results obtained confirm and extend the data contained in the Transmission Line Reference Book - 345 kV and Above, published by EPRI in 1975

EPRI PERSPECTIVE

PROJECT DESCRIPTION

Project UHV (ultrahigh voltage) was initiated by the Electric Research Council in 1967 to study overhead transmission lines with voltages in excess of 1000 kV ac. Project UHV evolved from Project EHV, the research facility built and funded by General Electric in 1958-1964 to provide data for EHV transmission in the 400-750 kV range.

With the support of the Edison Electric Institute and the Tennessee Valley Authority in 1965 and 1966, Project EHV completed the study of EHV transmission and incorporated all available data in the EHV Transmission Line Reference Book, published by the Edison Electric Institute in 1968.

In 1967 the Electric Research Council, using funds provided by the Edison Electric Institute and the Bonneville Power Administration, started a research program intended to cover a voltage range from 1000 to 1500 kV ac.

Instrumentation and equipment from Project EHV, already in place for research on EHV problems, were modified and used for the new research, and the project was renamed Project UHV in January 1967, to better describe its expanded activities.

In the early stages of this program, three-phase research was not justifiable from an economic point of view until single-phase work had defined the problems and assessed study priorities. Therefore, a single-phase test line was constructed and energized for the initial period of research from 1967 to 1971. The single-phase program was extended to 1973 when it became apparent that additional research was necessary to investigate further subjects of most importance for UHV transmission, such as audible noise and electrostatic effects. In 1973, Project UHV was transferred to the jurisdiction of the Electric Power Research Institute (EPRI), which has since published a new transmission design book, which updates and extends the previous EHV Reference Book. The new book, Transmission Line Reference Book - 345 kV and Above, covers the electrical aspects of transmission line design from 345 kV to 1500 kV. The design data for ultrahigh voltages were obtained during the single-phase UHV program from 1967 to 1973.

Means for conversion to three-phase performance from single-phase test results had to be developed for each phenomenon being considered. It should be noted that single-phase testing was limited by the fact that research for transmission above 1300 kV could not be effectively performed with the available single-phase equipment. In fact, for the same applied voltage, single-phase lines have conductor surface gradients that are 10 to 30% lower than three-phase lines.

In order to verify and extend the single-phase results, a new three-year program to construct and operate a three-phase test line in the range of 1000 to 1500 kV was started by EPRI in 1974.

The present report is an account of the work accomplished in the period 1974-1976. In this period a three-phase test line was built and operated with voltages up to 1500 kV (line-to-line). This construction of the three-phase test line was a major task of this research program. New electrical equipment and structures were added to existing single-phase facilities. Energization of the three-phase UHV test line occurred on January 25, 1975. The 1500-kV test capability makes the Project UHV test line the highest voltage experimental three-phase line in the world.

The work performed is described in the three sections following the Summary. Section 2 describes the three-phase test line and its test capabilities. Section 3 contains the detailed results of the tested conductor line configurations. Section 4 describes the insulation research performed at Project UHV in the period 1974-1976. Research on electric field effects and on measures to reduce the electric field is being conducted at Project UHV under EPRI RP566 and will be the subject of a future report. From February 1975 to December 1976 six different conductor and line configurations were tested on the three-phase test line of Project UHV, at voltages between 100 and 1300 kV. The electrical performance of each configuration was determined during long-term (3 to 5 months) exposure to natural weather conditions.

PROJECT OBJECTIVES

Specific research objectives for Project UHV are as follows:

- Develop an understanding of coronal phenomena that affect conductor selection. Make long-term measurement of radio and TV influence, audible noise, and corona loss. Develop predictive methods useful in designing lines. Investigate means for reducing corona-generated effects.

- Investigate insulation requirements for UHV transmission lines. Define 60-Hz performance of contaminated insulators and develop application data.
- Develop a clear understanding of nonbiological effects of electric fields. Develop instrumentation and predictive methods. Measure induced potentials and currents on objects such as vehicles, fences, etc., that appear near transmission lines.

CONCLUSIONS AND RECOMMENDATIONS

The research has primarily been experimental testing using the three-phase 1500-kV line, contamination chamber, and corona cages, with some necessary theoretical work.

The major emphasis in recent years has been to increase the scope of work relating to electric field research, and to qualify bundled conductor configurations. As a result of the work completed thus far, researchers have:

- Assembled statistical data relating to potentials and currents induced in vehicles parked under a transmission tree.
- Developed the equivalent circuit for spark discharge between a person and an object.
- Developed a personal body current monitor instrument that integrates electric field strengths at ground level.
- Developed data on three-phase conductor configurations from tests on 8- and 12-conductor bundles. Radio influence, audible noise, and corona-loss predictive methods have been verified for these conductor arrangements.
- Established electric field measurement and prediction techniques that are now being used by utilities nationwide.
- Developed and tested methods to reduce electric fields in vicinity of lines using underbuilt grounded wire grids or energized circuits.
- Performed phase-to-phase switching surge tests on a transmission line span, rather than the usual very short laboratory mock-up.
- Sufficiently demonstrated the benefits of asymmetrical bundle geometry to qualify it for consideration by utilities in designs.
- Demonstrated that horizontal and vertical grids of grounded wire, together with underbuilt energized low voltage lines, can now be considered where special electric field problems exist.

The new empirical and test data developed in the past year will enable designers to plan UHV lines using conventional guidelines with but minor modifications.

The project will be continued through 1979. Then a revision of Transmission Line Reference Book - 345 kV and Above will be published.

Richard E. Kennon, Program Manager
Electrical Systems Division

ACKNOWLEDGEMENTS

The authors are indebted to all the personnel of Project UHV who have helped accomplish the results that made the writing of this report possible. In addition to the authors, the staff of Project UHV consisted of: Joseph R. Doyle, Development Engineer, Facility Construction; Don W. Deno, Principal Investigator, Electric Field; George T. Baer; John P. Benedict; J. Roland Devoe; Lawrence A. Gattasso; Hazel Mazza; David M. Milone; Clark W. Nicholls; Clifton Waite; and Frederick Wood. Particular acknowledgement should be made to the Project UHV Steering Committee. This Committee, comprised of a team of experienced professionals from Electric Utilities of the United States, helped with its advise to keep the research effort directed toward the most important and practical needs. Members of the Steering Committee during the period 1974-1976 were: (Chairman) George Balderston - Philadelphia Electric Co.; Earl H. Boesenberg; Robert W. Flugum; Ralph S. Gens; Gene H. Huston; Fred R. Klumb; Ross King; Benjamin D. Miller; Brendan J. Ware. The authors are grateful to EPRI program manager Frank S. Young for his support and advise. Also acknowledged are the contributions of the two previous EPRI Program Managers, P. Luther Kolarik (presently with Philadelphia Electric Co.) and Alan Johnson (presently with Portland General Electric Co.)

TABLE OF CONTENTS

	Title	Page
SECTION 1	INTRODUCTION AND SUMMARY	1-1
SECTION 2	THREE-PHASE UHV TEST LINE	2-1
	PROJECT UHV: A TRANSMISSION RESEARCH CENTER, PAST HISTORY AND PRESENT OBJECTIVES	2-1
	UHV STATION	2-2
	THREE-PHASE UHV TEST LINE	2-4
	INSULATOR STRINGS	2-10
	INSTRUMENTATION FOR DATA ACQUISITION	2-14
	Data Acquisition Computer	2-14
	Instrumentation Systems	2-16
	OTHER FACILITIES	2-20
	CONDUCTOR AND LINE CONFIGURATION TESTED	2-20
	REFERENCES	2-22
SECTION 3	CORONA EFFECTS	3-1
	INTRODUCTION AND SUMMARY OF CORONA RESEARCH	3-1
	Audible Noise	3-2
	Radio and Television Interference	3-4
	Corona Loss and Ozone	3-5
	AUDIBLE NOISE	3-6
	Philosophy of "Long-term" Testing	3-6
	Interpreting Measurements During Periods of Low Line Noise or High Ambient Noise	3-8
	Three-Phase Test Line Configurations	3-14
	Eight-Conductor Bundle - Effect of Change in Line Geometry	3-16
	Twelve-Conductor Bundle - Effect of Changes in Voltage Level	3-28
	Twelve-Conductor Bundle - Effect of Changes in Bundle Geometry	3-30
	Fair Weather Noise	3-36
	Ambient Noise	3-40
	Cage Tests of Three-Phase Line Bundle Geometries	3-41
	Bundle Geometry Optimization	3-52
	Conductor Aging	3-61
	Refinement of Design Rules	3-70

TABLE OF CONTENTS (cont.)

	Title	Page
SECTION 3	RADIO INTERFERENCE	3-75
	Interpreting Measurements of RI from Short Lines	3-75
	Results of Long-term Monitoring on 3-Phase Line	3-80
	Correlation of RI with Audible Noise	3-89
	TELEVISION INTERFERENCE	3-93
	Instrumentation	3-94
	Three-Phase Line Testing	3-94
	CORONA LOSS	3-101
	Three-Phase Line Testing	3-101
	OZONE	3-104
	Three-Phase Line Testing	3-105
	REFERENCES	3-115
SECTION 4	INSULATION RESEARCH	4-1
	CONTAMINATION PERFORMANCE OF LONG INSULATOR STRINGS	4-1
	Introduction	4-1
	Test Facilities for UHV Research	4-2
	Indoor Test Results	4-8
	Outdoor Natural Humidity Tests	4-17
	Design Rules	4-22
	Future Work Required	4-23
	NEW INSULATOR TECHNOLOGIES	4-25
	Introduction	4-25
	Electrical Considerations for UHV Insulators	4-25
	Voltage Grading and Contamination Performance	4-26
	Semiconductive Glaze Insulators	4-36
	Non-Ceramic Insulators	4-43
	Mechanical Loading Considerations	4-45
	Future Work	4-51
	INFLUENCE OF THE TEST PARAMETERS	4-53
	Introduction	4-53
	Description of Available Circuits	4-53
	Test Results with Different Circuits	4-56
	Influence of Wetting Conditions	4-65
	CONTAMINATION PERFORMANCE OF STATION POST INSULATORS	4-67
	Introduction	4-67
	Effect of Diameter	4-71
	Effect of Length	4-79
	ICE FLASHOVER PERFORMANCE	4-84
	Introduction	4-84
	Test Procedure with Ice Thickness as a Seventy Parameter	4-86
	Standard Insulators	4-88
	Plastic Insulators	4-93
	Results on Antifog Units and EHV/UHV Comparison	4-101
	Post Insulators	4-105

TABLE OF CONTENTS (cont.)

	Title	Page
SECTION 4	UHV INSULATOR DESIGN FOR CLEAN AREAS	4-109
	Introduction	4-109
	Full Scale Tests in Artificial Rain	4-109
	Design Limits - Hangers, Switching Surges, Corona	4-111
	INSULATOR STRING HARDWARE	4-112
	Introduction	4-112
	Effect of Attachment on Contamination Flashover	4-112
	Corona Single-Phase Tests	4-113
	Corona on Three-Phase Test Line Insulators	4-131

LIST OF ILLUSTRATIONS

Figure	Title	Page
2-1	UHV Station	2-3
2-2	Plan - Profile, Towers 1-4.	2-5
2-3	Plan - Profile, Towers 1-2.	2-5
2-4	Winch Behind Tower 4.	2-6
2-5	Outline - Tower 2.	2-6
2-6	Outline - Tower 4.	2-7
2-7	Screw Anchor Installation.	2-8
2-8	Falsework on Tower 2, Lifting Bridge Into Place.	2-8
2-9	Bull Wheel Tensioner.	2-9
2-10	Single Suspension Insulator.	2-12
2-11	Double Suspension Insulator.	2-12
2-12	Triple Suspension Insulator.	2-13
2-13	Quadruple Suspension Insulator.	2-13
2-14	Suspension Hardware.	2-14
2-15	Dead-End Shield.	2-15
2-16	Dead-End Shield.	2-15
2-17	Data Acquisition System.	2-16
2-18	Audible Noise Test Strip.	2-18
2-19	Original Ozone Trailer and Pole.	2-19
3-1	Typical Frequency Spectra of Ambient Noise, Corona Noise, and Total Noise: A Weighted Ambient Noise Same as Corona Noise.	3-11
3-2	Typical Frequency Spectra of Ambient Noise, Corona Noise, and Total Noise: A Weighted Ambient Noise 5 dB Above Corona Noise.	3-12
3-3	Typical Frequency Spectra of Ambient Noise, Corona Noise, and Total Noise: A Weighted Ambient Noise 10 dB Above Corona Noise.	3-12
3-4	View of 3-Phase Test Line: 8-Conductor Bundle, Horizontal Configuration, 50 ft Phase Spacing.	3-15
3-5	View of 3-Phase Test Line: 8-Conductor Bundle, Triangular Configuration.	3-15

LIST OF ILLUSTRATIONS (Cont)

Figure	Title	Page
3-6	Statistical Distribution of Audible Noise During Rain and 100% RH: 8-Conductor Bundle, 50 ft Phase Spacing, Measuring Location 50 ft From Outside Phase.	3-17
3-7	Statistical Distribution of Octave Band Noise Levels: 8-Conductor Bundle, 50 ft Phase Spacing.	3-18
3-8	Statistical Distribution of Octave Band Noise Levels: 8-Conductor Bundle, 50 ft Phase Spacing.	3-18
3-9	Octave Band Frequency Spectra: 8-Conductor Bundle, 50 ft Phase Spacing.	3-20
3-10	Lateral Profile of A Weighted Audible Noise: 8-Conductor Bundle, 50 ft Phase Spacing.	3-20
3-11	Variation of Noise Level With Voltage: 8-Conductor Bundle, 50 ft Phase Spacing.	3-21
3-12	Statistical Distribution of Audible Noise During Rain and 100% RH: 8-Conductor Bundle, Triangular Configuration, Measuring Location 50 ft From Outside Phase.	3-22
3-13	Statistical Distribution of Audible Noise During Rain: 8-Conductor Bundle, 65 ft Phase Spacing; Measuring Location 50 ft From Outside Phase.	3-22
3-14	Comparison of Statistical Distribution of A Weighted and 8-kHz Octave Band Levels: 8-Conductor Bundle, Triangular Configuration.	3-24
3-15	Comparison of Statistical Distribution of A Weighted and 8-kHz Octave Band Levels: 8-Conductor Bundle, 65 ft Phase Spacing.	3-24
3-16	Comparison of Measured and Calculated Lateral Profiles: 8-Conductor Bundle, 50 ft Phase Spacing.	3-26
3-17	Comparison of Measured and Calculated Noise Levels for Different Voltages: 8-Conductor Bundle, 50 ft Phase Spacing.	3-26
3-18	Comparison of Measured and Calculated Noise Levels for Different Voltages: 8-Conductor Bundle, Triangular Configuration.	3-27
3-19	Comparison of Measured and Calculated Noise Levels for Different Voltages: 8-Conductor Bundle, 65 ft Phase Spacing.	3-27
3-20	Statistical Distribution of Audible Noise During Rain at Different Voltages: 12-Conductor Bundle, 50 in Diameter; Measuring Location 50 ft From Outside Phase.	3-29
3-21	Comparison of Calculated and Measured Noise Levels; 12-Conductor Bundle, 50 in Diameter.	3-29
3-22	Statistical Distribution of Audible Noise During Rain: 12-Conductor Bundle, 20 in Diameter.	3-32

LIST OF ILLUSTRATIONS (Cont)

Figure	Title	Page
3-23	Measured and Corrected Statistical Distribution of Audible Noise During Rain: 12-Conductor Bundle, 80 in Diameter.	3-35
3-24	Measured and Corrected Statistical Distribution of Audible Noise During First 660 Minutes of Rain: 12-Conductor Bundle, 80 in Diameter.	3-35
3-25	Comparison of Measured and Calculated Noise Levels: 12-Conductor Bundle at 1200 kV.	3-36
3-26	Comparison of Frequency Spectra in Rain and in Fair Weather: 12-Conductor Bundle, 50 in Diameter.	3-37
3-27	A Weighted and 8 kHz Octave Band Noise Levels for Different Voltage Levels: 8-Conductor Bundle, Triangular Configuration.	3-38
3-28	A Weighted and 8 kHz Octave Band Noise Levels for Different Voltage Levels: 8-Conductor Bundle, 65 ft Phase Spacing.	3-39
3-29	A Weighted and 8 kHz Octave Band Noise Levels for Different Voltage Levels: 12-Conductor Bundle, 50 in Diameter.	3-39
3-30	Conductor Test Cage.	3-42
3-31	Audible Noise Measured in Cage: 8-Conductor Bundle.	3-43
3-32	Comparison of Heavy Rain Audible Noise Generation of 8-Conductor Bundle with Reference Book Data.	3-44
3-33	Comparison of Measured 3-Phase Line Audible Noise With Levels Calculated From Cage Tests: 8-Conductor Bundle, 50 ft Phase Spacing.	3-45
3-34	Variation of Maximum Gradient Around an 8-Conductor Bundle.	3-47
3-35	UHV Cage, Bundle Offset (Simulation of Outer Phase).	3-48
3-36	Comparison of 3-Phase Line Maximum Gradient Distribution With Those Obtained in Test Cage.	3-48
3-37	Comparison of Audible Noise Generation of Center and Outer Phase Bundles in Test Cages.	3-49
3-38	Comparison of Measured and Calculated Audible Noise Levels: 12-Conductor Bundles of Different Diameters.	3-50
3-39	Comparison of Measured and Calculated Audible Noise Levels: 12-Conductor Bundles of Different Diameters.	3-51
3-40	Audible Noise Measured During Cage Tests on Regular and Asymmetric Bundles, Plotted Versus the Average of the Maximum Surface Gradients of all the Subconductors. Bundles of 8 x 3.3cm Diameter Conductors.	3-55
3-41	Audible Noise Measured During Cage Tests on Regular and Asymmetric Bundles, Plotted Versus the Average of the Maximum Surface Gradients of all the Subconductors.	3-56

Figure	Title	Page
3-42	Asymmetric 6-Conductor Bundle.	3-56
3-43	Audible Noise Versus Asymmetry for the Center Phase of an 8-9-8 Line Configuration.	3-58
3-44	Audible Noise Versus Asymmetry for the Outside Phases of an 8-9-8 Line Configuration.	3-58
3-45	Comparison of a Regular 8-8-8 With an Optimized 8-9-8 Line Configuration; Phase Spacing is 60 ft.	3-59
3-46	Appearance of an Untreated Wet Conductor in Corona (Maximum Gradient = 17 kV/cm)	3-62
3-47	Appearance of Treated Wet Conductor in Corona (Maximum Gradient = 17 kV/cm)	3-62
3-48	Test Cage Used for Screening Tests.	3-65
3-49	Comparison of Audible Noise Performance of "As Manufactured" and Treated 6-Conductor Bundles.	3-66
3-50	Formation of Water Drops on Conductors After Accelerated Life Test.	3-68
3-51	Variation of Audible Noise Throughout Accelerated Aging Period.	3-69
3-52	Wet Conductor Generation Versus k; Subconductor Diameter d = 1.427 in; α = Angular Position of Water Drops Relative to Point of Maximum Gradient.	3-72
3-53	Difference Between Measured and Calculated Noise Levels: 12-Conductor Bundles.	3-73
3-54	Variation of Audible Noise With Bundle Diameter: 8-Conductor Bundle; 1200 kV; Wet Conductor.	3-73
3-55	Variation of Audible Noise With Bundle Diameter: 12-Conductor Bundle; 1200 kV; Wet Conductor.	3-74
3-56	Variation of Air Absorption Coefficient With Frequency, Temperature and Humidity.	3-75
3-57	Comparison of Short Line and Long Line RI Frequency Spectra for Open Ended Terminations (Short Line Length = 1625 ft).	3-77
3-58	Mode 1 Contribution to RI of Figure 3-57.	3-78
3-59	Comparison of Short Line and Long Line RI Frequency Spectra for One End Open and the Other End Terminated in 100 pF to Ground on Each Phase.	3-79
3-60	West-Phase UHV Station Showing Transformer, Surge Arrestor and Coupling Capacitor.	3-80
3-61	RI Choke Coil Connected Between Flexible Jumpers and Line Conductors.	3-81

Figure	Title	Page
3-62	RI Frequency Spectra - 8-Conductor Bundle.	3-81
3-63	Cumulative Frequency Distribution of RI for Configuration 1 - Horizontal Configuration - 105 ft Laterally From Center Phase.	3-82
3-64	Cumulative Frequency Distributions of RI for Configuration 2 - Triangular Configuration - 105 ft Laterally From Center Phase.	3-83
3-65	Cumulative Frequency Distributions of RI for Configuration 3 - Horizontal Configuration - 105 ft Laterally From Center Phase.	3-83
3-66	Cumulative Frequency Distributions of RI for 12-Conductor Bundle, 50 in Diameter, 105 ft Laterally From Center Phase, Loop Antenna.	3-86
3-67	Comparison of RI Measurement Made With Rod and Loop Antennas for 12-Conductor Bundle, 50 in Diameter.	3-88
3-68	Comparison of RI Measurements Made With Rod and Loop Antennas for 12-Conductor Bundle, 20 in Diameter	3-89
3-69	Variation of RI and Audible Noise Before, During and After a Rain Period.	3-90
3-70	Correlation Between RI and Audible Noise for the Period Covered by Figure 3-69.	3-91
3-71	Variation of RI and Audible Noise During and After a Period of Fog.	3-91
3-72	Variation of RI and Audible Noise During a Period of Snow.	3-92
3-73	Correlation of RI and Audible Noise. Short Term Variations, Voltage Range 1150-1300 kV.	3-93
3-74	Correlation of RI and Audible Noise. Long Term Variations.	3-93
3-75	6-Day Variation of Quasi-Peak TVI Levels; 8-Conductor Bundle, 65 ft Phase Spacing.	3-96
3-76	Variation of Peak, Quasi-Peak, and FI Levels of TVI During a Period of Rain; 8-Conductor Bundle, 65 ft Phase Spacing.	3-99
3-77	Comparison of RI and TVI Variations for Period Covered by Figure 3-76.	3-99
3-78	Correlation of RI With TVI (FI) for Period Covered by Figure 3-76.	3-100
3-79	Correlation of RI With TVI (QP) for Period Covered by Figure 3-76.	3-101
3-80	Corona Loss of the Test Line at 1050 kV in Two Different Periods of Rain, July 7 and 14, 1975.	3-102
4-1	Outline of New 1500/$\sqrt{3}$ kV Plastic Sheet Window Bushing in the UHV Contamination Building.	4-3

LIST OF ILLUSTRATIONS (Cont)

Figure	Title	Page
4-2	Outer Sheet of the Plastic Window Bushing Feed Wire Passing Through Circular Opening in the Sheet.	4-4
4-3	Plastic Window Bushing as seen from Inside the Contamination Chamber. Insulator String Shown in Figure 4-1 for Support of Feed Wire may also be seen here Through Circular Openings.	4-4
4-4	Corona Streamers on Feed Wire Inside UHV Contamination Chamber During Fog Test at 1450/$\sqrt{3}$ kV.	4-5
4-5	UHV Contamination Building with Plastic Window Bushing Overhead Door Open.	4-6
4-6	UHV Contamination Building with Protective Door for Plastic Sheet Window Bushing Closed.	4-6
4-7	1500/$\sqrt{3}$ kV Porcelain Bushing Being Installed in UHV Contamination Chamber on Wall Opposite Plastic Sheet Window Bushing.	4-7
4-8	Porcelain Bushing Installed in UHV Contamination Chamber.	4-7
4-9	Center Phase Insulator String on Suspension Tower of UHV Test Line Contains 39 Units per Side (8.6m) of High Strength Antifog Units and was Used for Natural Humidity Contamination as well as Clean Wet Tests.	4-9
4-10	Geometrical and Mechanical Characteristics of Standard and Antifog Insulators used in this Study.	4-9
4-11	Voltage as a Function of Fifty Percent String Length for Vertical Strings of Standard Insulators.	4-13
4-12	Voltage as a Function of Fifty Percent String Length for Vertical Strings of Antifog Insulators.	4-13
4-13	Time Exposure (~30 sec) Photograph of Scintillation Discharge Activity on Long Vertical String of Standard Units in Early Stage of Contamination Test at 1450/$\sqrt{3}$ kV. Note arc in air Bridging First Three Insulators and Absence of Activity on Some Units.	4-14
4-14	Time Exposure (~30 sec) Photograph of Scintillation Discharge Activity during Later Stage of Same Test as in Figure 4-13. Note Increased Intensity of Activity and Fewer Units on Which no Discharges Appear. Only a Portion of the Total String Length (about 3m out of 11m) is Visible.	4-15
4-15	Quadruple Vertical String of Standard Insulators and Single String Which was Sometimes Tested in Parallel	4-16
4-16	Crane Lifted Platform Used for Bringing Operators Near Insulator String During Contaminated Application in Natural Humidity.	4-18
4-17	Platform of Figure 4-16 Adjacent to Insulator String in Preparation for Natural Humidity Test.	4-18

Figure	Title	Page
4-18	Lineman Applying Contaminant to Center Phase V-String Before Natural Humidity Test.	4-19
4-19	Results of Outdoor Natural Humidity Tests on V-Strings Compared with Results of Indoor Tests on Vertical Strings.	4-21
4-20	Long String Efficiency for Vertical Standard Insulators Using Present Results Compared with Previous Results.	4-23
4-21	Long String Efficiency Vs kV for 40/10 and 40/20 Contaminants.	4-24
4-22	Voltage Distribution on 30 Unit Insulator String.	4-26
4-23	Cross-Sectional View of the High Capacitance Insulator.	4-27
4-24	Voltage Distribution on a 25-Unit String of High-Capacitance Insulators.	4-28
4-25	Voltage Distribution on a 27-Unit String of Standard Insulators.	4-29
4-26	Voltage Distribution on an Externally Graded String of 25 Standard Insulators.	4-31
4-27	Experimental Test Setup for External Capacitive Grading Using Wired Connections to High Capacitance Insulators. String on Right Contains 22 High Capacitance Units, While Other Two Strings Contain 22 Standard Insulators Each. Only the String on the Left was Contaminated. The Purpose of the String in the Center was to Insure that the Wires to the Contaminated String Would be Parallel and Uniformly Spaced.	4-32
4-28	Experimental Test Setup for External Field Grading of an Insulator String. The 25-Unit Insulators in the Center of the 4 Rings were Contaminated. The Voltage on the Rings was Controlled by Connections to the Capacitor-Divider Stack on the Right.	4-33
4-29	External Field Grading with 2 Additional Rings to Improve the Voltage Distribution Obtained with the Apparatus in Figure 4-28.	4-34
4-30	Voltage Distribution on Field Graded Insulator Strings for the Case of 4 Rings (Figure 4-28) and 6 Rings (Figure 4-29).	4-34
4-31	Experimental Setup Used to Obtain Nonuniform Voltage Distribution with External Field Grading. Top Three Rings Grounded, Other Two Electrically Floating.	4-35
4-32	Nonuniform Voltage Distribution Obtained by External Field Grading Setup of Figure 4-31.	4-36
4-33	Resistance of Insulator String as a Function of Time for Different Lengths of Application of Voltage.	4-40
4-34	Fifty Percent Flashover Strength as a Function of String Length.	4-42

LIST OF ILLUSTRATIONS (Cont)

Figure	Title	Page
4-35	Fifty Percent Flashover Voltage Expressed as kV/Insulator.	4-43
4-36	Shape and Dimensions of a Single Unit Silicone Rubber, Glass-Fiber Reinforced Long-Rod Insulator.	4-44
4-37	Shed Surfaces of Long-Rod Insulators After Being Contaminated and Dried.	4-46
4-38	Experimental Test Setup for EHV Contamination Tests on the Single Unit Vertical Configuration.	4-47
4-39	Experimental Test Setup for EHV Contamination Tests on a Single Unit V-Configuration.	4-47
4-40	Experimental Test Setup for UHV Contamination Tests on a Double Unit V-String.	4-48
4-41	Contamination Performance of Silicone Rubber, Glass-Fiber Reinforced Long-Rod Insulators. The Curves Marked T-25, T-50, V-25, and V-50 Represent the Performance of Standard Cap and Pin Insulators in Vertical (T) and V-Configurations Having Lengths of 25 and 50 Units.	4-49
4-42	V-String on East Phase of the UHV Test Line, Tower 2, Consisting of Rosenthal RODURFLEX Units, Installed in October 1975.	4-52
4-43	V-String on East Phase of the UHV Test Line, Tower 3, Consisting of Ohio Brass HI-LITE Units, Installed in February 1976.	4-52
4-44	Short Circuit Strength and R/X Characteristics of the Power Supplies Available at Project UHV.	4-55
4-45	The Range of R/X and I_{sc} Values for the Test of Table 4-11.	4-57
4-46	Test Results Showing Characteristics of Test Circuit.	4-58
4-47	Region of R/X-I_{sc} Diagram Occupied by Tests of Figure 4-46.	4-59
4-48	Currect (top) and Voltage During a Typical Scintillation Burst at 780 kV.	4-60
4-49	Current and Voltage Just Prior to Flashover at 780 kV	4-60
4-50	Current and Voltage During a Scintillation Burst of 470 mA Showing a 5-6% Voltage Drop.	4-61
4-51	Current and Voltage Prior to Flashover. Note no Measurable Voltage Drop.	4-62
4-52	Current and Voltage During Scintillation. Note no Measurable Voltage Drop.	4-62
4-53	Current and Voltage Just Prior to Flashover with same Circuit as in 4-52. Here Again there is no Measurable Voltage Drop.	4-63

Figure	Title	Page
4-54	Voltage and Current During Scintillation with a Highly Resistive Circuit. Note Voltage Distortions.	4-64
4-55	Current and Voltage During Scintillation Leading to Flashover with a Reactive Circuit. Note Distorted Voltage Shape.	4-64
4-56	Relative Humidity as a Function of Time for Test 2-5. Arrows Indicate Times at Which Scintillation Activity Began.	4-65
4-57	Relative Humidity as a Function of Time for Test 1. Arrows Indicate Times at Which Scintillation Activity was Observed.	4-66
4-58	Relative Humidity During 1975 Tests.	4-67
4-59	Single Sections of Post Which Have Identical Shed Design and Leakage Distance but Different Diameters.	4-69
4-60	Large and Small Diameter Insulator Columns in UHV Test Chamber. Insulator in Upper Right Corner was Used to Support Connection Wires.	4-69
4-61	Flashover Voltage Probability Distribution from Table 4-15, Assuming all Posts Identical.	4-72
4-62	Scintillation Discharges on Post Insulator.	4-73
4-63	Scintillation on the Large Diameter Post.	4-78
4-64	Scintillation on the Large Diameter Post.	4-78
4-65	Energized 12-Conductor Bus Placed Between Posts to Modify Voltage Distribution. Hipot Wire also Extends to Conventional Insulators at far Right.	4-81
4-66	Voltage Distribution on Small Diameter Column with and without Nearby Energized Electrodes. Measurements in Absence of Electrodes was made with Conventional Technique and with Space Potential Probe.	4-81
4-67	Voltage Distributions During Outdoor Natural Humidity Tests on Two Small Diameter Columns Having 14 Sections.	4-82
4-68	Voltage Distributions on Large Diameter Column with and without Nearby Energized Electrodes. Measurements made with Space Potential Probe. "Section" Corresponds to a Length of About 5 ft.	4-83
4-69	Ice Accumulation on Insulators and Tower in the Ontario Hydro 230-kV System.	4-85
4-70	Alternate View of the Same Tower Shown in Figure 4-69.	4-85
4-71	EHV Poleyard Showing Boom of Truck From Which Water was Sprayed on Insulators.	4-87

Figure	Title	Page
4-72	Copper Pipe Ice Monitor. Ice Thickness Measured on Top Surface.	4-88
4-73	Experimental Setup for Effect of Length on Ice Flashover Strength. Standard Unit Strings of 30, 27, 27 and 24 Units are Shown.	4-89
4-74	Flashover Voltage as a Function of Ice Thickness Measured on Pipe Monitor for Vertical Strings of Standard Insulators with Different Lengths.	4-90
4-75	Flashover Voltage as a Function of Radial Ice Thickness Measured on Insulator Strings on Morning After Tests.	4-90
4-76	Typical Appearance of Vertical Insulator String After Ice Test.	4-93
4-77	Generalized Sketch of Sheds and Hardware on Synthetic Long Rod Insulators R1-R4.	4-95
4-78	Ice Accumulation on Vertical Configuration of Long-Rod Insulators.	4-95
4-79	Flashover Voltage per Unit and Per-Unit Length of Ice-Coated Standard and Long-Rod Insulators as a Function of Monitor Ice Thickness. Shaded Band Indicates Range of Insulation Strength for Standard Units.	4-96
4-80	Synthetic Long Rod Insulator Type R4 Having 6 Groups of Sheds Separated by a Gap of 14cm.	4-97
4-81	Synthetic Long-Rod Insulators After Ice Test. From Left Types are R3, R4, R2, R1.	4-99
4-82	Ice Accumulation on Insulator Type R2 After Test.	4-99
4-83	Ice Accumulation on Insulator Type R3 After Test.	4-100
4-84	Ice Distribution on Long Rod Insulator Type R4. Note that Large Gaps Between Groups of Sheds Remain Free of Ice Bridging.	4-100
4-85	Pre-Flashover Scintillation Activity on Insulator Type R3 During Ice Test. Note Partial Arcs at Both Ground and Energized Ends of the Unit.	4-101
4-86	Partial Arcs on Type R4 Insulator. Corona Type Glow may be seen at Energized End and Across Gap Between First Two Shed Groups.	4-102
4-87	Heavy Scintillation Activity Across All Gaps and Some Sheds of Type R4 Insulator.	4-102
4-88	Characteristics of the Antifog Glass Insulator.	4-103
4-89	Ice on a 20-Unit V-String of 66,000-lb Glass Insulators Used to Compare EHV and UHV Performance.	4-104

Figure	Title	Page
4-90	Comparison of Ice Flashover Voltages Expressed in Voltage/Connection Length as a Function of Icing Severity for Standard Suspension Units and Post Insulators.	4-106
4-91	Ice on Post Type A After Test. Sheds at Bottom (Ground End) no Longer Bridges. Large "Whisker" in Center of Hardware on Which Partial Discharges were seen are Also Present in Figure 4-92.	4-107
4-92	Ice on Post Insulator Type C After Test. Note Nonuniform Distribution of Ice Around Column. Sheds at Top (Energized End) Lost Ice During Scintillation.	4-108
4-93	Ice Accumulation on Post Type D After Test. Pipe Monitor in Lower Right Hand Corner.	4-108
4-94	Rain Spray Produced by Artificial Rain System Above Center Phase on Tower 2. Note Water Dripping From Individual Units.	4-110
4-95	Center Phase Insulator String Showing Shorting Wires Used in Test Sequence to Change String Length in Clean Wet Tests.	4-110
4-96	Suspension Plate Used for Testing of V-Strings.	4-113
4-97	Test Setup for Corona Observations on Suspension Insulators and Hardware.	4-115
4-98	Original Hardware for Single V-String Illustrated with Sediver 120,000-lb. Units.	4-116
4-99	Corona on Hardware and Insulators of Original Design for Single V-String at 1400 kV.	4-117
4-100	Two Shield Ring Designs Which were Employed for Suppressing Corona on Original Design for Single String. Single Ring on Left and "Butterfly" on Right all Composed of 3-in Tubing Formed into 2-ft Circle.	4-117
4-101	Corona Activity on Single String With Encircling and "Butterfly" Shields at 1400 kV.	4-118
4-102	Single and Triple V-Strings Attached Directly to Suspension Plate.	4-119
4-103	View of Composite Single/Triple String From Below.	4-119
4-104	Corona on Composite Single/Triple String at 1400 kV Without Shield Rings.	4-120
4-105	Alternate View of Corona on Composite Single/Triple String at 1400 kV Without Shield Rings.	4-121
4-106	Composite Single/Triple With 2-ft Ring of 3-in Tubing on Single and 3-ft Ring of 6-in Tubing on Triple String.	4-121

Figure	Title	Page
4-107	Composite Single/Triple with 3-ft Ring of 6-in Tubing on Both Single and Triple Strings.	4-122
4-108	Corona Activity at 1400 kV on Composite Single/Triple with Shields Described in Figure 4-107.	4-122
4-109	Same as Figure 108, but in the Absence of Illumination in Order to Verify Corona Activity.	4-123
4-110	Attachment Hardware for Double Strings, Illustrated for Sediver 66,000-lb Units.	4-123
4-111	Corona on Double V-String at 1400 kV Without Shield Rings.	4-124
4-112	Shield Rings 3 Feet in Diameter (6-in Tubing) on Double V-String.	4-125
4-113	Corona Activity at 1400 kV on Double V-String with Whield Rings.	4-125
4-114	Attachment Hardware for Quadruple V-String of Locke 40,000-lb Insulators.	4-126
4-115	Alternate View of Quadruple String Hardware from Below.	4-126
4-116	Corona on Quadruple V-String at 1400 kV.	4-127
4-117	Summary of Insulator String Corona Performance as Noted by Visual Observations for Different Voltage Levls.	4-128
4-118	Corona Activity at 1300 kV on Single V-String in Natural Rain.	4-128
4-119	Corona at 1300 kV on Single String and Conductors in Heavy Artificial Rain.	4-129
4-120	Corona Activity at 1400 kV on Double V-String in Heavy Artificial Rain.	4-130
4-121	Voltage Distribution of Single Insulator String Showing Effects of Shield Rings and Hardware Modification.	4-131
4-122	Voltage Distribution of Double Insulator String Showing Effects of Shield Rings.	4-132
4-123	Voltage Distribution of Triple and Quadruple Strings.	4-132
4-124	Corona on Shield Ring of Double Porcelain String seen from Tower Bridge.	4-133
4-125	Corona on Shield Ring of Triple Porcelain String seen from Tower Bridge.	4-134
4-126	Corona on Units of Double Glass String seen from Tower Bridge.	4-134
4-127	Corona at Base of Caps and on Shield Ring of Single Porcelain String.	4-136

LIST OF ILLUSTRATIONS (Cont)

Figure	Title	Page
4-128	Corona on Single Glass V-String.	4-137
4-129	Comparison of Corona Performance of Single Glass Insulator V-String on One-Phase Mock-up with its Performance on the Three-Phase Line.	4-137
4-130	Corona Activity During Wet Test with Artificial Rain Spray System Above the Single Porcelain Center Phase String.	4-138

LIST OF TABLES

Table	Title	Page
2-1	Suspension Insulator V-String Configurations on the 3-Phase Test Line.	2-11
3-1	Relative Total Noise for Varying Levels of Corona Noise, and Constant Ambient Noise of 49 dB(A).	3-13
3-2	Amount of Rain Data Collected for Each Test Period.	3-14
3-3	Comparison of Measured and Calculated Noise Levels Measured at 15m (50 ft) Laterally From Outside Phase.	3-25
3-4	Comparison of Measured and Calculated Audible Noise Levels for 12 x 1.302 x 50 in Bundle Configuration.	3-30
3-5	Typical Bundle Geometries and K Values for Operating Lines.	3-33
3-6	Comparison of Losses of Regular and Asymmetric Bundles - Typical for 1100 kV.	3-60
3-7	Comparison of RI Data With Calculations - 8-Conductor Bundles - 1050 kV.	3-85
3-8	Number of Minutes of Data Covered by Distribution Curves of Figure 3-66.	3-87
3-9	Comparison of RI Data with Calculations.	3-87
3-10	Results of Statistical Analysis of TVI Data Recorded During Rain for 8-Conductor Bundle, 19.8m (65 ft) Phase Spacing.	3-97
3-11	Comparison of TVI Levels Derived From RI Measurements and RI Calculations With TVI Levels Actually Measured.	3-98
3-12	Comparison of Measured and Calculated Corona Loss Levels for 8- and 12- Conductor Bundles.	3-104
3-13	50% Ozone Concentrations for Different Categories - 1050 kV, March 1975.	3-112
3-14	50% Ozone Concentrations for Different Categories - Ambient, March 1975.	3-112
4-1	Test Series on Standard and Antifog Insulators. Results Aligned in Same Vertical Column were Obtained During the Same Test Period. Voltage 375 kV (ℓ-g) "Fifty Percent String Length" = 32.3 Standard, 15.9 Antifog Units.	4-11
4-2	Fifty Percent String Length, ℓ_{50}, and Corresponding Fifty Percent Flashover Voltage in kV/Insulator for the Standard Units Shown in Figure 4-10.	4-12

Table	Title	Page
4-3	Quantities Related to 50% Flashover Probability, Namely, Fifty Percent String Length, ℓ_{50}, and Corresponding Fifty Percent Flashover Voltage in kV/Insulator for the Antifog Units Shown in Figure 4-10.	4-12
4-4	Flashover Test Results on a Quadruple Vertical String of Standard Insulators and Comparison with Single String Data, Either From Table 4-2 (*), or From Tests Made Simultaneously with a Single String Present. Spacing Between Individual Strings in Quadruple was 46cm (18 in).	4-15
4-5	Natural Humidity Tests on Center Phase V-String of Antifog Insulators on UHV Test Line. Entries for Each Test Give the Number of Insulators on Each Side of the String.	4-20
4-6	Cold Switch-on Test Series Performed on Conventional and Semi-Conducting Glaze Units. Insulators Contaminated Only Before Beginning of Test Series. Total Time of Test:2 Hours.	4-41
4-7	Fifty Percent Cold Switch-on Flashover Voltage of Conventional and Semiconducting Glaze Insulators.*	4-41
4-8	Summary of Contamination Test Results on Plastic Insulators.*	4-50
4-9	Plastic Insulators Installed on the UHV Test Line.	4-51
4-10	Circuit Parameters for Contamination Test Equipment at Project UHV.	4-54
4-11	"Fifty Percent" String Lengths and Flashover Voltages in kV/Insulator for Different Test Circuits.	4-57
4-12	Posts Used to Investigate Effect of Diameter in Tests at Low Voltage Connection Length 76cm (30 in).	4-68
4-13	Geometrical Characteristics of Long Insulator Columns.	4-70
4-14	Results of Contamination Tests on Single Unit (30 in) Posts. Symbold Denote Post Types (S, M, L) and the Order in Which Flashovers Occurred. Numbers Indicate Standard Units Which Flashed over. Asterisks Indicate Tests in Which Six Posts Were Present (No Standard Units). (W) Indicates all Insulators Withstood.	4-74
4-15	Calculation of Flashover Probability for Each Voltage Level. Numbers of Flashovers (FO) and Withstands (WS) for Each Insulator Types at Different Voltage Levels are Shown.	4-75
4-16	40/5 Mixture Tests on Small Diameter Post 7.82m (25.7 ft) in Length.	4-76
4-17	40/40 Mixture. Tests on Large and Small Diameter Column 7.6m (25 ft) in Length. X = Flashover, 0 = Withstand. Avg. Salt Deposit - 0,1 mg/cm^2. Tests in the Same Column Were Performed Simultaneously.	4-77

LIST OF TABLES (Cont)

Table	Title	Page
4-18	Tests on Large Diameter Column with Vertical Strips of Various Widths Contaminated with 40/40. Numbers in Parenthesis Below Each Test Indicate Width of Contaminated Strip (Lower Sections). Entire Circumference of Column is Approximately 250cm.	4-79
4-19	Comparison of Flashover Voltages of Small Diameter Posts in Long Stacks (7.82m) with Data Obtained in Short (103 section) Columns.	4-80
4-20	Contamination Tests on Large and Small Diameter Posts with Modified Voltage Distribution. Voltage 300 kV.	4-83
4-21	Ice Flashover Tests on Vertical and V-Strings of Standard Insulators. Note: Tests 1-6, Vertical; 7 V-String.	4-92
4-22	Characteristics of Plastic Long Rod Insulators Used for Ice Tests.	4-94
4-23	Ice Tests on Plastic Insulators of Type R1 During First Test Period.	4-94
4-24	Ice Tests on Plastic Insulators During Second Test Period.	4-98
4-25	Ice Tests on a 20-Unit Glass V-String of Antifog Insulators.	4-104
4-26	Geometrical Characteristics of Post Insulators Used in Ice Tests.	4-105
4-27	Ice Tests on Post Insulators.	4-106
4-28	Fifty Percent Flashover Voltage as a Function of String Length for 40,000 kg (90,000 lb) Anti-Fog Units in Clean, Wet Tests.	4-111
4-29	First V-String Configurations for Three Phase Test Line.	4-114
4-30	Corona Activity Observed on Suspension Insulator Strings From Bridges of Portal Towers During Dry Conditions. 0 Denotes no Activity.	4-135

Section 1

INTRODUCTION AND SUMMARY

Electric power transmission research with Ultra High Voltages (UHV), i.e. line voltages above existing 800 kV ac, has been proceeding in the United States for a number of years.

UHV overhead transmission offers the most efficient means now available for the transmission of large blocks of power. It uses the least of the nation's raw materials, creates the least heat, requires the least amount of fuel to be continuously burned to supply its losses, and eliminates the necessity for more extensive lower voltage line construction. One of the objectives of UHV overhead transmission research is to develop the technology of designing these major carriers of power so that they have a minimum impact on the ecology and the environment, yet can function effectively to supply the increasing power demands of the United States.

Most of UHV transmission line research in the United States has been performed since 1967 at Project UHV, an organization staffed by the General Electric Company and funded by America's electric utility companies, originally through the Electric Research Council and since 1973 through the Electric Power Research Institute.

During the period 1967-1973, a research program using a single-phase test line was completed and UHV line design data were developed and presented in the "Transmission Line Reference Book - 345 kV and Above" published by EPRI in 1975 [1-1]. The present report is an account of the work accomplished in the period 1974-1976. In this period a 3-phase test line was built and operated with voltages up to 1500 kV (line-to-line). The construction of the 3-phase test line has been a major accomplishment of this research program. New electrical equipment and structures were added to existing single-phase facilities. Energization of the 3-phase UHV test line occurred on January 25, 1975. The 1500 kV test capability makes the Project UHV test line the highest voltage

experimental 3-phase line in the world.

The work performed is described in the next three sections. Section 2 describes the 3-phase test line and its test capabilities. Section 3 contains the detailed results of the tested conductor and line configurations. Section 4 describes the insulation research performed at Project UHV in the period 1974-1976. Research on electric field effects and on measures to reduce the electric field is being conducted at Project UHV under EPRI project RP 566 and will be the subject of a future report. From February 1975 to December 1976 six different conductor and line configurations were tested on the 3-phase test line of Project UHV, at voltages between 1000 and 1300 kV. The electrical performance of each configuration was determined during long term (3 to 5 months) exposure to natural weather conditions.

A major objective of the 3-phase test line was the verification of the design rules previously obtained with a single-phase line, but which could not be reliably established because of the following physical differences between 3-phase and single-phase testing:

- For the same line-to-ground voltage, the electric field (voltage gradient) on the surface of the conductors is 10 to 30 percent higher for 3-phase tests than for single-phase tests. Conversely, single-phase tests require a higher voltage in order to obtain the same surface gradient.
- The gradient distribution among the subconductors of a bundle of a three-phase line is different from that of the same bundle on a single-phase line.
- The audible noise, radio noise, corona loss, and electric field caused by a three-phase line are the combination of the effects of all three phases.

The results obtained during three-phase tests generally confirm the calculation methods developed during the single-phase test period which have been published in the Reference Book [1-1]. The following conclusions have been reached:

- Corona generation of ac transmission lines depends on the electric field in the immediate vicinity of the conductors. The electric stress can be characterized by the surface gradient calculated without accounting for space charge. It is possible to duplicate the physical phenomena occurring in close proximity of a bundle if the conductor surface gradient is kept the same. For the same surface gradient the corona generation is practically independent of the applied voltage and of the proximity of the other conductors and ground.
- Small differences between the surface gradients of subconductors of a bundle resulting from different modes of energization, e.g.

single-phase or three-phase, have a negligible effect on corona if the average bundle gradient is maintained constant.

- Three-phase tests have confirmed that audible noise caused by corona in wet weather is one of the most important problems impacting on line cost and performance.
- For most of the configurations tested, the measured audible noise which is exceeded for 50% of the time (L_{50}) during rain practically coincides with the "wet conductor" audible noise defined and calculated according to the Reference Book [1-1].
- The measured value of audible noise which is exceeded for 5% of the time (L_5) during rain, practically coincides with the "heavy rain" audible noise [1-1].
- Fair weather audible noise produced by UHV transmission lines is negligible, provided that the lines are designed to have an acceptable noise performance in wet weather.
- Audible noise in fog can reach levels as high as the L_5 noise in rain.
- Radio interference measured for the three-phase line configurations tested was about 5 dB higher than the levels calculated from the Reference Book [1-1]. Efforts are underway to determine the reasons for this difference, with special attention given to the conversion from a short test line to long operating lines.
- An estimate of Television Interference (TVI) produced by corona during rain can be derived from Radio Noise measurements at 1 MHz as described in Reference [1-1]. The levels of TVI caused by corona of UHV transmission lines are generally low compared with other possible sources on interference.
- Ozone generated by corona can be measured in small amounts (up to 5 ppb) in close proximity of the conductors of UHV lines; however, the levels measured are totally negligible compared with daily variations of 50 to 80 ppb in ambient ozone levels.

The three-phase test line has been instrumental in demonstrating the feasibility of UHV transmission, and to identify the most important problems which impact on line costs and performance. In addition to providing confirmation of the basic corona performance of practical line configurations, new design data were obtained, which were not available from previous single phase testing.

- For bundles of many subconductors (8-12), a small bundle diameter, which is advantageous in reducing ice loading and electric field at ground level, and increasing air clearances, can result in much larger levels of corona than expected. For an optimum corona performance, rather large (1.2 to 1.7m) bundle diameters are needed.
- A method to correct audible noise measurements to account for ambient noise was devised. This method utilizes the differences in the frequency spectra between corona noise and the noise from various ambient sources.
- The noise of UHV transmission lines has been found to be statistical dependent on the weather, and the minimum time required for "long-

term" testing has been determined. For instance, it has been found that 2000 minutes of rain are practically sufficient to represent all the rain periods.

The insulation of UHV transmission lines has been studied using one of the three UHV transformers of the test line, and on several occasions the test line itself. The insulator strings of the test line, three "V" strings at each of the two suspension towers, have been selected to represent practical suspension insulator strings which can be used to withstand the mechanical and the electrical stress of UHV lines up to 1500 kV. These include multiple strings of ordinary type insulators, single porcelain and glass insulator strings of high mechanical strength and non-ceramic insulators, especially supplied to provide experience with these types of insulators up to 1500 kV. The corona performance of insulator strings on the UHV test line has been made acceptable using large shield rings. Without these rings excessive visual corona on the hardware would be present.

In addition, a large program of flashover tests on artificially contaminated insulators was conducted in the UHV test chamber of Project UHV. The program included long vertical strings of different types of insulators (ordinary, antifog, semiconductive glaze, non-ceramic), multiple strings, post insulators, and the study of the effects of various parameters. The main conclusions reached are:

- The relation between flashover and insulator length is non-linear, is a function of the type of insulation, and requires full scale tests.
- The long string efficiency for "vertical" insulator strings at ultra-high voltages is about 90%, much higher than reported in [1-1].
- Tests on "V" strings for UHV have not yet been performed in the chamber. However, tests on the UHV test line during natural humidity indicate that the long string efficiency of V-strings is much higher than reported in the Reference Book [1-1]. Then, data had been obtained on "V" strings with an insufficient mechanical load to form a "V".
- The loss of efficiency of long insulator strings had previously been associated with proximity effects and non-linear voltage distribution along the string. However, attempts to improve the voltage distribution have not resulted in an improved long string efficiency.
- Semiconductive glaze insulators are effective in eliminating the contamination flashover problem. The constant power loss of these insulators, however, limits their potential application to areas with severe contamination problems.
- Post insulators for UHV are very vulnerable to contamination flashover. Posts for contaminated areas will require special design solutions or expensive maintenance programs.

- The flashover mechanism of insulators for UHV is still not completely understood, despite useful additional experimental information. The leakage current pulses and the impedance requirements of the test source have been found to be independent of string length and of flashover voltage.

During the contract period (1974-1976) a study of the switching surge breakdown development in long air gaps was made in the Outdoor Area of the General Electric's High Voltage Laboratory in Pittsfield, Mass. This was an independent effort sponsored by General Electric Company parallel to the UHV program sponsored by EPRI. The results of this study have been published in the technical literature [1-2]. The tests performed have provided additional experimental information for use in developing a model of long gap flashover. The studies included measurements of corona inception, leader inception, and leader propagation characteristics. These data were obtained for practical configurations, such as conductor-tower air gaps, and include influences of hardware and weather.

References

(1-1) - Transmission Line Reference Book - 345 kV and Above, Research Reports Center, P.O. Box 10090, Palo Alto, CA 94303.

(1-2) - Switching Surge Breakdown Development in Large Conductor - Tower Air Gaps, by E. J. Los and H. M. Schneider, presented at the summer power meeting of the IEEE, Mexico City, July 1977.

Section 2

THREE PHASE UHV TEST LINE

PROJECT UHV: A TRANSMISSION RESEARCH CENTER, PAST HISTORY AND PRESENT OBJECTIVES

Project UHV (Ultra High Voltage) was initiated by the Electric Research Council in 1967, to study overhead Transmission Lines with voltages in excess of 1000 kV ac. Project UHV evolved from Project EHV, the research facility built and funded by General Electric in 1958-1964 to provide data for ehv transmission in the 400-750 kV range.

With the support of the Edison Electric Institute and the Tennessee Valley Authority in 1965 and 1966, Project EHV completed the study of ehv transmission and incorporated all available data in the "EHV Transmission Line Reference Book", published by the Edison Electric Institute in 1968. [2-1]

In 1967 the Electric Research Council, using funds provided by the Edison Electric Institute and the Bonneville Power Administration, started a research program, intended to cover a voltage range from 1000 to 1500 kV ac.

Instrumentation and equipment from Project EHV, already in place for research on ehv problems, were modified and utilized for the new research, and the Project was renamed Project UHV in January, 1967, to better describe its expanded activities.

In the early stages of this program, three-phase research was not justifiable from an economic point of view until single-phase work had defined the problems and assessed study priorities. Therefore, a single-phase test line was constructed and energized for the initial period of research from 1967 to 1971. The single-phase program was extended to 1973 when it became apparent that additional research was necessary to investigate further subjects of most importance for uhv transmission, such as audible noise and electrostatic effects. In 1973, Project UHV was transferred to the jurisdiction of the Electric Power Research Institute (EPRI), which has since published a new transmission design book which updates and extends the previous "EHV Reference Book". The new book "Transmission

Line Reference Book - 345 kV and Above" [2-2] covers the electrical aspects of transmission line design from 345 kV to 1500 kV. The design data for ultra high voltages were obtained during the single phase UHV research program from 1967 to 1973.

Means for conversion to three-phase performance from single-phase test results had to be developed for each phenomenon being considered. It should be noted that single-phase testing was limited by the fact that research for transmission line above 1300 kV could not be effectively performed with the available single-phase equipment. In fact, for the same applied voltage, single-phase lines have conductor surface gradients which are 10 to 30% lower than three-phase lines.

In order to verify and extend the single-phase results, a new 3-year program to construct and operate a 3-phase test line in the range of 1000 - 1500 kV ac was started by EPRI in 1974.

In addition to three-phase overhead line testing, it was important that efforts in basic research and development be continued at Project UHV to stimulate innovation and development of new design concepts. This could be accomplished with single-phase testing using existing UHV facilities during 3-phase line construction and stringing, and using the available EHV facilities. Such efforts were concentrated in the areas of improved corona performance of bundles and contamination performance of insulators for UHV. The results of these are illustrated in Section 3 (Corona Effects) and Section 4 (Insulation Research) respectively.

UHV STATION

A view of the UHV station is shown in figure 2-1. The voltage to the test line is supplied by 3 single phase auto-transformers. Each auto-transformer is rated 33 MVA, with a BIL of 2550 kV. Taps are provided for $193/\sqrt{3}$ kV and $143/\sqrt{3}$ kV input points for connection to a 73 step regulating transformer capable of varying the voltage + or -30% around its $110/\sqrt{3}$ kV rating. The use of the $143/\sqrt{3}$ kV tap and a +30% regulator setting gives a maximum voltage of $1500/\sqrt{3}$ kV. With a suitable combination of the UHV transformer taps and regulator setting the test line can be energized at any selected line-to-line voltage in the range between 600 kV and 1500 kV. The 650 kV 3-phase transformer which is still in place from Project EHV [2-3], can further extend the voltage capabilities since it covers the range of line voltages between 400 kV and 700 kV and can also provide an additional source for tests on double circuit or 6-phase EHV line configurations.

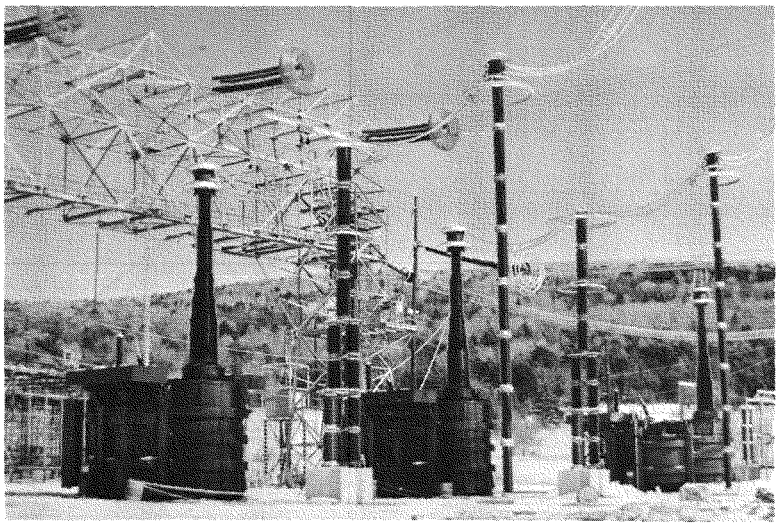


Figure 2-1. UHV Station

Protection of the UHV transformers from lightning and switching surges is provided by 900 kV lightning arresters, which are also shown in figure 2-1.

The east phase bus is the original bus used for the single phase test line, and contains a high-precision SF_6 insulated, 2550 kV BIL, gas capacitor and radio noise coupling capacitor. The bus itself consists of six aluminum pipes 6cm (2.5 in) diameter, with a bundle diameter of 90cm (36 in). Large toroidal shields 4.12m (13 ft) in diameter are used on each end of this bus to eliminate corona from the end hardware, and to reduce the dielectric stress on the strain insulators used for support. These shields are built of aluminum tubing 11cm (4.5 in) in diameter, arranged in an array of six rings spaced about 46cm (18 in) apart.

The other two buses, for the center and the west phase of the line, consist of 3 or 4 flexible aluminum tubes, suspended directly from the corona shields of the equipment. The flexible tubes have a diameter of 10cm (4 in) and are about 46cm (18 in) apart. The center and west phase buses contain a coupling capacitor which can be used both for conducted radio noise and for corona loss measurements. It is possible to make corona loss measurements using standard instead of precision capacitors by periodically calibrating the loss measuring system at low voltage in fair weather, when the loss is negligible (two orders of magnitude less) with

respect to the loss at normal voltage in foul weather.

Each bus was originally connected to the test line by means of flexible tubing terminating in a wave trap. These lightweight flexible tubings proved satisfactory from the corona standpoint. However, they had little resistance to fatigue bending at spacers and junctions caused by the wind, and the connections broke down several times. The flexible tubing was replaced with bundles of eight stranded cables (3.3cm in diameter), which are satisfactory electrically and mechanically. The wave traps serve the purpose of terminating the line at the bus side in a high impedance in the radio frequency range of 0.5 to 2 MHz. The wave traps can be short-circuited in order to measure the radio noise current conducted through the coupling capacitors.

Short circuit current for insulation testing is limited by series resistors. The resistor for the 1500 kV UHV transformer is a wire resistor consisting of 1820m (6000 ft) of #6 nichrome wire with a value of 200 ohms. The resulting short circuit current is 20.3 amps at the lowest voltage (346 kV to ground) and 36.8 amps at the upper limit (866 kV to ground).

THREE-PHASE UHV TEST LINE

A plan-profile of the UHV test line is shown in figure 2-2. The line is supported on two portal type suspension towers with a main span of 340 meters. The conductors are dead-ended in a pair of steel cables which are supported by an end structure and terminated in an anchor system set behind the towers at ground level (see figures 2-3 and 2-4). Sag, and therefore ground clearance, is adjustable over a range of approximately 12 meters. This can be accomplished even with the line energized. Under high ice and wind loads, the conductors are slacked as shown in figure 2-3 to prevent overloads on the towers.

An outline of the suspension towers is shown in figure 2-5, and of the tower 4 end structure in figure 2-6. The suspension towers are guyed structures resting on a ball and socket joint. The 4.75cm (1.825 in) bridge pins join the leg to the truss. The towers are constructed of A-36 galvanized steel; each leg weighs 13,600 kg (15 tons) and the truss weighs 60,000 kg (66 tons). Each leg foundation is supported by four 7m (23 ft) deep pressure injected uncased footings with a design load capability of 63,000 kg (70 tons) each.

The guy cables are attached to multi-helix power installed screw anchors, with an average depth of 10m (35 ft). Figure 2-7 shows a triple-helix unit just starting

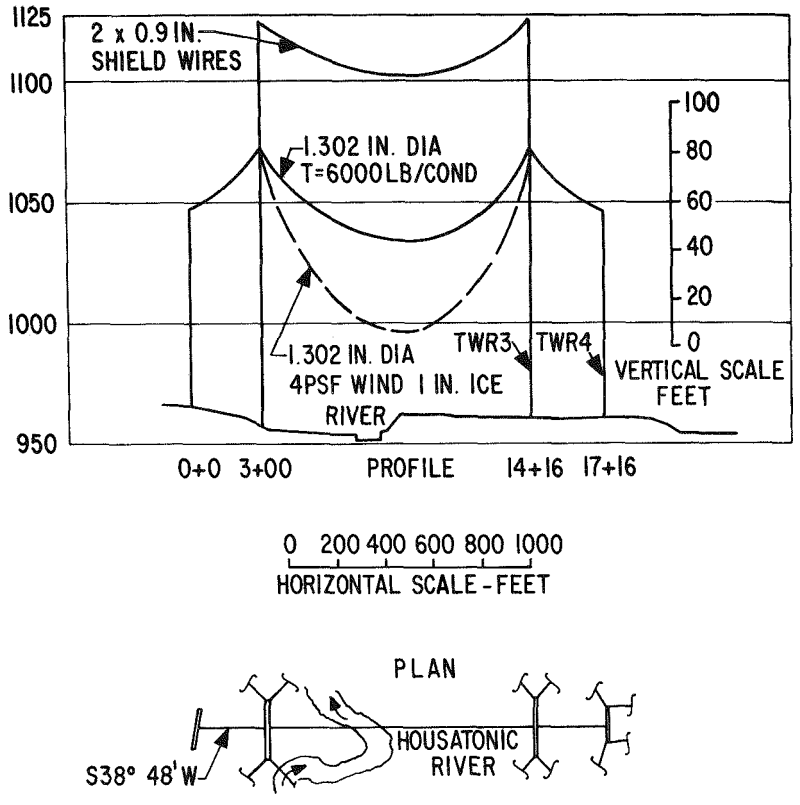


Figure 2-2. Plan-Profile, Towers 1-4.

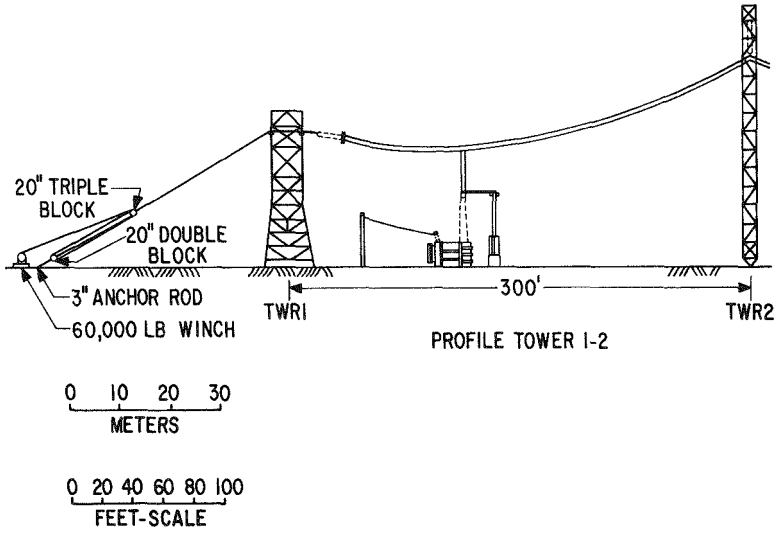


Figure 2-3. Plan-Profile, Towers 1-2.

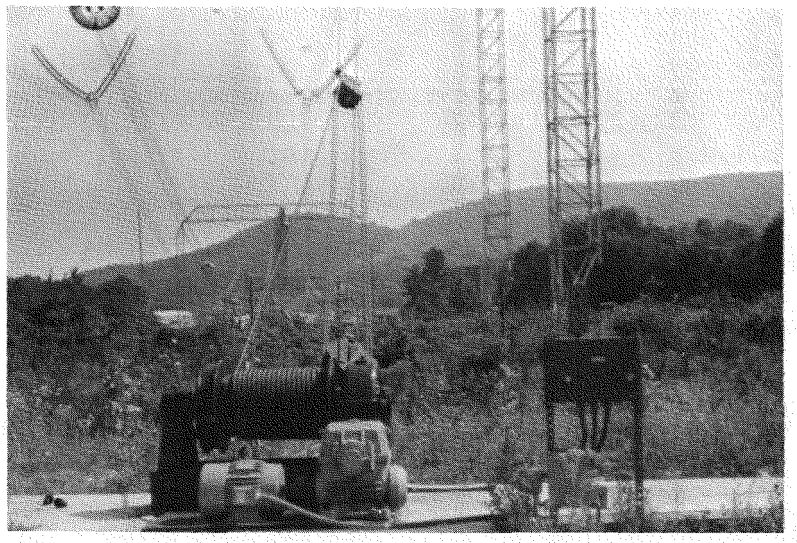


Figure 2-4. Winch Behind Tower 4.

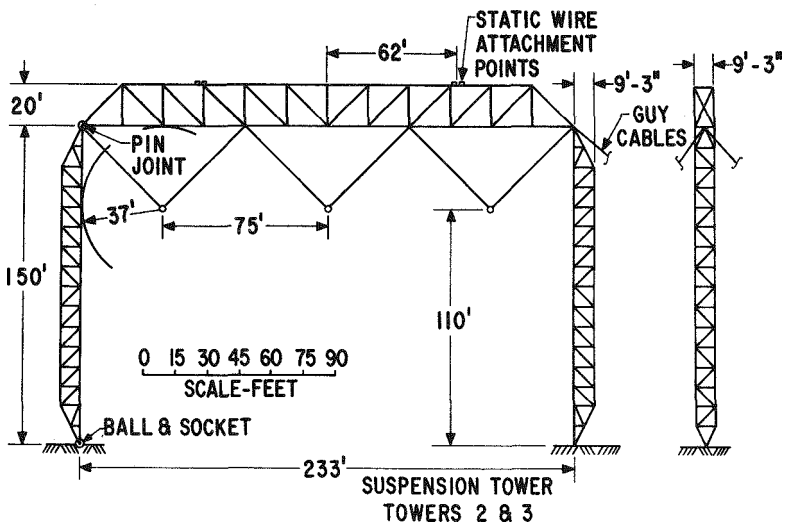


Figure 2-5. Outline - Tower 2.

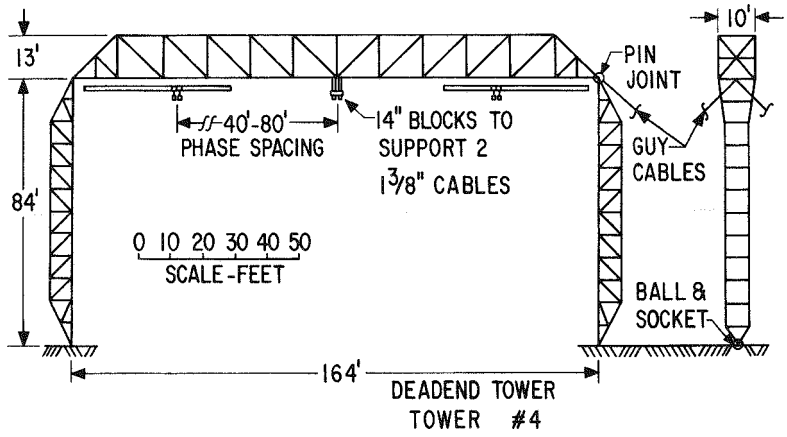


Figure 2-6. Outline - Tower 4.

into the ground. A shear pin type torque wrench is between the anchor and the Kelly bar to indicate when desired torque is attained. The guy cable is 6 x 19 wire rope, with a breaking strength of 26,000 kg (58,000 lb). It is terminated on both ends in helical guy grips.

Erection of the trusses on the suspension towers was completed without large cranes, by using the legs as gin poles. First the legs were erected, and temporary guys installed. Falsework was then installed on top of the leg (see figure 2-8), and the truss lifted into place using a 5-part hitch pulled by available line tensioning winches.

The design capabilities of the UHV test line are as follows:

Total length	523m	(1716 ft)
Main suspension span	340m	(1116 ft)
Phase spacing	9 - 24m	(30-80 ft)
Tower-to-ground clearance	46m	(150 ft)
Height above ground	21 - 30m	(70-100 ft depending on conductor size)
Working tension 22,700 kg	(50,000 lbs/phase)	
Maximum tension 45,400 kg	(100,000 lbs/phase)	



Figure 2-7. Screw Anchor Installation.

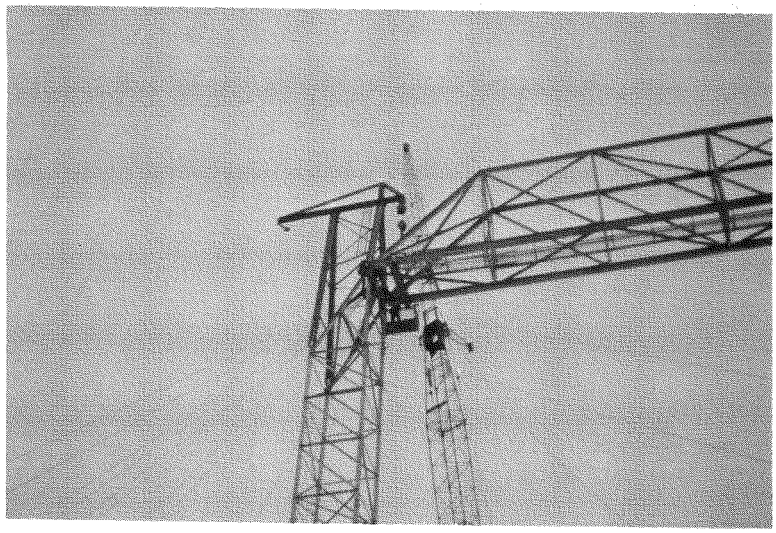


Figure 2-8. Falsework on Tower 2, Lifting Bridge Into Place.

Towers, winches and dead-ends are designed for the following bundles with either 1.27cm (1/2") of ice and 190 N/m^2 (4 lb/ft^2) wind, or no ice and 430 N/m^2 (9 lb/ft^2) wind:

16 x 3.3cm (1.302 in)
11 x 4.6cm (1.8 in)
8 x 10cm (4 in) expanded

The facilities include tension and stringing equipment (see figure 2-9) with capability of stringing up to 10cm diameter conductors at 9000 kg tension at a speed of 1.8 m/s (4 mi/h).

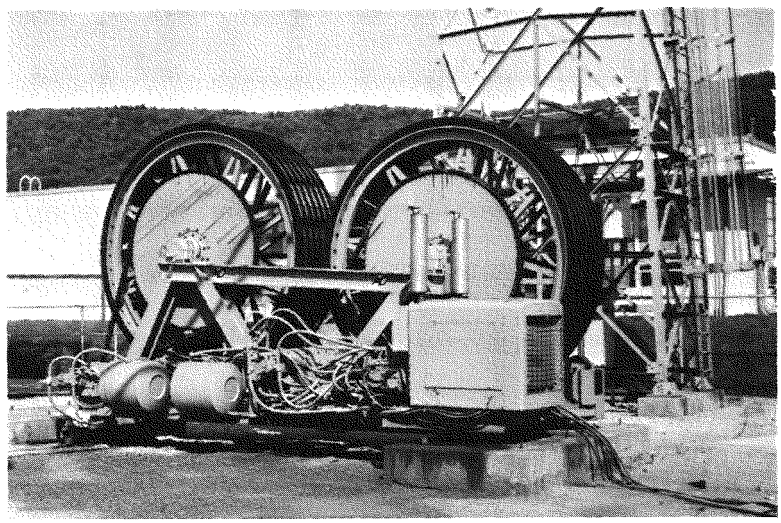


Figure 2-9. Bull Wheel Tensioner.

INSULATOR STRINGS

The three-phase Project UHV test line is being used to illustrate some of the alternative suspension insulator string designs which satisfy the electrical and mechanical constraints imposed by transmission voltage levels up to $1500/\sqrt{3}$ kV. All the suspension strings are V-type, since the long vertical strings necessary for UHV systems would allow unacceptably large wind swing displacements.

For the initial insulator configurations, the total length of each leg of the V-strings was chosen to be 8.6 meters (28 ft). The insulators are suspended from the test towers with long hangers. However, it is possible to duplicate practical tower structures by means of suitable mock-ups for both center and outer phase simulation.

Mechanical considerations of the National Electric Safety Code heavy loading conditions with 1.27cm (0.5 in) ice and 18 m/s (40 mi/hr) horizontal wind on the 16 x 3.3 cm (1.3 in) conductor bundle showed that the maximum working tension in each leg of the V-strings should be 22,700 kg (50,000 lb). Such high mechanical strengths could be achieved by using single strings, or by paralleling two or more sub-strings of lower strength so that the multiple strings have the necessary total strength. The combinations chosen for the initial construction of the test line are shown in table 2-1. The double glass, single porcelain, and double porcelain strings were located in one portal tower, whereas the triple porcelain, single glass, and quadruple porcelain are in the other tower. It should be noted that all the insulator strings except the single porcelain have sufficient mechanical strength for the 16-conductor bundle mentioned above.

Circular metallic rings of flexible tubing with a diameter of 15cm (6 in) have been installed near the conductor yoke plate on all the suspension insulator strings. The ring diameter is 0.9m (3 ft) on the single strings and 1.2m (4 ft) on the multiple strings. These rings were designed to suppress corona on the basis of visual observations made during full scale tests performed with a single phase line before the three phase line was constructed. The appearance of the single, double, triple, and quadruple strings is shown in figures 2-10 to 2-13, whereas figure 2-14 illustrates the hardware in the vicinity of the 8 x 3.3cm (1.3 in) conductor bundle which was the first bundle tested.

The insulator strings at the dead-end towers are quadruple, with each substring containing 45 standard type porcelain units with a mechanical strength of 22,700 kg

TABLE 2-1

SUSPENSION INSULATOR V-STRING CONFIGURATIONS ON THE THREE PHASE TEST LINE

Type	Material	Mechanical Strength/Unit kg	(lbs)	Length (Each Substring) m	(ft)	Number of Units/ Substring	Ratio of Leakage/ Spacing	cm Leakage/kV (1500 kV)
Single	Porcelain	40,900	(90,000)	8.60	(28.2)	39	3.34	3.3
Single	Glass	54,500	(120,000)	8.68	(28.5)	38	3.16	3.2
Double	Porcelain	22,700	(50,000)	8.57	(28.1)	54	2.20	2.2
Double	Glass	30,000	(66,000)	8.57	(28.1)	45	3.11	3.0
Triple	Porcelain	18,100	(40,000)	8.57	(28.1)	58	2.20	2.2
Quadruple	Porcelain	18,100	(40,000)	8.57	(28.1)	54	3.04	3.0

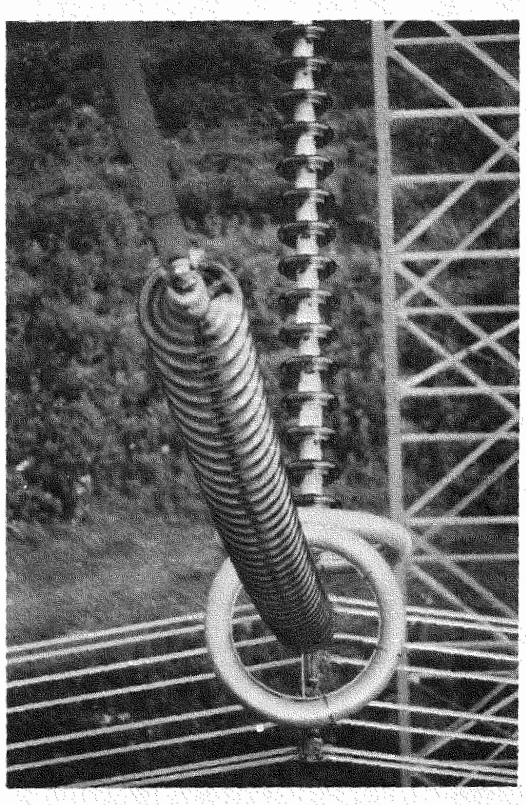


Figure 2-10. Single Suspension Insulator.

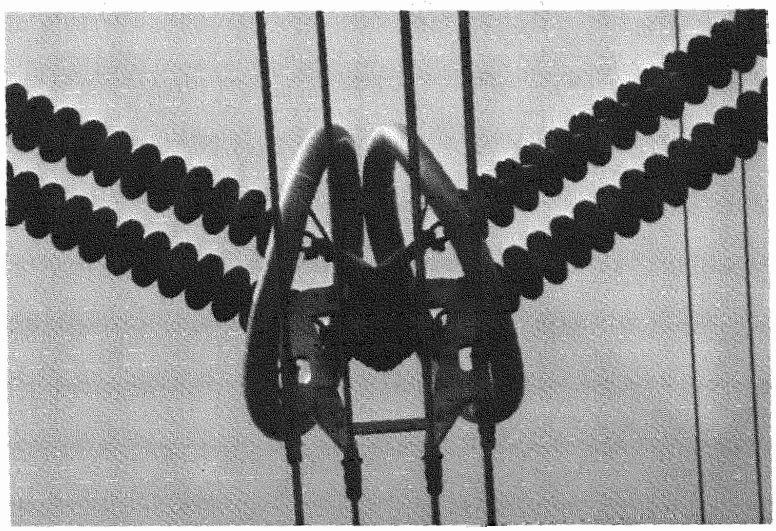


Figure 2-11. Double Suspension Insulators.

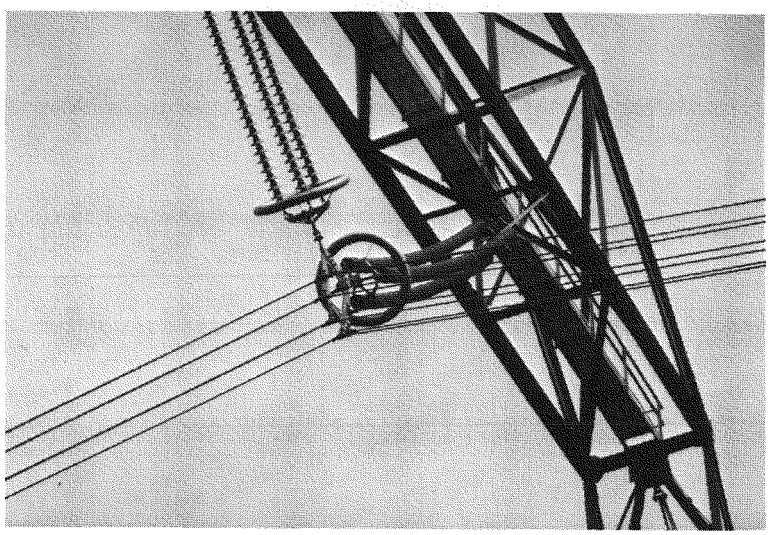


Figure 2-12. Triple Suspension Insulator.

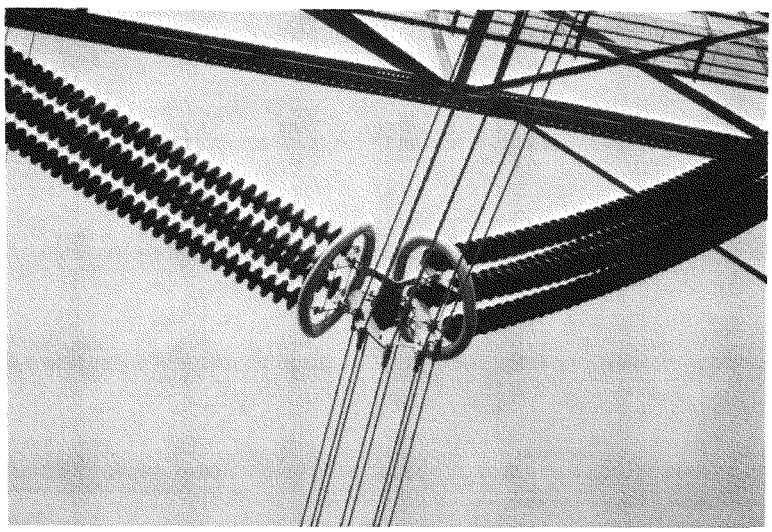


Figure 2-13. Quadruple Suspension Insulator.

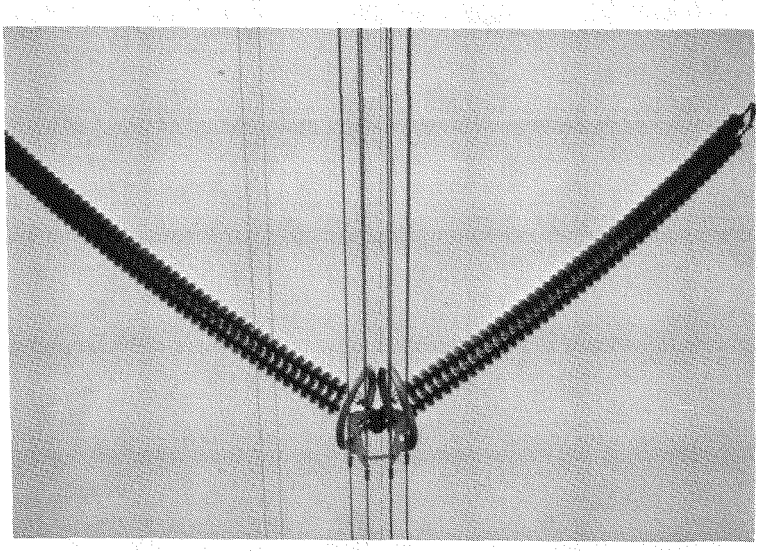


Figure 2-14. Suspension Hardware.

(50,000 lbs) and a string length of 7.7m (25 ft). Two types of toroidal shields are being used at the termination of the conductor bundles on the insulator strings. One, shown in figure 2-15, consists of a composite of 5 circular rings constructed from 10cm (4 in) diameter tubing, with an overall diameter of 3m (10 ft). The other type of dead-end shield, shown in figure 2-16, is a composite of 17 circular rings 3.3cm (1.3 in) in diameter, with an outer toroid diameter of 3m (10 ft).

A rain spray system has been installed on one portal tower in order to make tests for determining the required UHV insulator string lengths in clean conditions.

Two of the V-strings described here have been later replaced with insulators of composite materials containing a fiberglass rod which provides the mechanical strength and a shell of synthetic material, to illustrate the application of this new technology for UHV transmission lines. (See Section 4).

INSTRUMENTATION FOR DATA ACQUISITION

Data Acquisition Computer

The heart of the data acquisition system is a Hewlett-Packard 2100S digital computer (see figure 2-17) operating in the software environment of the H-P Real Time

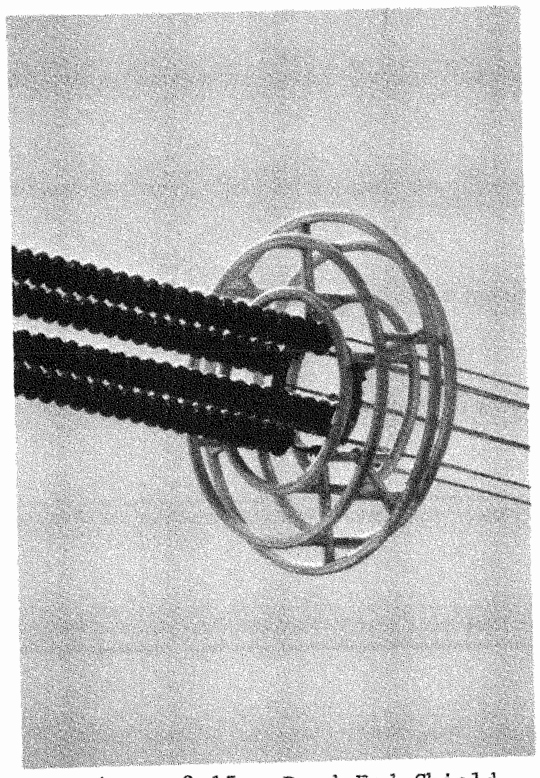


Figure 2-15. Dead-End Shield.

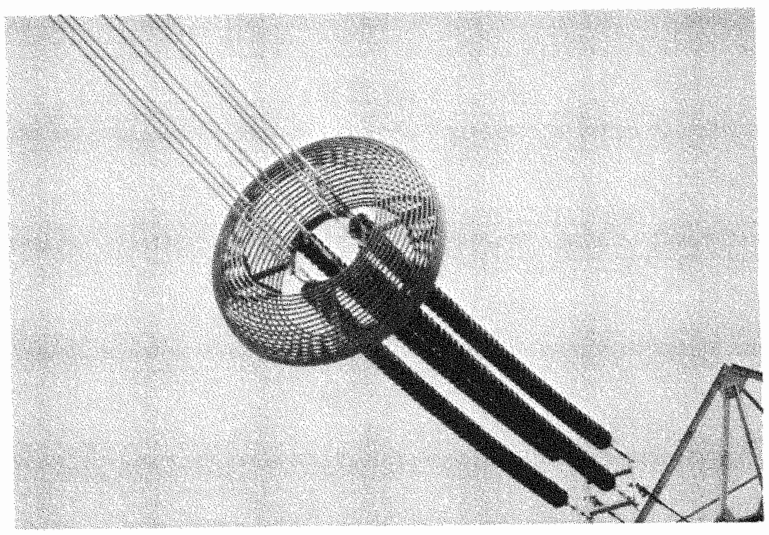


Figure 2-16. Dead-End Shield.

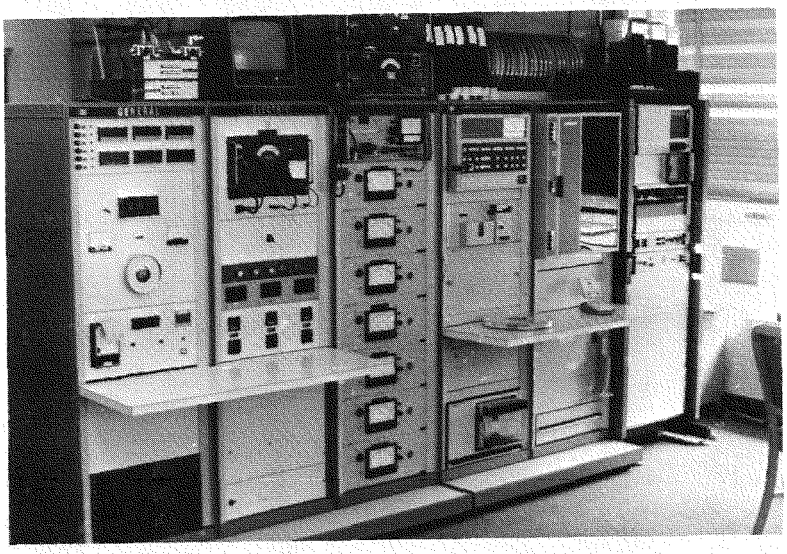


Figure 2-17. Data Acquisition System.

Executive - Basic Language System. Computer hardware includes a 16K core memory, a high speed paper tape reader and punch, a magnetic tape drive unit and a 30 character/s teletype terminal. In addition to the regular features of the Basic Language, the system incorporates special program calls for the sampling and handling of data inputs.

The computer is programmed to sample each data input channel every 20 seconds. Each minute an average of the previous 3 readings is determined for each channel. The averaged data is then converted to the desired engineering units and stored on magnetic tape for future analysis. Concurrently with storage on magnetic tape certain operator-selectable channels are printed out on the teletype terminal for a real-time record of the performance of the line.

Instrumentation Systems

Inputs to the computer are derived from separate instrumentation systems for voltage, weather conditions, audible noise, radio interference, corona loss, television interference and ozone. A typical system consists of a sensor located in the field connected with a measuring instrument located in the control room. The instrument while interfaced with the computer for data acquisition purposes, also provides a visual indication of the condition of the parameter being measured. Following is a brief description of the various instrumentation systems.

Voltage. The voltage to ground of each phase is derived from the capacitive taps on the high voltage bushings of the UHV transformers. Voltage readings are displayed on Weston meters having a special modification for analog output.

Weather Parameters. Parameters measured are air temperature, dew-point, air pressure, wind speed and direction, and rainfall. Air temperature is measured by a Foxboro Dynatherm Resistance Bulb, while the dewpoint is obtained from a Foxboro Dewcell element measurement. These sensors are located, along with the wind speed and direction transmitters manufactured by the Belfort Instrument Company, approximately 15m (50 ft) above ground at the 1/4-span point. The air pressure, measured by a Fairchild Controls pressure transducer, and rainfall, measured by a Meteorology Research Inc. tipping bucket rain gauge, are monitored close to ground level. The catch area of the rain gauge has been enlarged tenfold so that each tip of the bucket corresponds to a rainfall of 0.025mm (0.001 in).

Audible Noise. Microphones for audible noise measurements are located at mid-span in a specially prepared region referred to as the "test strip" (see figure 2-18). The microphones are of the ceramic type manufactured by the General Radio Company, as is all the equipment in this system. Pre-amplifiers are required to overcome the loss in 365m (1200 ft) of cable connecting the sensors with the real-time analyzer in the control room. The analyzer permits sequential scanning of networks A, B, C, and Flat and all octave bands from 31.5 Hz to 16 kHz for up to 16 microphones. Microphones are located under the center phase and at 15m (50 ft) intervals laterally therefrom. With the present configuration of the system complete scanning of the 7 microphones located at the test strip, including storage of the data, can be accomplished in approximately 15 seconds.

Radio Interference. Single-frequency Singer NM21FFT quasi-peak meters are used to monitor the radio interference detected by tuned rod antennas located along the test strip at the electrical center of the line. In addition to a location under the center phase, antennas are also positioned at 15, 30 and 60m (50, 100 and 200 ft), respectively, from the center of the line. Radio-frequency traps provide a high-impedance termination for radio frequency currents, a condition desired for field measurements of radio interference. The facility exists, however, to make conducted current measurements via high voltage coupling capacitors connected to the station buses. A frequency of 1.035 MHz has been chosen for all measurements, this being a frequency relatively free from "interference" from radio broadcast signals and which falls practically mid-way between resonant frequencies of the line.

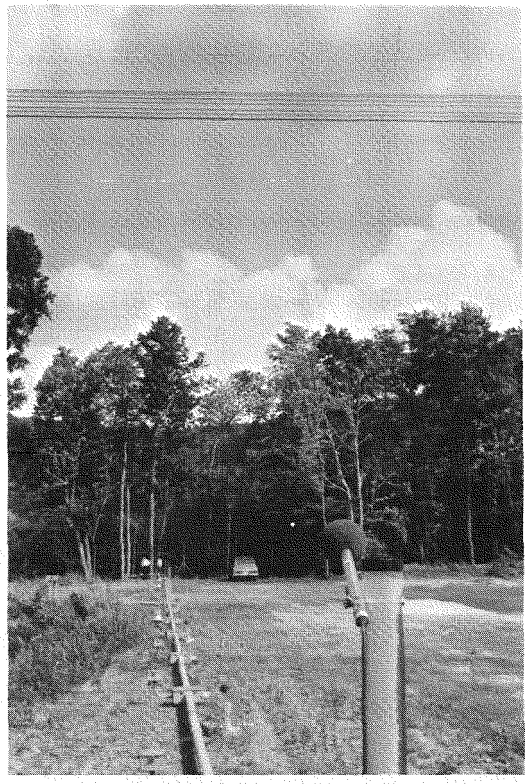


Figure 2-18. Audible Noise Test Strip.

Corona Loss. A voltage proportional to line current is transmitted via an FM telemetric link to ground to serve as the signal input to a phase-sensitive detector which is used for the measurement of corona loss. The output of the detector is proportional to the product of the signal magnitude and the cosine of the angle between the signal and a reference voltage. The reference voltage is obtained from a capacitive divider connected to the station bus. When properly calibrated the detector output is given by

$$V_d = K\ I \cos \phi$$

where I is the line current and ϕ the phase angle between line current and line-to-ground voltage. K is a proportionality constant. For a given voltage the detector output is proportional to power input to the line which is practically the corona loss. Each phase of the line has its own corona loss system.

Television Interference. Three measures of the television interference are recorded from a single Electrometrics Corp. dipole antenna. Peak and quasipeak

measurements are made by Stoddart NM30A meters, while an Electrometrics EMC25 is used for average (field intensity) measurements. A frequency of 75 MHz, falling between TV channels 4 and 5, is used for these measurements.

Ozone. One of five sensors, located on a wood pole at heights ranging from ground level to 29.3m (95 ft) above ground, can be selected for monitoring by a Meloy chemiluminescence ozone meter. The monitoring location was originally 33.5m (110 ft) from the center of the line at 1/3 span (see figure 2-19), when the phase spacing was 15m (50 ft) and the voltage was 1050 kV. When the line voltage was increased to 1300 kV and the phase spacing was changed to 20m (65 ft), the wood pole was exposed to a much stronger electric field, and electrostatically induced current caused the pole to catch fire at a point about 3m (10 ft) from ground. This occurred in misty weather after a long period of dry weather. Since then the ozone measurements have been made with sensors on a new wood pole at midspan and at a distance of 61m (200 ft) from the line center.

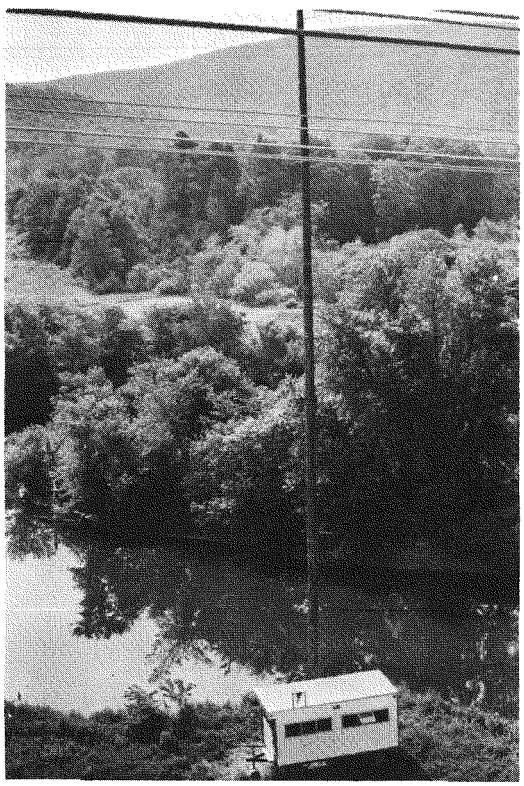


Figure 2-19. Original Ozone Trailer and Pole.

OTHER FACILITIES

Instrumentation and equipment already in place for the single phase UHV research program have been used during the work reported here for basic research and test work. They include:

- UHV Contamination building 24.4m in diameter and 24.4m height. A porcelain bushing for 866 kV to ground (the single phase equivalent of 1500 kV 3-phase) was installed in August 1976. A detailed description of this facility is contained in Section 4.
- EHV Contamination building for tests up to 350 kV to ground.
- UHV outdoor test areas for natural humidity and ice tests (see Section 4).
- EHV outdoor test yard for natural humidity and ice tests (see Section 4).
- One UHV test cage (7.6 by 7.6 by 15.2m) (see Section 3).
- Two EHV test cages (5.34 by 5.34 by 6.1m).

CONDUCTOR AND LINE CONFIGURATIONS TESTED

Different line configurations have been tested in 1975 and in 1976. They are listed in the following:

(1) January, 1975 - July, 1975

Bundle of 8 conductors 3.3 cm (1.302 inches) in diameter, with a bundle diameter of 1m (40 inches). Horizontal line configuration with 15.25m (50 ft) phase spacing.
Voltage: 1050 kV

(2) August 1975 - September 1975

Bundle of 8 conductors, 3.3cm in diameter (same as for the previous configuration). Triangular phase arrangement with 24.4m (80 ft) horizontal spacing between the two outside phases and 9.15m (30 ft) vertical offset of the center phase.
Voltage: 1050 kV

(3) October 1975 - December 1975

Bundle of 8 conductors, 3.3cm in diameter (same as for the two previous configurations). Horizontal line configurations with 19.8m (65 ft) phase spacing.
Voltage: 1050 kV

(4) February 1976 - March 1976

Bundle of 12 conductors, 3.3cm (1.302 in) in diameter. Bundle diameter 127cm (50 in). Horizontal line configuration with 19.8m (65 ft) phase spacing.
Voltage: 1300 kV

(5) April 1976 - June 1976

Bundle of 12 conductors as for the previous configuration, with the same phase spacing.
Voltage: 1200 kV (for a two week period the line was energized at

1150 kV

(6) July 1976 - September 1976

Bundle of 12 conductors, 3.3cm in diameter, bundle diameter 51cm (20 in) - Phase spacing 19.8m (65 ft).
Voltage: 1050 kV (for a two week period the line was energized at 1200 kV)

(7) October 1976 - December 1976

Bundle of 12 conductors, 3.3cm in diameter, bundle diameter 203cm (80 in). Phase spacing 19.8m (65 ft).
Voltage: 1200 kV

The test program for the period 1977 - 1979 is listed in the following:

(8) February 1977 - June 1977

Optimized line configuration with asymmetric 8 conductor bundles in the outside phases and asymmetric 9 conductor bundles in the center phase. The bundle parameters are: 3.3cm (1.302 in) conductor diameter, 100cm (40 in) bundle diameter, and asymmetry

$$E_o = 2 \text{ (see reference 2-4)}$$

Phase spacing 19.8m (65 ft)
Voltage: 1200 kV

(9) July 1977 - September 1977

Line configurations as in (8)
Voltage: 1050 kV

(10) October 1977 - December 1977

Same bundle as in (1): 8 by 3.3cm regular. Phase spacing 19.8m (65 ft)
Voltage: 1050 kV
The purpose of this test is to verify the effect of aging (about 2.5 years with voltage applied about 50 percent of the time, the remainder of the time being spent for line restringing and other tests such as contamination and cage tests).

(11) March 1978 - June 1978

Bundle of 16 conductors 3.3cm (1.302 in) diameter, with a bundle diameter equal to 142cm (56 in). Phase spacing 19.8m (65 ft).
Voltage: 1500 kV and higher (above 1500 kV tests will be single phase only)

(12) July 1978 - November 1978

Same configuration as in (11), but with the bundle asymmetric.

(13) March 1979 - June 1979

Regular bundle of large diameter expanded conductors, for instance 8 conductors 5.6cm (2.2 in) in diameter.
Voltage: 1300 - 1500 kV

(14) August 1979 - December 1979

Same configuration as in (13), but with an asymmetric bundle.
Voltage: 1500 kV and higher (above 1500 kV tests will be single phase only)

REFERENCES

(1) "EVH Transmission Line Reference Book", Edison Electric Institute, 750 3rd Ave., New York, 1968

(2) "Transmission Line Reference Book - 345 kV and Above", (Electric Power Research Institute, 3412 Hillview Ave., Palo Alto, California 04304, 1975).

(3) J.J.LaForest, D.B.Lindh, D.D.McCarthy, F.Olsen, M.W.Schultz, Jr., "Radio Noise and Corona Loss Results from Project EHV", IEEE Trans. Power Apparatus and Systems, Vol. 82, pp. 735-748, 1963.

(4) M.G.Comber, L.E.Zaffanella, "Audible Noise Reduction by Bundle Geometry Optimization", IEEE Trans. Power Apparatus and Systems, Vol. PAS 92, pp. 1782-1791, Sept./Oct. 1973.

Section 3

CORONA EFFECTS

INTRODUCTION AND SUMMARY OF CORONA RESEARCH

The choice of transmission line conductors has a major influence on the overall cost of construction and operation of the line. If the effects of corona are neglected, the optimum conductor configuration corresponds to the minimum total cost, calculated by adding the capitalized power loss (I^2R) to the material and installation costs. At ehv and uhv levels, however, corona effects cannot be neglected and their inclusion as parameters in the conductor selection process may result in an increase in conductor material beyond the optimum, and consequently an increase in total cost. At the lower ehv levels, the controlling factor is often the requirement to limit the amount of radio interference resulting from corona, while at uhv levels it appears likely that corona-produced audible noise will be the limiting criterion. In particular instances, perhaps for certain sections of a line route in which television signal reception is very weak, television interference could also be an influencing factor. Corona loss is also a consideration in the economic analysis but it rarely dictates the selection of conductors.

The extent to which the conductor configuration, number and diameter of conductors and their spacing, affects radio and TV interference, audible noise and corona loss has been studied extensively at Project UHV. Up to the end of 1973 all investigations were carried out either on a single phase overhead test span or on relatively short sections of conductors in test cages. Analytical procedures were developed in order to relate corona effects of single phase test conductors to those of three-phase transmission lines. These procedures together with conductor design data were subsequently published in the "Transmission Line Reference Book - 345 kV and Above." [3-1]

To the extent possible, the validity of the design procedures was checked by comparing calculated levels with published data from operating lines. However, such data was found to be limited in quantity and few checks were possible.

The subsequent construction of the three-phase test line presented an opportunity to demonstrate the validity of the techniques, with particular emphasis on the uhv range above 1000 kV. Consequently, a major portion of the 1974 - 76 research period was devoted to the three-phase testing of different line configurations, different bundle configurations, and different voltage levels, under a wide variety of climatic conditions. Particular emphasis was given to the analysis of the audible noise performance of the various test configurations since this aspect of corona is believed to control conductor design at uhv levels.

During this period, use of the test cage as a research tool continued. In addition to testing bundle configurations identical to those tested on the three-phase line, many special investigations were carried out. These included studies into the effects of conductor aging and tests to generate design data for asymmetric bundles.

A major objective of the research program was to substantiate the information provided in the Reference Book related to corona effects with particular emphasis on uhv levels above 1000 kV. Wherever the resulting data has justified the process, refinements to the calculation techniques have been made. A description of the corona research activities and reporting of the data collected are covered in detail in subsequent portions of this section. The key findings and conclusions of this work are reported in the following.

Audible Noise

A major portion of the program was devoted to this area of research. Much of the investigation was concentrated on the long-term performance of different three phase test line configurations. Audible noise data were collected for six configurations, one of which was tested at three voltage levels, and another at two voltage levels, yielding a total of nine test periods. The main findings were:

- A generally good agreement was found between the results of long-term measurements and calculations performed following the Reference Book [3-1]. In four of the nine test periods the L_5 audible noise level* in rain differed from the calculated "heavy rain" value by 0.5 dB or less. The maximum difference was found to be 1.8 dB (with the exceptions of two tests with reduced conductor spacing - see next paragraph). In four of the nine test periods the L_{50} audible noise level* in rain differed from the calculated "wet conductor" value by 1.2 dB or less. The maximum difference was found to be 3.1 dB (with the same exceptions as that referred to above). Results obtained during periods of fog, which occurred for some of the configurations tested, have indicated that the maximum noise levels during fog approximate the L_{50} levels during rain.

* The L_x level is that level of noise which is exceeded x% of the time. If the time period considered is qualified as "in rain" only noise occurring during periods of rain are considered.

- For bundles in which the spacing between subconductors is much less than "typical", the audible noise produced is much higher than the levels determined by Reference Book calculations. Tests on a 12-conductor bundle in which the ratio of subconductor spacing to subconductor diameter was approximately 4.0, the L_5 audible noise level exceeded the calculated "heavy rain" value by 9.6 dB, while the L_{50} level exceeded the "wet conductor" value by 13.2 dB. Typical spacing to diameter ratios for which the Reference Book calculation method is applicable range approximately from 7 to 15. Lower ratios result in a very nonuniform distribution of surface gradient on the subconductors which requires special consideration. A means of taking the gradient distribution into account is described later in this section.
- The audible noise produced by a line is dependent on the prevailing weather conditions. For most areas of the country rain represents the most important weather condition in the assessment of the noise impact of a line. The long-term noise performance of a line can be expressed in terms of its L_{50} level in rain. A period of testing which includes a minimum of 2000 minutes of rain can be used to obtain a reasonable estimate (within ± 2 dB) of this long-term performance.
- During periods of high ambient noise, or low line noise, measurements of the line noise may be affected by ambient noise intrusions. Most ambient noises, however, are predominantly low frequency (below 1 KHz) noises whereas corona noise has a significant high frequency content. A means of adjusting the overall A-weighted [dB(A)] measure, based on this difference in frequency content, can be employed to compensate for the influence of ambient noise.

The single-phase test cage facility was used throughout the three year period covered by this report. Investigations utilizing the cage included: Tests under artificial rain of conductor geometries used on the three-phase test line, simulation of an outer phase of a three-phase line, study of the effect of corona on conductor aging, evaluation of the feasibility and benefits of artificial aging of conductors, and tests on individual subconductors to generate design data for asymmetric bundles. The main conclusions of these investigations may be summarized as follows:

- Further evidence that cage tests can be utilized to provide a preliminary estimate of actual line performance was obtained through comparison of results of artificial rain tests in the cage with the performance of identical bundles on the three-phase test line.
- Gradient conditions representative of those on an outer phase of a horizontal three phase line can be reproduced by offsetting the test bundle from the cage center while the center phase is more closely represented when the bundle is centered. The small change in the gradient distribution amongst the subconductors from the bundle-centered to the bundle-offset

condition was found to contribute very little to the change in overall level of audible noise. It was found that the performance of a regular bundle is practically dependent on the "average maximum bundle gradient"; that is, the arithmetic mean of the individual subconductor maximum gradients.

- Conductors exhibiting the surface wetting characteristics of well-aged conductors can result in significant noise reductions over new conductors. The rate of natural aging is a function of the environment, and can be accelerated by the presence of corona. Artificial pre-aging of conductors appears feasible, and because of the extent of the potential benefits, especially when coupled with the concept of asymmetric bundles, could provide one of the most attractive means of solving the audible noise problem of uhv transmission lines.
- Asymmetric bundles appear to be an attractive means of reducing audible noise levels in light to medium rains without increasing conductor materials. The performance of an asymmetric bundle can be calculated from knowledge of the performances of its individual subconductors. Mechanical problems associated with asymmetric bundles appear to be manageable and do not require costly solutions.

Radio and Television Interference

Radio and television interference (RI and TVI) research was mainly centered around long-term measurements on the three-phase test line. In addition, some work was undertaken to understand the relationship between RI on a short test line to that on a long operating line. The following general conclusions can be reached:

- The RI for a long operating line can be reasonably well estimated from the geometric mean, in terms of $\mu V/m$ of the successive maxima and minima of the frequency spectrum measured on a short test line of the same design and voltage, and under the same weather conditions. (This had previously been postulated for three-phase lines, but had been shown analytically to be valid only for the single-phase case). It is not essential that the test line be terminated in open-circuit to radio-frequencies, only that the termination be reactive in nature, containing no lossy elements.
- The translation of data from short to long-line is a function of the frequency at which the data is measured. The results of long-term measurements at 1.035 MHz on the uhv test line, when translated to a long line appear to be generally some 5-6 dB higher than levels calculated according to the Reference Book [3-1]. Because of the frequency-dependency of the adjustment factor (to translate from short to long line) it is essential that accurate measurements of the short line frequency spectrum be made. The procedure for measuring this quantity is presently being reviewed as a possible source for the discrepancy between calculated and measured RI levels.
- Simultaneous measurements of RI using rod and loop antennas indicate good agreement between the two types of antennae during fair

weather. During foul weather, however, the rod antenna appears to result in RI levels higher than those measured with the loop. Possible reasons being investigated are 1) a change in the rod antenna effective ground plane when the earth becomes wet, 2) station corona noise being directly radiated and sensed by the omni-directional rod antenna. This noise is blocked from entering the line by RI wave traps and would not be detected by the loop antenna directed for optimum response to line corona.

- Results of long-term measurements of TVI agree reasonably well with calculated levels according to the Reference Book. The calculation method is based on an extrapolation of RI data to television frequencies which inherently assumes a linear relationship between RI and TVI. A comparison of RI and TVI variations during periods of rain indicate that this assumption might be valid for light rains and during drying periods after rain, but that for heavier rains there is evidence that TVI increases at a faster rate than RI; for these conditions, a 1 dB increase in RI is accompanied by an approximate 2 dB increase in TVI.
- On many occasions, the TVI levels measured in fair weather exceeded those resulting from corona on the test line during foul weather. The fair weather TVI was found to be predominantly contributed by a near-by 115 kV transmission line, serving to illustrate that uhv corona may not produce greater levels of TVI than those presently caused by lower voltage lines. TVI from sub-transmission and distribution lines can, however, be usually traced to sparking hardware or a similar problem for which remedial action could be taken.

Corona Loss and Ozone

Instrument failures and the consequent time required for repairs rendered both the corona loss and ozone measuring systems to be inoperative for significant periods of time. However, sufficient data has been collected to allow for the following conclusions:

- Corona loss is an extremely variable quantity, being especially sensitive to the weather (primarily rain) and conductor surface conditions. The average loss measured during rain on the uhv test line approximated the value computed according to the Reference Book for long lines (maximum loss in terms of W/m for lines in the Northeast United States).
- Ozone can be detected in the vicinity of uhv transmission lines only under unusual conditions of operation. Ozone concentrations which could be definitely attributed to corona on the test line were measured only during periods of higher than normal voltage, in rain and for extremely low wind speeds less than about 0.9m/s (2 mi/h). The turbulent effect of higher wind speeds disperses the ozone produced to extremely low levels. In no instance was the 80 ppb Environmental Protection Agency limit for hourly average concentration exceeded on occasions when corona related ozone was measured. Maximum increases of concentrations above ambient, averaged over a one-hour period, were of the order of 5 ppb.

AUDIBLE NOISE

Philosophy of "Long-term" Testing

The corona performance of a proposed three-phase transmission line can be assessed by "long-term" testing of a three-phase test line of similar geometry. The test line can be relatively short in length - 1 or 2 span-lengths typically - providing that end effects, if any, are properly taken into account. For the specific case of audible noise, the length of line required such that end-effects are negligible is relatively small. It is necessary only that the line length be of the order of 6-8 times the radial distance from the line to the measuring location. A single 365m (1200 ft) span is adequate for noise measurements out to 45-60m (150-200 ft) from the line center. Noise levels thus measured can be directly translated to those which would be anticipated from the full-scale line under the same operating conditions. The phase "same operating conditions" implies not only the same electrical conditions (i.e. conductor surface voltage gradients) but also identical weather conditions. Weather conditions are inherently variable, from day-to-day and from season-to-season, and it is this aspect of variability which causes one to ask for how long must one test in order to obtain an accurate assessment of long-term performance of the operating line.

What is meant by "long-term performance". Before one can determine how long a test must continue to provide adequate data for assessing long-term performance, it is necessary to define what we mean by "long-term performance." In a study of radio interference (RI) performance of transmission lines, reference [3-2] states that "at present, long-term RI levels for a period of one year are used to design proposed EHV lines." Indeed, based upon the general repeatability of weather patterns on an annual basis, it is reasonable to assume that the performance of a line in any one year would be statistically the same as in any other year. This would apply not only to RI but to all other aspects of the line performance which are dependent on the weather, including audible noise.

Thus one could describe long-term performance in statistical terms, such as a cumulative frequency distribution of noise levels over a one-year period.

Assessment of the long-term performance. A cumulative frequency distribution describes the long-term performance of a particular line for a particular climatic region. The same line in another climate could yield a very different distribution. Thus statistical analyses of data collected at a particular test site over

a period of a year can, in the strictest sense, only be used for predicting the performance of lines which will be situated in a region having the same climate as that in which the test site is located. Data would be more generally useful if they were separated into defined categories such as fair weather, rain, fog, snow, etc. Then the overall, all-weather distribution for some other region could be assessed by combining individual distributions for the various weather categories according to the probabilities (or percentage of time) of occurrence of those weather conditions. This approach assumes that, although the total period of a particular condition (say rain) may differ from region to region, the statistical performance during that condition is invariant. That is, the cumulative frequency distribution is the same, for a given weather category, irrespective of the location. For a great many situations this assumption would probably lead to reasonably accurate assessments. (Obviously a great deal of caution must be exercised when attempting to translate between extremes of climate).

It may be noted that we are now talking in terms such as "probably" and "reasonably accurate" since the assumption previously stated is rather broad and certainly not absolutely valid. At this point, one may begin to question the reasoning behind testing a particular line geometry for periods of a year or more. The reasoning generally put forward is that one whole year of testing encompasses all variations in the weather, therefore increasing the validity of the findings. It is accepted that this would be the case if the proposed line is to be built in the same area as the test line. For general purposes, however, findings based on one-year's-worth of data may be no more reliable than those based on only a few months or even a few weeks. Thus the problem essentially reduces to one of whether or not testing for periods of less than one year can be used for "reasonably accurate" assessments of performance; if it is possible, then what is the minimum length of time required for testing?

A measure of line performance. As is the case for other ac transmission line corona effects, audible noise reaches its highest levels during foul weather. During fair weather the audible noise levels will generally be difficult to distinguish from ambient levels, for a design generally considered acceptable. Thus the weather conditions of importance in the analysis of audible noise are those which can be classified as "foul"; that is, rain, fog, snow, etc. For measures of the acceptability of ehv lines the L_{dn}* level and the L_{50} level in

*The L_{dn} measure of a varying noise is the average of the squared noise pressure over a daily, weekly, monthly or annual period of time, with a nighttime penalty of 10 dB added to the noise pressures occurring between 10:00 pm and 7:00 am.

rain have been suggested [3-3, 3-4]. Of these, the latter is the more easily determined measure given a particular data base of periodic measurements of noise and the climatic conditions under which the measurements were made. For at least one case, which might be considered reasonably typical of most areas of the United States excluding the relatively dry Southwest, the L_{dn} computed on an annual basis (including both fair and foul weather) was within 1 dB of the L_{50} level in rain [3-3]. For convenience, therefore, the more simply determined L_{50} level in rain is used here as a measure of the line performance.

Through an analysis of the variation of the L_{50} level computed for varying periods of rain, it has been concluded that data collected over a total period of 2000 minutes of rain, with data samples being taken once per minute, would provide a reliable estimate ($\pm$ 2 dB) of the long-term audible noise performance of a line. Details of the analysis performed are given in Appendix A.

Interpreting Measurements During Periods of Low Line Noise or High Ambient Noise

Many times the problem facing the investigator of transmission line noise is not one of making the measurements, but one of interpreting them. In general, audible noise from transmission lines is of concern only during foul weather. If during foul weather the noise from the line increases appreciable above the general background (ambient) level then there should be no difficulty in detecting when this occurs and properly attributing the noise to the line. However, when the line noise is of the same order as, or only a few dB greater than, the ambient noise then the determination of the contribution from the line is not so straightforward.

As a hypothetical example, assume that prior to the commencement of the foul weather period a steady level of 45 dB(A) is being recorded. Suppose that it is known that during fair weather the line is inaudible so that this 45 dB(A) is without doubt attributable to ambient noises. Then during the following foul weather period, suppose that the noise level quickly attains a level of 60 dB(A), maintaining this level until the end of the foul weather period. Given these circumstances one could say that the line noise during the foul weather period was 60 dB(A). Indeed, if the ambient noise remained at 45 dB(A) during the foul weather period then this statement would be essentially correct [if ambient noise and line noise are both assumed to be random in nature (i.e. incoherent noise sources) then the actual contribution from the line would be 59.9 dB(A)].*

*Total noise = 60 dB(A) = 0.02 N/m^2
Ambient noise = 45 dB(A) = 0.00036 N/m^2
Random noises add according to the square root of pressure squared. Thus,
Line noise = $[0.02^2 - 0.00036^2]^{1/2}$ - 0.01998 N/m^2 = 59.9 dB(A)

Even if the ambient level varied during the foul weather period, say increased to 50 dB(A), the line noise contribution would still be 59.5 dB(A) if the total noise measured was 60 dB(A), and thus little error would be incurred if the actual measured noise during foul weather was attributed entirely to the line.

Now assume, however, that the measured noise increased to only 51 dB(A) during the foul weather period. If the ambient level remains at 45 dB(A), then the line contribution would be 49.7 dB(A). But if the ambient noise was 50 dB(A), the line contribution would be only 44.1 dB(A), actually less than the ambient. In either case, and in particular the latter, significant error is incurred if the 51 dB(A) noise level during foul weather is attributed to the line. It is apparent, therefore, that a certain amount of care has to be taken in interpreting the noise measurements. For conditions of low line noise (or high ambient noise) it would be desirable to "correct" the measured noise level to account for the ambient contribution.

Correction using an ambient microphone. If at all times, for a particular measuring location, both the ambient noise and the total (line plus ambient) noise were known, then the contribution from the line could be determined. It is not possible, however, due to the directional characteristics of the noise sources and the microphones to place two microphones at the same location to independently measure the desired quantities. To determine the level of ambient noise, an "ambient microphone" could be placed at a sufficiently large distance from the line, at a point where the line noise would be attenuated far (10 dB or more) below the lowest expected ambient. In most instances this would require situating the microphone several hundred feet away from the line, in which case one could not reliably say that the ambient level detected by this microphone is the same as the ambient level existing close to the line where the "line microphone" is situated. This may be because the "ambient microphone" is, for example, closer to a highway or nearer to trees (where noise may be higher due to birds or wind-rustled leaves), or registers differently to certain aircraft flyovers. Use of the "ambient microphone" noise level as a basis for moment-by-moment correction is therefore subject to substantial error. In many cases, the "ambient microphone" might measure higher levels than the "line microphone," falsely indicating that the addition of line noise actually resulted in a reduction of total noise.

Recognizing this problem, one might consider putting a range on the difference between levels far from and near to the line, and then discarding data which fall in this range from analysis, in favor of data which can more certainly be attributed to the line. However, this approach has a serious drawback; namely that a great many of the lower levels of line noise will be omitted from the analysis, thereby forcing any measure of the line noise (e.g. mean, 50% level) upwards from its true level. In an example cited earlier, total noise was (assumed) 51 dB(A) while the ambient was 50 dB(A). Under the range criteria chosen, this data may be omitted from future analysis, which for completeness and accuracy should include a corrected measurement [line noise contribution is actually 44.1 dB(A), corrected for effect of ambient]. In the extreme, if the ambient noise never dropped below 50 dB(A), then the line noise would be assessed as being greater than 50 dB(A) under all conditions.

Consequently, the use of an "ambient microphone", although yielding useful information, may not provide a satisfactory means of correcting the data to account for ambient intrusions.

Correction based on frequency content. All noise sources can be characterized by frequency content. The dB(A) measure is a single number which takes into account the complete frequency range of the noise, weighting the energies contained in different frequency bands by differing amounts. Being a single number, the dB(A) measure does not itself provide information about the frequency makeup of a particular noise. Two noises which differ greatly in their frequency content can have the same dB(A) measure. Significantly more information concerning a source of noise is provided by the frequency spectrum of the noise.

Most of the noises which are main contributors to the general background noise (vehicles, aircraft, wind, etc.) have the major part of their energies concentrated in the lower frequency region of the spectrum while corona noise has a significant high frequency component. In fact, corona noise has been shown to be fairly "flat" up into the ultrasonic frequency range [3-5] (generally used one-inch microphones will not show this to be so due to a pronounced drop-off in their frequency responses above 10 kHz). These contrasting characteristics of ambient and corona noises can be used to detect when the noise measurement is affected by ambient intrusions and also, with one assumption relating to the frequency spectrum of corona noise, to provide a means of "correcting" the measurement. The assumption made is that the shape of the spectrum of corona noise remains the same

even though the intensity of the noise may vary; that is, each component of noise increases or decreases the same amount due to, say, variation in the intensity of rain or variation in line voltage. The dB(A) measure will automatically vary in the same manner; that is, if each frequency component of the noise increased by x dB then the dB(A) level will also increase by x dB. Thus, if any frequency component of corona noise is plotted against the dB(A) measure of the corona noise a linear relationship would be obtained. However, since the actual noise measurement contains contributions from both the line corona and general background noise this relationship will not generally be found. To illustrate this fact, consider figures 3-1 to 3-3. Figure 3-1 shows typical octave band frequency spectra for ambient noise and line corona noise. In this instance, the two noises have the same dB(A) measure of 49 dB(A). Also shown in this figure is the resulting total noise spectrum if the ambient noise and line noise are present at the same time. The net A-weighted level would be 52 dB(A). Now figure 3-2 illustrates what happens if the corona noise is reduced by 5 dB while the ambient is unchanged; and figure 3-3 depicts the effect of reducing the corona noise a further 5 dB, to 39 dB(A). It is noted that the resultant total noise spectrum resembles more and more the ambient spectrum as the corona noise contribution diminished. Let us examine how each component of the total noise varied as the corona noise was reduced. Table 3-1 shows the total noise relative to its original level [when am-

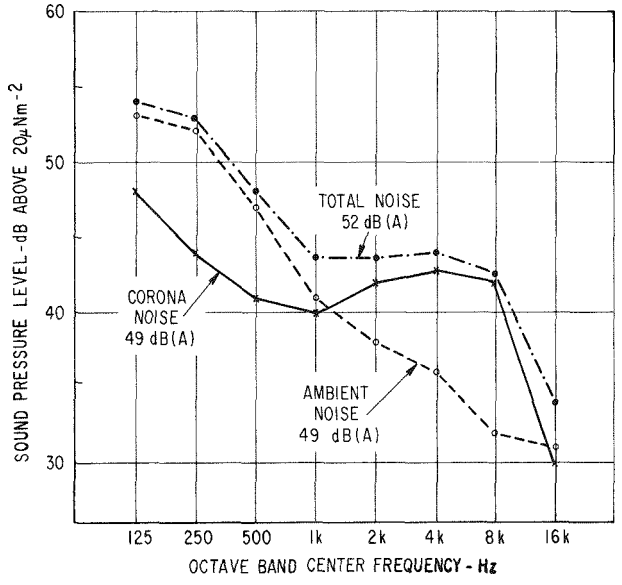


Figure 3-1. Typical Frequency Spectra of Ambient Noise, Corona Noise, and Total Noise: A Weighted Ambient Noise same as Corona Noise.

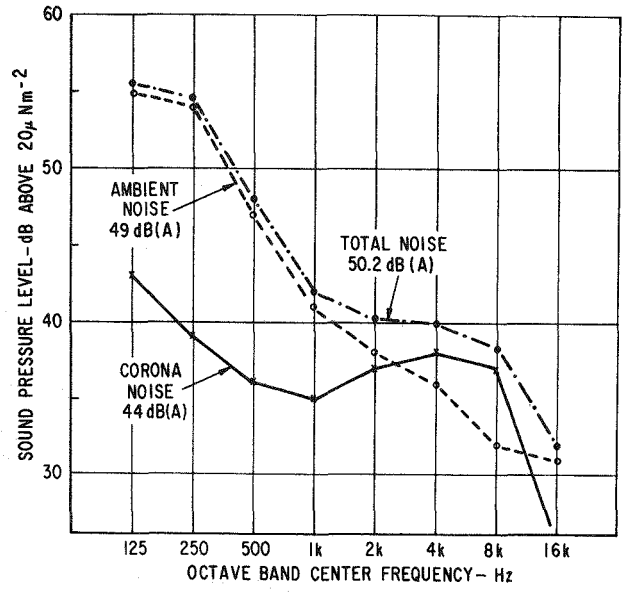


Figure 3-2. Typical Frequency Spectra of Ambient Noise, Corona Noise, and Total Noise: A Weighted Ambient Noise 5 dB Above Corona Noise.

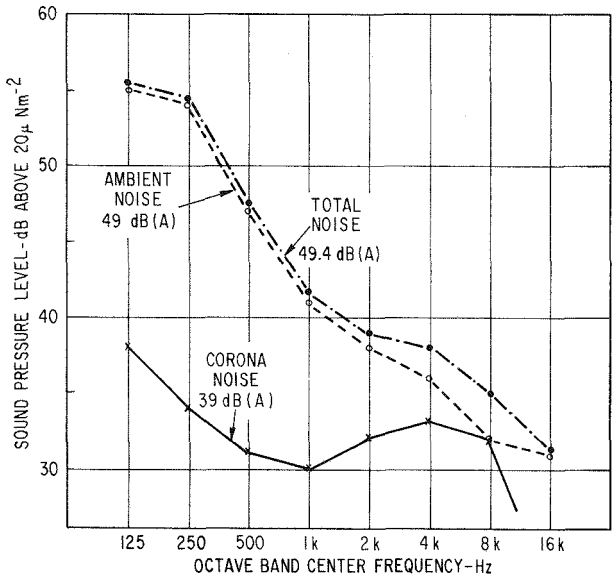


Figure 3-3. Typical Frequency Spectra of Ambient Noise, Corona Noise, and Total Noise: A Weighted Ambient Noise 10 dB Above Corona Noise.

bient and corona noises were both 49 dB(A)]. It illustrates that the dB(A) measure of total noise is not a good indicator of the behavior of the corona noise, since when the corona noise decreases by 5 and 10 dB(A), respectively, the total noise only falls off by 1.8 and 2.6 dB(A). It can be seen that the best indicator would be the 8 kHz level whose variation matches most closely that of the A-weighted level of the line noise. The last column of table 3-1 relates to a situation in which the corona noise is 10 dB(A) below the total measured noise. This would appear to be the limit to which one could consider a one-for-one relationship between A-weighted corona noise and the actual measured 8 kHz level. However, now we have a means of "correcting" the measured noise to take account of the ambient contribution, at least to a point where the corona noise is 10 dB(A) less than the ambient. This should be sufficient for the majority of cases. Situations in

TABLE 3-1

RELATIVE TOTAL NOISE FOR
VARYING LEVELS OF CORONA NOISE, AND CONSTANT AMBIENT NOISE OF 49 dB(A).

Noise Component	Relative total noise when corona noise is: 49 dB(A)	44 dB(A)	39 dB(A)
dB(A)	0	-1.8	-2.6
125 Hz	0	-0.8	-1.1
250	0	-0.4	-0.6
500	0	-0.6	-0.9
1000	0	-1.6	-2.2
2000	0	-2.9	-4.5
4000	0	-4.6	-8.4
8000	0	-4.8	-9.1
16000	0	-3.2	-5.0

which this would not be satisfactory would be those of very low line noise or very high ambient noise. In this example, when the corona noise has an A-weighted level of 49 dB, its 8 kHz component is 42 dB. According to our original assumption, this 7 dB difference is maintained even though the absolute levels may increase or decrease. Then, in order to "correct" the measured dB(A) noise (which includes both line noise and ambient noise) one simply needs to look at the 8 kHz level of the measured noise and add 7 dB to obtain the dB(A) level of the line noise alone.

An example of how this approach can be applied to a practical case is shown in Appendix B. (It is a coincidence that the "correction" factor computed in Appendix B for a particular line geometry and measuring location is 7dB, the same value as that for the example above. In general a correction factor must be determined for each line geometry and measuring location.)

Three-Phase Test Line Configurations

In total, six different line configurations were tested over the period February 1975 to December 1976. These configurations are described in Section 2. Long-term tests were conducted at selected nominal voltages for each of the configurations. One configuration was tested at three different voltage levels while another was tested at two levels, yielding a total of 9 test periods.

A key quantity in the assessment of the audible noise performance of a line based on test line results is the amount of test data recorded during periods of rain. Table 3-2 gives this information for the various configurations tested.

TABLE 3-2

AMOUNT OF RAIN DATA COLLECTED FOR EACH TEST PERIOD

No. of Conductors	Bundle Diameter (cm)	Bundle Diameter (in)	Phase Spacing (m)	Phase Spacing (ft)	Nominal Voltage (kV)	Rain Data* (min)
8	102	40	15.2	50	1050	4987
8	102	40	Triang		1050	2454
8	102	40	19.8	65	1050	4333
12	127	50	19.8	65	1300	2326
12	127	50	19.8	65	1200	2566
12	127	50	19.8	65	1150	1058
12	51	20	19.8	65	1200	711
12	51	20	19.8	65	1050	2292
12	203	80	19.8	65	1200	2208

* At nominal voltage; each minute of data represents one record of data.

Note: Subconductor diameter of 3.31cm (1.302 in) used throughout.

A view of flat and triangular configurations is given in figures 3-4 and 3-5.

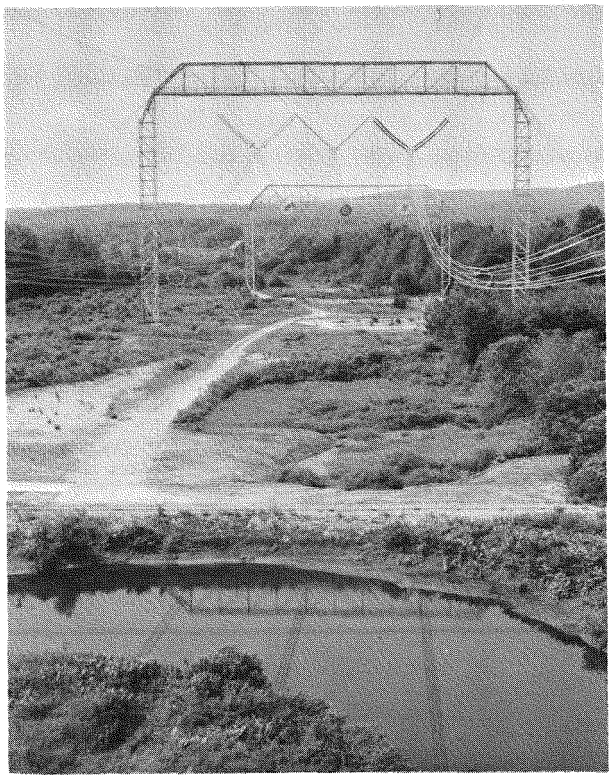


Figure 3-4. View of 3-Phase Test Line: 8-Conductor Bundle, Horizontal Configuration, 50 ft Phase Spacing.

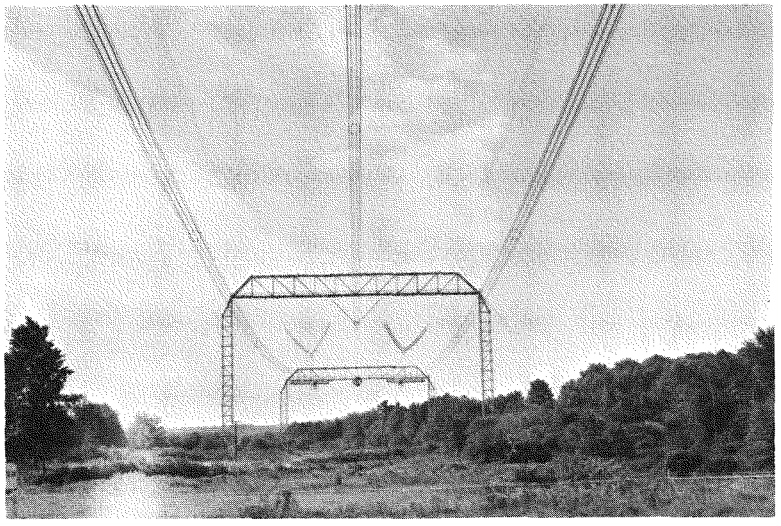


Figure 3-5. View of 3-Phase Test Line: 8-Conductor Bundle, Triangular Configuration.

Eight-Conductor Bundle Line Tests - Effect of Change in Line Geometry

The three configurations utilizing eight-conductor bundles differed only with respect to their phase arrangements. The bundle geometry and the nominal voltage for long-term data collection were maintained the same throughout.

For long term measurements, microphones were located at ground level under the center and east phases, and at 1.5m (5 ft) above ground at locations 15m, 30m and 45m (50 ft, 100 ft and 150 ft) from the outside (east) phase. In addition to the data collected during rain a considerable amount of data was also collected during conditions of fog. However, the existence or non-existence of fog cound not always be precisely determined since the station was run in an unmanned mode during nights and weekends and no instrumentation was employed for the function of fog detection. It was felt preferable, therefore, to report data for conditions of 100% relative humidity (RH), occurring for the well-defined periods when the dew-point and air temperatures are equal.

Results of Test Line Measurements. Data collected over the long-term are best presented in some statistical form; for example, in the form of cumulative frequency distributions. Figure 3-6 shows two such distributions for the first 8-conductor configuration tested. The levels shown refer to a measuring location 15m (50 ft) laterally from an outside phase. They show, for instance, that the noise produced by the line during rain is less than 60 dB(A) for approximately 40% of the time, while during 100% RH conditions the noise is less than this level for approximately 90% of the time.

The distribution of noise in rain is essentially comprised of two separate distributions which approach Gaussian (a Gaussian or Normal distribution would appear as a straight line with the probability scale used here); that is, one Gaussian distribution predominating above the 15-20% probability region, and the second distribution of greater variance below this region. The former is considered representative of the statistical distribution of the noise during rains in which the conductor is fully wetted (i.e. when rain is sufficient to cause the conductors to become saturated with water drops), while the latter is considered related more to the initial periods of rain or rains of short duration in which the conductors are in the process of becoming wetted but have not yet become saturated.

In conditions of 100% RH, the line performance, as measured by the noise distribution curves, is quite different to that in rain. The 100% RH distribution also

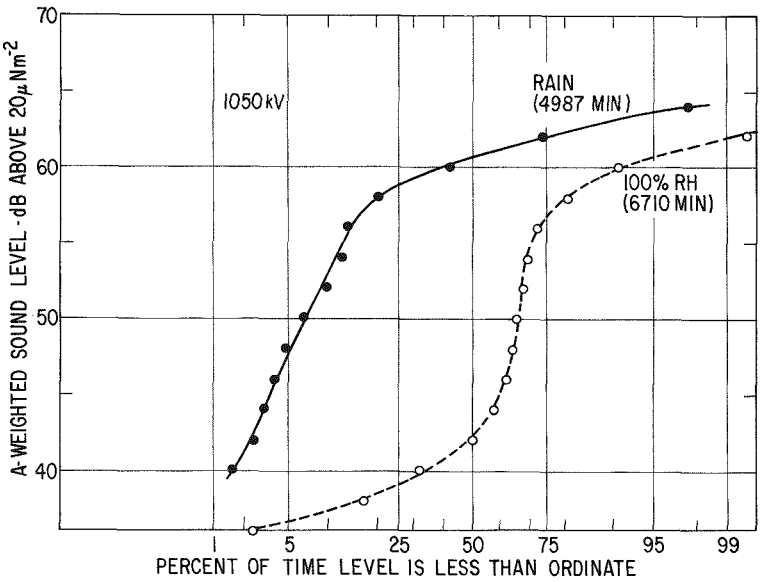


Figure 3-6. Statistical Distribution of Audible Noise During Rain and 100% RH: 8-Conductor Bundle, 50 ft Phase Spacing, Measuring Location 50 ft From Outside Phase.

appears to be the combination of two more-or-less Gaussian distributions, but both of fairly low variance. One predominates in the low noise range, up to the 50-60% region, while the second is a major influence above this region. The lower portion of the curve is representative of the performance of dry conductors; that is, the high humidity has not yet caused water drops to form on the conductor surfaces. The upper section of the curve represents wetted conductors, wetted either by an extended period of high humidity or by rain which is then followed by 100% RH conditions.

In a discussion in an earlier section of "correcting" noise measurements to account for ambient noise intrusions, it was assumed that each frequency component of the line noise varied in the same manner, and therefore the dB(A) measure varied similarly. This assumption is somewhat verified by figure 3-7 which shows the distributions of 1 kHz to 16 kHz octave band levels of the noise measured during rain. The shapes of these distributions are essentially similar to one another, particularly over the upper low-variance portions, although their absolute levels differ. However, for lower frequencies the degree of similarity between the distributions diminishes, as can be seen in figure 3-8. This is primarily attributed to the influence of ambient noises such as road and air traffic and wind,

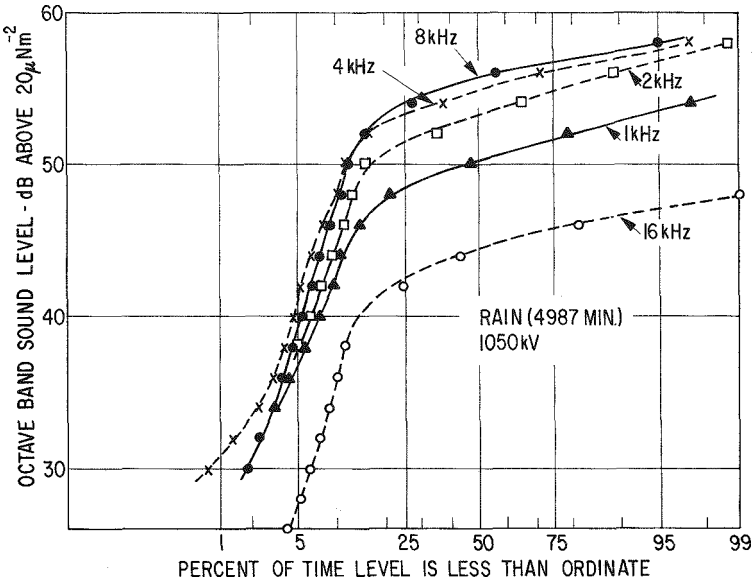


Figure 3-7. Statistical Distribution of Octave Band Noise Levels: 8-Conductor Bundle, 50 ft Phase Spacing.

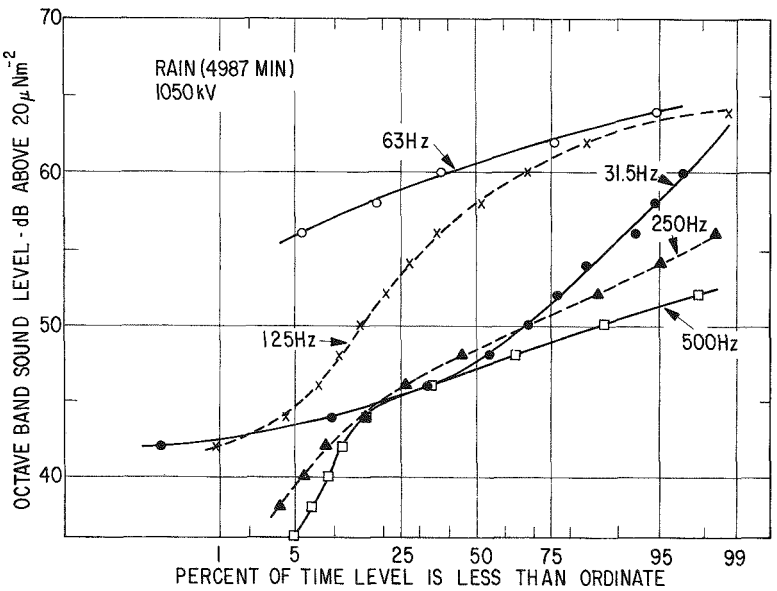


Figure 3-8. Statistical Distribution of Octave Band Noise Levels: 8-Conductor Bundle, 50 ft Phase Spacing.

which have most of their energies concentrated in the low frequency region where the line noise has a relatively small energy content. The 125 Hz distribution is perhaps an exception to this reasoning since corona on the line can result in a significant 120 Hz pure tone, which could be the predominant contribution to the 125 Hz octave band measurement. The 125 Hz distribution differs from those of the higher frequencies (above 1 kHz) in that it has no distinct "knee". This could be attributable to the fact that the 120 Hz pure tone component of the noise is a result of the motion of space charge under the influence of the alternating electric field in the vicinity of the conductors, which is quite different to the random corona-discharge pulse mechanism responsible for the broad-band noise measured in the higher frequency range. The exceptionally high 63 Hz level is attributable to a 60 Hz electrical "pickup" which was not corrected at this stage of the program (this high level, however, does not influence the dB(A) measure since the 63 Hz band level is attenuated 26 dB by the A-weighting network of the sound level metering equipment).

From figures 3-7 and 3-8 it is possible to construct octave band frequency spectra. For example, by taking the L_{50} (50%) levels of each octave band one could construct an L_{50} frequency spectrum such as shown in figure 3-9, which also shows spectra for the L_5, L_{25}, L_{75} and L_{95} levels in rain. Corresponding dB(A) levels are shown to the left of the spectra.

Figures 3-6 and 3-7 to 3-9 all relate to a measuring location 15m (50 ft) laterally from the outside phase. Data were also obtained from other locations ranging from directly under the center phase to 60m (200 ft) from the center phase. From statistical distributions of noise at these locations, lateral profiles can be constructed. Figure 3-10 shows lateral profiles of the L_5 and L_{50} dB(A) measures for conditions of rain. These profiles indicate the rather low attenuation with distance associated with this type of noise source.

In addition to the long-term gathering of data providing statistical information on the variation of the noise, a number of relatively short duration voltage runs were conducted in both rain and fair weather conditions. Typical results are shown in figure 3-11 which illustrates why ac transmission line audible noise is considered only a foul weather problem. In this instance, for voltages at which the noise level in rain is in the range 55-60 dB(A), which could be considered unacceptably high, the fair weather noise is essentially ambient. In fair weather, line corona noise is hardly evident below 1200 kV at which voltage the

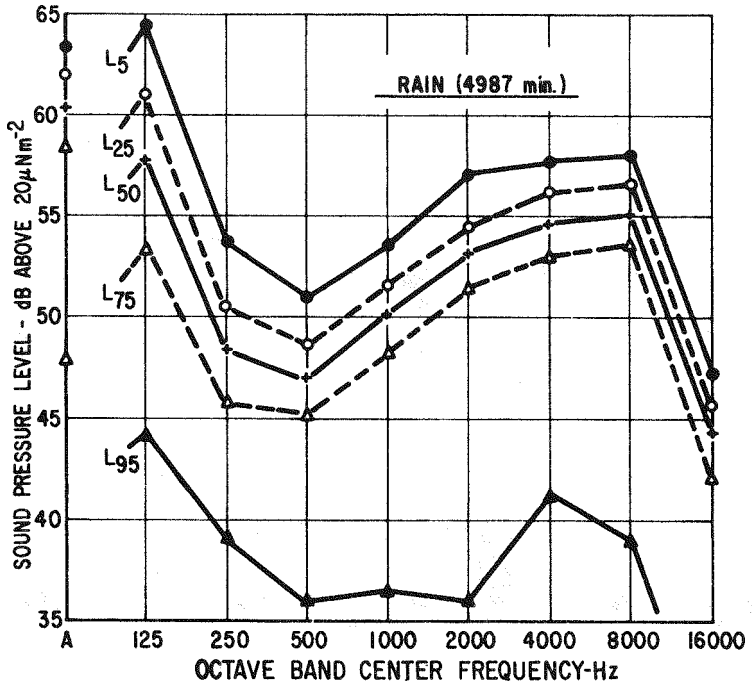


Figure 3-9. Octave Band Frequency Spectra: 8-Conductor Bundle, 50 ft Phase Spacing.

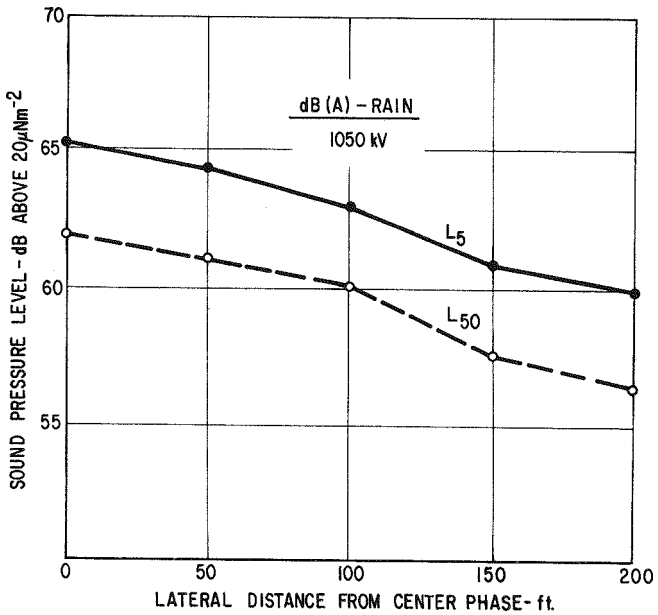


Figure 3-10. Lateral Profile of A-Weighted Audible Noise: 8-Conductor Bundle, 50 ft Phase Spacing.

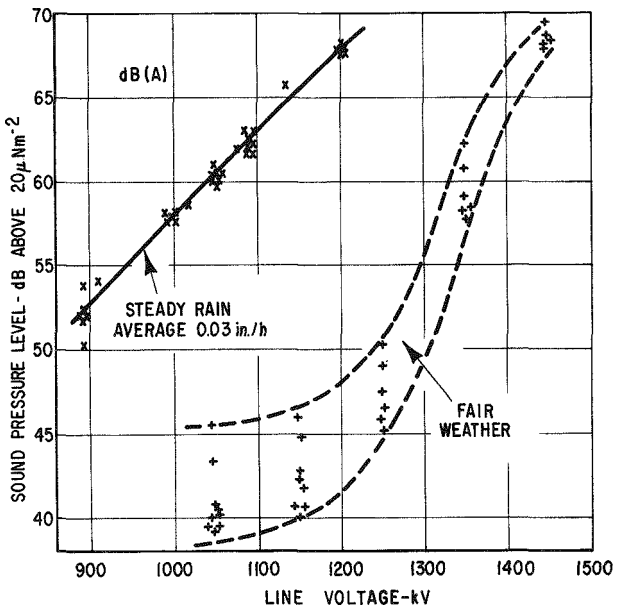


Figure 3-11. Variation of Noise Level With Voltage: 8-Conductor Bundle, 50 ft Phase Spacing.

noise in rain attains an extremely high level in the region of 68 dB(A).

All results presented above pertain to the first configuration tested. Similar data collections and analyses were conducted for subsequent configurations. Figures 3-12 and 3-13 show statistical distributions of the dB(A) measure for the second and third 8-conductor bundle line configurations; namely, the triangular and the horizontal [19.8m (65 ft) phase spacing] arrangements. In each instance, the measuring location is 15m (50 ft) from the outside phase, corresponding to 27.5m (90 ft) from the center phase for figure 3-12 and 35m (115 ft) from the center phase for figure 3-13. The total period of 100% RH conditions encountered during the testing of the horizontal configuration was not sufficient to yield meaningful statistics. The distributions of figures 3-12 have characteristics generally similar to those obtained for the first configuration (figure 3-6). The lower portion of the rain curve (up to the 7-8% probability level) which now appears is attributed to the generally higher ambient "floor" than was encountered during the previous tests. It would appear that the ambient levels during 100% RH conditions were significantly lower than those during rain. This may be explained by the fact that 100% RH was obtained almost exclusively during the late-night and early-morning hours when ambient levels are generally much lower than during daytime hours, while more than 75% of the rain data were recorded during the daytime between 6:00 am and 8:00 pm.

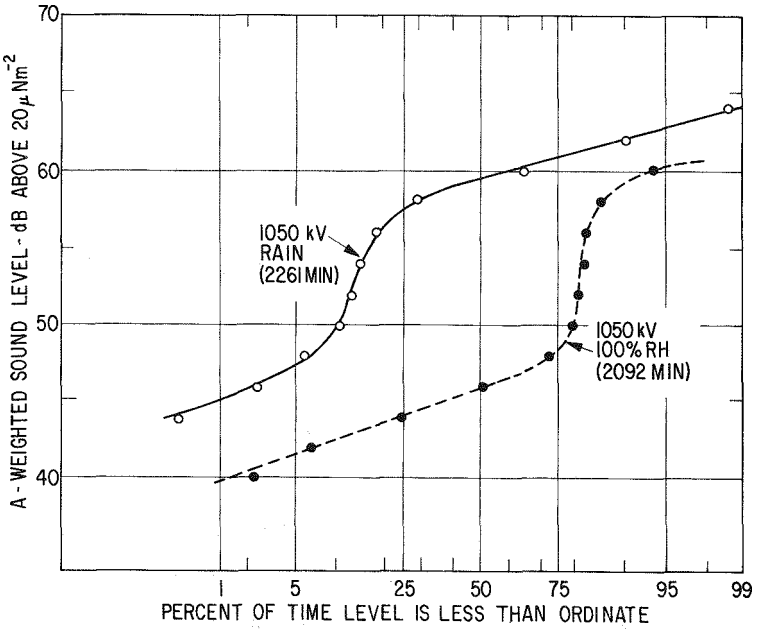


Figure 3-12. Statistical Distribution of Audible Noise During Rain and 100% RH: 8-Conductor Bundle, Triangular Configuration, Measuring Location 50 ft From Outside Phase.

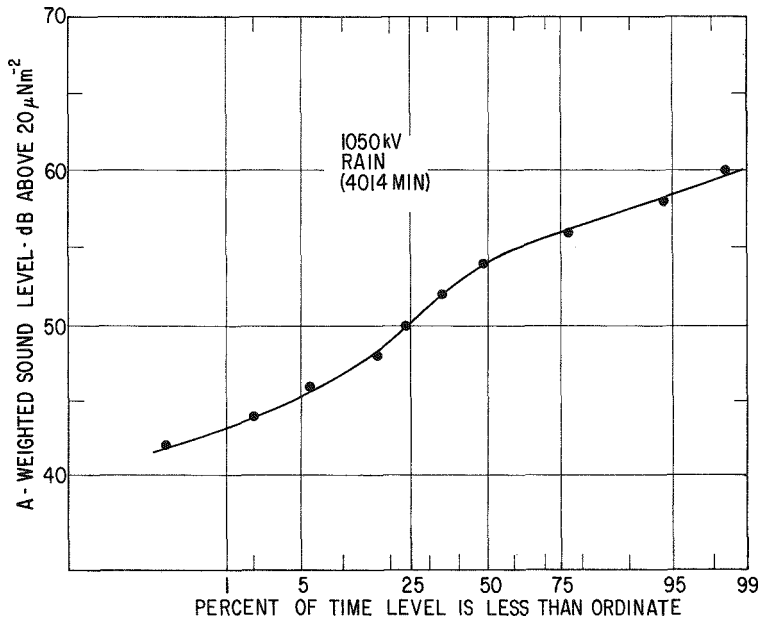


Figure 3-13. Statistical Distribution of Audible Noise During Rain: 8-Conductor Bundle, 65 ft Phase Spacing; Measuring Location 50 ft From Outside Phase.

The horizontal configuration resulted in significantly lower noise levels during rain, as evidenced by figure 3-13, this being due to the reduced conductor surface gradients resulting from the increased phase spacing. Consequently, since the ambient "floor" is relatively unchanged, the overall distribution is much flatter than for the previous configurations. To illustrate that the lower portions of the dB(A) distribution curves are significantly affected by the ambient noise, one can compare side-by-side the dB(A) and 8 kHz distributions, as in figures 3-14 and 3-15. In fact, if one were to use the A-weighted ordinate scale with the 8 kHz distribution curve the resulting product would be the dB(A) distribution "corrected" for ambient, according to the procedure described earlier.

Comparison with Calculations. Methods for predetermining the corona performance of any line configuration are described in Reference 3-1. Noise levels under two conditions can be calculated; 1) heavy rain, which is considered to be equivalent to the L_5 level during rain, and 2) wet conductor, which is considered to be equivalent to the L_{50} level during rain or the L_5 level during 100% RH conditions. This relation of heavy rain and wet conductor values to long-term statistical levels is based on previous comparisons of published audible noise data on 500-800 kV lines [3-8,3-9] with levels calculated according to Reference 3-1. Results reported here provide a test of the validity of this relationship for voltages in the uhv range. However, since the two levels - heavy rain and wet conductor - would correspond to only two points on a distribution curve, the predetermination method does not provide a means of determining the complete distribution of the noise. However, as has been noted earlier, the portion of the distribution curve which can be associated with fully wetted conductors (generally above the 20-30% probability level) approaches a Gaussian or Normal distribution. Thus with two points, such as L_5 and L_{50}, one can construct this portion of the distribution curve to permit a prediction of other probability levels such as L_{10}, L_{20}, etc.

Table 3-3 compares measured A-weighted levels with those calculated according to the methods described in Reference 3-1. As indicated by figures 3-14 and 3-15 (and also by figures 3-6 and 3-7) little or no correction for ambient is required at the L_5 and L_{50} levels in rain. The levels reported in Table 3-3 are as measured.

For the first configuration, measured valued were found to be higher than calculated. At the time this was first noted, it was theorized that this could be attributable to the fact that the conductors were still relatively new, whereas

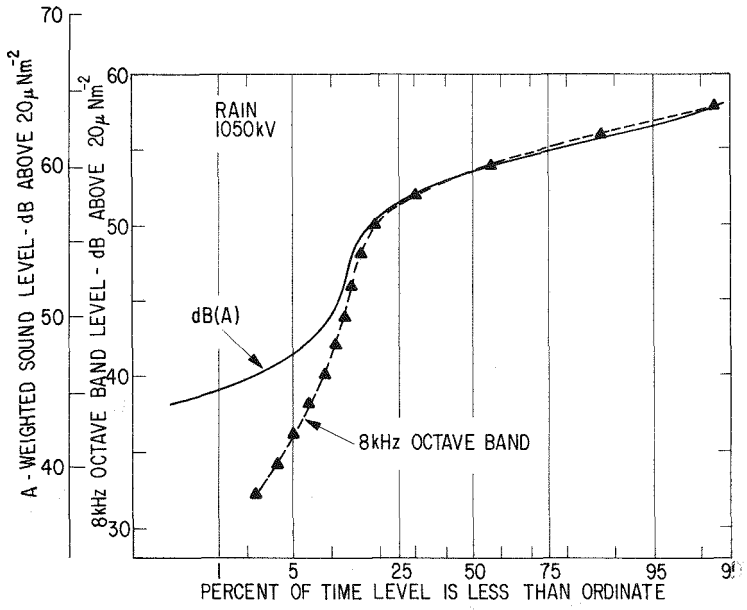


Figure 3-14. Comparison of Statistical Distribution of A-Weighted and 8-kHz Octave Band Levels: 8-Conductor Bundle, Triangular Configuration.

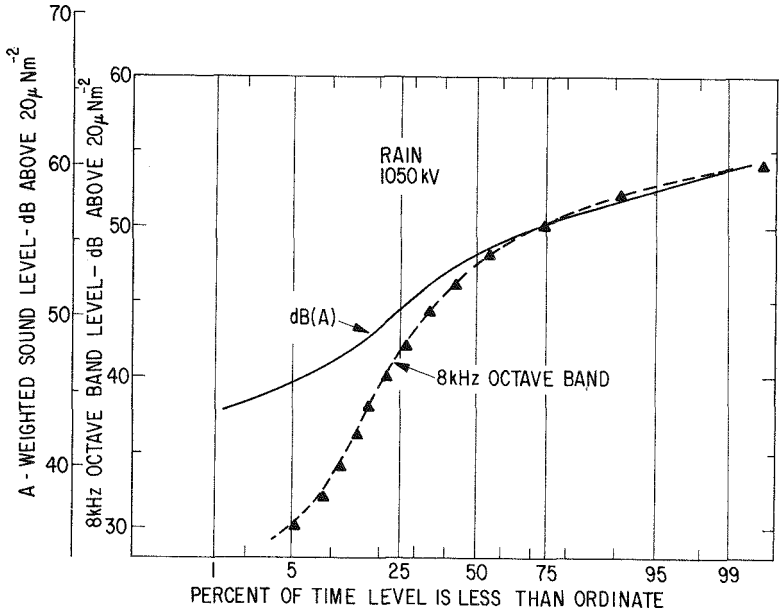


Figure 3-15. Comparison of Statistical Distribution of A-Weighted and 8 kHz Octave Band Levels: 8-Conductor Bundle, 65 ft Phase Spacing.

the calculations relate to partially aged conductors. It was anticipated that as the conductors began to age, better agreement between measured and calculated values would be obtained. The results of tests on the second and third configurations tended to confirm this theory.

Also of note in Table 3-3 is the good correspondence between L_{50} rain and L_5 100% RH levels.

TABLE 3-3

COMPARISON OF MEASURED AND CALCULATED
NOISE LEVELS MEASURED AT 15m (50 FT) LATERALLY FROM OUTSIDE PHASE

	Configuration *		
	1	2	3
For measured levels refer to:	Figure 3-6	Figure 3-12	Figure 3-13
Calculated "heavy rain"	61.5	62.3	58.2 dB(A)
Measured L_5 (rain)	63.3	62.8	58.4 dB(A)
Calculated "wet conductor"	57.5	58.3	52.1 dB(A)
Measured L_{50} (rain)	60.4	59.5	54.0 dB(A)
Measured L_5 (100% RH)	60.7	60.2	- dB(A)

1 - Horizontal, 15m (50 ft) phase spacing
2 - Triangular
3 - Horizontal, 19.8m (65 ft) phase spacing
} All 1050 kV

Figure 3-16 compares calculated and measured lateral profiles for the first configuration. The rate of attenuations are very similar although, as noted above, the absolute levels of the measured values are somewhat higher (1-3 dB) than the calculated levels. Comparisons of measured and calculated levels for voltages other than the nominal 1050 kV are presented in figures 3-17 to 3-19. Overall agreement was found to be very good.

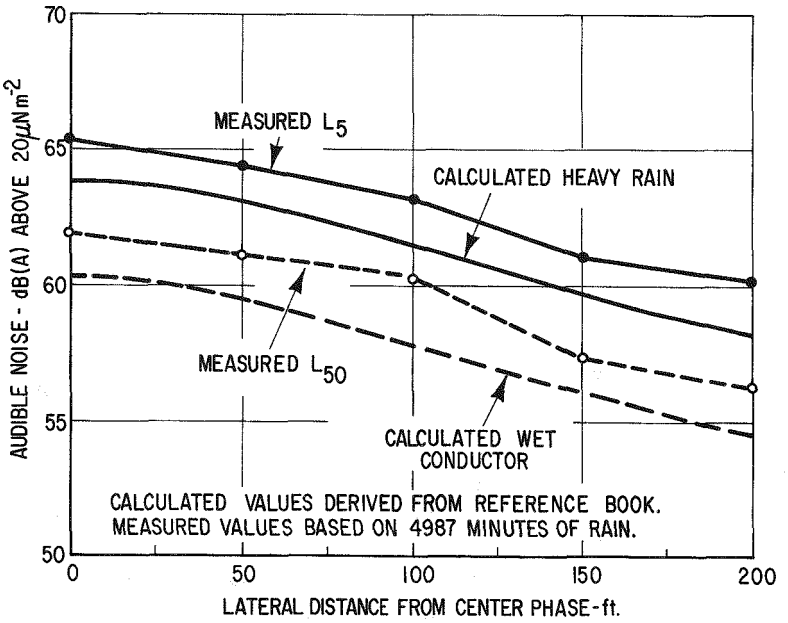


Figure 3-16. Comparison of Measured and Calculated Lateral Profiles: 8-Conductor Bundle, 50 Feet Phase Spacing.

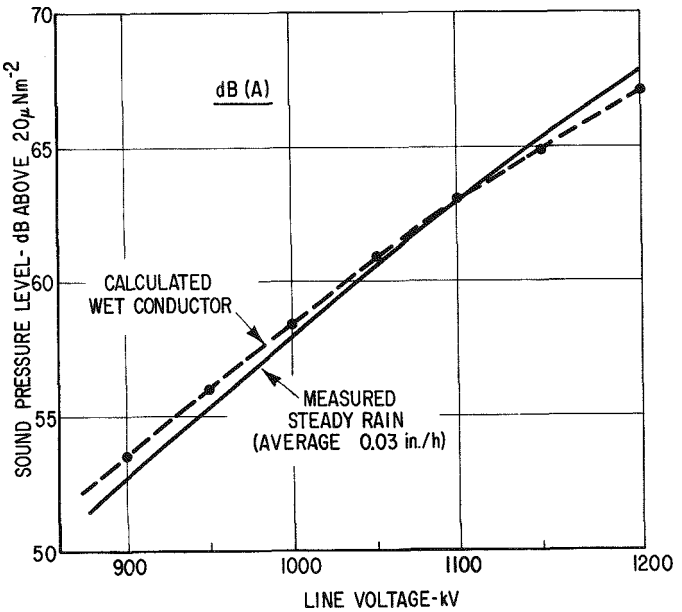


Figure 3-17. Comparison of Measured and Calculated Noise Levels for Different Voltages: 8-Conductor Bundle, 50 Feet Phase Spacing.

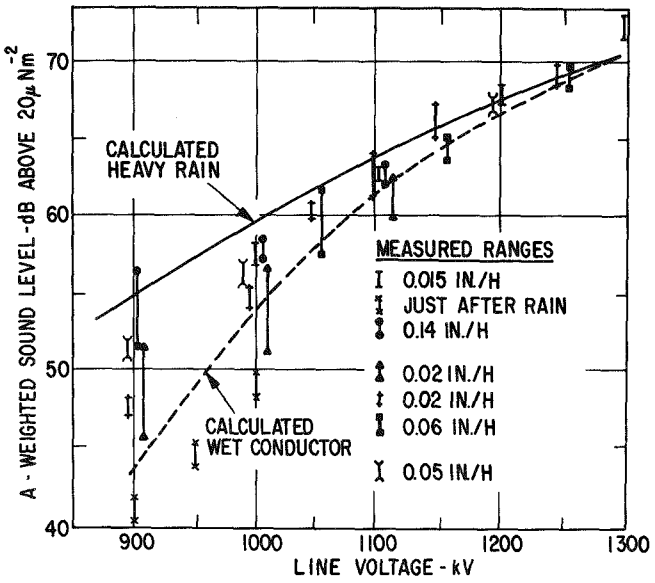


Figure 3-18. Comparison of Measured and Calculated Noise Levels for Different Voltages: 8-Conductor Bundle Triangular Configuration.

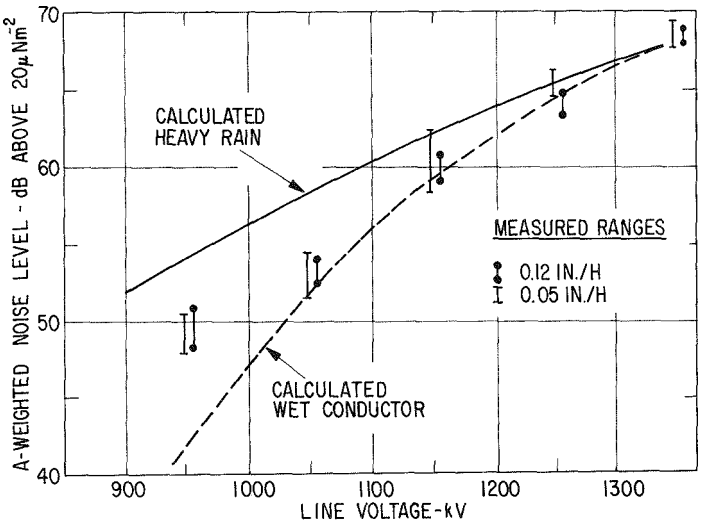


Figure 3-19. Comparison of Measured and Calculated Noise Levels for Different Voltages: 8-Conductor Bundle, 65 Feet Phase Spacing.

Twelve-Conductor Bundle Line Tests - Effect of Changes in Voltage Level

Testing of the 12-conductor bundle configuration began in February, 1976. Initially, a nominal voltage of 1300 kV was chosen for the 127cm (50 in) diameter bundle. After having gathered a sufficient quantity of data at this voltage level, the nominal test voltage was lowered in order to obtain audible noise statistics at relatively low conductor gradients. According to Project UHV calculations, the difference between "heavy rain" and "wet conductor" (i.e. L_5 and L_{50}) noise levels in rain increases as the conductor gradients decrease. This has particular significance if conductor design is to be based on L_{50} levels. Presently differing opinions exist among researchers as to the dependence of the L_{50} level on the design parameters of the line.

Initially a voltage of 1150 kV was selected, but the low levels of line noise coupled with an abnormally high ambient level apparently prevented good data from being obtained, and consequently after approximately 1000 minutes of data collection during rain, the line voltage was raised to 1200 kV. It should be noted that the means for "correcting" measured noise levels to account for ambient had not been developed at this time. It was subsequently determined that the data gathered at 1150 kV could be analyzed through adoption of the correction technique.

Figure 3-20 shows the results of correcting the dB(A) distributions as previously described. (In all cases this was equivalent to adjusting the 8 kHz octave band level upwards by 7 dB. The same adjustment factor applied to all cases since the line configuration, measuring location and microphone all remained unchanged). The L_5 and L_{50} levels from figure 3-20 are plotted versus voltage level and compared to calculated values in figure 3-21. Results are also summarized in Table 3-4.

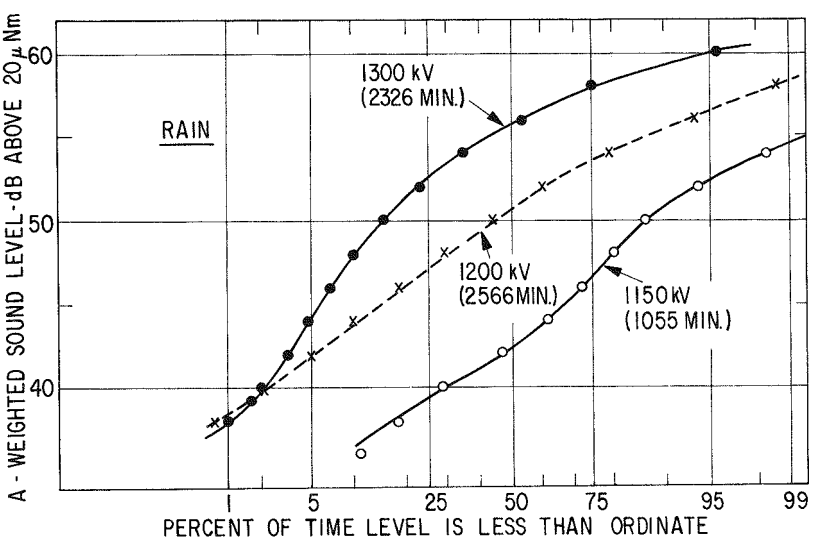


Figure 3-20. Statistical Distribution of Audible Noise During Rain at Different Voltages: 12-Conductor Bundle, 50 in Diameter; Measuring Location 50 Feet From Outside Phase.

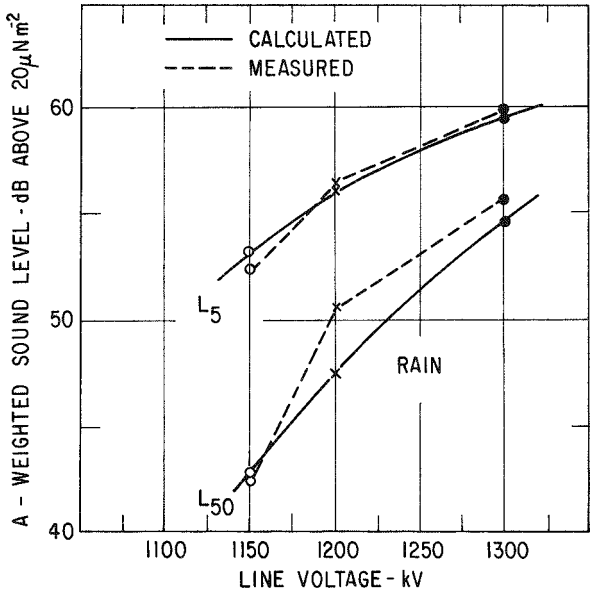


Figure 3-21. Comparison of Calculated and Measured Noise Levels: 12-Conductor Bundle, 50 in Diameter.

TABLE 3-4

COMPARISON OF MEASURED AND CALCULATED
AUDIBLE NOISE LEVELS FOR 12 x 1.302 x 50-in BUNDLE CONFIGURATION

	LINE VOLTAGE		
	1300 kV	1200 kV	1150 kV
Data records included in analysis	2326	2566	1055 dB(A)
Measured L_5 (rain)	59.9	56.0	52.2 dB(A)
Calculated "heavy rain"	59.6	55.6	53.3 dB(A)
Measured L_{50} (rain)	55.8	50.5	42.4 dB(A)
Calculated "wet conductor"	54.7	47.4	42.8 dB(A)
Difference between measured L_5 and L_{50} (rain)	4.1	5.5	9.8 dB(A)
Difference between calculated "heavy rain" and "wet conductor"	4.9	8.2	10.5 dB(A)

* Corrected for ambient
(For measured values refer to figure 3-20)

Agreement with calculations is generally very good. The greatest difference between measured and calculated values occurs at the L_{50} level for 1200 kV. The significant outcome of these data is the indication that the difference between the L_5 and the L_{50} level in rain is dependent on the operating conductor surface gradient, the difference increasing as the surface gradient decreases. All previously available data relating to the audible noise performance of operating lines [3-8, 3-9] have indicated that the difference between L_5 and L_{50} levels would be no greater than about 4 dB(A). The data presented here clearly indicates that, in fact, this is not the case at the lower operating gradients which might be required in order for future transmission lines to meet specific noise limitations. This is of particular importance since every dB of overestimation of the noise that will be produced by a line could translate into a substantial economic penalty paid by the utility.

Twelve-Conductor Bundle Line Tests - Effect of Changes in Bundle Geometry

The effect of very small and very large bundle diameters was examined using the 12-conductor bundles previously tested at a 127cm (50 in) bundle diameter. Bundles with small overall diameter promise a significant advantage with respect to reduction of ice loading and to reduction of the magnitude of the electric field at ground level. Large diameter bundles might be used to advantage to limit

wind induced oscillation, in improvement of conductor to ground flashover performance and in shielding of insulators and associated hardware without the need for other corona shields. However, such advantages should be weighed against any increase in corona activity. Previous studies have indicated that a 127cm (50 in) diameter is close to optimum, with reference to corona performance, for a 12-conductor bundle. Any reduction or increase of the diameter should result in higher noise levels. In order to investigate the effect of the bundle diameter, the 12-conductor bundle was tested at diameters of 51cm (20 in) and 203cm (80 in). Subconductor spacing to diameter ratios ranged from 4:1 for the 51cm (20 in) bundle to 16:1 for the 203cm (80 in) bundle. Both bundle configurations were tested at 1200 kV, permitting a comparison with results obtained with the 127cm (50 in) bundle at the same voltage level. In addition, the 51cm (20 in) bundle was tested at 1050 kV.

51cm (20 in) Bundle. It was discovered very early in the testing of this bundle that the audible noise levels were much higher than had been anticipated. Calculations had indicated that levels should be 4-7 dB greater than those produced by the 127cm (50 in) bundle for the same 1200 kV test voltage while in practice the increase was found to be in the order of 13-20 dB. Testing at this voltage level was terminated after about 700 minutes worth of rain data had been collected. It was evident that the noise performance was little affected by variations in rain intensity once the conductors had become fully wetted. The statistical distribution of the dB(A) measure is shown in figure 3-22. The general shape of this curve resembles very much the rain noise distribution of the first 8-conductor bundle tested (figure 3-6), having a distinct "knee" around the 15% probability level. This appears to be the characteristic shape of corona noise distributions for high levels of noise which are not particularly sensitive to variations in rain intensity (i.e. difference between L_5 and L_{50} is small.) For configurations resulting in lower noise generation having greater sensitivity to weather variations, the distributions appear somewhat more smooth (e.g. figures 3-15 and 3-20).

For the 51cm (20 in) bundle, L_5 and L_{50} levels of 68.6 dB(A) and 67.4 dB(A), respectively, were obtained with the noise level being greater than 66 dB(A) for over 85% of the time during rain [for a measuring location 15m (50 ft) from an outside phase]. Calculated L_5 and L_{50} levels were 59.2 dB(A) and 53.9 dB(A) respectively. The reason for the large discrepancy between calculated and measured levels is not immediately apparent. The maximum voltage gradients of 14.2 kV/cm for the center phase and 13.3 kV/cm for the outer phases were only 7-8% higher than those

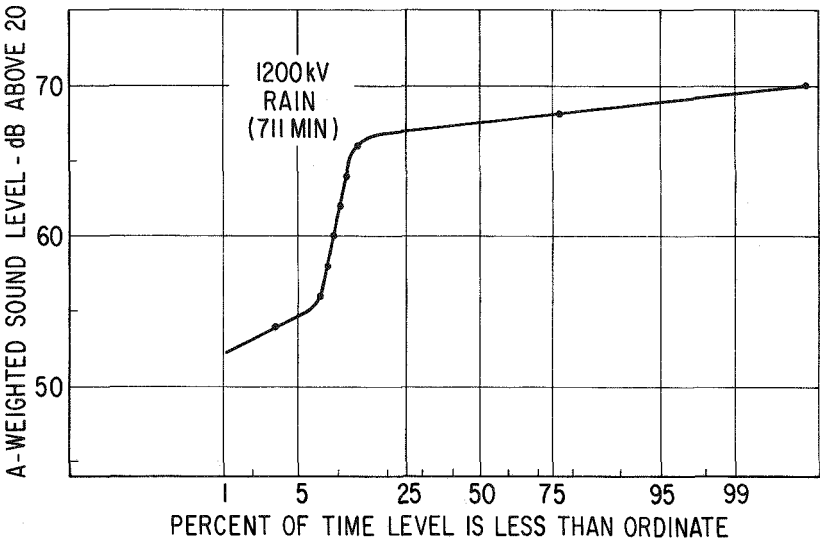


Figure 3-22. Statistical Distribution of Audible Noise During Rain: 12-Conductor Bundle, 20 in Diameter.

for the 127cm (50 in) bundle previously tested. This alone accounts for the 4-7 dB increase in noise expected from calculations. It is evident that another factor contributes to the noise generation, but which must generally be only of secondary importance since in all other instances measured noise levels have been in relatively close correspondence with calculated levels. Earlier analytical work [3-7] had indicated that noise generation is a function of subconductor diameter [same for 127cm (50 in) and 51cm (20 in) bundles], maximum subconductor gradient (accounting for 4-7 dB increase only), location of corona sources (i.e. water drops, assumed to be the same for both bundles) and, lastly, the distribution of gradient around the surface of the subconductors. It is this last factor which is considered to be responsible for the large increase in noise beyond that attributable to the increase in maximum gradient.

The distribution of gradient around a subconductor can be expressed approximately by

$$E_\theta = \frac{E_{max}}{k} (1 + [k-1] \cos \theta) \qquad (3\text{-}1)$$

where θ is the angular position around the subconductor, E_{max} is the maximum surface gradient on the subconductor, and k is the ratio of maximum to average subconductor gradient. For regular bundles the ratio k can be expressed in terms

of the bundle geometry

$$k \simeq (n-1)\, d/D \qquad (3\text{-}2)$$

where n is the number and d the diameter of the subconductors, and D is the bundle diameter. For the 127cm (50 in) bundle, with n = 12 and d = 3.31cm (1.302 in), we have k = 1.29, while for the 51cm (20 in) bundle we have k = 1.72. The former value is comparable to that for the 8-conductor bundle previously tested (k = 1.23) and represents an upper limit for all bundles tested during the single-phase era of Project UHV to generate the design data incorporated into the Transmission Line Reference Book. For reference, Table 3-5 lists k values corresponding to typical operating lines. The bundle to be used on the Bonneville Power Administration 1100/1200 kV prototype line, 8 x 4.07 x 107cm (8 x 1.602 x 42 in), has k = 1.27. The value k = 1.72 for the 51cm (20 in) bundle therefore represents an unusually high degree of non-uniformity of conductor surface gradient, with the maximum gradient (172% of the average gradient) being approximately 6 times that of the minimum gradient (equal to 28% of the average). For k = 1.29, the ratio

TABLE 3-5

TYPICAL BUNDLE GEOMETRIES AND K VALUES FOR OPERATING LINES

Line Voltage (kV)	Bundle Geometry n	d cm (in)	D cm (in)	k
500	2	4.07 (1.602)	45.7 (18)	1.09
500	3	3.31 (1.302)	53.3 (21)	1.12
765	4	3.51 (1.38)	64.8 (25.5)	1.16

of maximum to minimum gradient is only 1.8. It can be shown analytically that the rate of attenuation of gradient away from the surface of a conductor decreases as the degree of non-uniformity of the surface gradient increases. Thus, for the same subconductor diameter and maximum gradient, we could expect longer corona streamers from a bundle with high k than from a bundle with low k. Therefore, providing other factors, such as the number of subconductors and the location of sources, remain the same then the noise generated will increase with increasing k. For values of k in the more typical range of 1.1-1.3 this effect is small, however, and little error is introduced if the "k-effect" is neglected.

During the contract period covered by this report, a series of special cage tests were carried out to determine the influence of the "k-effect" on noise generation

(these are described later in this Section). However, values of k only up to 1.35 were obtained. Based on those tests and the 3-phase line findings a rough correction factor to account for the "k-effect" can be developed. However, in order to develop a more accurate means of predicting the performance of bundles with high k, further experimental work is necessary.

Since it was found that the 51cm (20 in) bundle generated levels of noise which could not be considered acceptable, it was decided to reduce the nominal test voltage to 1050 kV. The maximum gradients at this voltage were 12.4 kV/cm and 11.6 kV/cm for center and outer phases respectively. The reduced gradients resulted in a larger difference between L_5 and L_{50} levels during rain. Over a test period of 2292 min, L_5 and L_{50} levels of 63 dB(A) and 58 dB(A) were obtained. However, for the same reason put forward for the 1200 kV energization, the measured levels far exceeded, by 11-20 dB, the levels expected from calculations. At 1050 kV, the 51cm (20 in) bundle configuration was still some 2-4 dB higher than the 127cm (50 in) bundle at 1300 kV.

These results indicate that the use of reduced-diameter bundles for the purposes of reducing ice-loading is not very practical. If the area traversed by the line was one in which noise generation was of no concern, then such a solution might be considered. However, under such circumstances, other solutions such as using fewer larger conductors might be more attractive.

203cm (80 in) bundle. As of the writing of this report, tests on this bundle were still in progress. To this date approximately 2000 min of data have been collected during periods of rain. However the test period was noted for its exceptionally low rain rates. Rain rates in excess of 2.8mm/h (0.11 in/h), i.e. moderate and heavy rains, occurred for only about 10% of the time compared to a yearly average of about 25%. Consequently the audible noise levels recorded for this bundle were significantly less than expected on the basis of calculations and previous good correlation between measurements and calculations. Results are shown in figure 3-23. "Corrected" L_5 and L_{50} levels of 55.2 dB(A) and 45.3 dB(A) were obtained. These compare to calculated levels of 57.9 dB(A) and 52.0 dB(A).

Although overall the rain was lighter than normal, some 660 minutes of rain at the beginning of the period was distributed much closer to the normal yearly distribution with the 2.8mm/h (0.11 in/h) rate falling at the 78% probability level (i.e. that rate was exceeded 22% of the time). An analysis of the audible noise perfor-

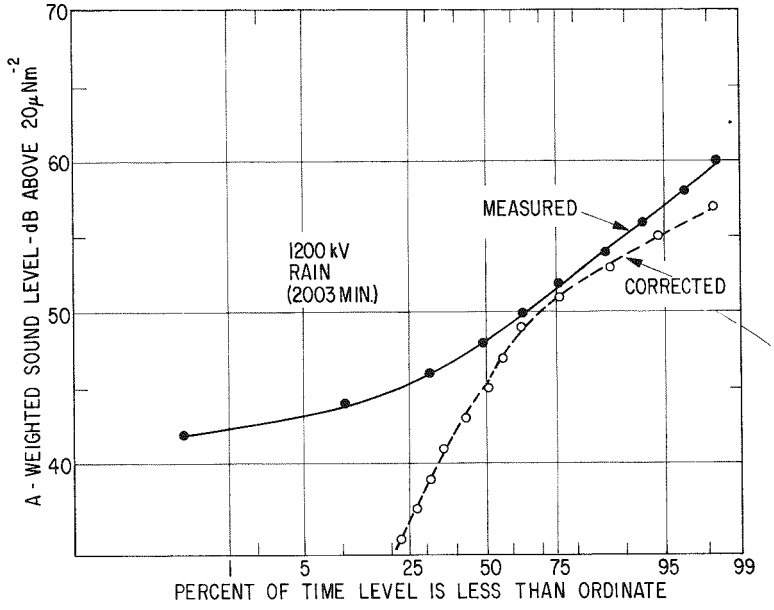


Figure 3-23. Measured and Corrected Statistical Distribution of Audible Noise During Rain: 12-Conductor Bundle, 80 in Diameter.

mance during this rain period shows a much better agreement with calculated levels. Figure 3-24 indicates L_5 and L_{50} levels of 57 dB(A) and 52.4 dB(A). As described in

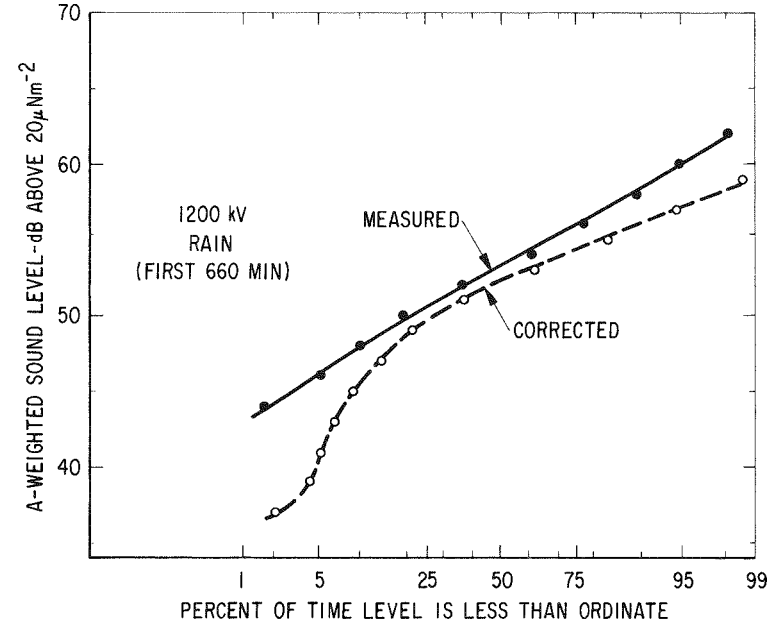


Figure 3-24. Measured and Corrected Statistical Distribution of Audible Noise During First 660 Minutes of rain: 12-Conductor Bundle, 80 in Diameter.

Appendix A it is desirable to have both a rain rate distribution near to the normal yearly distribution and 2000 min of data or more during rain for a reasonable degree of confidence that the field measurements accurately represent the long-term performance. Both requirements were not met together in this bundle test; however, it is considered that the results of figure 3-24 are more representative of the actual long-term performance.

Figure 3-25 shows the comparison of calculated and measured levels for the complete range of bundle diameters tests.

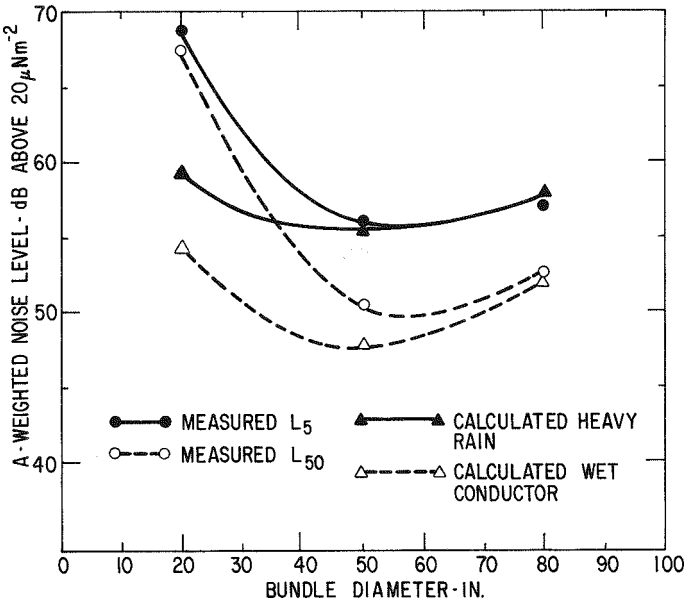


Figure 3-25. Comparison of Measured and Calculated Noise Levels: 12-Conductor Bundle at 1200 kV.

Fair Weather Noise

As previously mentioned, audible noise produced by transmission lines should be of a negligible level in fair weather provided the lines are designed to have acceptable noise performance in foul weather. Figure 3-11 illustrated this general observation. A further illustration is given in figure 3-26 which shows the L_{50} octave band levels for the 12 x 3.31 x 127cm (12 x 1.302 x 50 in) bundle at 1200 kV in both rain and fair weather. The A-weighted level is indicated to the left

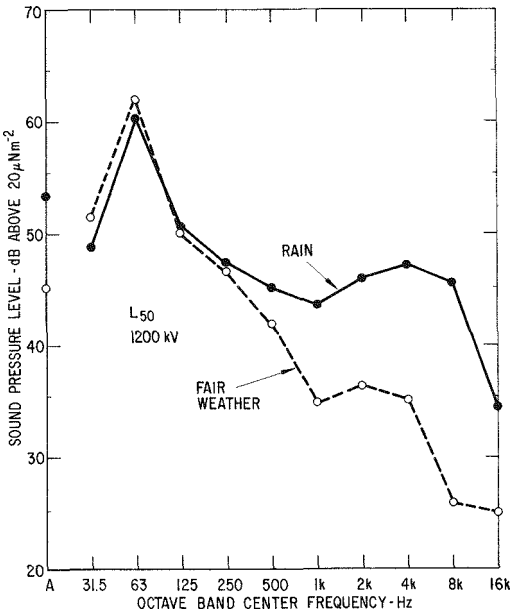


Figure 3-26. Comparison of Frequency Spectra in Rain and in Fair Weather: 12-Conductor Bundle, 50 in Diameter.

of the octave band levels. Over 10,000 data records are included in the fair weather analysis. It is fairly evident that ambient noises control the levels below 500 Hz, but the foul weather line corona noise is clearly dominating in the higher frequency region. In the frequency range over which the human ear is most sensitive (1-4 kHz) the line noise is some 8-12 dB above the fair weather levels for this example. The fair weather noise levels indicated are more likely to be due to ambient noises rather than the line itself. A categorical statement to this effect cannot be made on the basis of this information, however, since it is known that corona does in general occur also in fair weather. This is evidenced by the fact that high voltage transmission lines can generate fair weather radio interference (RI) which exceeds normal ambient levels; the corona resulting in the RI must also generate acoustic pressure waves, even though these may not always be detected due to the presence of overriding ambient noises.

It is possible to obtain some information concerning the contribution from the line itself in fair weather by examining the behavior for higher than nominal voltages. If the voltage is raised sufficiently, the noise produced by the line will measurably exceed the ambient levels. If one makes the assumption that the shape of the frequency spectrum of corona noise is invariant (i.e. as corona activity varies, the noise spectrum varies in overall level but maintains the same

relationship between octave band levels) then one would first notice line noise exceeding the ambient at the higher frequencies where ambient levels are lowest. Consequently a measure such as the 8 kHz octave band level is a better indication of the line corona noise than, say, the dB(A) measure. Figure 3-27 shows the results of plotting both the 8 kHz level and the dB(A) level measured during voltage runs, in rain and fair weather, for the triangular 8-conductor bundle configuration. Similar data are presented for the 8-conductor bundle configuration with 19.8m (65 ft) phase spacing in figure 3-28, and for the 12-conductor bundle of 127cm (50 in) diameter in figure 3-29.

With reference to figure 3-27 it is fairly evident that above 1250 kV line noise predominates in both dB(A) and 8 kHz levels, the difference between the two quantities being the same (approximately 7 dB) in both rain and fair weather. At low voltages this same 7 dB difference is evident in the data for rain, indicating that the line noise is still significantly above ambient, but in fair weather the correlation between the two quantities ceases to exist due to the effect of ambient noises which affect the dB(A) measure more than the 8 kHz. Let us assume that 45 dB(A) is an acceptable level of line noise in fair weather at the edge of the right-of-way, and 55 dB(A) the corresponding acceptable level in rain (L_{50} value). At the center of the line, to which noise levels of these figures corre-

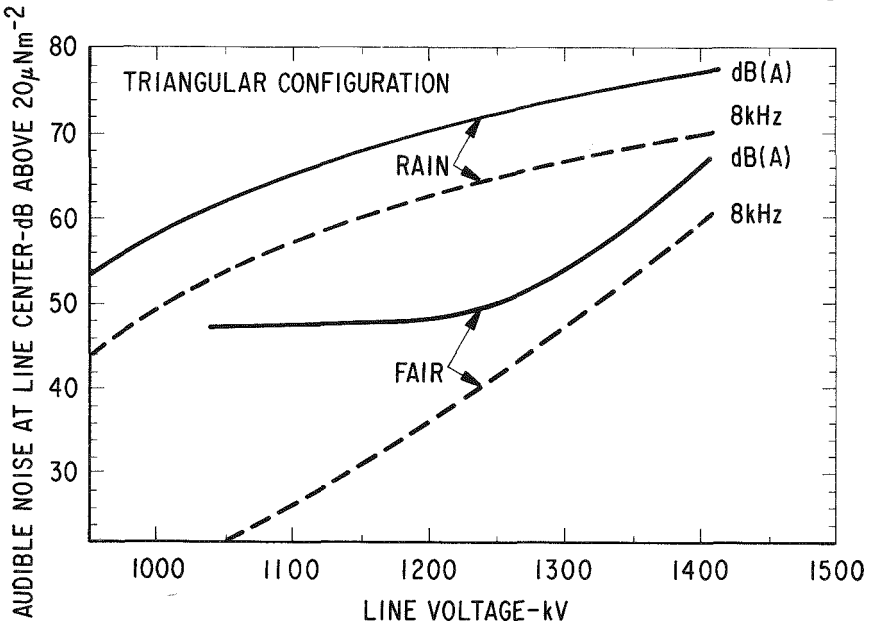


Figure 3-27. A-Weighted and 8 kHz Octave Band Noise Levels for Different Voltage Levels: 8-Conductor Bundle, Triangular Configuration.

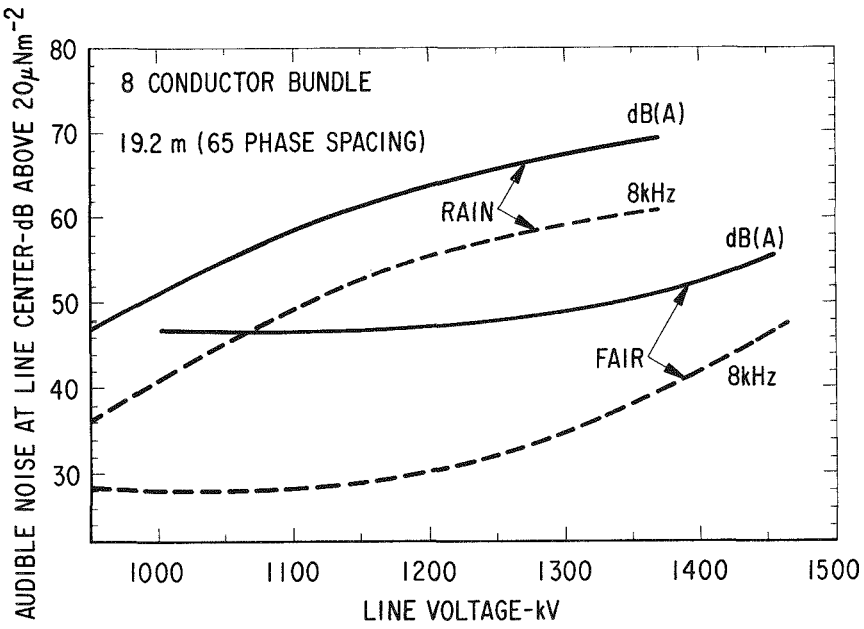


Figure 3-28. A-Weighted and 8 kHz Octave Band Noise Levels for Different Voltage Levels: 8-Conductor Bundle, 65 ft Phase Spacing.

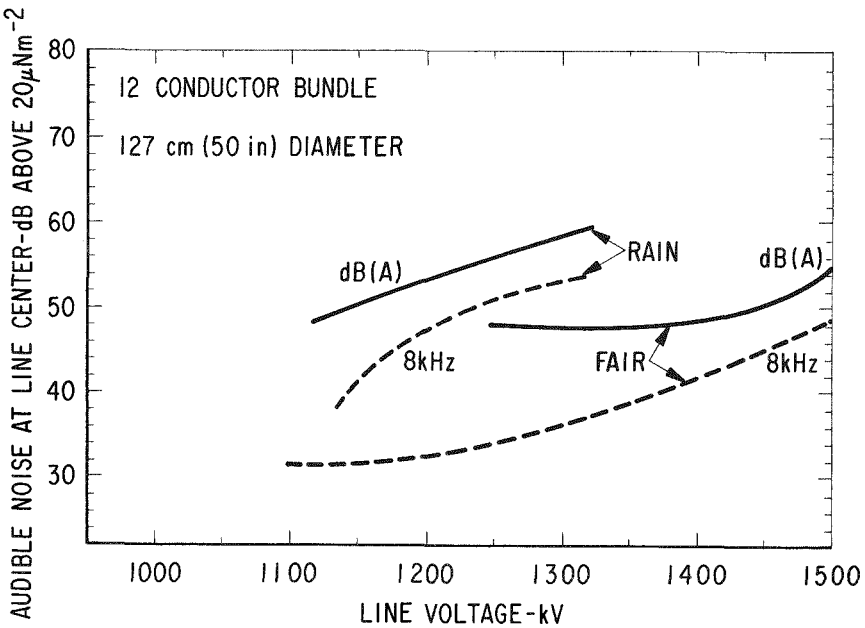


Figure 3-29. A-Weighted and 8-kHz Octave Band Noise Levels for Different Voltage Levels: 12-Conductor Bundle, 50 in Diameter.

spond, the levels would be approximately 6 dB higher, for a 105-120m (350-400 ft) right-of-way, resulting in acceptable levels of 61 dB(A) in rain and 51 dB(A) in fair weather under the center phase of the line. In terms of voltage these levels translate to 1075 kV and 1300 kV respectively. Thus, if the line was designed for acceptable wet weather performance, an operating "safety-margin" of approximately 22% in voltage is available in fair weather. On the basis of the 8 kHz vs. dB(A) correlation, the fair weather line noise would be approximately 22 dB(A) at the edge of the right-of-way at 1075 kV, much lower than ambient levels generally encountered.

In certain areas of the country where rain occurs very infrequently, one may not consider the audible noise performance in rain as being an important design consideration. In such a situation one could consider operating at higher voltage or, given the same voltage, design the line with smaller or fewer conductors to the point where the fair weather noise becomes the limiting factor. The 22% figure mentioned above provides some indication of what margin in design modifications is available. (Of course, for such a case other factors might determine the conductor design; for example, radio interference. The situation would have to be considered on a case by case basis).

A similar operating margin, approximately 23%, is obtained for the horizontal configuration of figure 3-28. At low voltages the effect of ambient is noticeable also on the 8 kHz level. For the 12-conductor bundle, figure 3-29, a margin of only about 8% is indicated. However, it is apparent that the fair weather noise shown is primarily due to a source other than the line since the levels differ only slightly from those of the 8-conductor bundle with the same phase spacing (previous figure). It is thought that the noise levels could be affected by noise from the station hardware at voltages approaching 1500 kV.

Ambient Noise

Ambient noise is a very variable quantity, due to the inherent variability of the sources contributing to it. Typical sources are: wind, which can have a direct effect in passing over the head of the microphone (limited by use of a specially designed windshield) and indirectly by whistling through shrubbery and rustling of leaves on trees; traffic such as motor vehicles, airplanes and construction machinery, which can vary in nature from an almost continuous drone to short duration bursts; animals, such as birds, frogs (in swampy areas) and crickets which can result in fairly continuous and high levels of noise. Most of these

sources produce low frequency noise, typically below 1000 Hz. Animal noises tend generally to be in the higher frequency region; for example, young frogs (spring peepers) produce noise predominantly in the 2 and 4 kHz octave bands, while a certain type of grasshopper has been observed to produce noise in the 16 kHz band. The level of noise produced by the combination of these sources will obviously depend on the location of the observer. At Project UHV, the combination of these sources result in noise levels generally much lower than the noise produced by line corona in wet weather, and consequently do not pose problems of measurement of the corona noise, and would not create a masking effect on the noise (on the occasions when this is not the case - i.e. for periods of abnormally high ambient noise or low line noise - methods of identifying the contribution of the line noise to the total measured are available, as previously described in this report). However, during wet weather, there exists another potential source of noise which could possibly result in higher ambient levels and consequent masking of the line noise, and that is the noise of the rain itself falling on the ground, on structures and on leaves of trees.

A fairly extensive study conducted elsewhere [3-10] indicated that the noise produced by the rain might raise an average ambient level of 37-39 dB(A) by 3 or 4 dB. A limited analysis of data gathered at Project UHV during periods of line denergization during night-time hours has indicated a similar increase from an average level of around 41 dB(A) to around 45 dB(A). A lack of data prevented any similar conclusion to be drawn for daytime hours.

From the data available it is apparent that for lines designed to meet acceptable noise levels in average foul weather conditions (most likely in the 50-55 dB(A) range), the additional masking effect of the rain superimposed on other ambient noises will be minimal. However, measurement of ambient noise levels will continue whenever possible in order to determine whether or not this conclusion is valid in every case.

Cage Tests of Three-Phase Line Bundle Geometries

A part of a continued investigation of the relationship between single-phase cage and three-phase line, bundle conductors identical in geometry to those tested on the three-phase line have also been tested in the "uhv" cage shown in figure 3-30. Artificial rain tests in the cage yield two values characterizing the performance of the bundle; namely, "heavy rain" and "wet conductor" noise generations. Heavy rain generation is determined from measurements of corona generated noise during the application of a rain spray, simulating conditions of natural heavy rain. Wet

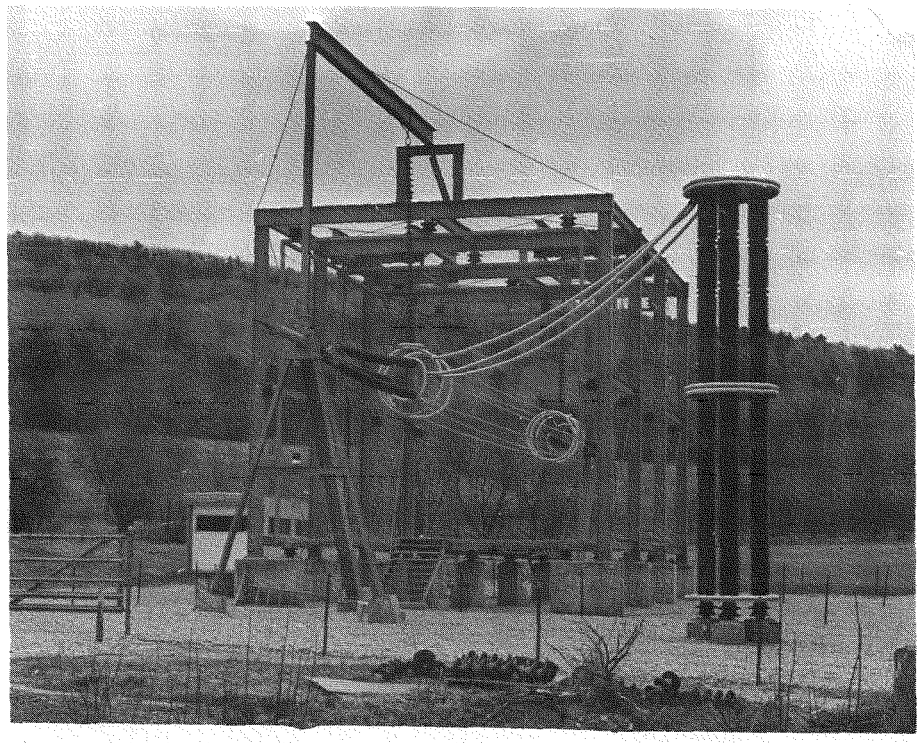


Figure 3-30. Conductor Test Cage.

conductor generation is derived from the average of measurements taken from one to two minutes after the rain spray is turned off; during this time water drops still remain on the conductors simulating a condition which is obtained during periods of light rain or heavy fog when the moisture in the air is sufficient to maintain water drops on the conductors.

The cage is 13.7m (45 ft) long and has a 7.9m (26 ft) square cross section. The microphone is situated at bundle height and is 4.39m (14.4 ft) from the bundle center. The relationship between P, the measured A-weighted sound level, and A the acoustic power generated by the bundle is given by

$$P^2 = \frac{\delta c A}{2\pi r} \tan^{-1}\left(\frac{\ell}{2r}\right) \qquad (3\text{-}3)$$

where δ is the air density, c is the sound wave propagation velocity, r is the distance from the bundle axis to the microphone and ℓ is the length of the conductor in the cage. For normal temperature and pressure conditions $\delta = 1.225\ kg \cdot m^{-3}$ and $c = 344\ m \cdot sec^{-1}$, giving

$$P = 15.28A \qquad (3\text{-}4)$$

which is dimensionally correct if P is in $N \cdot m^{-2}$ and A is in $W \cdot m^{-1}$. If P is given in dB relative to $20\mu Nm^{-2}$ (a standard means of expressing sound level) then the

generated acoustic power may be found from

$$A = 26.2 \times 10^{(P/10-12)} \quad W \cdot m^{-1} \tag{3-5}$$

or

$$A = P - 45.8 \text{ dB above } 1\mu W \cdot m^{-1} \tag{3-6}$$

Tests are generally performed to determine A as a function of conductor surface gradient. Then, through methods described in Reference 3-1, three-phase line performance can be calculated.

As previously mentioned in this report, the three-phase line performance calculated from "heavy rain" data has been considered to be comparable to the L_5 level of a long-term statistical distribution of noise in rain, while "wet conductor" performance has been considered comparable to the L_{50} level in rain.

Eight-conductor bundle. The first three-phase line also to be tested in the cage was the 8 x 3.3 x 102cm (8 x 1.302 x 40 in) bundle. This was strung with conductors taken from the same reels as those used for the three-phase line stringing to ensure that line and cage conductors had identical surface conditions. Results of cage tests are depicted in figure 3-31. Each data point represents the

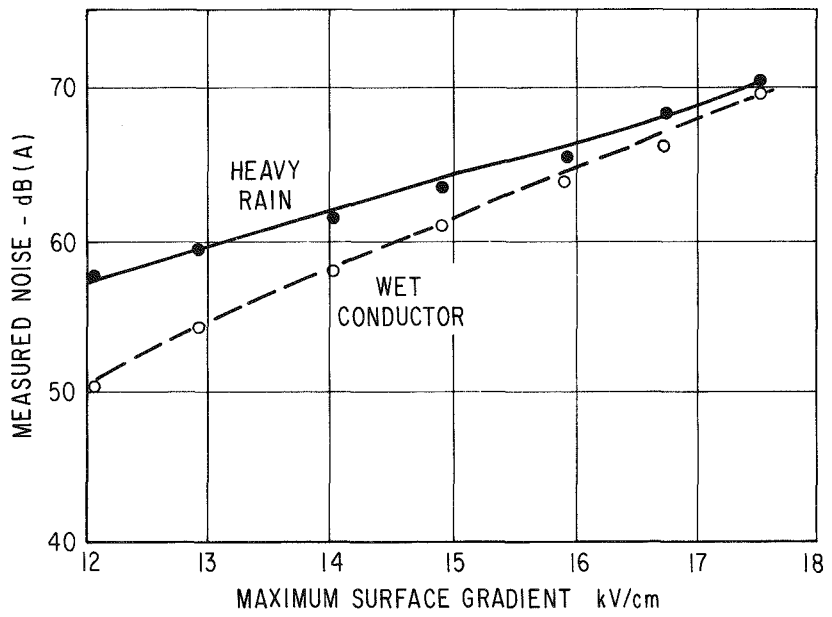


Figure 3-31. Audible Noise Measured in Cage: 8-Conductor Bundle.

average of results obtained from several individual tests conducted on different days. (In an effort to obtain reproducibility, particularly of wet conductor data, care was taken to test the conductors only during periods of calm, generally early in the morning or late in the afternoon; hot sunny days with low humidity were avoided).

The Reference Book [3-1] presents a generalized curve of generated acoustic power versus conductor gradient, this being the result of reducing data from a very large number of configurations tested during the period 1970-1973. By reducing the heavy rain data of figure 3-31 according to the same formula, the comparison of figure 3-32 can be made. Agreement over the range of gradients tested is quite good. At the low end of the range, the Reference Book curve underestimates the generation by around 2-4 dB. At the upper end of the range, very good agreement is indicated. It may be noted that the Reference Book states that the data presented therein "apply to conductors with a moderate degree of aging," whereas the 8-conductor bundle reported on here had new conductors recently taken off the reel. The differences seen between the Reference Book curve and the 8-conductor bundle data in figure 3-31 are consistent with observations made many times before at Project UHV; namely that the dependence of noise generation on surface conditions is very

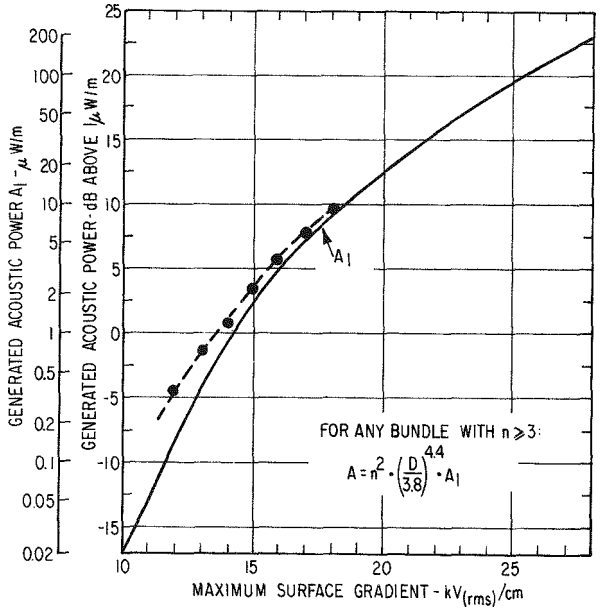


Figure 3-32. Comparison of Heavy Rain Audible Noise Generation of 8-Conductor Bundle with Reference Book Data.

much a function of operating gradient. At low gradients a new conductor will be noisier than an aged conductor, the difference decreasing as the gradient increases to a point where the effect of surface condition is negligible. The effect of surface condition is generally more noticeable for the wet-conductor situation, and this case appears to be no exception. For example, the Reference Book calculation procedure indicates that the "6 dB gradient" (that gradient at which the wet-conductor generation is 6 dB less than the heavy rain generation) is 14.8 kV/cm for this 8-conductor bundle, at which gradient the new conductors only show a 3 dB difference (figure 3-31). At this gradient, the heavy rain generation is approximately 1.5 dB higher than the Reference Book value (figure 3-32), making the wet conductor level approximately 4.5 dB higher than predicted by the Reference Book.

However, when the cage results are translated to the three-phase geometry of the test line and compared directly with test line data, very good agreement is indicated in figure 3-33 which shows the translated cage data superimposed on line data taken from figure 3-10. It is considered that the similarity in conductor surface conditions is primarily responsible for this agreement which is measurably better than that obtained between the initial test line data and Reference Book calculations (figure 3-16).

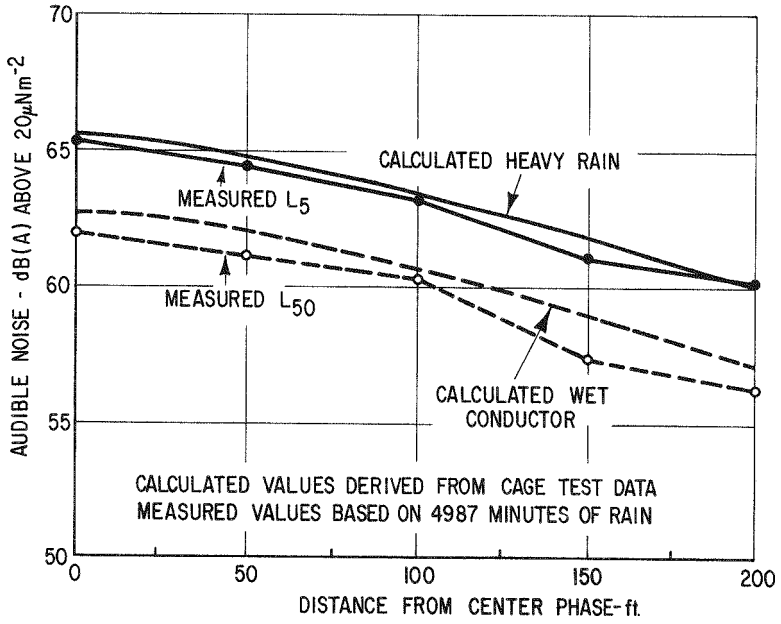


Figure 3-33. Comparison of Measured 3-Phase Line Audible Noise with Levels Calculated From Cage Tests: 8-Conductor Bundle, 50 Feet Phase Spacing.

Conductor aging experiment. Subsequent to the tests described above, a special test was conducted on the 8-conductor bundle to determine to what extent the presence of corona affects the aging process. The test procedure and results are described in more detail in a later section on Conductor Aging. However, it is pertinent to mention the tests here since the outcome had an influence on the results of later cage tests which used the 8 conductors subjected to the aging experiment. At the conclusion of the experiment, which in total comprised 300 hours of energization in heavy rain at a maximum conductor surface gradient of 18 kV/cm (20-30% above "normal" for such a bundle), the wet-conductor noise levels were found to be from 5-10 dB lower (depending on the operating gradient) than at the beginning of the aging period. The lower noise generation is evident in the results of later tests utilizing the same conductors.

Simulation of an outside phase. During cage tests on bundled conductors, the bundle has always in the past been centered in the cage. The resulting distribution of surface gradients on the conductors represents very closely that of a similar bundle in the center phase of a three-phase line. For practical purposes, the maximum gradient can be considered the same on all subconductors of the center phase bundle. However, on the outer phase bundles there is a marked asymmetry of maximum gradient values. Figure 3-34 illustrates this for 8-conductor bundles used on a 1100 kV three-phase line. The distributions of maximum gradient are shown relative to the mean value of the individual subconductor maximums, which for this particular case are 15.7 kV/cm for the center phase and 14.3 kV/cm for the outer phases. The greatest deviation from this "mean-maximum" gradient is about 0.2% for the center phase and 3.5% for the outer phases. For a bundle centered in the cage, the distribution of maximum gradients is uniform (i.e. plotted in figure 3-34 it would be equal to unity for each subconductor). In translating cage data to three-phase line cases, the "mean-maximum" value has always been used as the basis for calculations, this being considered to result in little loss of accuracy even for the outer phases.

However, in order to check this conjecture a series of tests were performed in which the gradient distribution of an outside phase was duplicated in the cage. This can be achieved by offsetting the bundle from the cage center. The amount Δ and direction α of the offset will depend on the asymmetry of the gradient distribution to be reproduced. The amount is given by

$$\Delta \simeq 1.2\ \alpha A^2/4D \qquad (3\text{-}7)$$

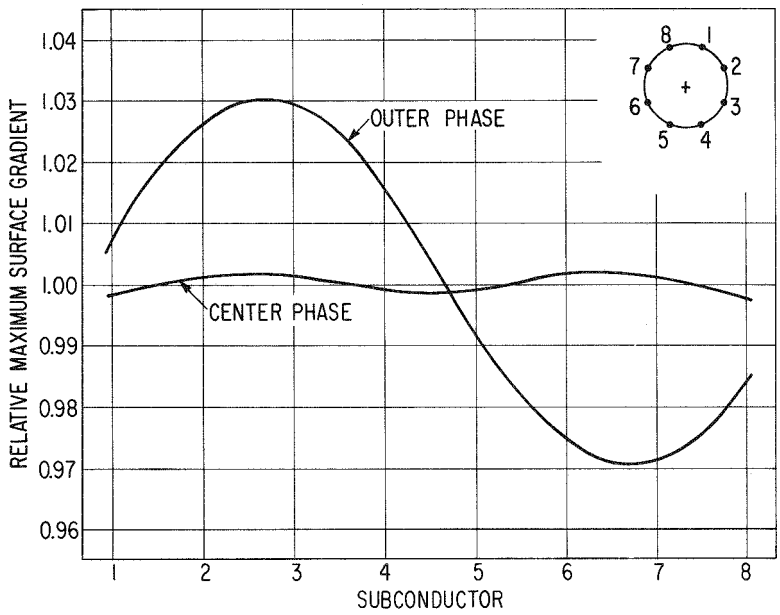


Figure 3-34. Variation of Maximum Gradient Around an 8-Conductor Bundle.

where δ is the greatest deviation, in per unit, of the distribution of maximum gradients (see figure 3-34), D is the bundle diameter, and A is the equivalent diameter of the cage.* The direction of the offset is determined by the point at which the gradient distribution reaches a peak. To reproduce the distribution shown in figure 3-34, the calculated offset was

$$\Delta = 66\text{cm (26 in)}, \quad \alpha = -8.5^\circ$$

Figure 3-35 illustrates the arrangement in the cage to achieve this offset, and figure 3-36 compares the distributions of cage and line for the centered and offset conditions.

Typical results expressed in terms of generated acoustic power versus surface gradient are shown in figure 3-37. Since it was felt that differences being

*It can be demonstrated by use of the method of multiple images that the equivalent diameter of a square cage of side S is given by

$$A \simeq 1.08S$$

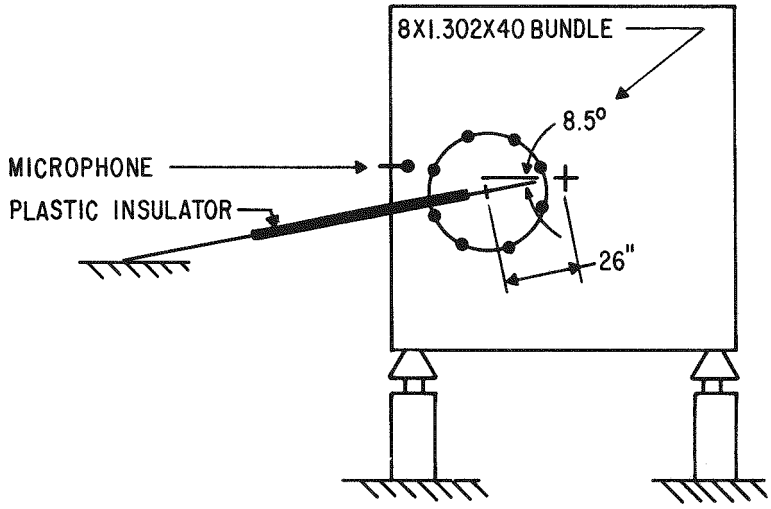


Figure 3-35. UHV Cage, Bundle Offset (Simulation of Outer Phase).

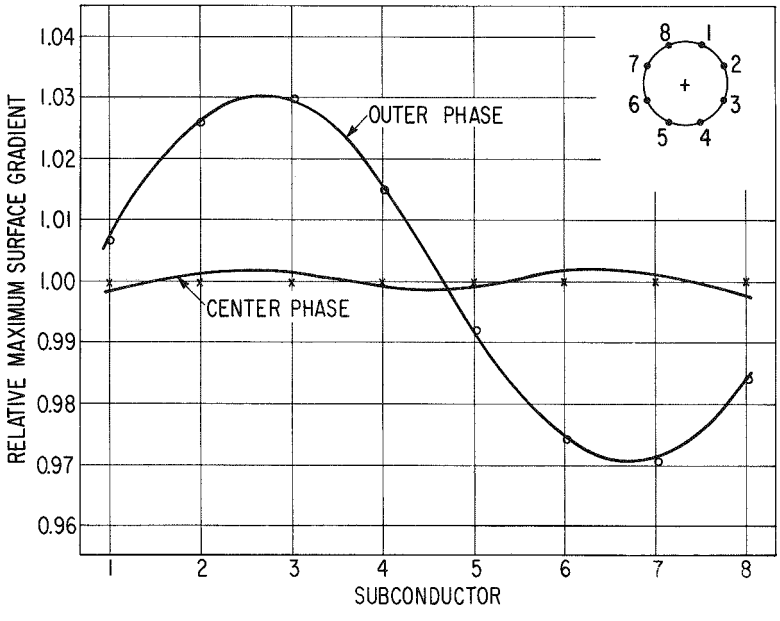


Figure 3-36. Comparison of 3-Phase Line Maximum Gradient Distribution With Those Obtained in Test Cages.

sought would be no more than a few dB at most, care was exercised to compare the performance of the two bundle arrangements in as close to identical weather conditions as possible by testing bundle centered and bundle offset alternately over a period of about 3 hours. The fact that the bundle was approximately 0.6m (2 ft) closer to the microphone for the offset condition than for the centered condition causes the relationship between measured noise and generated acoustic power to be slightly different between the two conditions. This effect has been taken into account in figure 3-37 (the net effect is minor, causing only about 1 dB lower generation for the same measured noise).

It was concluded from the experiment that the difference in generation between center and outer phases, for the same "mean-maximum" gradient, is small and for

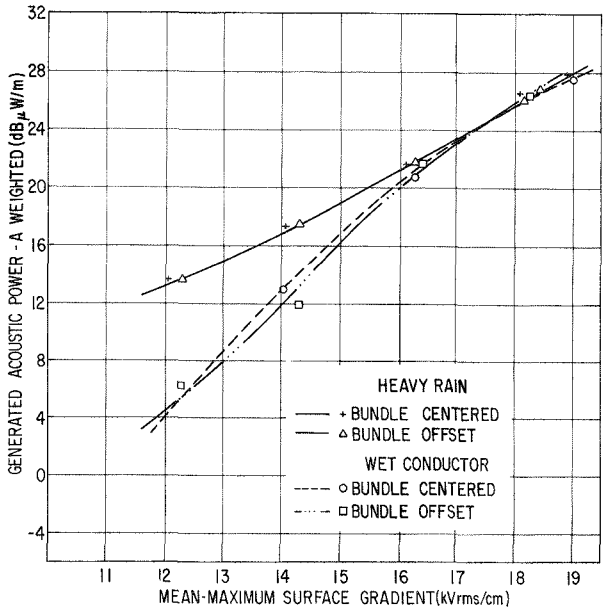


Figure 3-37. Comparison of Audible Noise Generation of Center and Outer Phase Bundles in Test Cages.

practical purposes can be neglected when translating from cage to three-phase line.

(It should be noted that the generated acoustic power values presented in figure 3-37 refer to the quantity "A" and not "A_1" in figure 3-32. For this bundle, one would find A_1 by subtracting 15.4 dB from A).

Twelve-conductor bundle. The 12-conductor bundle was tested with four different bundle diameters; namely, 51, 81, 127 and 203cm (20, 32, 50 and 80 in). Results of artificial rain tests, translated to the case of the 1200 kV 3-phase line, are presented in figures 3-38 and 3-39 where they are compared to noise levels calculated according to the Reference Book and to levels obtained from actual 3-phase line measurements.

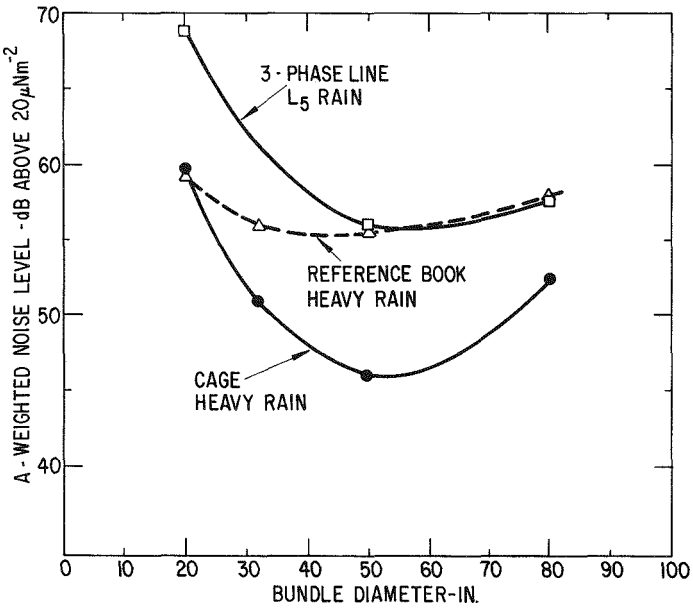


Figure 3-38. Comparison of Measured and Calculated Audible Noise Levels: 12-Conductor Bundles of Different Diameters.

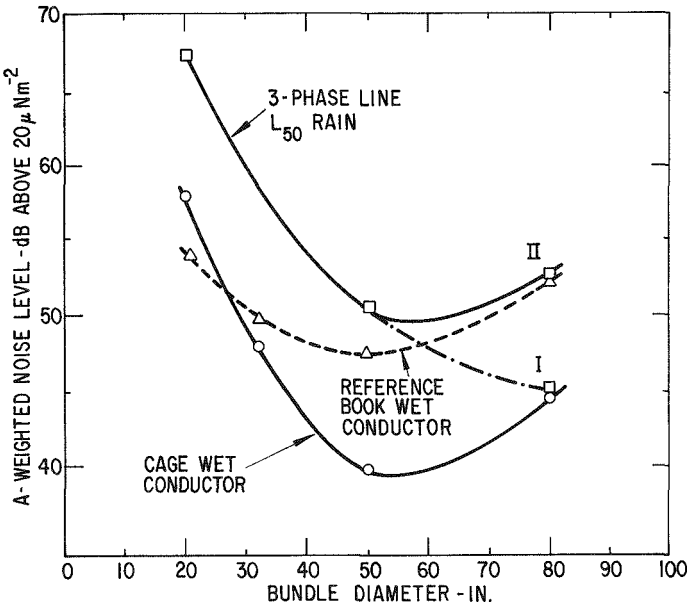


Figure 3-39. Comparison of Measured and Calculated Audible Noise Levels: 12-Conductor Bundles of Different Diameters.

The 3-phase line L_{50} level for the 203cm (80 in) bundle was 45 dB(A) - corrected - for the total period analyzed (point I in figure 3-39). As explained earlier in this report it is felt that this level is not a good indicator of the long-term performance of the line due to the abundance of very light rain encountered. The level indicated by point II corresponds to a period during which the distribution of rain more closely matched that of the normal yearly distribution for the Northeast and regions of similar climate. The reasons for the discrepancy between Reference Book calculations and 3-phase line measurements for small bundle diameters have been discussed earlier. A large difference between 3-phase measurements and levels calculated directly from cage data is observed over the complete range of diameters. This is attributed to the fact that 8 of the 12 conductors had significantly reduced generations due to being subjected to the accelerated aging process described above. Although the absolute levels do not compare well because of this fact it is interesting to note that relatively the effect of changes in the bundle diameter is similar for line and cage. This is further indication that the Reference Book calculations do not properly take into account the high degree of non-uniformity of the subconductor surface gradient distributions which occur for small subconductor spacings.

Bundle Geometry Optimization.

The concept of bundle geometry optimization was introduced in Chapter 6 of the Transmission Line Reference Book [3-1]. In wet weather, a bundle of conductors regularly spaced has different corona activity for each individual subconductor. Because water drops form on the bottom surface of the conductors, the bottom conductors of a regular bundle generate more corona (radio noise, audible noise, and corona loss) than the conductors in the upper part of the bundle.

It was shown that the corona generation of each conductor could be made the same by proper positioning of the subconductors. The "asymmetric" bundles so formed have a total noise generation lower than that of regular bundles. This fact was demonstrated with cage tests and single-phase line tests on 6 and 8-conductor bundles.

The noise reduction appears substantial for the "wet-conductor" condition representing light rain, fog, or after rain. In heavy rain the effect of asymmetry tends to disappear.

It was also shown that asymmetry is beneficial particularly for well aged conductors. Bundles with new conductors, on which water drops form all around the surface, do not lend themselves to an effective optimization.

Noise Generation of Individual Subconductors. Optimization of bundle geometry to obtain the minimum audible noise generation requires the calculation of the noise of many different bundle configurations, which in turn is possible if the noise generation of individual subconductors can be calculated.

It has been shown [3-7] that the noise of a subconductor is determined by the following parameters:

1) the subconductor diameter
2) the maximum surface gradient
3) the ratio "k" between maximum and average surface gradient
4) the point of maximum gradient on the conductor surface in relation to the point where water drops form (the bottom of the conductor for well aged conductors).

The noise generation of individual subconductors, determined experimentally with tests in a small cage, was given in the Reference Book, which also illustrated a method to determine the optimum bundle geometry.

A more complete series of tests was performed in 1976 and the results are reported in Reference 3-7. These tests were performed in the uhv cage of Project UHV and made use of a new experimental technique consisting of stringing a test conductor at different distances from a symmetrical 12-conductor bundle. The dimensions of the 12-conductor bundles were such that, when the complete set-up (12 conductor bundle plus test conductor) was energized, the noise was generated only by the test conductor.

Reference 3-7 contains a complete set of experimental curves for various diameters, gradients, k, and positions of point of maximum gradient. The curves were incorporated in a versatile computer program for the computation of audible noise generation of multiconductor bundles of any geometrical configuration.

The results of computations compared favorably with full scale tests performed on an asymmetric 6-conductor bundle tested on the Project UHV single phase line in 1973.

The limitations of the results on which the computer program is based are the following:

- diameter between 2.96cm and 4.63cm (1.165 in and 1.823 in)
- maximum gradient between 13kV/cm and 23 kV/cm
- k values between 1.0 and 1.35
- angle between point of maximum gradient and water drops between 0 and 120 degrees

Outside these ranges the results must be viewed with caution. The ranges cover most practical cases, with few exceptions. One such exception, tested in 1976, was a bundle of 12 conductors with bundle diameter of 51cm (20 in) which had k = 1.7. The experimental results showed an unexpectedly higher noise than anticipated by extropolation of available data.

Corrections to the design rules for regular bundles are required in such cases. A means of making the necessary correction is described later in this report.

Calculation of noise generation of a bundle. The audible noise generation of a bundle may be calculated by the computer program "CONOP3" (the program description and user guide have been made available to EPRI).

The program computes the wet conductor audible noise generation of bundles having up to 12 subconductors. Any line configuration can be handled, whether it be a single phase or a three phase line. Any diameter and location of the individual subconductors in the bundle may be input. The program calculates the potential coefficients and the surface gradients (maximum, average, distribution on the surface). Empirical data contained within the program permits the calculation of the noise generation of individual subconductors. The total generation of the bundle is calculated by summing up the generations of individual subconductors.

The following sample output of CONOP3 illustrates some of the program capabilities (underscored numeric values indicate user responses):

Number of Phases? 3

* Phase to be studied is designated as Phase 1
Number of Conductors in thie Phase? 4

* Phase voltages - real and imaginary components - kV
Phase 1? 441.7,0
Phase 2? -220.8,382.5
Phase 3? -220.8,-382.5

* Geometrical Data for Phase 1
Do you wish to input: (1) Individual Subconductor Data
or (2) Asymmetry Limits? 1

Subconductor Diameter and Position - D(I), X(I), Y(I) - inches
1. ? 1.382,9,651
2. ? 1.382,9,669
3. ? 1.382,-9,669
4. ? 1.382,-9,651

* Geometrical Data for Phases 2 and 3
No. of Subconductors, subconductor diam. bundle diam.
and bundle position - N(I), D(I), A(I), X(I), Y(I) - inches
Phase 2? 4,1.382,25.5,-540,660
Phase 3? 4,1.382,25.5,540,660

#	D (IN)	X (IN)	Y (IN)
1	1.382	9	651
2	1.382	9	669
3	1.382	-9	669
4	1.382	-9	651

#	MAX GRAD (KV/CM)	K (PU)	ALPHA (DEG)	WATER GRAD (KV/CM)	GENERATION (DB)
1	18.4301	1.16332	45.0913	17.6696	18.5817
2	18.4061	1.16312	134.795	14.0068	-1.95051
3	18.4062	1.16312	134.795	14.0047	-1.94946
4	18.4303	1.16332	45.0909	17.6677	18.5823

TOTAL GENERATION = 21.6303 DB(A) ABOVE 1 μW/M

Cage tests of asymmetric bundles. Cage tests have been performed on several asymmetric bundles in the past. Such results are shown in References 3-1 and 3-7. Asymmetric bundles of 8 and 9 subconductors were tested in anticipation of tests on similar bundles on the 3-phase test line. The results of the cage tests are shown in figures 3-40 and 3-41. The asymmetric conductors tested had a degree of asymmetry of 2. The degree of asymmetry is defined as the ratio between the arc distance between the upper pair and the arc distance between the bottom pair of subconductors, as shown in the example figure 3-42.

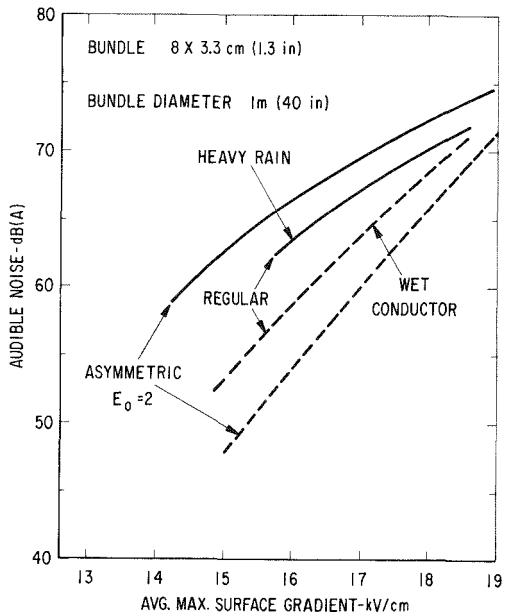


Figure 3-40. Audible Noise Measured During Cage Tests on Regular and Asymmetric Bundles, Plotted Versus the Average of the Maximum Surface Gradients of all the Subconductors. Bundles of 8 x 3.3cm Diameter Conductors.

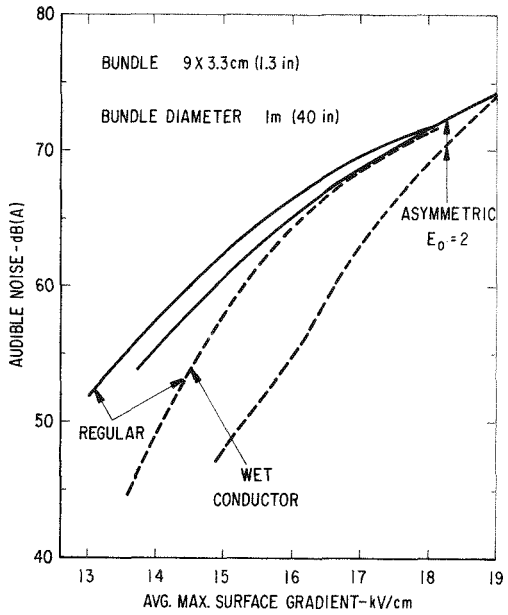


Figure 3-41. Audible Noise Measured During Cage Tests on Regular and Asymmetric Bundles, Plotted Versus the Average of the Maximum Surface Gradients of all the Subconductors.

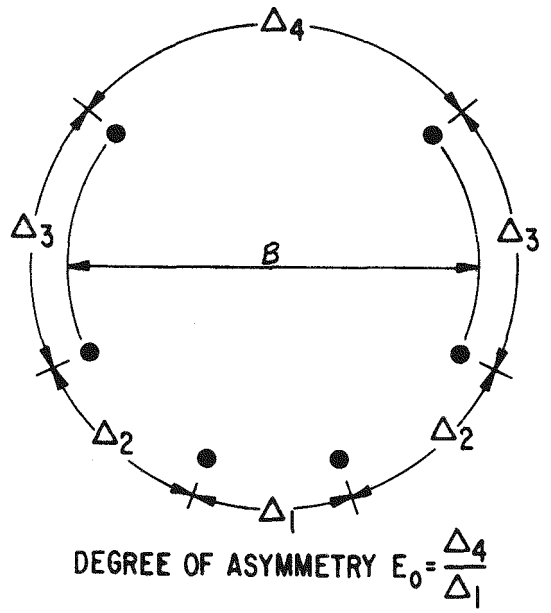


Figure 3-42. Asymmetric 6-Conductor Bundle.

The figures show that asymmetric bundles do not bring about any noise reduction in conditions of heavy rain, but a substantial reduction is indicated for wet conductor conditions. This is significant in that the wet-conductor level, considered representative of the level in light rain conditions, will generally factor into the design of a line much more than the level in heavy rain which occurs for only a small fraction of the total time.

Calculations for 8 and 9 conductor bundles show that the optimum asymmetry is approximately equal to 2. These calculations were performed for a 3-phase line having a flat configuration and bundles of 8 x 3.3cm (1.302 in) in the outside phase, and a bundle of 9 x 3.3cm (1.302 in) in the center phase. The results are shown in figure 3-43 and 3-44. Using these figures, bundles with different asymmetries can be compared with regular bundles (E_o=1). For instance for E_o=2, at 1100 kV there is about a 7 dB noise reduction for both 8 and 9 conductor bundles. This compares with a 5 to 10 dB reduction measured in the cages. There is the need to evaluate the advantage of asymmetric conductors with long term tests using the 3-phase uhv test line. These tests are in program for 1977. Calculations for a 3-phase line for regular and asymmetric conductors (E_o=2) are shown in figure 3-45. At 1200 kV the optimized line shows a reduction of 15 dB over the regular 8-8-8, 10 dB over the regular 8-9-8, and 8 dB over the regular 8-8-8 using 4.1cm (1.6 in) diameter subconductors used on the Bonneville Power Administration prototype 1100/1200 kV line.

Design considerations. As has been shown, asymmetric bundles may have a large advantage over regular bundles with respect to audible noise generation in wet weather. It has been shown [3-12] that in wet weather radio noise and corona loss also are reduced.

This makes asymmetric bundles economically attractive because it allows the use of smaller (more economical) subconductors. However, because of the asymmetry, a number of other possible negative effects should be considered. In fact, the asymmetry causes an imbalance in the current among the subconductors, which in turn causes additional resistive loss, difference in temperature and sag among the subconductors, and current flow between subconductors when they contact each other during short-circuits. In addition, there is an increased probability of subconductor oscillation because of the closer distance between the bottom pair of subconductors.

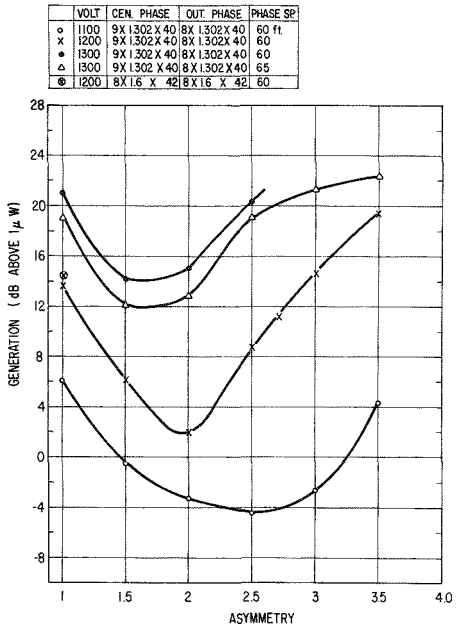


Figure 3-43. Audible Noise Versus Asymmetry for the Center Phase of an 8-9-8 Line Configuration.

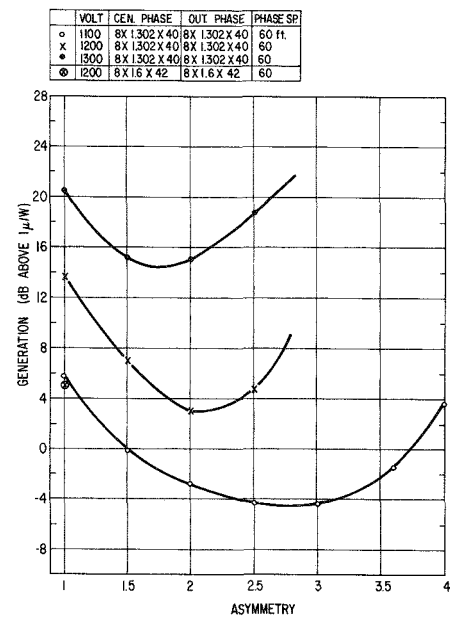


Figure 3-44. Audible Noise Versus Asymmetry for the Outside Phases of an 8-9-8 Line Configuration.

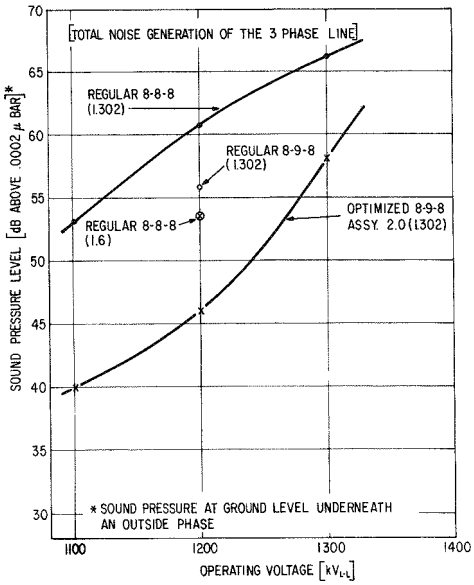


Figure 3-45. Comparison of a Regular 8-8-8 With an Optimized 8-9-8 Line Configuration; Phase Spacing is 60 Feet.

In order to evaluate the impact of this effect on the line design, calculations were performed for an asymmetric 8-conductor bundle, for an 1100 kV line carrying 10 GVA (5250 Amperes per phase).

For an optimum asymmetry (E_o = 2.3) the current distribution would be 780 A, 695 A, 610 A, and 540 A respectively for the four pairs of subconductors, from top to bottom. In the worst case (still air, hot day, maximum load) the temperature difference between upper and lower pairs would be 9°C. For a 500m (1600 ft) span without spacers, this would correspond to a differential sag of about 45cm (18 in). The presence of the spacers would probably reduce this effect, although the differential elongation might be concentrated in the central subspan. The study of the system with spacers is very complex and requires full scale tests or sophisticated calculations for which the spacer characteristics (such as their longitueinal flexibility) must be taken into account.

Indications are that the presence of the spacers would be beneficial, although asymmetric bundles might require an increased number of spacers (especially in the center of the span). An increased number of spacers would help also eliminate subconductor oscillations.

Resistive losses of asymmetric bundles would be about 2% higher than those of a regular bundle. However, this increase may be compensated by a reduction of corona loss; an example, for an 1100 kV line is shown in Table 3-6.

TABLE 3-6

COMPARISON OF LOSSES OF REGULAR AND ASYMMETRIC BUNDLES - TYPICAL FOR 1100 kV

	REGULAR BUNDLE		ASYMMETRIC BUNDLE	
	kW/km	(kW/mi)	kW/km	(kW/mi)
Average Resistive loss	62	(100)	63	(102)
Average Corona loss	9	(14)	6	(9)
Average Total loss	71	(114)	69	(111)

Another consequence of the current unbalance is the unequal tension in the subconductors caused by different temperatures. However, the differential tension would reach modest values ($\pm$ 8%) only in conditions which do not coincide with the conditions of maximum load (wind and ice) for which the line is designed.

Creep, that is non elastic elongation of the cables under different tensions and temperatures, would tend to equalize the sag and the tensions and the tendency of the bundle to rotate, because of the greater sag of the upper conductors, would be balanced by the natural restoring moment of the bundle against twisting.

Possible remedies to the current unbalance were proposed and studied. The most promising include:

1) The use of different expanded conductors. An average expansion of 0.87 (ratio between the cross section area of expanded and full conductors) was found sufficient to obtain temperature balance.
2) Use of conductors with different diameters. A difference of $\pm$ 20% in diameters and an asymmetry $E_o \approx 3$ would achieve both temperature balance and minimum audible noise.
3) The transposition of the subconductors at each dead end tower, combined with the use of insulating spacers and insulating suspension hardware.

Other concepts were examined and found less practical or ineffective, such as the use of steel on the outside of the cables, and the addition of dummy conductors.

Conclusions and future work. Asymmetric bundles, optimized to generate a minimum amount of audible noise in wet weather, represents the best practical method of audible noise reduction, using present technology. It is conceivable that the reduction in noise achieved by bundle geometry optimization is sufficient to practically eliminate audible noise as a parameter on which the cost of transmission is dependent.

However, asymmetric bundle conductors present a number of problems, mainly related to the unbalanced current distribution among the subconductors. Although it appears that these problems are manageable, and do not require expensive solutions, full scale tests are necessary to evaluate the performance. An optimized line design, with asymmetric 8-conductor bundles in the outer phase, and an asymmetric 9-conductor bundle in the center phase will be tested in 1977 to ascertain the extent of the audible noise reduction and to evaluate (without voltage) the effect of the current unbalance on conductor temperatures and sags, and forces on the spacers.

Conductor Aging

Benefit of Conductor Aging. A conductor which is freshly removed from a reel will have a somewhat greasy surface which causes water (from rain or dense fog) to bead up in small droplets all over the conductor surface. Each droplet is a potential source of corona and therefore audible noise. Such a conductor can be said to have a "hydrophobic" (non-wettable) surface property. Figure 3-46 shows an example of corona from a "Drake" conductor, 2.81cm (1.108 in) diameter, at a gradient of 17 kV/cm. If the conductor is part of a bundle of similar conductors, there will be sources of corona in the vicinity of the maximum gradient on all conductors of the bundle.

As the conductor continues to be exposed to the elements it gradually takes on a surface property, presumably due to some form of oxidation of the surface, which can be described as "hydrophilic" (wettable). This results in water drops being drawn up by capillary-like action into the strands of the conductor, to ultimately appear as large drops on the underside of the conductor. These drops tend to be much fewer than the many droplets observed on a new conductor, and the resulting overall corona activity tends to be reduced. Figure 3-47 shows the corona activity on a conductor which has a good hydrophilic property. The conductor is again "Drake" at 17 kV/cm under the same conditions of rain as the conductor shown in figure 3-46. Furthermore, on bundled conductors, the water drops on the uppermost conductors form towards the inside of the bundle in a low field region, re-

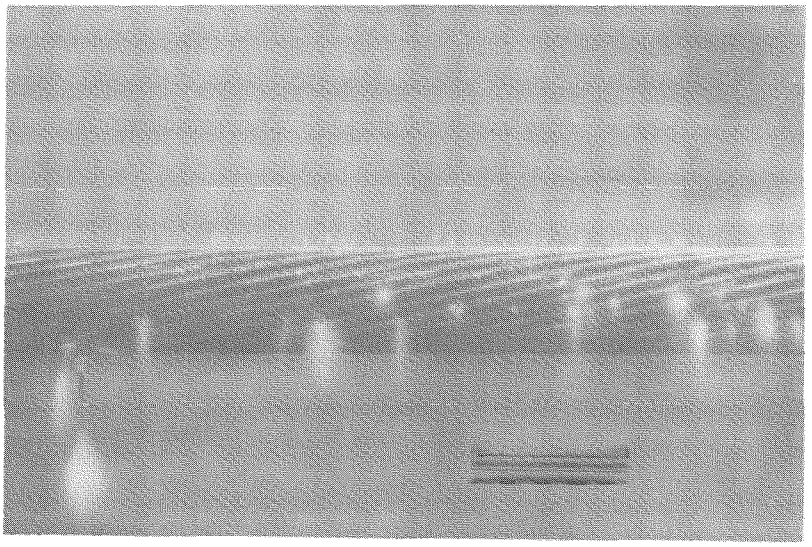


Figure 3-46. Appearance of an Untreated Wet Conductor in Corona (Maximum Gradient = 17 kV/cm)

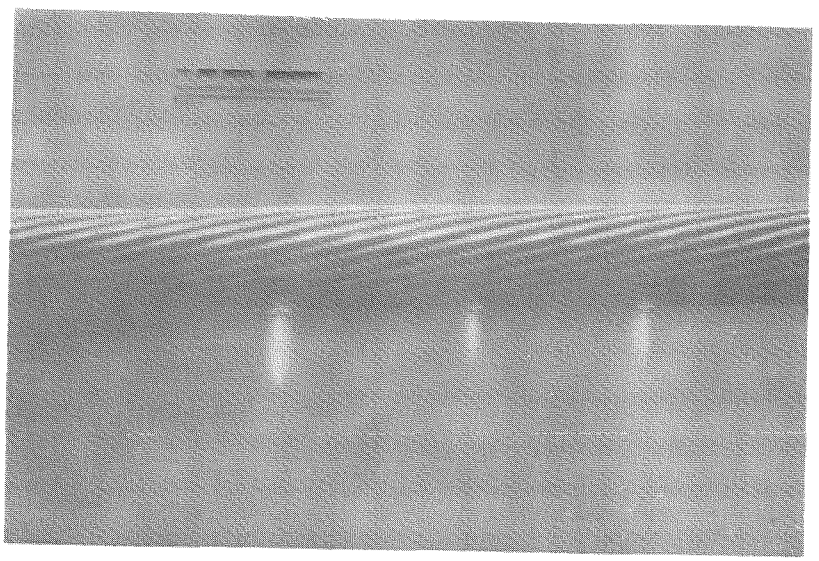


Figure 3-47. Appearance of Treated Wet Conductor in Corona (Maximum Gradient = 17 kV/cm)

ducing corona on those conductors to even lower levels.

The reduced corona activity associated with conductors which have been "aged" by exposure to the weather results in lower levels of audible and radio noise and corona loss. The extent to which these effects are reduced is a function of the degree of aging (i.e. the degree of surface wettability) and the gradient at which the conductors are operating. It has been repeatedly found at Project UHV that the achievable reduction increases as the gradient is decreased, this being particularly evident for light rain conditions. For a conductor configuration operating at a high gradient, little or no benefit might be derived through aging of the conductor.

Through suitable choice of the bundle geometry, the hydrophilic property of conductors can possibly be used to further advantage as described earlier in this report.

Natural vs. Artificial Aging. The aging process will occur naturally over a period of time which might be dependent on a number of factors such as the climate, the air quality and the presence of corona. One unpublished study indicated that, of many samples removed from transmission lines of varying ages, those exhibiting a good degree of aging had been in service (i.e. post energization) for 25 months or more. A sample which had 17 months of service still had noticeable beading of water droplets around the surface.

Generally, a utility will not be in a position where it can wait for the natural aging process to take place since greatest public awareness of the line and its effects will exist early in the life of the line. Consequently, the conductors must be designed for acceptable corona performance from the outset. However, it is conceivable that the benefits which could ultimately be derived through the natural aging process could be achieved by means of an "artificial aging" of the conductors sometime prior to their energization. For example, some chemical treatment of the conductors to produce a hydrophilic surface property could possibly be implemented at the time of manufacture. Any additional process, of course, will result in an increase in conductor cost which would have to be weighed against the cost of improving the corona performance a similar amount by the traditional approach of using larger or more conductors.

A number of experimental investigations were carried out at Project UHV to demonstrate that conductor treatments can result in significant reductions of audible noise. These were intended as feasibility studies only; no attempt was made to determine whether such treatments were economically viable.

The natural aging process was not systematically investigated. However, a special experiment was conducted to determine if the presence of corona could significantly contribute to the conductor aging.

Results of Tests on Artificially Aged Conductors. The potential benefit of artificial aging was demonstrated during the previous contract period. In those investigations the aging was accomplished by sandblasting the conductor surfaces. However, it has been observed that such a surface treatment does not truly reflect the properties of a naturally aged conductor since the desired hydrophilic property is obtained only after the conductor surface has been thoroughly wetted. It is clear that such a surface is not the solution for actual transmission line conductors.

These tests, although demonstrating the benefits, did not demonstrate the feasibility of an artificial aging process. The surface condition desired is one in which water flow is immediate for even the lightest of rainfalls.

A number of possibly suitable treatments were proposed by a conductor manufacturer. To evaluate these treatments a 3-stage program was formulated:

1) Short-sample testing
   Screening tests to select the most likely candidates. Tests made with short lengths of conductors in an indoor test cage.
2) Bundle testing
   Corona performance evaluation. Promising candidates determined by screening tests to be used on bundles of realistic dimensions and tested in outdoor test cage at representative levels of operating gradient.
3) Accelerated life testing
   Evaluation of the operating life of a treatment. Samples subjected to abnormal surface stress levels, under artificial rain, for a determined time period.

Stage 1 utilized an indoor test cage shown in figure 3-48. The corona photographs of figures 3-46 and 3-47 were taken during this investigation. The conductor of figure 3-47 was considered the most promising of all treatments, determined both qualitatively and quantitatively. Qualitatively, the treatments were evaluated

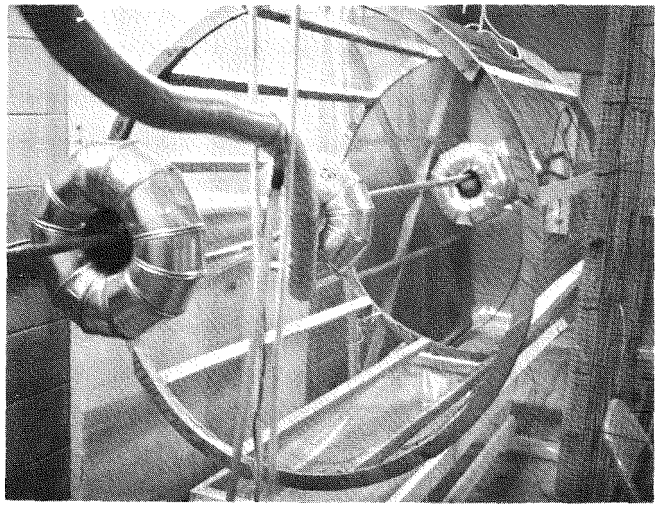


Figure 3-48. Test Cage Used for Screening Tests.

by visual observation of the formation of water drops on the surface of the conductors. Quantitatively, the evaluation was by a measure of the audible noise generation in artificial rain and after rain at 3 different gradients, 14.2, 15.6 and 17.0 kV/cm. At the highest gradient, the best performer had a heavy rain noise generation about 4 dB(A) less than the new conductor, while under wet-conductor conditions the generation was about 7 dB(A) less. Included in the evaluation were conductors whose surfaces had been treated by blasting with different grades of Alumina, by a degreasing agent and wire brushing, by vapor degreasing, by coating with a commercially available wetting agent, and by a variety of experimental finishes basically consisting of oxide coatings. Also evaluated was an "as manufactured" sample having no special treatment, and a commercially available non-specular conductor. The most promising treatment comprised an oxide coating formed in a mild alkaline solution, somewhat similar to an anodizing process.

The second stage of the program called for testing a bundled-conductor treated with this coating. A 6 x 2.96 x 76cm (6 x 1.165 x 30 in) bundle was selected for test. For comparison, a similar bundle of "as manufactured" conductors was tested. Conductors of this bundle had no special surface treatment, being of a condition similar to that of conductors newly received from the manufacturer.

It was apparent from visual observations that the initial delivery of treated conductors was dissimilar to the short sample which performed so well in the screening tests. It was felt that this was due to the slightly different formulation required to treat large lengths of conductor. Observations during rain showed that water drops did not flow easily on the conductor surface, although wetting was notably better than on the as-manufactured conductors.

A modified formulation was used to treat a second delivery of conductors, which exhibited an excellent water-wetting property, very similar to that of the short-sample. Quantitatively, as determined by audible-noise measurements, the performance of these latest conductors was far superior to the as-manufactured conductors. Results of tests are shown for as-manufactured, treated (batch 1), and treated (batch 2) conductors in figure 3-49.

Significant improvements in performance, particularly under wet-conductor conditions, were obtained by using the treated conductors. It is evident that the benefit to be gained diminishes with increased operating gradient. Such observations have been made on previous tests using sandblasted conductors. Gradients for typical 800-kV transmission lines using this bundle configuration would be in the range of 15-17 kV/cm.

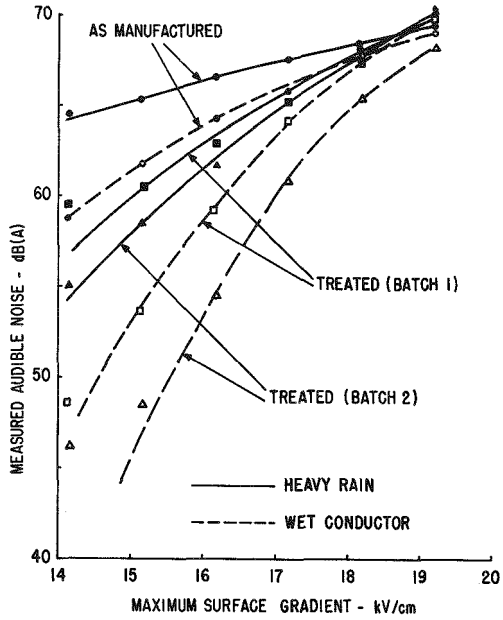


Figure 3-49. Comparison of Audible Noise Performance of "As Manufactured" and Treated 6-Conductor Bundles.

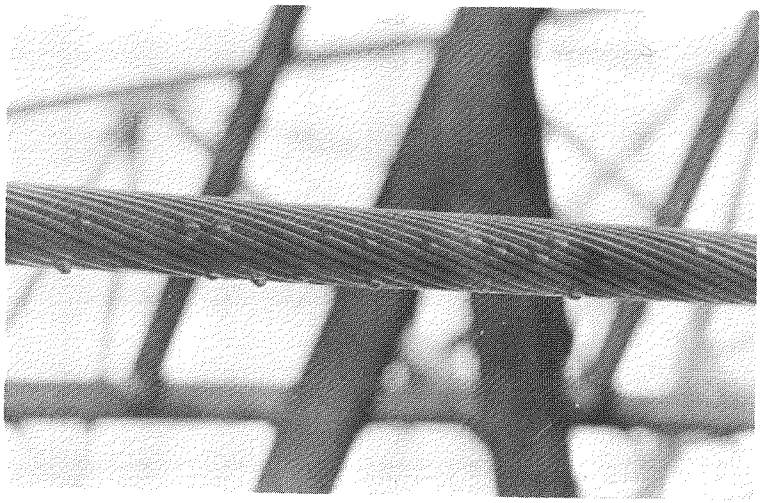
Quantitatively, the results confirmed previous findings that, if the hydrophilic property is achieved, reduced corona levels can be obtained. Further, qualitatively, these tests indicated that it is indeed feasible to treat the conductor in such a way that water-wetting is immediate. However, feasibility as demonstrated by these facts does not necessarily ensure practicality in terms of long-term application. An indication of this important aspect can be obtained by means of an accelerated life test, stage 3) of the program.

To simulate several months of normal operation, conductors strung in a triple-bundle arrangement, were subjected to a maximum gradient of 32 kV/cm for a period of 8 hours under artificial heavy rain. Based on calculations of the total kW of corona loss during this period, it was estimated that the accelerated test was equivalent to approximately 8 months of normal operation in a moderately wet climate such as in the Northeast United States. Each of the three surface conditions investigated in the bundle performance tests (stage 2) were represented in the accelerated life test.

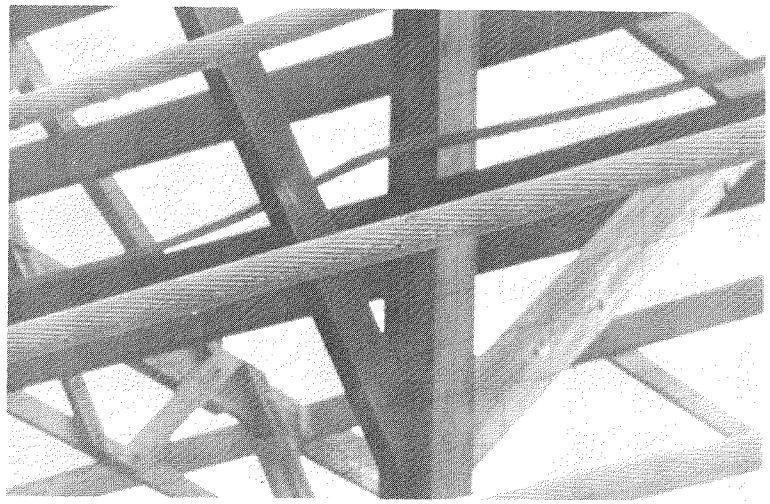
At the conclusion of the test it was observed visually that the properties of the treated surfaces had deteriorated to the point that there were few, if any, distinguishing features between these conductors and the as-manufactured conductors, a point which is clearly illustrated in figure 3-50.

The program demonstrated that the desired surface property can be achieved by a chemical process such as the oxide-coating described, but that such a treatment may not have the long life required for practical applications. Because of the large benefit to be gained from a good hydrophilic surface property, research into artificial aging should continue. Manufacturers should be encouraged to develop economically viable, long lasting treatments for future uhv transmission systems for which audible noise could be a limiting factor in the design of conductor configurations.

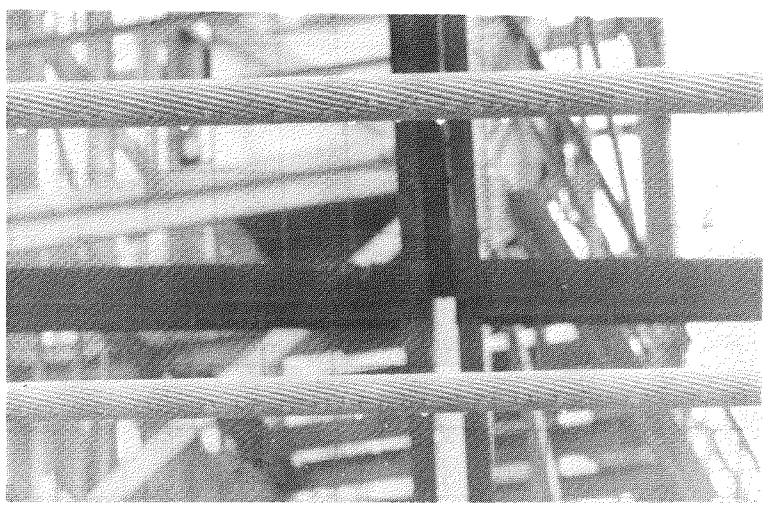
The Effect of Corona on Conductor Aging. It has been postulated that conductor aging is accelerated by the presence of corona; that a conductor which is exposed to the atmosphere but unenergized will take a longer period of time to age than a similar energized conductor. In an attempt to determine whether this is significant, an 8 x 3.3 x 102cm (8 x 1.302 x 40 in) bundle identical to that initially strung on the 3-phase line was subjected to 300 hours of energization under artificial



(a) Treated (batch 2)



(b) Treated (batch 1)



(c) As Manufactured

Figure 3-50. Formation of Water Drops on Conductors After Accelerated Life Test.

heavy rain conditions at a moderate-to-high surface gradient of 19 kV/cm. Periodically throughout the period, measurements of the corona performance were made.

Typical results are shown in figure 3-51. Measured noise levels for two gradients are presented relative to the heavy rain level recorded when the conductor surface was new. Results indicated that reduction in noise generation occurred from the outset of the aging period, with gains in performance attaining a maximum level after only about 50 hours of aging. Beyond that time, continued exposure of the conductor surfaces to corona had little effect on the corona performance of the conductors. Over the range of gradients tested (14-18 kV/cm), wet conductor performance was improved by 5-10 dB. Calculations of the 3-phase performance of this bundle at 1050 kV yielded levels approximately 5 dB below those determined for conditions of new conductors [calculations made for 15.3m (50 ft) phase spacing, 21.4m (70 ft) effective height - giving gradients of 16.5 kV/cm and 15.0 kV/cm for center and outer phases]. Subsequent cage tests on a 12-conductor bundle incorporating the 8 conductors subjected to this aging test resulted in data which, translated to a 3-phase line situation, were of the order of 10 dB lower than expected. Gradients for this case were in the region of 13-14 kV/cm.

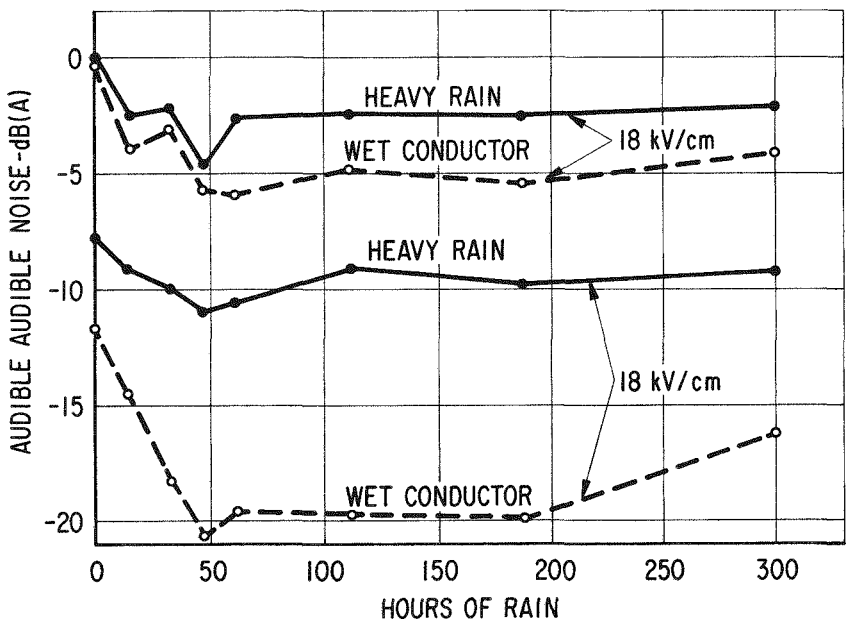


Figure 3-51. Variation of Audible Noise Throughout Accelerated Aging Period.

It is apparent that the conductors underwent some mechanism of aging, but it is not clear how the accelerated test reported here relates to actual operating conditions. If one considers the total kW·h of corona loss throughout the aging period, the 300h of testing could be related to 3-5 years of actual operation in a climate similar to that of the Northeast United States. The rate of rainfall produced was approximately 38 mm/h (1.5 in/h), so that in 300h of testing come 1143cm (450 in) of rain fell. For a moderately wet climate [normal annual precipitation of 127cm (50 in)] this would represent 9 years of exposure. However, the noise reduction occurred within the first 50h of the test which might be translated into 1-2 years of actual operation.

It is concluded that the presence of corona is a contributing factor to the aging process, but the extent to which it is practically significant was not satisfactorily determined. It is hoped that more information on this subject will be obtained when a retest of the original 8-conductor bundles will be performed on the 3-phase line, some 2 1/2 years after their initial energization.

Refinement of Design Rules

The k-Effect. In general the agreement between 3-phase line measurement and calculations according to the Reference Book [3-1] method have been found to be very good, and for the majority of cases no modifications to the design rules are suggested. However, it has been shown that the Reference Book approach does not adequately reflect the performance of bundles whose conductors have a very non-uniform distribution of surface gradient. The non-uniformity is measured in terms of k, the ratio of maximum subconductor surface gradient to average subconductor gradient. The Reference Book presents "base-case" design curves which give the audible noise levels for selected geometries for each voltage class. Additional "dB adder" curves are given to allow one to determine what adjustment to the base-case levels have to be made for variations from the base-case geometric parameters. For example, dB-adder curves to take account of changes in the bundle diameter are given; however, presently these reflect the effect of bundle diameter only in as much as variation of that parameter affects the maximum surface gradient; the "k-effect" is not accounted for, but could be incorporated into those curves. For a regular bundle (i.e. one whose subconductors are symmetrically spaced about the bundle circle), the k-value is practically the same for all subconductors. Typically, if the variation in the maximum gradient of the subconductors about the mean value is 3%, the variation in k is only of the order of ±0.5%.

Results of a special series of cage tests to determine noise generation as a function of the defining parameters gave information for $k \leq 1.35$. A typical set of curves derived from cage tests is shown in figure 3-52. For a given bundle gradient, the total noise generation of the bundle will increase with k but, according to the curves of figure 3-52, a leveling off of this increase would occur for k approaching 1.3. The maximum possible increase (for $\alpha = 0$) from the case k = 1.0 is seen to be only of the order of 5-6 dB. However, the results of 3-phase line tests on the 51cm (20 in) bundle indicated noise levels 10-14 dB higher than calculated. Since these 3-phase line data must be considered much more reliable than an extrapolation of the cage results to high k-values, any correction for the k-effect should be based on the line measurements.

The 12-conductor bundle was tested with 3 different bundle diameters: 51, 127 and 203cm (20, 50 and 80 in) corresponding to k-values, of 1.72, 1.29 and 1.18 respectively. In figure 3-53, the differences between measured and calculated noise levels are plotted against k. The differences indicated can be interpreted as correction factors to add to levels calculated according to the reference book. The few data points permit only a very rough correction factor, strictly applicable for the particular configuration tested. It is suggested that a linear correction factor be applied according to

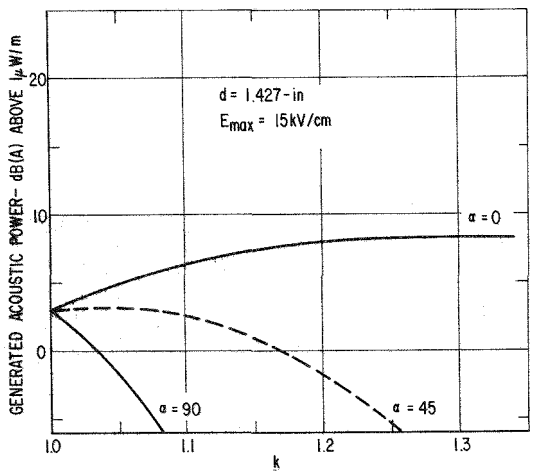
$$C_k = 20k - 24 \text{ dB} \tag{3-8}$$

for both L_5 and L_{50} (heavy-rain and wet-conductor) levels, k being determined from the bundle geometry,

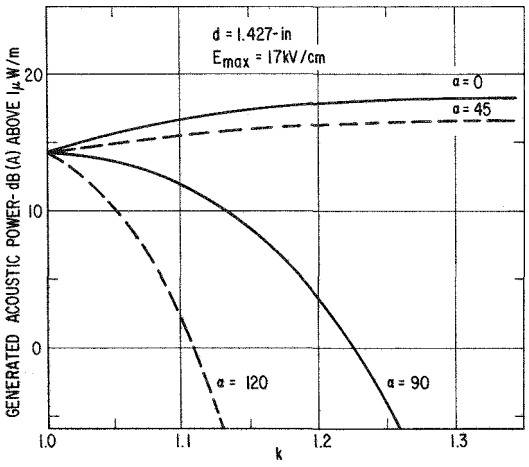
$$k = 1 + (n-1)\, d/D \tag{3-9}$$

where D is the bundle diameter. The correction should be applied only to multiconductor bundles with $n \geq 3$.

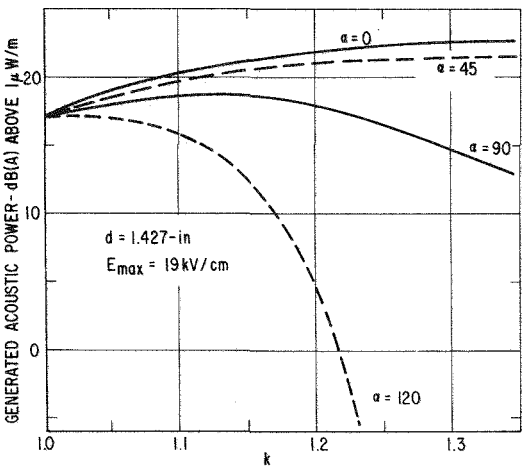
As an example of the effect of this correction, figures 3-54 and 3-55 compare the wet conductor "dB-adders" presented in the Reference Book for bundle-diameter variation of 1200 kV designs with new "dB-adders" corrected for the effect of k. The correction is clearly a function of both subconductor diameter and bundle diameter. For "normal" bundle diameters the effect is small. Apart from the pronounced effect for small k, the main effect is to increase somewhat the optimum bundle diameter.



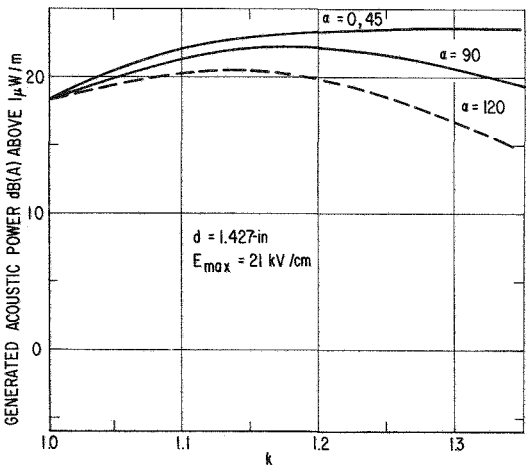
a) Max. Gradient 15 kV/cm



b) Max. Gradient 17 kV/cm



c) Max. Gradient 19 kV/cm



d) Max. Gradient 21 kV/cm

Figure 3-52. Wet Conductor Generation Versus k; Subconductor Diameter d = 1.427in; α = Angular Position of Water Drops Relative to Point of Maximum Gradient.

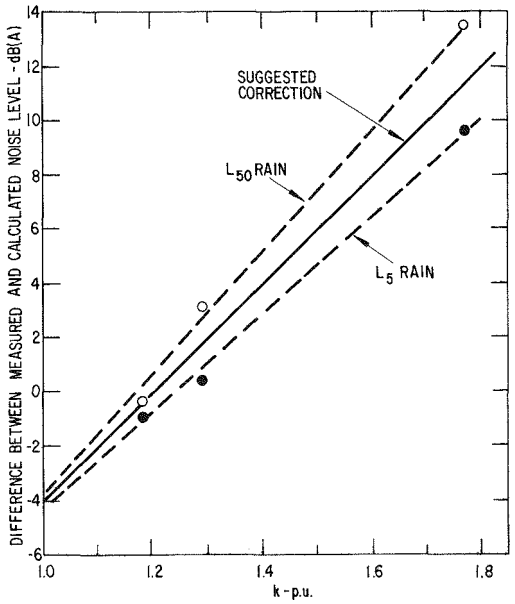


Figure 3-53. Difference Between Measured and Calculated Noise Levels: 12-Conductor Bundles.

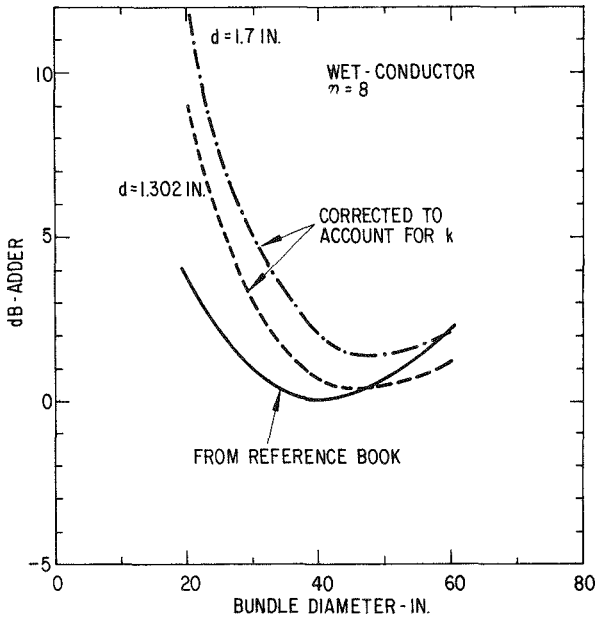


Figure 3-54. Variation of Audible Noise With Bundle Diameter: 8-Conductor Bundle; 1200 kV; Wet Conductor.

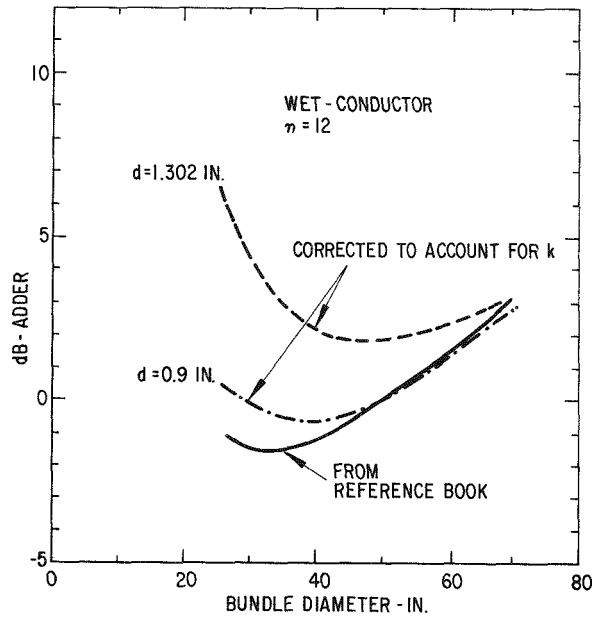


Figure 3-55. Variation of Audible Noise With Bundle Diameter: 12-Conductor Bundle; 1200 kV; Wet Conductor.

Air Absorption of Sound Energy. The sound pressure level attenuates away from a source due to 1) a divergence of the sound pressure waves, which for a line source results in a 3 dB attentuation per doubling of distance, and 2) absorption by the air of the sound energy. This latter effect is difficult to take into account analytically since the amount of absorption is a complex function of the frequency of the sound, the air temperature and the humidity, as illustrated by the experimental data [3-11] plotted in figure 3-56. For locations close to the transmission line the net effect of the sound absorption compared to that of the pressure wave divergence is small and little error is incurred if it is neglected entirely. At larger distances, however, the absorption effect becomes significant. For example, in going from 100m to 200m (330 ft to 666 ft) away from the line, the divergence effect would result in approximately 3 dB reduction in noise level (not exactly 3 dB due to the fact that the transmission line is not a true "line source") while over the 100m (330 ft) traversed the 4 kHz component of noise would be reduced by a further 3-4 dB and the 8 kHz component by a further 8-9 dB by air absorption [for 5°C (40°F), 90% relative humidity conditions].

Since the dB(A) measure is a composite of all frequency components it is only possible to specify an "A-weighted absorption coefficient" for a defined frequency spectrum of noise generated and for defined conditions of temperature and humidity.

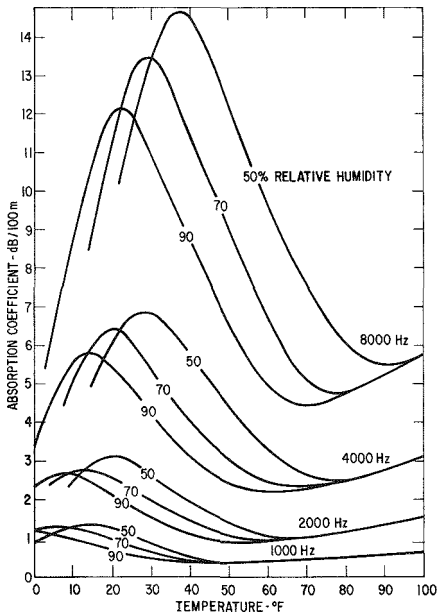


Figure 3-56. Variation of Air Absorption Coefficient With Frequency, Temperature and Humidity.

One can only make use of a "typical" value for calculation purposes. The Reference Book suggested that an absorption correction of 3.3 dB/100m (1 dB/100 ft) of distance traveled be used for calculations of A-weighted noise resulting from transmission line corona. It was subsequently found that this resulted in substantially lower levels than actually measured at large distances. A review of the situation has resulted in the use of 1.65 dB/100m (0.5 dB/100 ft) as a typical correction to be applied to account for air absorption.

RADIO INTERFERENCE

Interpreting Measurements of RI from Short Lines

For long transmission lines a condition of longitudinal uniformity of the radio interference (RI) field strength is approached. Measurements of RI frequency spectra at the center of one span will be essentially the same as those at the center of any other span provided 1) that the spans involved are sufficiently distant from an abrupt termination (such as a tee-point, or a substation termination) and 2) that the heights above ground of the conductors at the measuring locations are not significantly different. The frequency spectra will exhibit the characteristic of steadily decreasing level with increasing frequency. The use of rod and loop antennas practically result in the same field strength measurement, when expressed in terms of μV/m or dB above 1μV/m, irrespective of long-

itudinal location.

In the case of short lines, however, this situation does not exist. Due to reflections of corona-related voltages and currents at the line terminations, a standing wave pattern in the frequency spectrum is obtained. The spectrum is characterized by sharp peaks and broad valleys, the exact form being primarily dependent on the length of the line, the type of terminations, and the longitudinal location of the measuring point. For the idealized case of a perfectly horizontal single phase line with terminations which appear as open-circuits at radio-frequencies, the frequency spectrum at the exact center of the line is theoretically very well defined, with the sharp peaks occurring at regular intervals, at frequencies given by

$$f = n \cdot \frac{C}{L} \qquad n = 0,1,2,..... \tag{3-10}$$

for the electric field as measured by a vertical rod antenna, or

$$f = \left(\frac{2n + 1}{2}\right) \cdot \frac{C}{L} \qquad n = 0,1,2,..... \tag{3-11}$$

for the magnetic field as measured by a loop antenna, where C is the velocity of propagation of the voltages and currents, and L is the length of the line. For the 3-phase test line the resonant frequencies are approximately 0.6, 1.2, 1.8 MHz, etc., for electric field measurements. The minima of the broad valleys occur for frequencies mid-way between the frequencies of the peaks. For such an idealized case it can be demonstrated that the frequency spectrum of an infinitely long line of the same basic construction (conductor size, height above ground, etc.) coincides with the geometric mean, in terms of μV/m, of the successive maxima and minima of the short line spectrum. The standing-wave ratio, the ratio between maximum and minimum points, decreases with increasing line length as does the frequency interval between successive maxima and minima. If the RI field is expressed in terms of dB above 1μV/m, then the arithmetic mean in dB represents the long line value.

This approach which has been shown to be valid only for the idealized case cited, has nonetheless been adopted by several researchers for the case of three-phase lines. The application and validity of the approach was reviewed for 3-phase lines with generalized terminations. The analysis followed an approach similar to that of Perz [3-13] but extended to three-phase geometries. The details of the analysis are too lengthy to include in this report; however, the main results and conclusions can be outlined.

For the idealized case of perfectly open-circuit termination it was found that the geometric mean of the peaks and valleys of the frequency spectra did not coincide with the long-line frequency spectrum. The mean values were found to be some 2.5-3 dB higher than the long-line level, as indicated in figure 3-57. If, however, the total field is separated into each of its modal components, as shown in figure 3-58 for mode 1, it was found that the mean of maxima and minima do coincide precisely with the long-line spectrum for the respective modes. This latter finding is consistant with the findings of other researchers [3-13] who have considered the single-phase situation only, this being analagous to propagation of a single mode.

In practice, however, it is often difficult to approach the idealized open-circuited terminal condition. Generally one end of a test line (remote from the supply) can be considered an open circuit since the impedances of the terminations are very much greater than the mode surge impedances. At the supply end this may not be the case unless some special arrangement is made, such as the use of choke coils which offer a very high impedance to radio frequencies. Unless elaborate precautions are taken to eliminate the effects of stray capacitances, such a termination is likely to be less than perfect. With no special arrangement to make the end open, the termination will appear somewhere between an open circuit and a short circuit, and will be

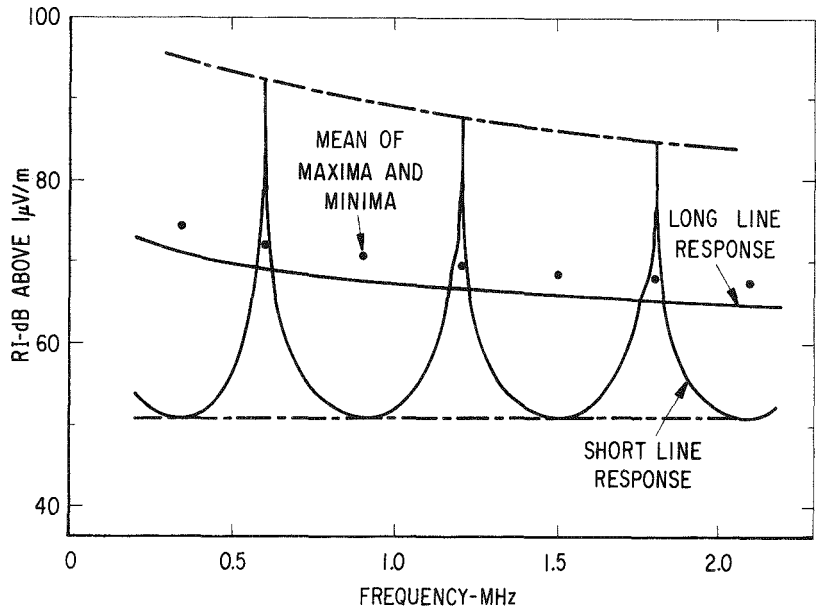


Figure 3-57. Comparison of Short Line and Long Line RI Frequency Spectra for Open Ended Terminations (Short Line Length ≈ 1625 ft).

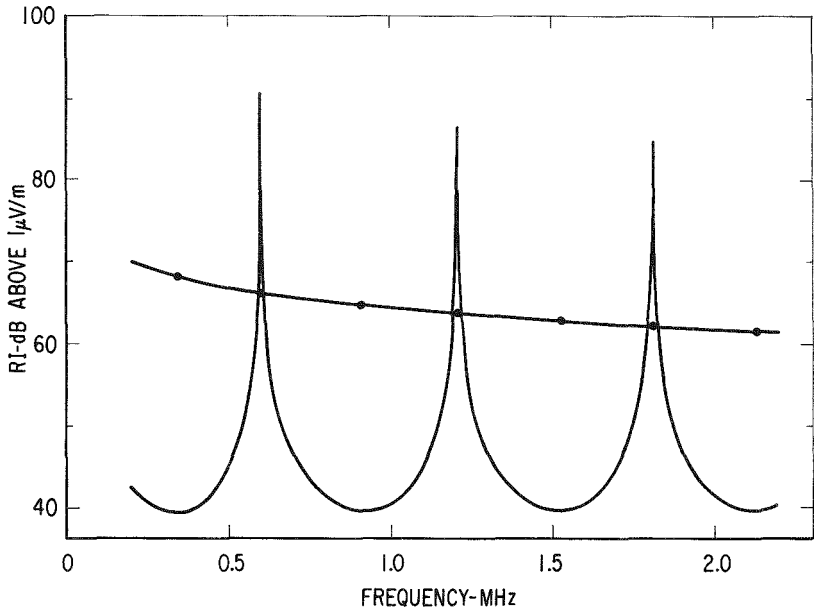


Figure 3-58. Mode 1 Contribution to RI of Figure 3-57.

predominantly reactive. It was found that the shape of the frequency spectrum of the short-line was dependent on the exact nature of the termination; often one would observe intermediate peaks of lower amplitude occurring between the major peaks. However, it was also found that, provided the termination was strictly reactive (capacitive or inductive) and contained no lossy elements, the relationship between the long-line spectrum and the mean of the minima and the major peaks of the short-line spectrum was very similar to the idealized case of open-circuit terminations. An example is shown in figure 3-59 for which one end of the line is considered open while the other is terminated in a capacitance of 100pF to ground on each phase. The mean of maxima and minima are again of the order of 2.5-3 dB above the long-line level. Further it was found that this same order of difference occurred for observer locations other than at the center of the line, even though the exact form of the frequency spectra may differ significantly from that of the idealized case of open-circuited terminations.

In practice the frequency spectra obtained will not be as well defined as those derived through a mathematical model. In part this is likely due to the non-ideal nature of the line. Varying height above ground, proximity effects at towers, types of line connections all add to the complexity of modeling of the line.

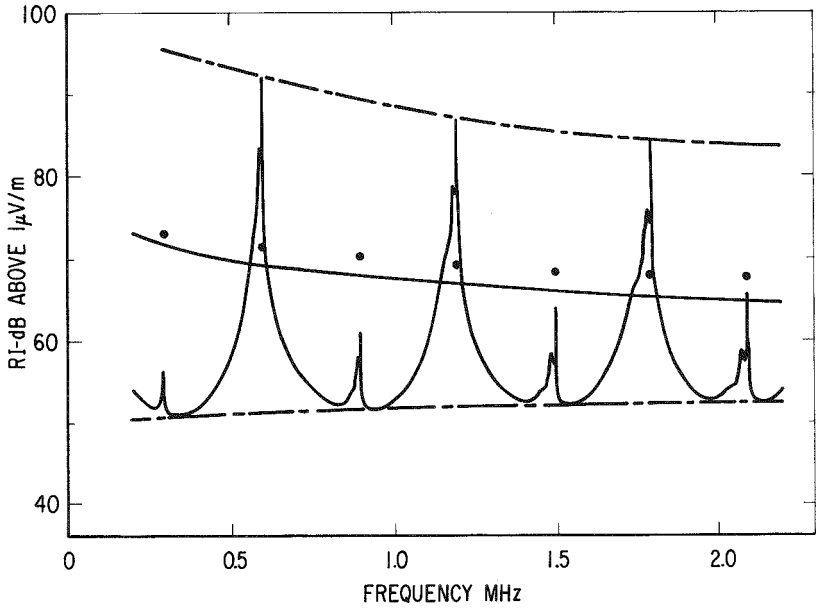


Figure 3-59. Comparison of Short Line and Long Line RI Frequency Spectra for One End Open and the Other End Terminated in 100 pF to Ground on Each Phase.

Notwithstanding these problems, it has been observed that the theoretical and practical cases have a great deal of commonality.

It is found in practice that the peaks of the spectrum are not as sharp as predicted by analysis due to the "smoothing" effect of the relatively wide bandwidth of the RI meter. This would have the tendency to lower the value of the mean of maxima and minima. For instance, a 6-8 dB smoothing of the peaks, which might be considered typical, results in a reduction of the mean level of 3-4 dB. This would then put the mean level close to the long-line value. The conversion from short-line to long-line could then be accomplished as follows:

1) Measure the RI frequency spectrum of the short-line, construct the best fit line through the minima and maxima and determine the mean level of these lines.

2) For the frequency of measurement, determine the difference $c_{s\ell}$ between the short-line spectrum level and the mean level determined in 1).

3) To measured levels of RI, add the factor $c_{s\ell}$ determined from 2); the result is the equivalent long-line RI level, for the particular frequency and conditions of measurement.

Results of Long-term Monitoring on 3-phase Line

The configurations tested on the 3-phase line have been previously described. For the 8-conductor bundles long-term measurements were made at a frequency of 1.035 MHz, close to a minimum in the frequency spectrum, using rod antennas factory tuned to this frequency. Tuning resulted in an antenna which was approximately 15-20 dB more sensitive than alternative broad-band rod or loop antennas. For the 12-conductor bundles, measurements were also made using a 42 x 36-in loop antenna for comparison with the measurements simultaneously obtained with the rod. The 1.035 MHz measuring frequency was maintained.

The South end of the line (remote from the supply) is dead-ended and not connected to any load, and consequently can be considered as an open-circuit to radio-frequency currents. At the supply end a choke-coil is inserted in the connection from the station to each phase (see figures 3-60 and 3-61). Calculations indicate that the inductance of this coil (265μH) provides a paralled resonance condition with the stray capacitance to ground (approximately 100 pF) at a frequency close to 1 MHz.

Eight-conductor bundles. Typical frequency spectra obtained at the mid-point of the line are shown in figure 3-62. It should be noted that in order to obtain RI

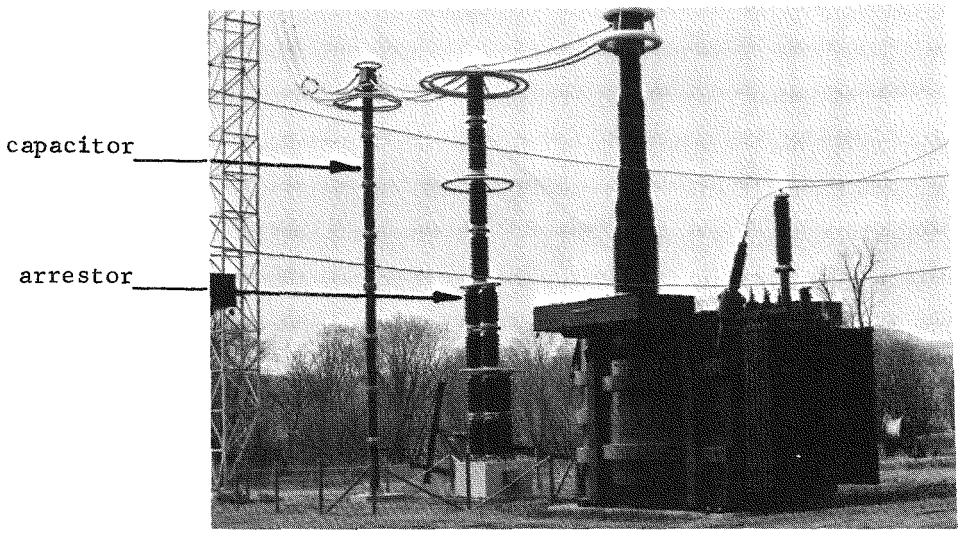


Figure 3-60. West-Phase UHV Station Showing Transformer, Surge Arrestor and Coupling Capacitor.

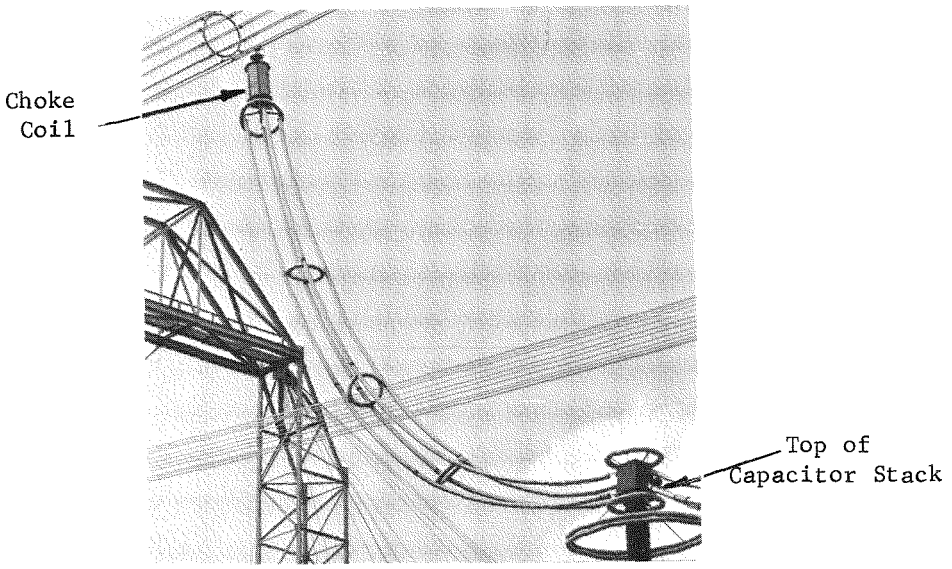


Figure 3-61. RI Choke Coil Connected Between Flexible Jumpers and Line Conductors.

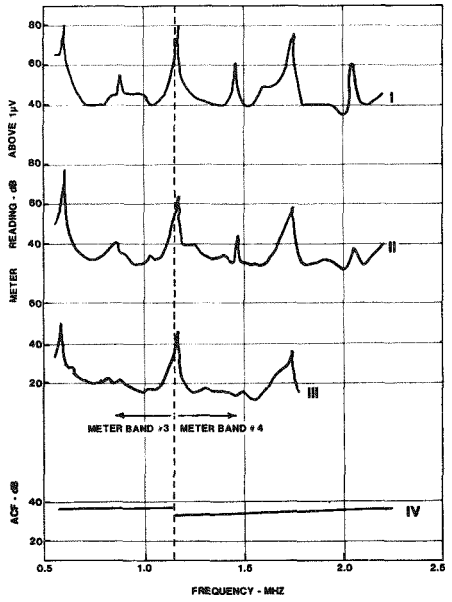


Figure 3-62. RI Frequency Spectra - 8-Conductor Bundle.

I, II 15.24m (50 ft) Phase Spacing, 1425 kV, Hot and Humid Weather, Meter #66AJ71, Rod Antenna Coupler #DC94.

III 19.81m (65 ft) Phase Spacing, 1300 kV, Sunny and Cold Weather, Meter #66AJ56, Rod Antenna Coupler #DC94.

IV Antenna Correction Factor for 104cm (41 in) Rod Antenna and Coupler #DC94.

levels sufficiently above ambient at all frequencies in fair weather it was found necessary to elevate the line voltage from its nominal value of 1050 kV. These are given in terms of meter readings in dB above 1μV; meter calibration was checked (using the internal calibrator provided) and adjusted if necessary before every reading. To obtain a spectrum in terms of dB above 1μV/m field strength the antenna correction factor must be added to the meter readings. After adjustment in this manner the best estimate of the short to long line conversion factor $c_{s\ell}$ was found to be ±12.5 dB for the 1.035 MHz measuring frequency. In the following, actual measured levels of RI are presented. It is necessary to add 12.5 dB to these to obtain the equivalent long-line value.

Figures 3-63 to 3-65 show statistical distributions of RI for the three different configurations tested. In all cases the measuring location is 32m (105 ft) laterally from the center phase of the line [it was convenient to fix the antenna at this location rather than adjusting the location for each configuration to correspond to the IEEE recommended location, i.e. 15m (50 ft) from an outside phase]. From the foul weather (rain and 100% RH) and all-weather curves, one can derive the fair-weather distribution. Since fair-weather periods outweigh, in terms of duration, the foul-weather periods by a factor of more than 7 to 1, the fair-

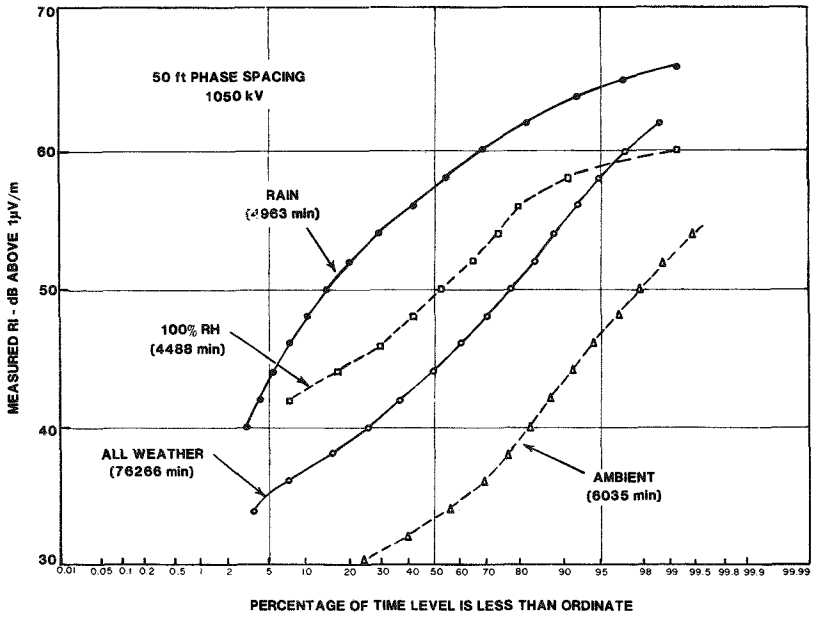


Figure 3-63. Cumulative Frequency Distribution of RI for Configuration 1 - Horizontal Configuration - 105 Feet Laterally From Center Phase.

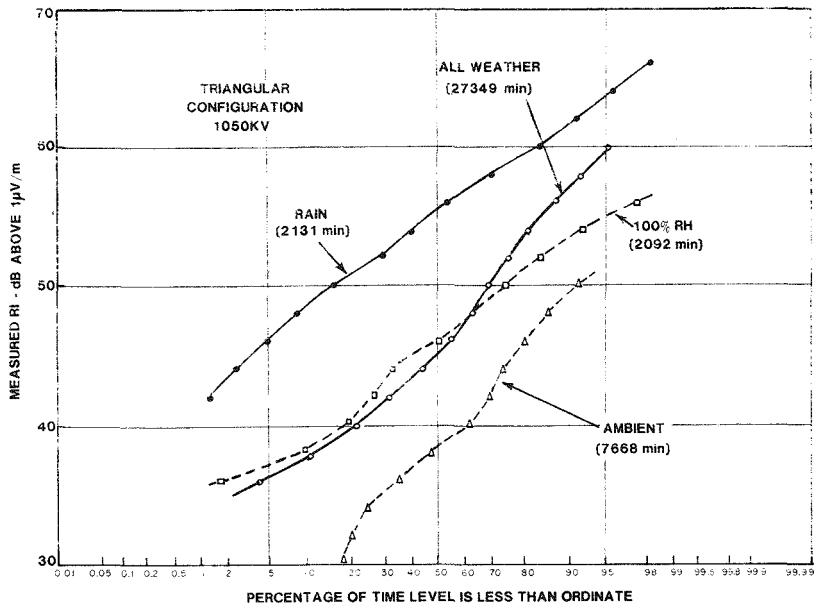


Figure 3-64. Cumulative Frequency Distributions of RI for Configuration 2-Triangular Configuration-105 ft Laterally from Center Phase.

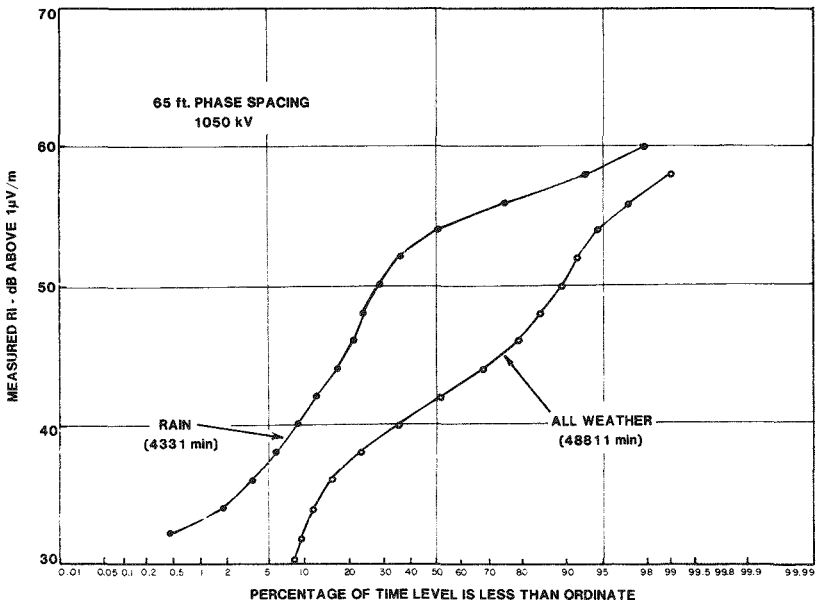


Figure 3-65. Cumulative Frequency Distributions of RI for Configuration 3-Horizontal Configuration-105 ft Laterally from Center Phase.

weather and all-weather curves are practically coincident except for the high percentage region (above the 80% point). For example, the 50% all-weather RI level from figure 3-63 is 44 dB above 1μV/m, while the 50% fair-weather level is 43.5 dB above 1μV/m. No significant fogs occurred during the test on the 19.8m (65 ft) phase spacing configuration and consequently no 100% RH data is presented for this case (figure 3-65). In addition, insufficient data were collected during periods of de-energization to provide a meaningful distribution for ambient conditions.

The measuring frequency of 1.035 MHz is mid-way between two AM broadcast carrier frequencies, 1.03 and 1.04 MHz. No radio station in the area transmits on these frequencies, the nearest station being WBZ in Boston, some 130 miles away, transmitting on 1.03 MHz. Since this is a powerful station (50,000W) we occasionally have "interference" from its broadcasts, this being particularly noticeable in the evening hours. However, as evidenced by figures 3-63 and 3-64, the noise produced by the line even in fair weather is sufficient to overcome any background "interference."

Translation of the measured levels to equivalent long-line levels is accomplished by means of the 12.5 dB adjustment factor described earlier.

Three different predicted levels can be derived from Chapter 5 of the Reference Book [3-1]; namely 1) "heavy rain," considered equivalent to the 99% foul weather level, 2) "wet conductor," considered equivalent to the 50% foul weather level, and 3) "average fair weather," taken to be 22 dB below the heavy rain value and equivalent to the 50% fair weather level. Data from figures 3-63 to 3-65 are translated to a long line value and compared with calculated values in Table 3-7.

The results are a mixture of rather poor agreement and rather good agreement. In all cases calculated levels are less than the values derived from field measurements. Best overall agreement is obtained for configuration 3, the 19.8m (65 ft) horizontal phase spacing. Best agreement within a category of weather occurs for the 50% foul weather/wet conductor comparison, where differences of less than 3 dB are noted. Differences between calculated and measured values of more than 4-5 dB are considered unacceptable. These occur in the 99% foul weather/heavy rain comparison for the first two configurations, and in the fair weather comparison for all configurations. In an attempt to rationalize the large differences occurring for the fair weather situation it may be noted that, during fair weather, insulator hardware on several

TABLE 3-7

COMPARISON OF RI DATA WITH CALCULATIONS - 8-CONDUCTOR BUNDLES-1050 kV

	1 (fig. 3-63)	2 (fig. 3-64)	3 (fig. 3-65)
99% foul weather	78.5 *	79.0 *	73.5 **
Calculated heavy rain	70.5	70.0	70.0
50% foul weather	69.5 *	68.0 *	66.5 **
Calculated wet conductor	67.0	65.5	64.0
50% fair weather	56.0	57.5	54.5
Calculated avg. fair weather	48.5	48.0	48.0

* combined rain and 100% RH
** rain only

All levels in dB above 1μV/m, quasi-peak.

suspension strings was audibly in corona and, at least to the ear, was more predominant than conductor corona. The hardware corona activity was more pronounced during tests on configurations 1 and 2 for which the phase spacings were smaller and voltage gradients correspondingly higher than for configuration 3. It may be noted that this corona activity exists even though the hardware has been equipped with shield rings.

In an attempt to rationalize the poor agreement between 99% foul weather and calculated heavy rain levels, it might be noted that the first two configurations (for which the poor agreement exists) were tested during periods of the year in which significant electrical storm activity occurs; namely July-September. Although obvious extreme and extraneous data were omitted from the analysis (during stormy weather RI levels would on occasion jump 10 dB or more for a short period of time without apparent reason and then return to a more stable level), it is possible that the upper parts of the statistical distributions are affected by non-line related RI, since for example the 99% point represents only 94 minutes for configuration 1 and 42 minutes for configuration 2.

These arguments were not entirely supported, however, by subsequent results of tests on the 12-conductor bundle which also point to higher noise levels than calculated although the conditions which would produce high ambient levels (i.e. electrical storms) were not in evidence.

Twelve-conductor Bundles. As of the writing of this report, tests on the 203cm (80 in) bundle were still in progress. However, sufficient data have been collected to provide meaningful statistics and results are therefore presented here. During the energization of the 51cm (20 in) bundle, the RI measurements appeared to be significantly influenced by the presence of a separate line strung under and to the West (in the direction of the RI antennas) of the 3-phase line. This stringing was conducted for purposes of research under a separate EPRI contract on the investigation of electric fields. During the periods of corona testing, the underbuilt line was left floating and consequently did not affect the line conductor gradients and corona generation. Audible noise measurements were not therefore affected by the presence of the underbuilt line, but it appears that the RI propagation and radiation characteristics were significantly affected. Consequently no RI data are presented for the 51cm (20 in) bundle.

Statistical distributions of RI measurements (with the loop antenna) for the 127cm (50 in) bundle are given in figure 3-66. The total number of minutes of data included in the analyses are given in Table 3-8. It is considered that the relatively few records obtained for 1150 kV causes that distribution to differ from those at 1300 kV and 1200 kV.

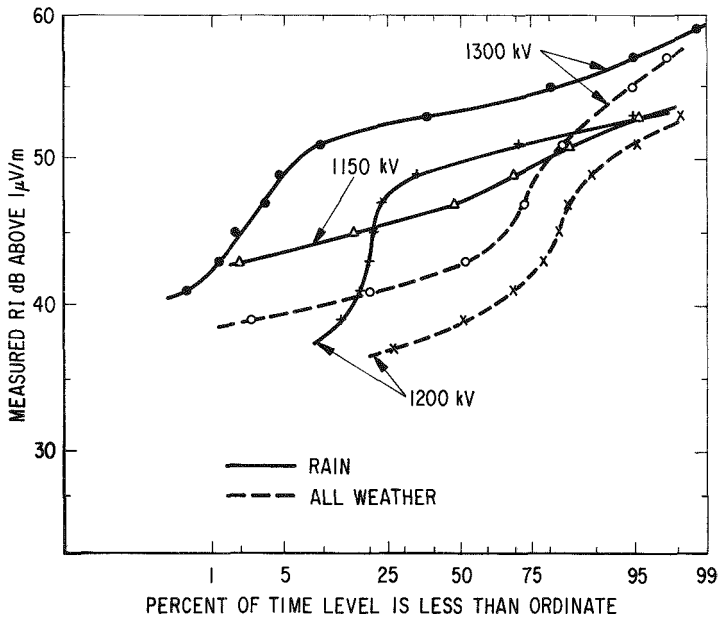


Figure 3-66. Cumulative Frequency Distributions of RI for 12-Conductor Bundle, 50 in Diameter, 105 ft Laterally from Center Phase, Loop Antenna.

TABLE 3-8

NUMBER OF MINUTES OF DATA COVERED BY DISTRIBUTION CURVES OF FIGURE 3-66

	Line Voltage		
	1300 kV	1200 kV	1150 kV
Rain	2227	2677	782 min.
All weather	30900	28900	- min.

The short to long line conversion factor for the loop antenna measurements was best estimated at 12.5 dB. The correspondence between this adjustment factor and that used earlier for rod antenna measurements arises from the fact that the long-term measurement frequency falls almost exactly mid-way between line resonant frequencies for magnetic field (loop-resonance at approximately 0.9 MHz) and electric field (rod-resonance at approximately 1.2 MHz). Levels taken from figure 3-66 are translated to the equivalent long line values and compared to calculated values in Table 3-9

TABLE 3-9

COMPARISON OF RI DATA WITH CALCULATIONS

12 x 3.3 x 127cm (12 x 1.302 x 50 in) BUNDLE

	Line Voltage		
	1300 kV	1200 kV	1150 kV
99% foul weather	72.5	66.5	66.5
Calculated heavy rain	67.0	63.5	61.0
50% foul weather	65.5	62.5	59.0
Calculated wet conductor	62.0	55.5	51.0
50% fair weather	55.0	51.0	-
Calculated Avg. fair weather	45.0	41.5	39.5

All levels in dB above 1μV/m, quasi-peak

Again the differences between measurements (translated to long-line levels) and calculations are significant. Overall, the levels appear to be some 6-7 dB on the high side. A reduction of all measurements by this amount would put all levels within 2-3 dB of calculated values. This suggests perhaps that the short to long line adjustment factor is different from that determined for this configuration.

RI as measured with the rod antenna is in fairly close agreement with loop antenna measurements for fair weather, but obvious differences occurred during foul weather,

as indicated by figure 3-67. The two antennas were located approximately 3m (10 ft) apart at the same lateral distance from the line. A similar result was obtained for RI measurements on the 203cm (80 in) diameter bundle. Figure 3-68 shows good agreement between the two antennas for fair weather, but during foul weather the rod resulted in higher levels than the loop. One possible reason for the difference between rod and loop in foul weather is that since the rod has an omnidirectional characteristic it might respond to noise emanating from station hardware approximately 230m (750 ft) away which is not conducted into the line because of the blocking effect of the RI chokes. The loop has a directional characteristic and is oriented for maximum response to the field produced by the radio frequency currents in the conductors. In fair weather the station noise is negligible, perhaps accounting for the better agreement between rod and loop measurements. To this point a certain amount of effort has been expended in reducing corona from station hardware; nevertheless, corona on shield rings and jumpers still persists during rain. An investigation to determine whether this could account for the observed differences between rod and loop will be undertaken.

Notwithstanding these differences, the measured noise levels when translated to long-line values still exceed the calculated levels by some 6-7 dB. For the 203cm (80 in) bundle, the 99% rain value is 69 dB compared to a calculated level of 63 dB

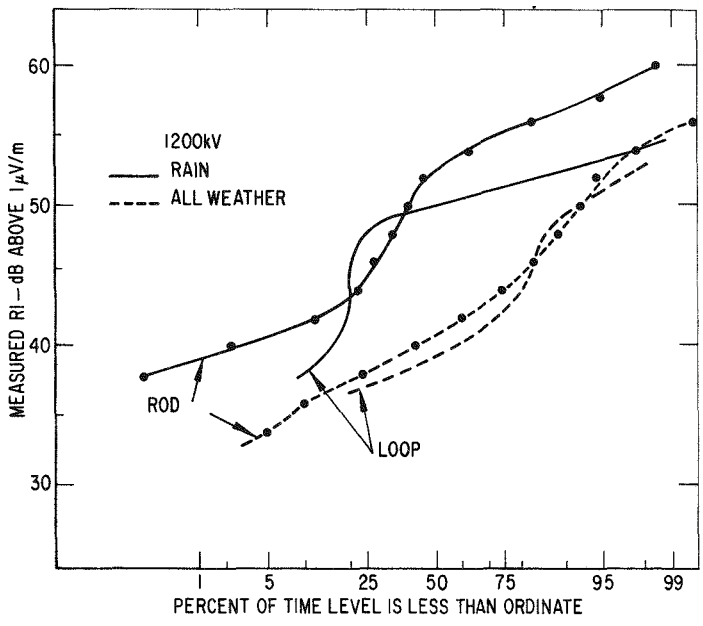


Figure 3-67. Comparison of RI Measurement Made With Rod and Loop Antennas for 12-Conductor Bundle, 50 in Diameter.

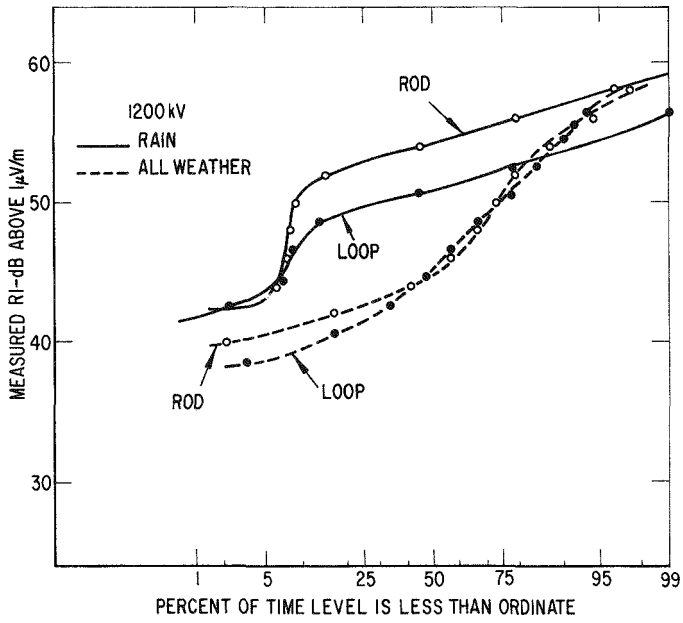


Figure 3-68. Comparison of RI Measurements Made With Rod and Loop Antennas for 12-Conductor Bundle, 20 in Diameter.

while the 50% rain value is 63 dB contrasted to 56 dB according to calculations. Investigations into the discrepancies are being continued. Special attention is being given to the methods by which the frequency spectra are measured and by which the short-to-long line correction factors are determined.

Correlation of RI with Audible Noise

It is generally considered that the positive streamer mode of corona is responsible for the broad band audible noise and the RI of transmission lines. If this is in fact the case one would expect a reasonable degree of correlation between the two quantities. Two situations can be investigated: 1) different weather conditions for fixed voltage, and 2) different voltage levels for fixed weather conditions.

Different Weather Conditions. Conditions which can be studied can generally be classified as fair weather, rain, fog, and snow. It is considered that other climatic variations such as air pressure and temperature have only a secondary effect on the corona generation for the range of these quantities encountered in a given location (an exception to this is the temperature during periods of snow, when temperatures near the freezing point will result in wet snow for which the generation can be considerably higher than in dry snow which is accompanied by much lower temperatures).

Within each weather category considerable variation in RI and audible noise levels can be experienced due, for instance, to variation in the rain intensity, the relative humidity, or the density of snow. In many instances a reasonably good one-for-one correlation between RI and audible noise was observed; that is for each dB variation in RI a corresponding 1 dB variation in audible noise occurred. An example for rain is shown in figures 3-69 and 3-70 (the 8 kHz rather than the dB(A) measure of audible noise has been used for reasons explained earlier). Rainfall is recorded in terms of the number of counts/min of a tipping bucket rain gauge, converted to rain rate in in/h (one tip of the gauge corresponds to 0.001 in of rainfall). The correlation is not always as well defined as this, however, as illustrated in figure 3-71 for fog and figure 3-72 for snow. Overall it would appear that the variation in RI is slightly less than that of audible noise for the same variation within a weather condition.

Different Voltage Levels. Information for this situation is available in the form of data recorded during short-term voltage runs where it was assumed that the weather conditions remained constant. Also of interest is the relationship between the median levels obtained from long-term tests of the same bundle at different voltages.

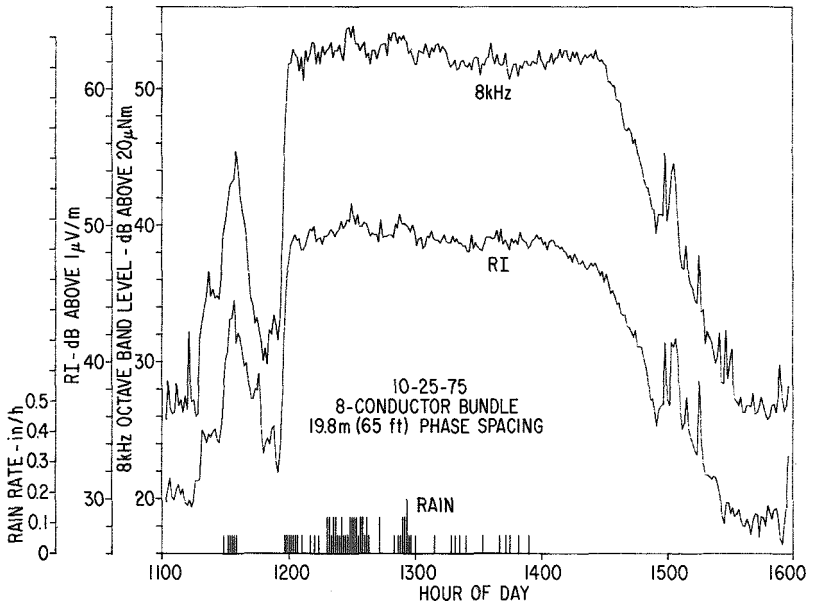


Figure 3-69. Variation of RI and Audible Noise Before, During and After a Rain Period.

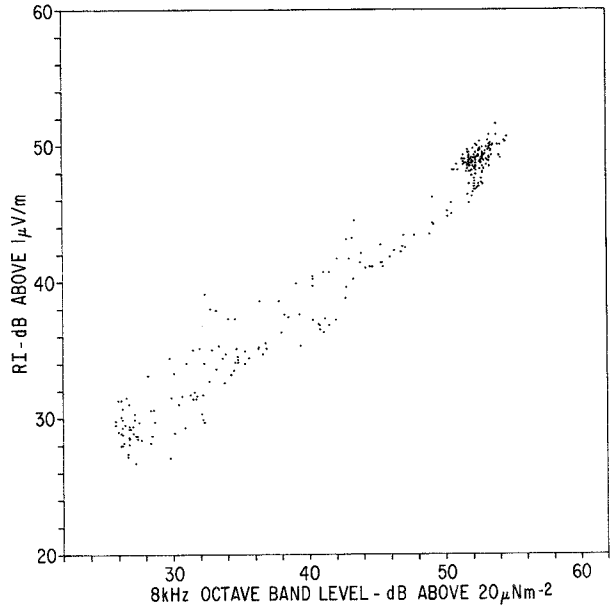


Figure 3-70. Correlation Between RI and Audible Noise for the Period Covered by figure 3-69.

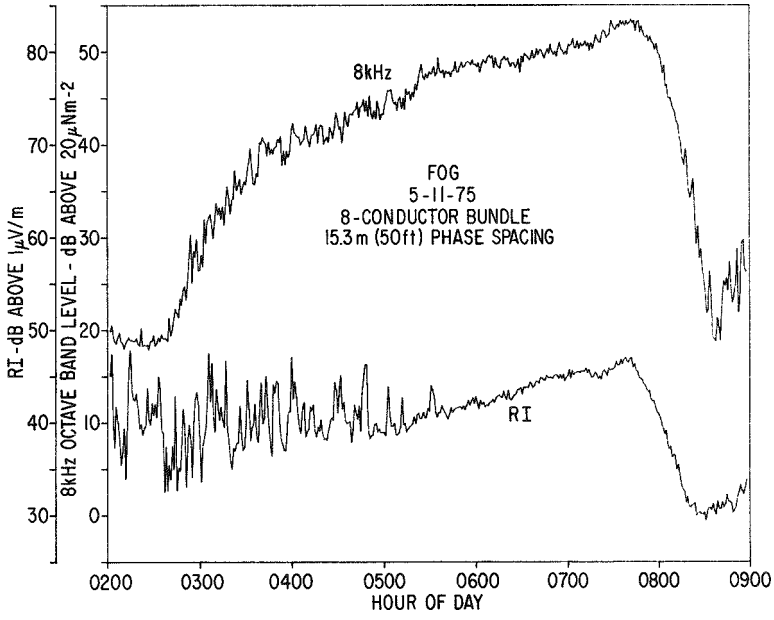


Figure 3-71. Variation of RI and Audible Noise During and After a Period of Fog.

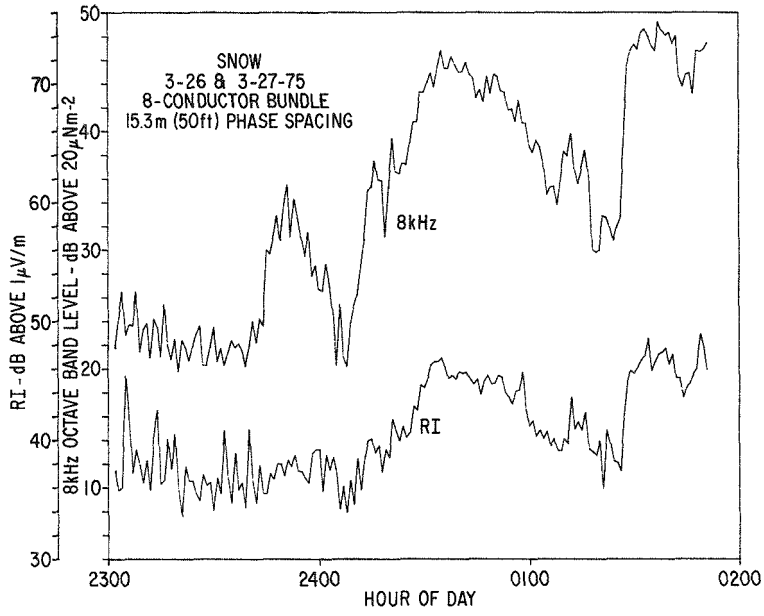


Figure 3-72. Variation of RI and Audible Noise During a Period of Snow.

An example of the short-term correlation is shown in figure 3-73 for conditions in which a fairly steady rain of 2.3 mm/h (0.09 in/h) was recorded. A good one-for-one correlation is noted. Figure 3-74 shows the comparison between long-term RI and audible noise for the 127cm (50 in) diameter, 12-conductor bundle which was tested at three different voltages. Here a good linear correlation is not obtained, although the voltage range covered, 1150-1300 kV, was identical to that of the short-term test reported in figure 3-73.

Observations which can be made on the basis of these few results are that for certain conditions, apparently those associated with well established corona generation, there is a reasonably good linear relationship, of slope 1 dB RI per 1 dB audible noise, while for other conditions where corona is less well established a linear relationship does not exist; in this latter case, a variation of less than 1 dB of RI accompanies each dB variation in audible noise. A more detailed investigation of a wider variation of conditions is required to determine whether these observations are generally valid.

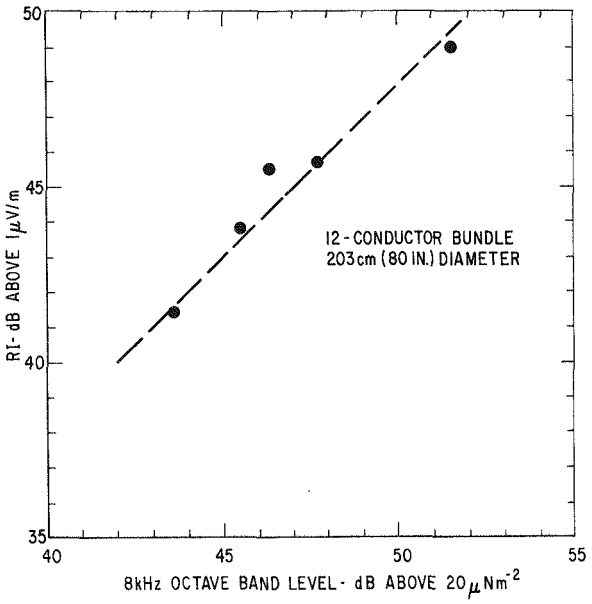


Figure 3-73. Correlation of RI and Audible Noise. Short Term Variations, Voltage Range 1150-1300 kV.

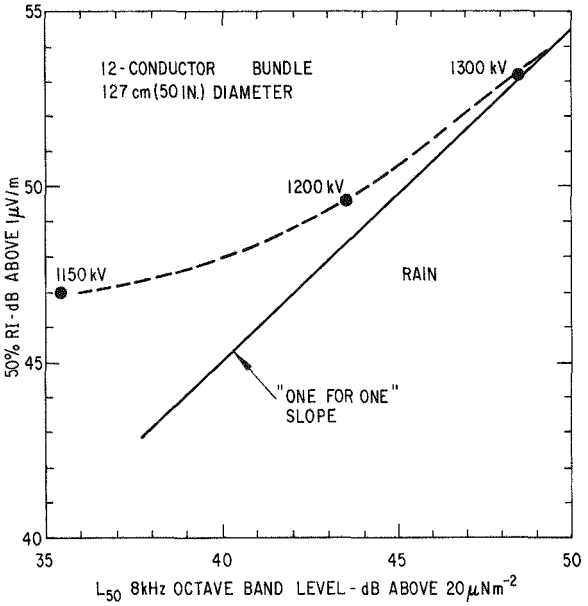


Figure 3-74. Correlation of RI and Audible Noise. Long Term Variations.

TELEVISION INTERFERENCE

It is generally considered that television interference (TVI) will not be a problem if the transmission line is designed for acceptable RI performance. There may be certain situations where this will not be the case, such as areas on the fringe of television signal areas. To design a line, or a section of a line, for such situations, which might be few and far between, would generally impose a severe economic penalty to the utility. Fortunately, any interference problems arising in these situations can often be ameliorated by relatively simple and inexpensive measures, such as relocating the user's antenna. Nevertheless, there is not yet sufficient evidence available to enable one to dismiss the TVI matter entirely.

In the Transmission Line Reference Book [3-1], it was noted that the suitability of available instrumentation to quantitatively assess the interfering effect of TVI was questionable. Some 3 years later, we find that the situation has not significantly changed. New instrumentation has become available, but for the most part this is based on standard principles. Notwithstanding this problem, an attempt was made at Project UHV to monitor the TVI performance of the various configurations of the 3-phase test line using commercially available instrumentation.

Instrumentation

A recent IEEE Committee Report [3-12] concluded that "presently available TVI instrumentation has as yet not been demonstrated to be adequate for measuring the annoyance quality of television interference." It was also suggested that efforts to prove or disprove their suitability should be undertaken. To this end, an IEEE Task Force is presently conducting a widespread subjective evaluation study, using recorded television signals with differing levels of superimposed gap and corona produced TVI obtained during a field trip from which data for the above mentioned report was obtained. While awaiting the outcome of this study, it is recommended that TVI measurement continue to be conducted using peak, quasi-peak and FI detectors of instruments which comply with current ANSI standards [3-13].

At Project UHV, three meters are used to accomplish this objective. Peak and quasi-peak measurements are made with Stoddart NM30A meters, while the FI (or average) noise value is measured with an Electrometrics EMC-25 meter. All three meters are fed from the same dipole antenna in the field via a broadband amplifier and low loss CATV cable and a 3-way signal splitter. The broad band dipole antenna for all measurements was located 61m (200 ft) laterally from the center phase at mid-span and oriented for maximum response to noise from the line (maximum response was obtained with the axis of the antenna elements oriented at approximately 90 degrees to the axes of the conductor bundles). 1200 kV transmission lines may require right-of-way of the order of 350-400 ft. The antenna location therefore represents a position near the edge of a typical right-of-way. Measurements were made at a frequency close to 75 MHz, the exact frequency being slightly different to this value due to a tuning for maximum meter response (the TVI frequency spectrum varies through successive peaks and valleys of some 5-8 dB peak-to-valley amplitude, this being due to reinforcement or cancellation of direct and ground reflected waves). The calibration of all meters accounted for the 6 dB loss experienced by each signal in passing through the 3-way splitter.

Three-Phase Line Testing

Several problems with the TVI measuring system were encountered during the periods covered by this report. Internal damage caused to the power supplies of the NM30A meters required factory repair, and on a separate occasion damaged input circuit boards also required repair, the net result of these situations being that data could not be collected for several months. The most complete data was obtained for the 8-conductor bundle with 19.8m (65 ft) phase spacing, for which over 3000 minutes of data were recorded during rain.

A general observation which could be made after examining all the data was that TVI resulting from line corona was, on a great many occasions, exceeded by the noise levels experienced in fair weather. In fair weather, when little corona activity exists, high noise levels are usually caused by spark discharges which can occur across small gaps formed for example by loosely connected hardware or by imperfect bonding between an insulator and its hardware. Much of this type of noise can be traced to lower voltage distribution system, and high levels of fair weather noise recorded near the 3-phase UHV test line are not necessarily attributable to the test line. This is demonstrated by the time-plots shown in figure 3-75. The configuration under test during the 6-day period shown was the 8-conductor bundle with 19.8m (65 ft) phase spacing. Quasi-peak (QP) TVI values are plotted along with the line voltage (nominally 1050 kV) and the rainfall. The QP values were found to be less erratic, in terms of short term variation, than the peak values. Here they have not been adjusted to account for antenna correction factor and cable loss and are therefore identified as "relative" levels. During the extended period of rain from 1900h on 10-18-75 to 0800h on 10-19-75 the relative QP level ranged from about 8 to 18 dB, while on occasion during fair weather levels of 25-30 dB were attained and levels 15-20 dB were quite common. It is interesting to note the wide variability of the noise particularly during 10-15-75 and up to the commencement of rain on 10-16-75. At the commencement of rain, however, the noise fluctuations were considerably reduced. Before rain, fluctuations of 10 dB or more from one moment to the next were not uncommon. During rain the short-term fluctuations were reduced in general to less than 5 dB. This can be explained by the following: during fair weather the noise is due to the spark discharges mentioned above; during rain, or periods of very high humidity, the small spark gaps become shorted out by moisture and the noise level drops considerably; as the rain continues the noise is a result of corona which occurs on the conductor and possibly on station hardware. As mentioned above, the fair weather noise may not be attributable to the test line. This is clearly indicated in the period from 0800h to 1600h on 10-16-75. For 75% of this time the line was deenergized without any noticeable reduction in the noise level.

Since it appears that the spark discharge noise is eliminated, or at least significantly reduced, during wet weather it is possible to analyze the TVI occurring during wet weather periods and attribute this to conductor corona. For the 8-conductor configuration mentioned, a statistical analysis of the rain periods yielded the results shown in Table 3-9.

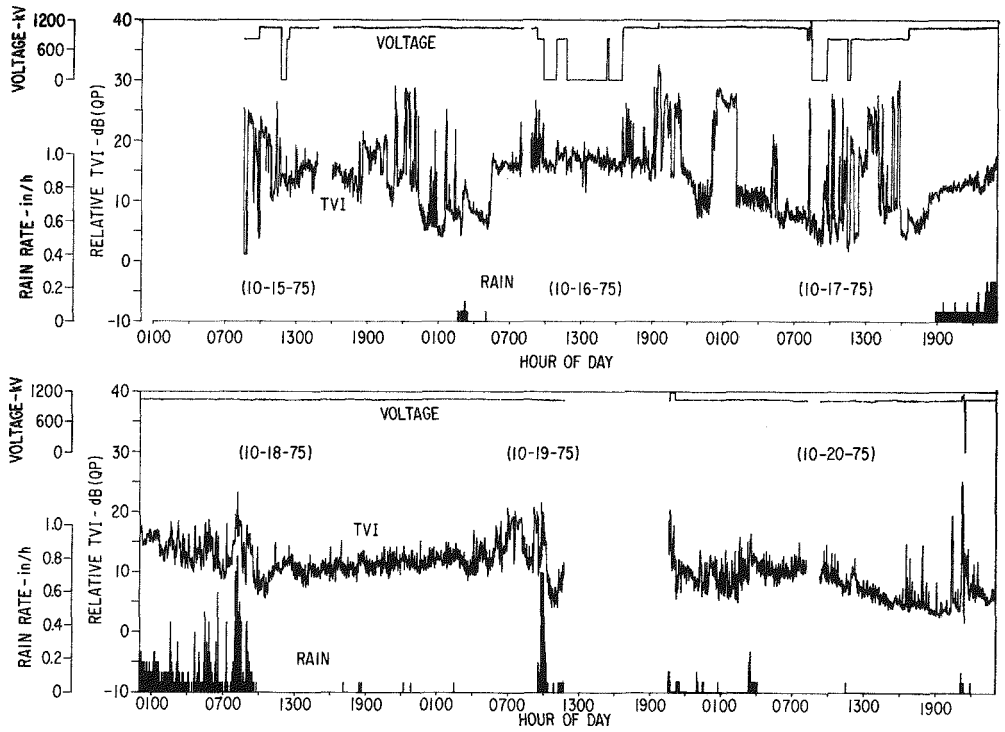


Figure 3-75. 6-Day Variation of Quasi-Peak TVI Levels; 8-Conductor Bundle, 65 ft Phase Spacing.

TABLE 3-10

RESULTS OF STATISTICAL ANALYSIS OF TVI DATA
RECORDED DURING RAIN FOR 8-CONDUCTOR BUNDLE, 19.8m (65 ft) PHASE SPACING

Probability Level	Detector Function Peak	QP	FI
99%	39.9	35.0	14.0
95%	35.0	30.5	12.0
75%	31.0	27.0	9.1
50%	28.1	25.1	6.8
25%	25.1	22.5	2.2
5%	12.6	14.6	-2.4
1%	6.4	12.5	-8.2

Total number of minutes = 3171

All levels in dB above 1μV/m = measured levels - $C_1 + C_2 + C_3$

C_1 = amplifier gain = 50 dB
C_2 = cable loss = 12 dB
C_3 = antenna factor = 6.6 dB
} at 75 MHz

The Reference Book [3-1] suggests that perhaps the best available means of calculating the TVI levels of a line (due to corona) is to assume that they vary linearly with RI levels. Then all one needs to determine is a conversion factor to apply to the various probability levels of RI to obtain corresponding levels of TVI. The conversion factor is a function of the bandwidth of the meter used for the measurement and the frequency of measurement. The bandwidth of the NM30A meters is nominally 150 kHz compared to the 5 kHz bandwidth of the RI meters, giving a bandwidth conversion factor, according to the Reference Book, of 20 log $\sqrt{150/5}$ = 14.8 dB. The noise level is assumed to fall off at the rate of 20 dB per frequency decade, such that the conversion from 1.035 MHz (used for RI measurements) to 75 MHz (used for TVI measurement) is -20 log (75/1.035) = -37.2 dB. One other factor needs to be taken into consideration, that being that the TVI measurements were made 29m (95 ft) further away from the line than were the RI measurements, accounting for a further reduction of approximately 14 dB according to the Reference Book. Thus the overall conversion factor is 14.8 - 37.2 - 14 = -36.4 dB. This quantity, added to the RI levels reported in a previous section should yield the TVI level reported here.

Applying the above to the RI levels reported for configuration 3 in Table 3-7, we obtain the results shown in Table 3-11. Considering the limited amount of information on which the suggested conversion between RI and TVI was based, the agreement seen here is remarkably good.

TABLE 3-11

COMPARISON OF TVI LEVELS DERIVED FROM RI MEASUREMENTS AND RI CALCULATIONS WITH TVI LEVELS ACTUALLY MEASURED

Condition	Level (dB)
99% foul weather[1]	37.1
Calculated heavy rain[2]	33.6
Measured 99% TVI	39.9 (peak) 35.0 (QP)
50% foul weather[1]	30.1
Calculated wet conductor[2]	27.6
Measured 50% TVI	28.1 (peak) 25.1 (QP)

[1]Derived from RI measurement

[2]Derived from Reference Book RI calculations

The Reference Book suggests that for better than "tolerable" reception within a television station's principal service community, TVI levels of 57 dB (peak) above 1μV/m, referred to a 3 MHz bandwidth, should not be exceeded. Translated to the 150 kHz bandwidth of the NM30A meters this would be 44 dB. The levels reported in Table 3-11 are well within this "limit", giving further indication that TVI arising from UHV transmission line corona will not be a general problem. However, for "fringe" areas, where lower signal strengths may be encountered, lesser amounts of TVI can be tolerated, and the levels given in Table 3-11 may result in less than acceptable reception during foul weather.

Table 3-10indicates a fairly constant difference, averaging about 19 dB, between QP and FI measurement over the complete range of probabilities. The difference between peak and QP is also reasonably constant over most of the range, this averaging about 3.5 dB. It should be borne in mind that these are long-term statistical values and that on the short-term the same differences may not be found, particularly between peak and QP since peak measurements are much more sensitive to spark discharges and isolated bursts of corona. Typical variations of peak, QP and FI levels during a period of rain are shown in figure 3-76, while figure 3-77 compares the variation of RI with QP and FI levels of TVI for the same period. Short-term variations of TVI appear somewhat greater than corresponding variations in RI. Even over the long-term there are indications that the correlation between TVI and RI may not be strictly one-for-one. For example, Table 3-11 indicates a difference between 99% and 50% RI in rain of 6-7 dB, while the corresponding difference in TVI is 10-11 dB. If we look at the relationship between the RI and TVI of figure 3-77, shown in figures 3-78 and 3-79, we also note that the correlation is not

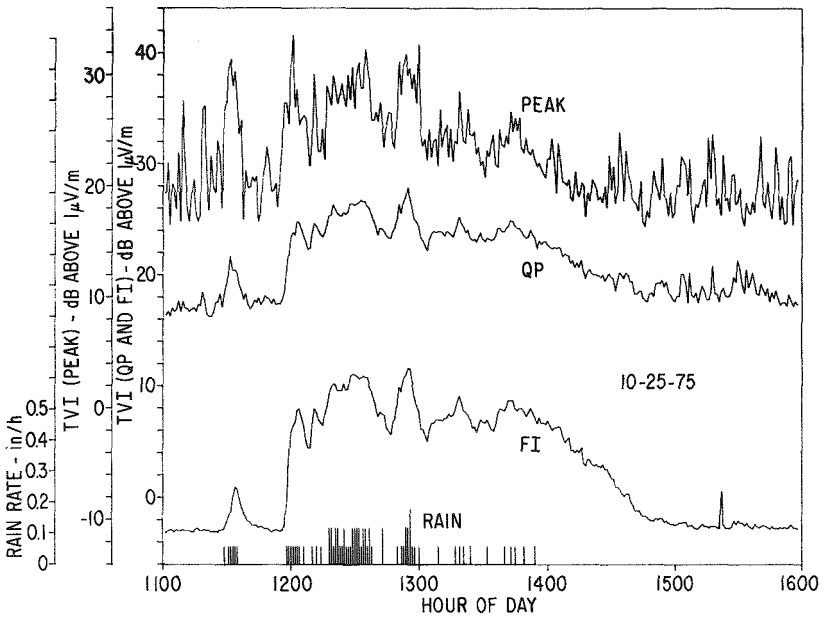


Figure 3-76. Variation of Peak, Quasi-Peak, and FI Levels of TVI During a Period of Rain; 8-Conductor Bundle, 65 ft Phase Spacing.

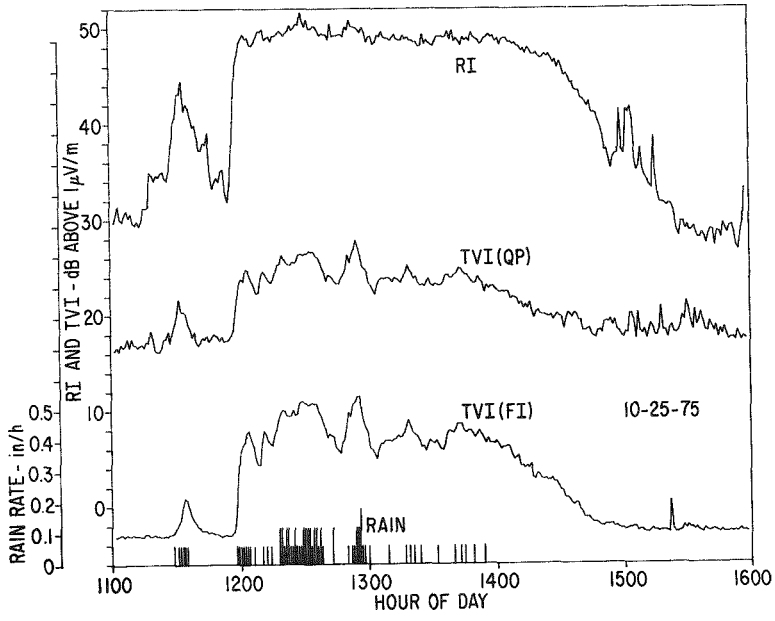


Figure 3-77. Comparison of RI and TVI Variations for Period Covered by Figure 3-76.

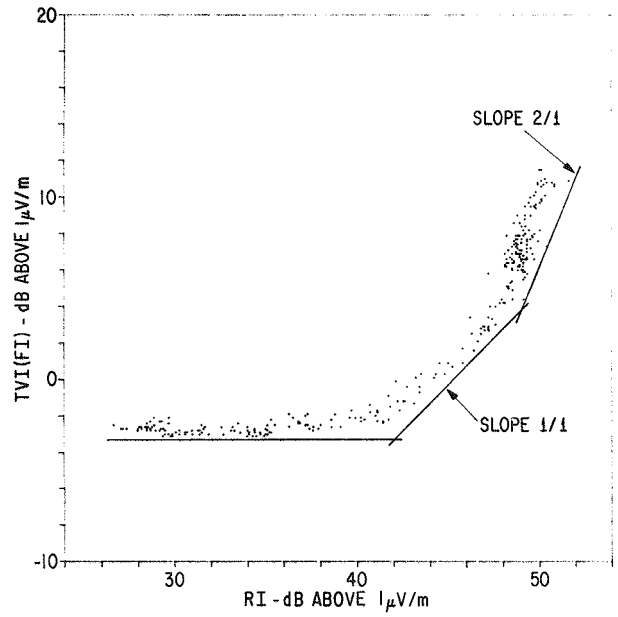


Figure 3-78. Correlation of RI With TVI (FI) for Period Covered by Figure 3-76.

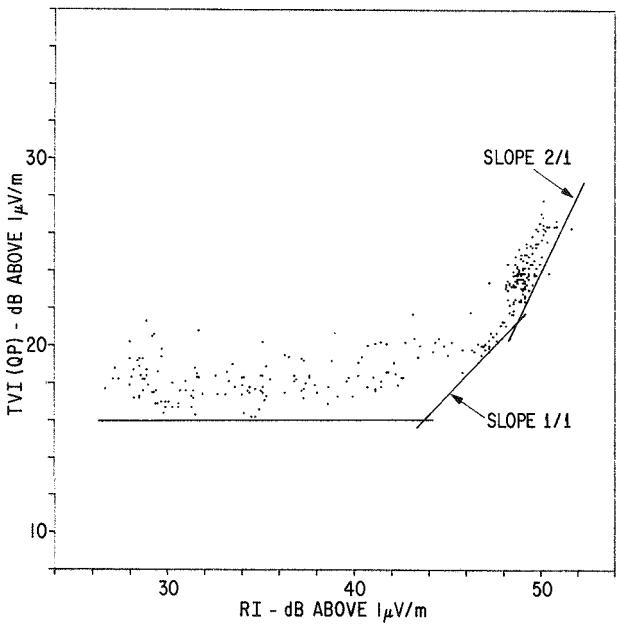


Figure 3-79. Correlation of RI With TVI (QP) for Period Covered by Figure 3-76.

one-for-one. In fact, there is an indication that the relationship varies, perhaps depending on the conditions of rain existing at the time. For instance, for the highest levels of RI and TVI the shape of the TVI/RI "curve" is about 2 dB TVI per 1 dB RI. The highest levels occur in the heaviest rains where water drops occurring at the conductors may result in microsparks between water drops and the conductors prior to physical contact. Such microsparks could result in higher levels of TVI than RI, the RI being predominantly from the positive corona streamer off the pendant water drops. For intermediate noise levels, the slope appears as if it might be more like 1 dB TVI per 1 dB RI, this occurring perhaps for lighter rains, or just after rain, when the microspark contribution is much reduced. For the lowest levels it appears as if the TVI levels are determined by factors other than line corona, and in the case of FI the lower levels are determined by the sensitivity threshold of the instrument.

CORONA LOSS

Corona loss is the power required for the movement of the ionized particles of air in the intense electric field which exists in the proximity of the conductors. It has been found [3-1] that corona loss increases with the line voltage proportionally less than the power transmitted, or the I^2R losses. Therefore, at ultrahigh voltages corona loss plays a diminishing role in the selection of conductor size and line geometry, which will be determined more by audible noise and radio noise requirements.

In addition, the ratio of fair-weather to foul-weather corona loss becomes very small at uhv levels, where corona loss in rain can be more than a hundred times greater than that in fair weather, with the results that fair weather loss will be insignificant for all practical purposes. Fair weather losses are not measured at Project UHV, because they are not considered important enough to justify the installation of the expensive precision instrumentation that would be required. The corona loss measuring system is calibrated (for zero loss reading) in fair weather at a low voltage, where no corona is present.

Three-Phase Line Testing

The corona loss measuring system which was installed on the Project UHV test line was based on the transmission of signals (proportional to the phase angle between voltage and current) from the UHV busses to receiving antennas on the ground. This was accomplished with three transmitters operating at different frequencies around 100 MHz. Unfortunately, the reliability of these transmitters has been

very poor, perhaps due to the very difficult environment (both physical and electrical) in which they have to operate. As a result, corona loss measurements have not been available for long periods of time.

Figure 3-80 shows the total loss of the test line, at 1050 kV, for two selected periods of rain. The bundle comprises 8 x 3.3cm (1.302 in) conductors, with phase spacing of 15.2m (50 ft). The loss varies rapidly and is sensitive to variations in rain intensity and wind. The average corona loss measured during the two periods of rain shown in figure 3-80 is approximately 160 kW/km (257 kW/mi). The maximum one-minute corona loss measured at 1050 kV was 375 kW/km (603 kW/mi), which occurred for a rain intensity of about 30mm/h (1.2 in/h).

Figure 3-81 shows the corona loss variations with line voltage for selected periods of rain and in fair weather. The figure shows that, for the 8-conductor bundle, the fair weather loss is negligible at voltages below 1250 kV. Figure 3-82 shows the total corona loss of the test line, at 1200 kV, for a bundle of 12 x 3.3cm (1.302 in), conductors measured during a period of rain.

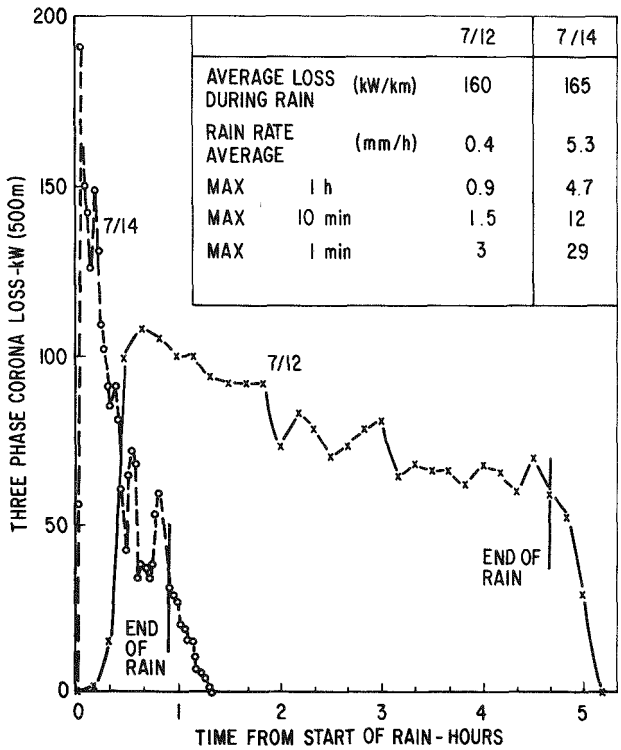


Figure 3-80. Corona Loss of the Test Line at 1050 kV in Two Different Periods of Rain, July 7 and 14, 1975.

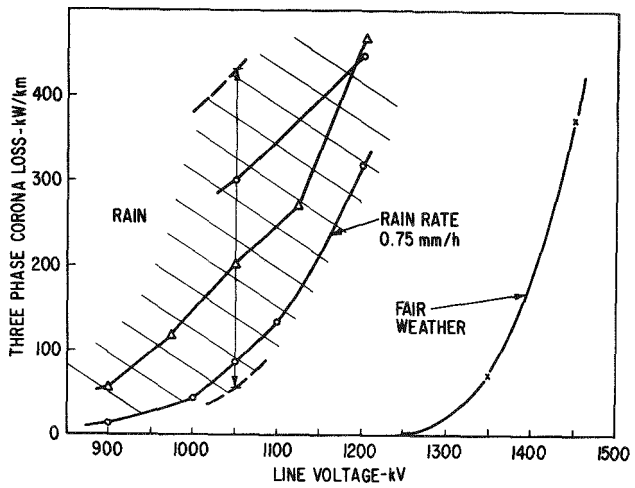


Figure 3-81. Corona Loss for Different Voltages and Weather Conditions for 8-Conductor Bundle, 15m (50 ft) Phase Spacing.

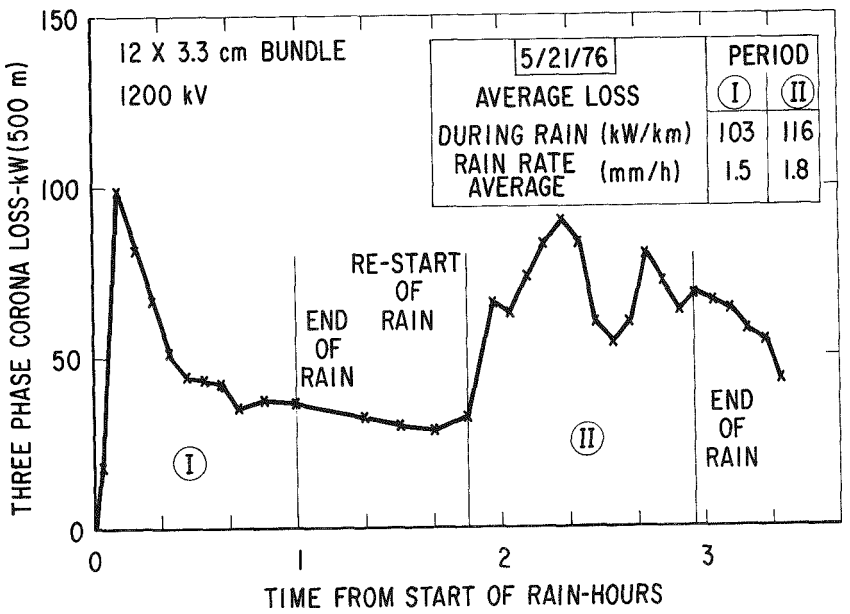


Figure 3-82. Three-Phase Corona Loss of the UHV Test Line at 1200 kV. 12-Conductor Bundle, 50 in Diameter.

Table 3-12 compares measured levels of corona loss with levels calculated for heavy rain, 12.5 - 25mm/h (0.5-1.0 in/h), according to the Reference Book [3-1]. The maximum corona loss of a long line, expressed for example in terms of W/m, is less than that of a single span due to the nonuniformity of the rain intensity along the line. The average loss measured during rain at Project UHV approaches the value calculated for a long line (maximum long line loss for the Northeast region). This shows that the procedures of Reference 3-1 can still provide a good estimate of the corona loss of UHV lines. This estimate is well within the dispersion of the data and the variability of the physical phenomenon of corona loss.

TABLE 3-12

COMPARISON OF MEASURED AND CALCULATED
CORONA LOSS LEVELS FOR 8- AND 12- CONDUCTOR BUNDLES

	kW/km	kW/mi	kW/km	kW/mi
Measured maximum loss	375	(603)	200	(322)
Measured average loss in rain	160	(257)	110	(177)
Calculated maximum loss (short section)	304	(489)	220	(354)
Calculated maximum loss (long line in Northeast)	225	(362)	162	(261)

OZONE

It has been established through laboratory tests that ozone is produced by corona on transmission line conductors. However reports of ozone monitoring near 765 kV power transmission lines [3-16, 3-17] indicated that no ozone produced by the lines could be detected. Tests performed at Project UHV have shown that ozone produced by corona on the three-phase UHV test line could be detected above ambient levels under certain special conditions. These tests utilized a chemiluminescence type ozone analyzer whereas less sensitive instrumentation was used for the previous field tests referred to. Although ozone generated by the test line has been detected, the levels have been found to be low and can be considered negligible compared to the normal ambient daily ozone variations. All indications are that these levels are not large enough to exceed the Environmental Protection Agency (EPA) standard for photochemical oxidants or to have any adverse effect on the environment.

The test set-up for monitoring ozone consisted of a 30m (100 ft) wood sampling pole located at quarter span of the center suspension span, positioned 34m (113 ft) laterally from the center phase of the line. Figure 3-83 shows the location of the wood pole near the UHV line. Sampling tubes have been installed on the pole at 29, 20, 9, and 2m (96, 66, 30 and 6 ft) above ground. Figure 3-84 shows the wood pole with the sampling tubes extending out. The height of the line at quarter span is approximately 23m (75 ft). The tubes are brought down the wood pole and into the ozone test trailer which is at the base of the sampling pole and is also shown in figure 3-83. Inside the trailer the sampling tubes are brought into the Meloy chemiluminescence ozone analyzer. This analyzer has a dc output proportional to the ozone concentration measured. This output is then recorded by the Data Acquisition System computer and, when desired, by a strip chart recorder.

Three-Phase Line Testing

Characteristics and Identification of Line Produced Ozone. Sample ozone recordings are presented in figures 3-85 to 3-92, which are copies of actual strip chart recordings for the 8 x 3.3cm (1.302 in) bundle geometry, 15.2m (50 ft) phase spacing. The strip chart recorder plots a reading proportional to the detected ozone concentration every 2 seconds. Gaps in the chart readings represent distinct sharp changes in the ozone concentration of the air being sampled. All recordings were taken with the 20m (66 ft) sensor, which is approximately at line height.

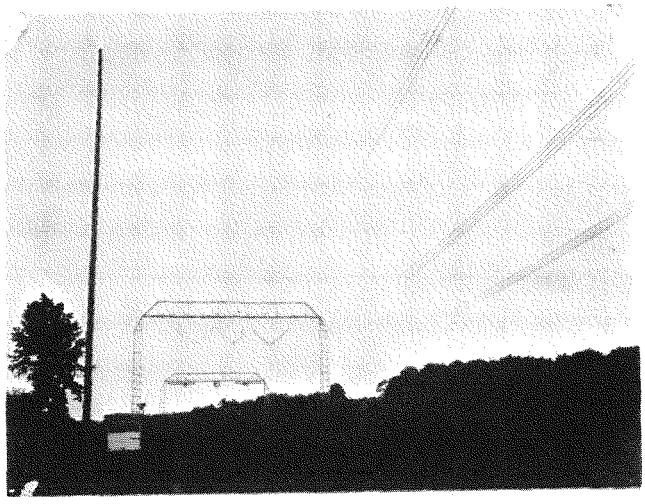


Figure 3-83. Ozone Test Pole, Trailer, and UHV Line.



Figure 3-84. Sampling Tubes Extending From Ozone Test Pole.

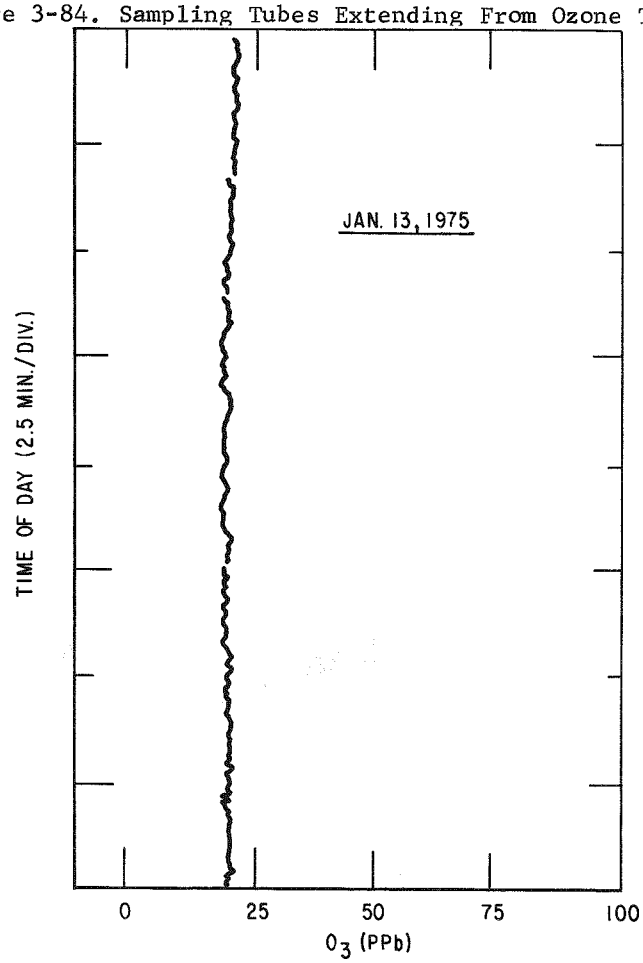


Figure 3-85. Ambient Ozone

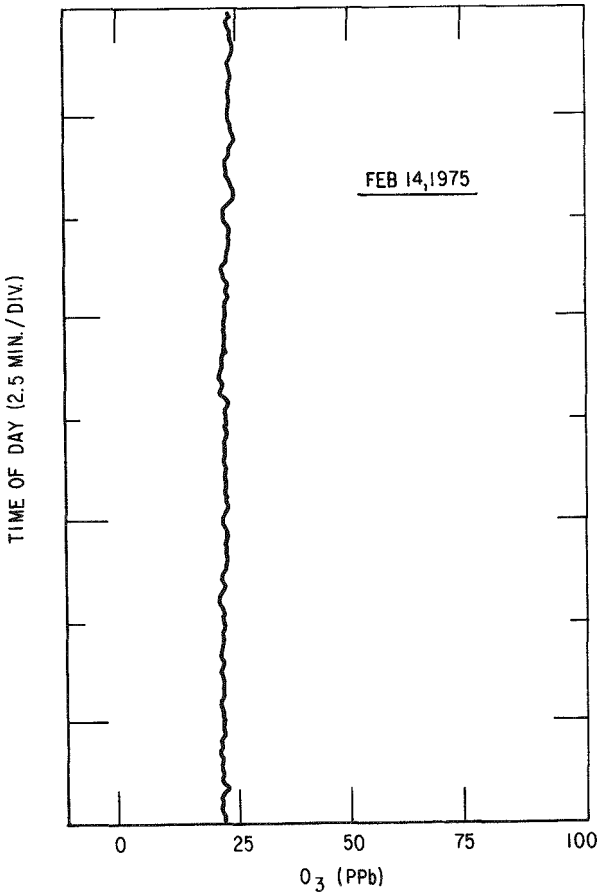


Figure 3-86. Ambient Ozone

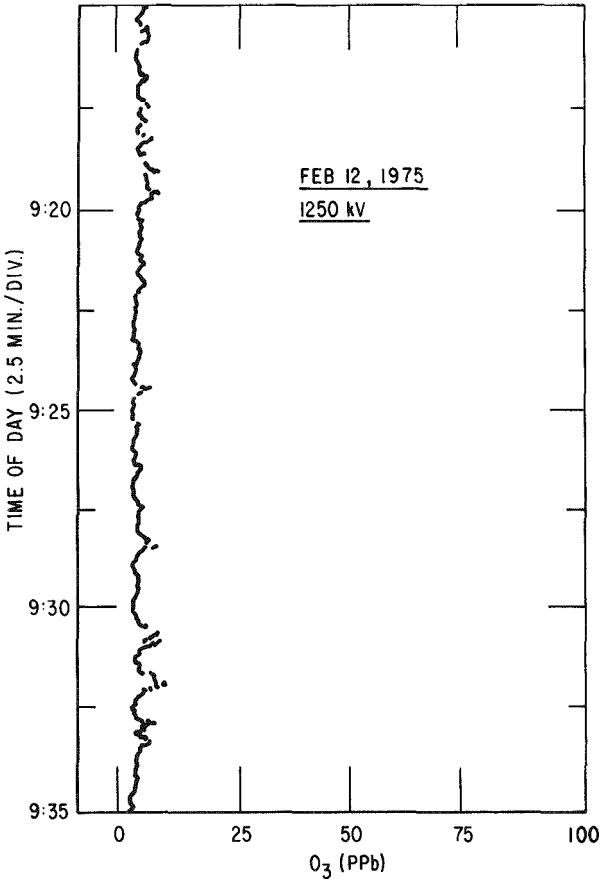


Figure 3-87. Detection of Ozone From the UHV Test Line.

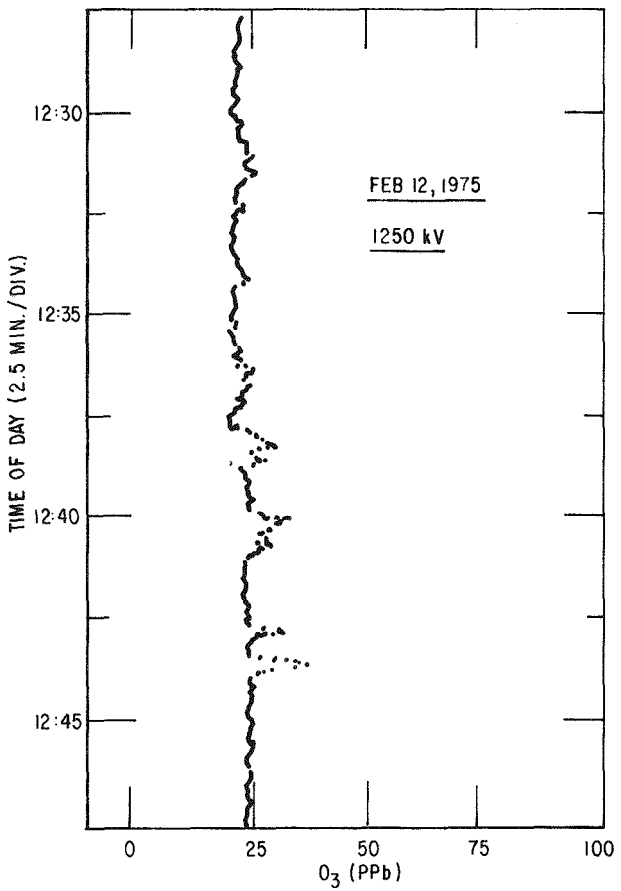


Figure 3-88. Detection of Ozone From the UHV Test Line.

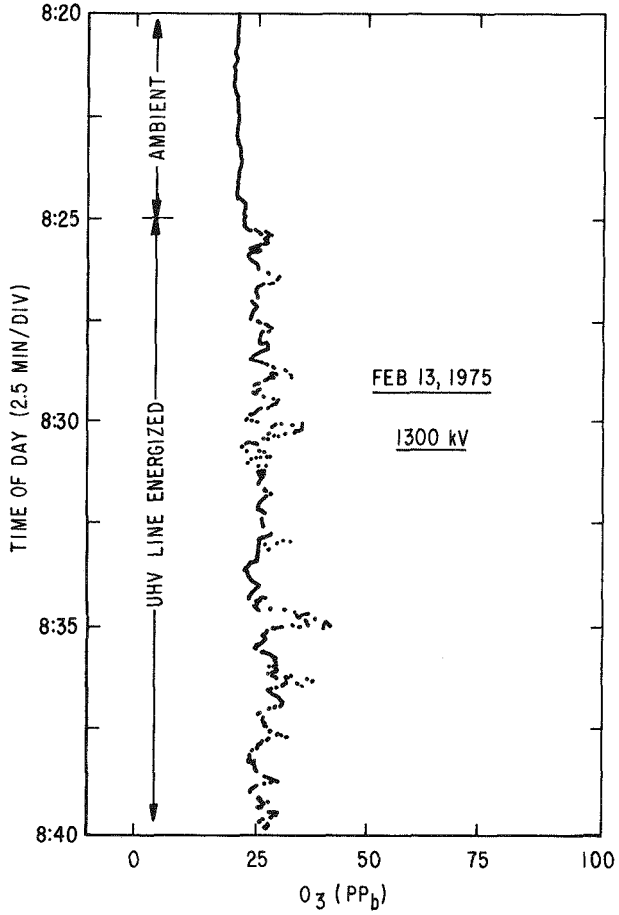


Figure 3-89. Detection of Ozone From the UHV Test Line.

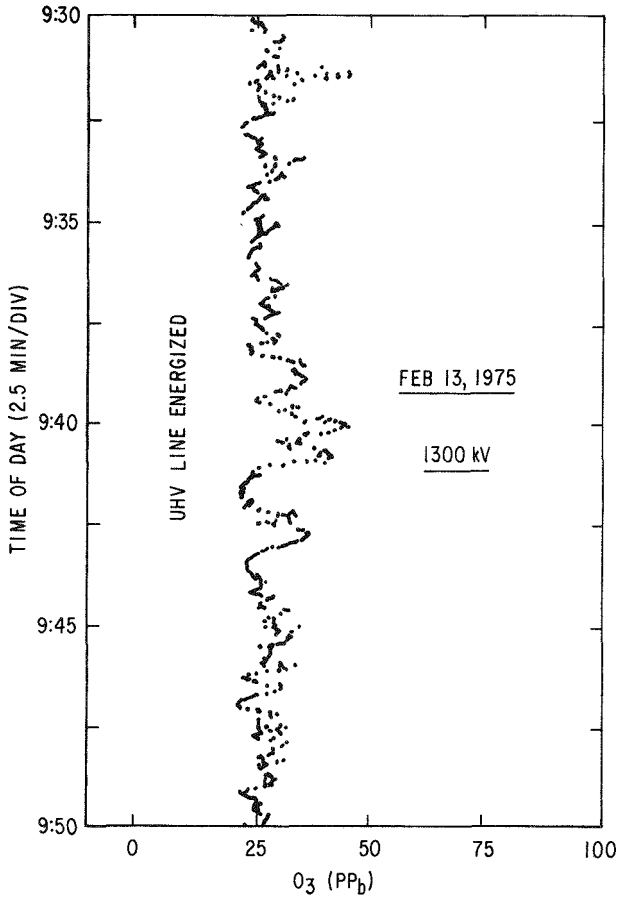


Figure 3-90. Detection of Ozone From the UHV Test Line.

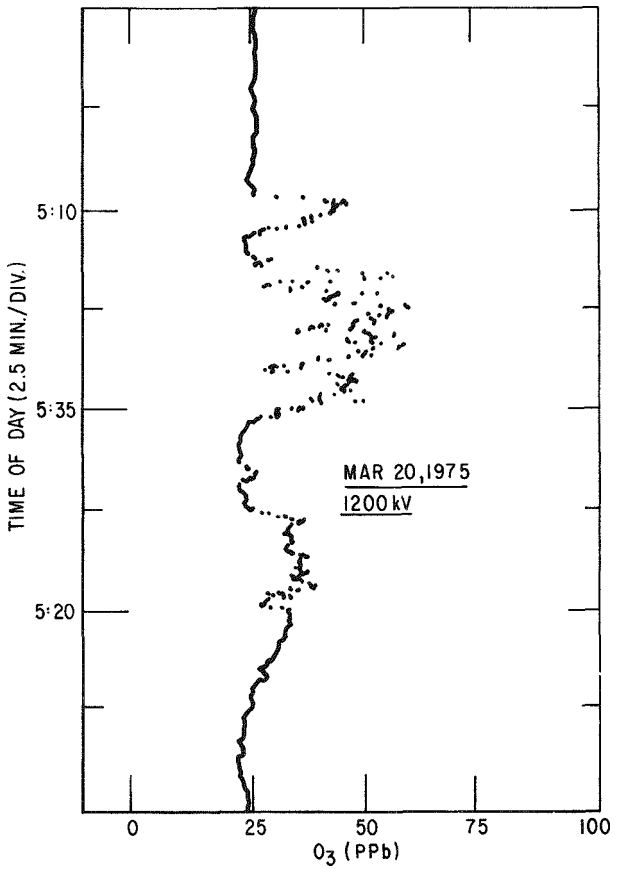


Figure 3-91. Detection of Ozone From the UHV Test Line in Calm Air.

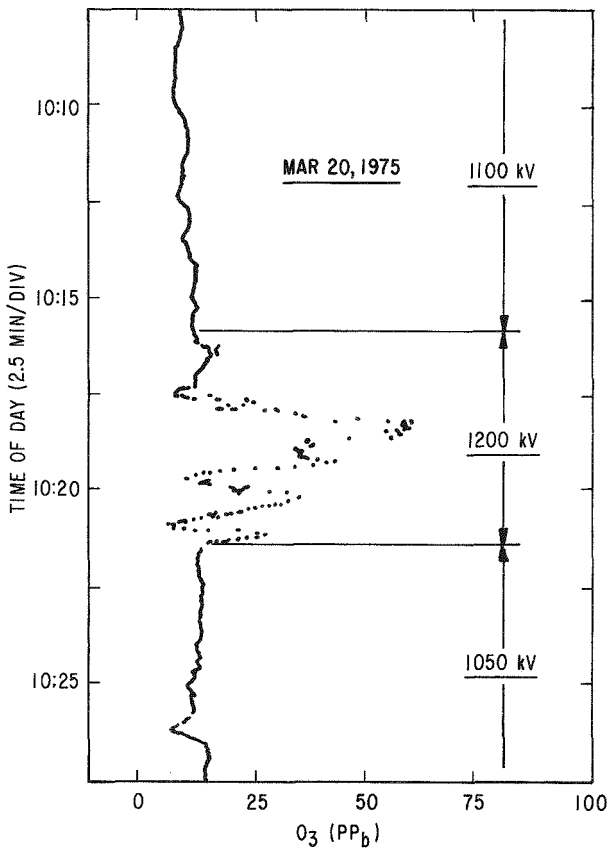


Figure 3-92. Detection of Ozone From the UHV Test Line in Calm Air.

Figures 3-85 and 3-86 are typical ambient ozone recordings. Very little fluctuation of the ozone concentration with time is observed.

Figures 3-87 and 3-88 indicate occasions when ozone generated by the test line was being detected. These recordings show a greater variation in the ozone levels. The recordings are composed of a series of peaks of short duration. This indicates that the sampled air contains pockets of ozone at concentrations in excess of the ambient.

Somewhat higher concentrations of ozone detected from the line are displayed in figures 3-89 and 3-90. These recordings are similar to those of figures 3-87 and 3-88 except that the peaks are larger and have a longer duration. The probable explanation of the higher levels is that the wind was less turbulent during these periods. Consequently the ozone pockets were not as dispersed as those of figures 3-87 and 3-88.

Figures 3-91 and 3-92 show instances of even higher levels of ozone produced by the line. These were obtained during periods when there was virtually no turbulence and only a very gentle breeze. Under calm conditions it is theorized that the pockets of ozone are dispersed much less than during more normal breezy conditions thereby resulting in higher levels of ozone above ambient.

Statistical Analysis. Analysis of strip chart recordings indicated that ozone concentrations above ambient can be detected only during short periods of time. The peaks of ozone do not appreciably affect the average values of the ozone concentration in a period of one hour. To analyze this point, the data acquisition system was used. The system collects a large number of measurements every minute. Among the data recorded is the average of a number of ozone readings. These average values were analyzed for periods of line energization and during periods when the line was not energized. The analysis was conducted for four different contitions.

1. No Westerly wind - Fair weather
2. No Westerly wind - Foul weather
3. Westerly wind - Fair weather
4. Westerly wind - Foul weather

- Westerly wind was defined as the wind generally perpendicular to the line (which has a general North-South direction) and blowing toward the ozone sensor at an angle between 45° and 135° (90° being perpendicular to the line).

- Foul weather was defined as the weather conditions causing an audible noise reading greater than 55 dB(A) under the center phase. This definition corresponds fairly well to the generation of corona from the line.

The resulting 50% levels obtained for the month of March 1975 are given in Tables 3-13 and 3-14. These figures indicate a possible contribution from corona on the line since the highest concentration occurred for the condition of line energization during foul weather with westerly wind (i.e. wind blowing from the line towards the sensor). The increase above average ambient or fair weather levels is in the order of 5ppb. Similar analyses for other test periods indicate increases above ambient, due to corona, in the range 2-5ppb. It is important to recognize that these results are based on measurements close to the line [19m (63 ft) from the nearest phase] and at line height [20m (66 ft) at the quarter span point]. Ground level measurements at the same lateral distance did not clearly indicate any contribution from the line. In addition, for points further from the line the contributions from corona measured at line height would be less than those reported above

TABLE 3-13

50% OZONE CONCENTRATIONS FOR DIFFERENT CATEGORIES-1050kV, MARCH 1975

	Fair Weather		Foul Weather	
	ppb	#min	ppb	#min
Westerly Wind	28.6	3159	33.1	1257
No Westerly Wind	28.4	5769	25.0	2618

#min indicates total number of minutes of data analyzed.

TABLE 3-14

50% OZONE CONCENTRATIONS FOR DIFFERENT CATEGORIES-AMBIENT, MARCH 1975

	All Weather	
	ppb	#min
Westerly Wind	25.0	858
No Westerly Wind	28.6	390

#min indicates total number of minutes of data analyzed

as a result of greater dispersion.

It is concluded that the net effect of uhv transmission line corona on ozone concentrations is negligible.

Ambient Ozone Levels. In order to determine the relative impact of any ozone that might be generated by the test line the normally existing ambient ozone level was monitored whenever possible. Figure 3-93 shows the variation of the ambient ozone level in Pittsfield over a two day period. This figure includes not only the data measured at Project UHV but also that measured by the Massachusetts Bureau of Air Quality Control. This shows a close agreement between the data collected by the State and that collected at Project UHV considering the fact that the two monitoring locations are approximately 12.8km (8 mi) apart.

Figure 3-93 also shows a daily ozone variation of about 50 ppb. This is fairly typical, with variations as much as 80 ppb occurring on occasion. A variation of 80 ppb is shown in figure 3-94 which shows the variation of the ambient ozone level over a 10-day period [5-20-75 to 5-30-75]. Considering that under the worst case

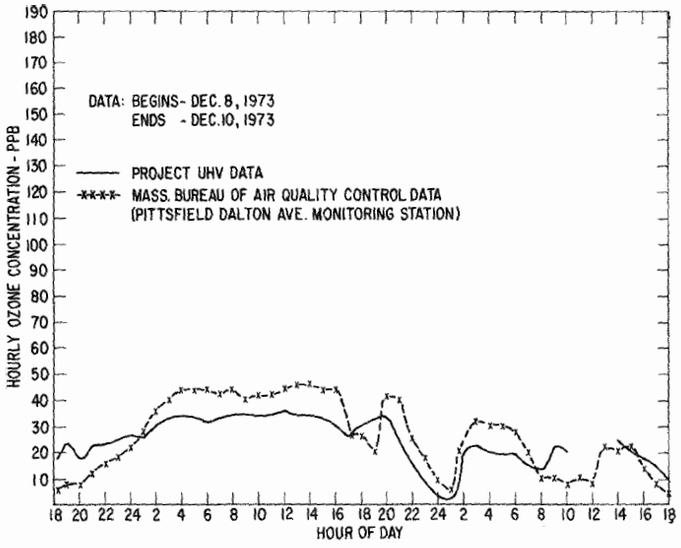


Figure 3-93. Ambient Daily Ozone Variation in Pittsfield, Mass.

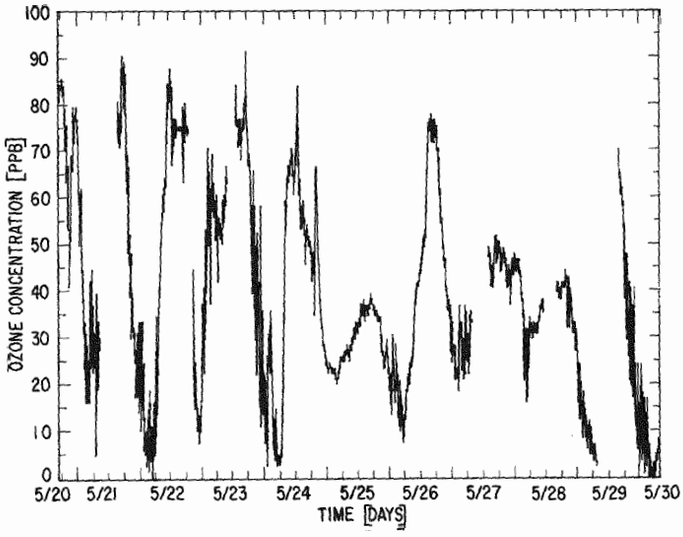


Figure 3-94. Ambient Ozone Variations for a 10 Day Period (5-20-75 to 5-30-75)

conditions ozone detected from the UHV line was on the order of 5 ppb above the ambient level, ozone generated by corona is negligible when compared to the normal ambient ozone variations that exist.

Further investigations in this area will be confined to routine monitoring of ozone concentrations for each of the line configurations tested to provide additional support to the findings reported here.

REFERENCES

3-1. Electric Power Research Institute, Transmission Line Reference Book - 345 kV and Above, Fred Weidner and Son Printers, Inc. New York: 1975.

3-2. V.L. Chartier, D.F. Shankle, N. Kolcio, "The Apple Grove 750-kV Project: Statistical Analysis of Radio Influence and Corona-Loss Performance of Conductors at 775-kV," IEEE Trans. on Power Apparatus and Systems, Vol. PAS-89, No. 5/6, May/June 1970, pp. 867-881.

3-3. Karl D. Kryter, Testimony before the State of New York Public Service Commission, Cases 26529 and 26559 - Common Record Hearings on Health and Safety of 765-kV Transmission Lines.

3-4. Karl S. Pearsons, Testimony before the State of New York Public Service Commission, Cases 26529 and 26559 - Common Record Hearings on Health and Safety of 765-kV Transmission Lines.

3-5. M. Sforzini, R. Cortina, G. Sacerdote, R. Piazza, "Acoustic Noise Caused by AC Corona on Conductors: Results of an Experimental Investigation in the Anechoic Chamber," IEEE Trans. on Power Apparatus and Systems, Vol. PAS-94, No. 2, March/April 1975, pp. 591-601.

3-6. M.G. Comber, R.J. Nigbor, "Audible Noise Performance of the First Three-Phase Ultra-High Voltage Transmission Test Line at EPRI's Project UHV," IEEE Trans. on Power Apparatus and Systems, Vol. PAS-95, No. 4, July/August 1976, pp. 1105-1114.

3-7. M.G. Comber, R. Cortina, "Audible Noise Generation of Individual Subconductors of Transmission Line Conductor Bundles," IEEE Trans. on Power Apparatus and Systems, Vol. PAS-95, No. 2, March/April 1976, pp. 525-535.

3-8. D. Perry, "An Analysis of Transmission Line Audible Noise Levels based upon Field and Three-Phase Test Line Measurements," IEEE Trans. on Power Apparatus and Systems, Vol. PAS-91, May/June 1972, pp. 857-864.

3-9. N. Kolcio, B.J. Ware, R.L. Zagier, V.L. Chartier, F.M. Dietrich, "The Apple Grove 750 kV Project - Statistical Analysis of Audible Noise Performance of Conductors at 775 kV," IEEE Trans. on Power Apparatus and Systems, Vol. PAS-93, May/June 1974, pp. 831-840.

3-10. N. Kolcio, J. DiPlacido, F.M. Dietrich, "Apple Grove 750-kV Project - Two Year Statistical Analysis of Audible Noise from Conductors at 775 kV and Ambient Noise Data," IEEE Trans. on Power Apparatus and Systems, Vol. PAS-96, No. 2, March/April 1977, pp. 560-570.

3-11. Society of Automotive Engineers, "Standard Values of Atmospheric Absorption as a Function of Temperature and Humidity for use in Evaluating Aircraft Flyover Noise," SAE Report ARP 866, Issued 8-31-64.

3-12. M.G. Comber, L.E. Zaffanella, "Audible Noise Reduction by Bundle Geometry Optimization," IEEE Trans. (Power Apparatus and Systems), Vol. PAS-92, pp. 1782-1791, September/October 1973.

3-13. M.C. Perz, "Method of Evaluating Corona Noise Generation from Measurements on Short Test Lines," IEEE Transactions on Power Apparatus and Systems, Vol. 82, December 1963, pp. 833-844.

3-14. IEEE Committee Report, "A Field Comparison of RI and TVI Instrumentation," Paper F76075-2, presented at the IEEE PES Winter Meeting and Tesla Symposium, January 25-30, 1976.

3-15. ANSI Standard C63.3, "Specifications for Radio Noise and Field Strength Meters 20 to 1000 MHz.

3-16. M. Frydman, A. Levy, S.E.Miller, "Oxidant Measurements In The Vicinity of Energized 765 kV Lines," IEEE Trans on Power Apparatus and Systems, Vol PAS-93, No. 3, May/June 1972, pp 1141-1148.

3-17. W.J.Fern, R.I.Brabets, "Field Investigation of Ozone Adjacent to High Voltage Transmission Line," IEEE Trans on Power Apparatus and Systems, Vol PAS-93, No. 5, Sept/Oct 1974, pp. 1269-1280.

APPENDIX A

DETERMINATION OF THE MINIMUM TIME REQUIRED FOR LONG-TERM TESTING

For a data base, let us consider the 4000 min. of rain data accumulated during the testing of the 8 x 3.3 x 102cm (8 x 1.302 x 40 in) bundle, horizontal phase configuration, 19.8m (65 ft) phase spacing, at 1050 kV. (Actually 4014 min. of data were collected during rain at 1050 kV, but for convenience we will consider only the first 4000 min.). Let us assume, for the time being, that this 4000 min. of data has been obtained from randomly sampling the results of one whole year's worth of test data on the same configuration, and that the cumulative frequency distribution of the audible noise levels during this 4000 min. matches that for the annual period. That is, the 4000 min. of data describes the long-term performance of the line. (In actual fact, the 4000 min. were taken over a 2 month period - the implications of this will be discussed later.) Figure A-1 shows the cumulative frequency distribution of this data. It may be noted that the L_{50} level is approximately 54 dB(A). If, as assumed, this data base represents the long-term performance of the line, then perhaps a reduced data base could provide a reasonable assessment of the long-term performance. Taking the very extreme situation, we could consider an individual minute of data. Obviously this would be a very unrealistic period of test since, as evident from figure A-1, this one-minute level could vary from less than 42 dB(A) to more than 60 dB(A). The confidence with which one could predict the "true" L_{50} level from a single minute of data would be extremely small indeed. Being a little more realistic we could consider 100 minute periods. Figure A-2 shows the variation amongst the L_{50} levels of the 40 consecutive 100-minute periods. A large dispersion is still evident, although the maximum spread has been reduced, from about 18-20 dB for the one-minute periods to about 11 dB for the 100-minute periods. We may note that a considerable number of levels (10 out of 40) fall within $\pm$ 1 dB of the long-term L_{50} level. However, the confidence with which we would predict long-term performance based on a single 100-minute period is still very small. Our estimate could be within a fraction of a dB of the long-term L_{50}, but it could equally as well be as much as 3 dB above or 8 dB below this level. Evidently a longer period must be considered.

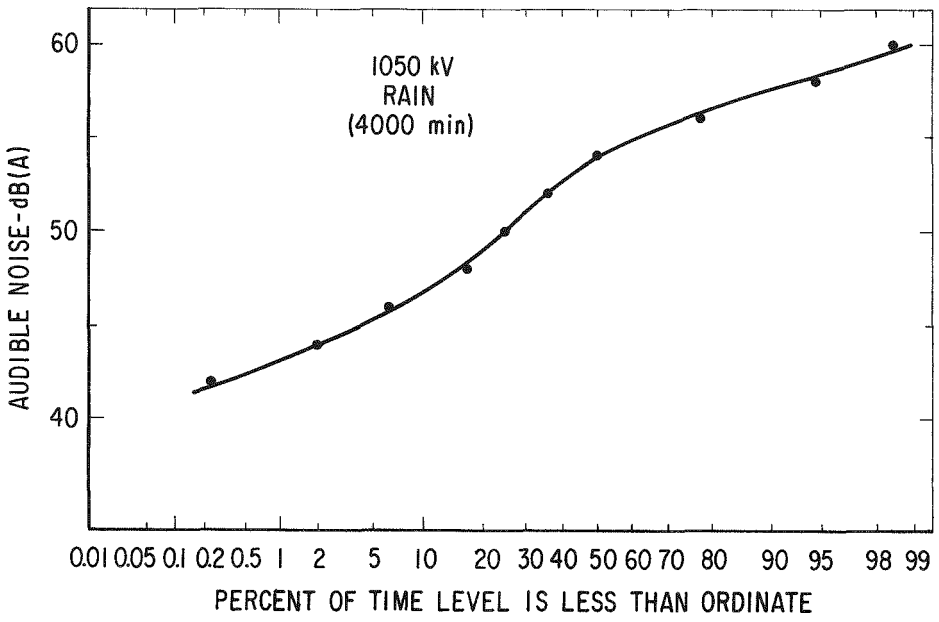


Figure A-1. Cumulative Frequency Distribution of Audible Noise in Rain, Measured at 50 ft From Outside Phase - 8 x 1.302 x 40 in Bundles, Horizontal 65 ft Phase Spacing, 1050 kV.

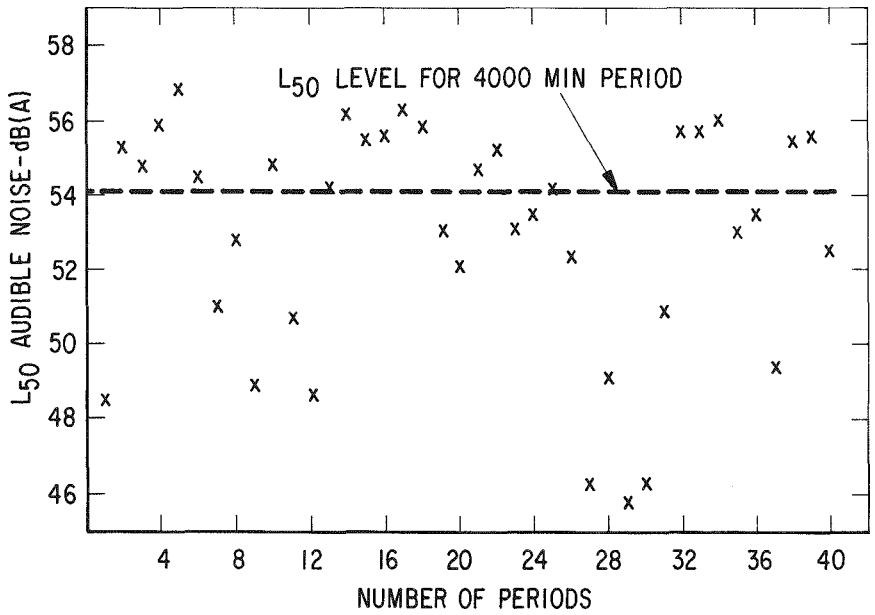


Figure A-2. Variation in L_{50} Audible Noise Levels for 100 min Periods of Rain.

By taking successively longer periods, we will inevitably obtain better and better estimates, to the point where we are taking the complete 4000 min. which gives us the (assumed) long-term L_{50} level. Results of this process are shown in figure A-3. Shown are the maximum and minimum L_{50} levels for periods of the length indicated. The difference between pairs of points (o and •) represents the maximum difference that would be obtained between any two periods of a given length (note that a period of 1000 min., for example, means a contiguous period of 1000 min.; that is, starting at some point in time, the next 1000 min. of rain). For instance, the figure indicates that selection of any 2000-minute period of rain would provide an estimate which is within ± 1 dB of the long-term L_{50} level. This is certainly considered to be within the range of error encompassed by the terminology "reasonably accurate." If one would accept an error of up to ± 2 dB, a test period of as little as 1200 min. (of rain) could be considered as adequate.

The decrease in dispersion amongst L_{50} levels with increasing length of period is accompanied by a decrease in dispersion amongst the distributions of rain intensities from period to period. For example, the system used for detecting rainfall at Project UHV measures in increments of .025mm (.001 in) of rain per minute. Rains of intensity above 2.5mm/h (0.1 in./h) are considered "medium" or "heavy" by

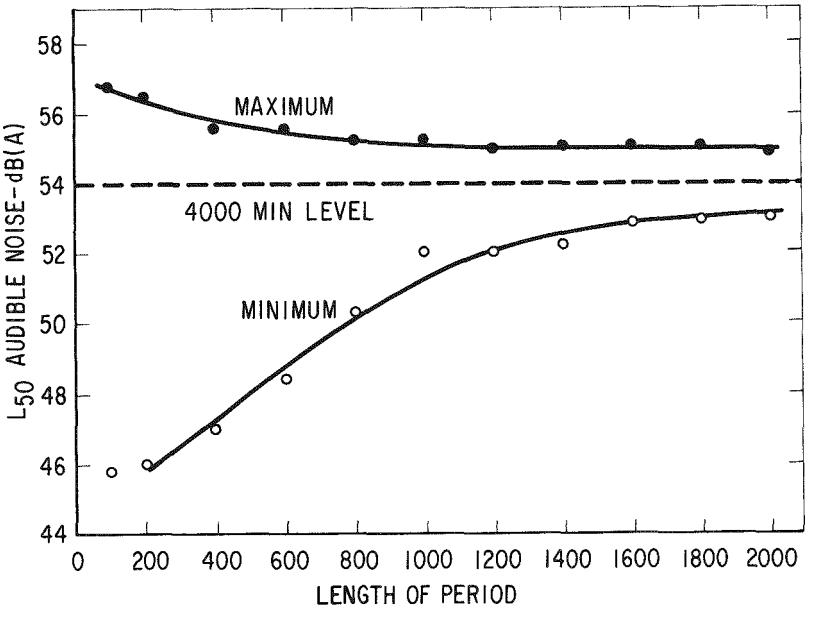


Figure A-3. Maximum and Minimum L_{50} Audible Noise Levels for Different Length Periods of Rain.

the U.S. Weather Bureau. A measure of the intensity in any given period could then be the percentage of time that the number of rain counts (recorded by the Project UHV measuring system) were 2 or more per minute; that is, when a rainfall of 3mm (0.12 in) or more - medium or heavy rain - was accredited to a particular minute. Figure A-4 shows the maximum and minimum values of this measure for the periods covered in figure A-3. One can observe that the values are converging, as the period selected increases, towards the long-term value.

The point being illustrated by figures A-3 and A-4 is that the uncertainty associated with predicting the long-term audible noise performance from short-term tests is also associated with the deviation of the rain distribution, during the test-period, from the long-term distribution. This is not a startling conclusion; in fact one could postulate such without resorting to any analytical techniques whatsoever. It must be borne in mind, however, that it is not concluded that if a period of any length yields the same rain distribution as for the long-term then that period will also yield the long-term noise performance. Perhaps the conclusion is better stated as follows: if there is a low probability that the rainfall distribution of a period of rain selected at random differs significantly from the long-term distribution, then there will be a correspondingly low probability of significant error in the estimate of the long-term audible noise performance.

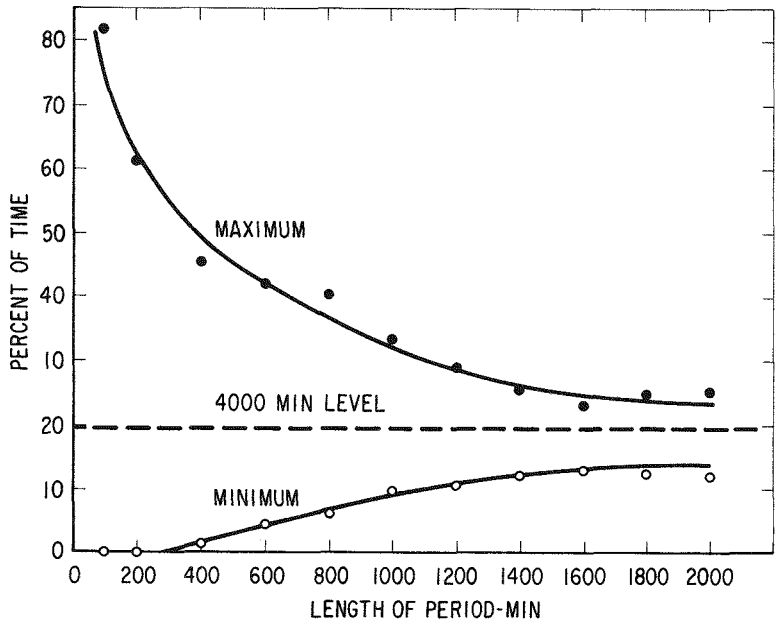


Figure A-4. Maximum and Minimum Levels of the Percentage of Time for Which Rain Counts/Min were Two or More, for Different Length Periods of Rain.

This leads us back to the original assumption that the data base of 4000 min. used in this study is representative of a year-long data base. Following the reasoning developed for sub-periods of the base 4000 min., we should merely need to show that the distribution of rainfall in any 4000 min. period is not significantly different to that for any other 4000 min. period. This represents a considerable computational effort, since if there is, for example, a total of 300h of rain in a year (a conservative estimate for the location of Project UHV), there would be a total of 14001 contiguous 4000 min. periods. However, an analysis of a very few periods can serve to illustrate the point. From late March to mid-December 1975, rain data were collected for 12728 min (~ 212h), representing approximately 65% of all rain during this 8 month period. Five sub-periods of between 3600 and 4300 minutes, according to figure A-5, were analyzed. Results are given in Table A-1.

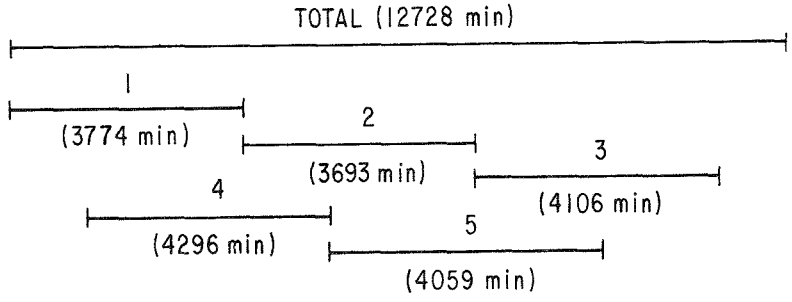


Figure A-5. Total Period and Sub Periods of Rain for Which Data was Recorded From Late-March to Mid-December 1975.

TABLE A-1

DISTRIBUTION OF RAINS IN 5 SUB-PERIODS

	Length (min.)	% of time rain counts ≥ 1	≥ 2
Total period	12728	49.3	19.7
Sub period 1	3774	51.0	20.1
Sub period 2	3693	47.5	18.0
Sub period 3	4106	47.5	20.3
Sub period 4	4296	51.8	26.0
Sub period 5	4059	47.5	19.4

The sub-periods selected follow no particular pattern, but were, for convenience, arrived at by combinations of analysis previously conducted on smaller periods for another purpose.

Thus it would appear that the probability of significant differences between periods of about 4000 min. is small, and thus any 4000 min. period is reasonably representative of the long-term situation. Consequently, an estimate of the long-term audible noise performance based on periods of 4000 min. can be made with a high degree of confidence. It is expected that the estimate of the L_{50} level would not differ from the long-term L_{50} level by more than 1 dB if the base period used for estimation is 4000 min. of rain or greater. Provided that the distribution of rain is similar to the long-term (normal annual) distribution then acceptably accurate estimates of the long-term audible noise performance can be obtained from as little as 2000 min. of data in rain. It is expected that the estimate in this case would differ from the actual long-term level by less than 2 dB.

APPENDIX B

"CORRECTION" OF AUDIBLE NOISE MEASUREMENTS TO ACCOUNT FOR AMBIENT NOISE

During the period January-June 1976 almost 5000 minutes of noise during rain was monitored in the vicinity of the Project UHV test line while the line was energized over the range 1100-1300 kV. Under test at that time was the 12 x 3.3 x 127cm (12 x 1.302 x 50 in) bundle. Figure B-1 shows the result of plotting the 8 kHz level of noise measured over this period against the dB(A) level [for microphone location 15.2m (50 ft) from outside phase]. Although there is a fairly wide dispersion there is a reasonable degree of one-for-one correlation at the higher levels where the ambient intrusions are less significant. At lower levels the data points break out of the trend lines due, it is assumed, to the greater influence of the ambient. If, indeed, the dispersion is attributable to ambient intrusions which result in an increased dB(A) measure of the total noise without significant effect on the 8 kHz component, then this dispersion should be consider-

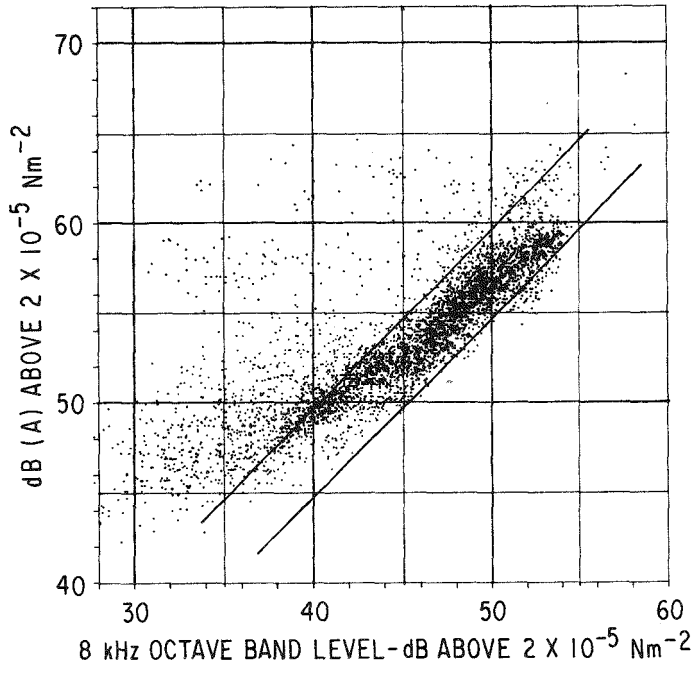


Figure B-1. Measured dB(A) Level Plotted Against 8 kHz Octave Band Level.

ably reduced if we were to plot the 8 kHz level with another high frequency level (such as 16 kHz) since it has been assumed that ambient noises have insignificant high frequency content compared to line noise. Figure B-2 confirms this hypothesis (the poorer correlation observed at the lower levels is attributable to the 16 kHz levels approaching the sensitivity threshold of the measuring system. One would expect that an effect of ambient intrusions here would cause the 8 kHz level to be relatively greater than the 16 kHz level). From these results it is assumed that the 8 kHz level is a good indicator, on a dB-for-dB basis, of the dB(A) level of the noise.

Figures B-3 to B-8 show the 8 kHz level plotted against 4 kHz, 2 kHz, 1 kHz, 500 Hz, 250 Hz and 125 Hz respectively (all octave bands). Progressively greater dispersion can be noted as the frequency, against which the 8 kHz is plotted, decreases. This indicates that the lower frequencies are more and more affected by ambient variations than by line noise variations.

In order to determine the most appropriate relationship between 8 kHz and dB(A) to use in "correcting" the dB(A) measure, the data represented in figure B-2 can be analyzed and replotted as shown in figure B-9. Each point in this figure represents the median dB(A) level of all points falling within 1 dB "windows" of the 8 kHz

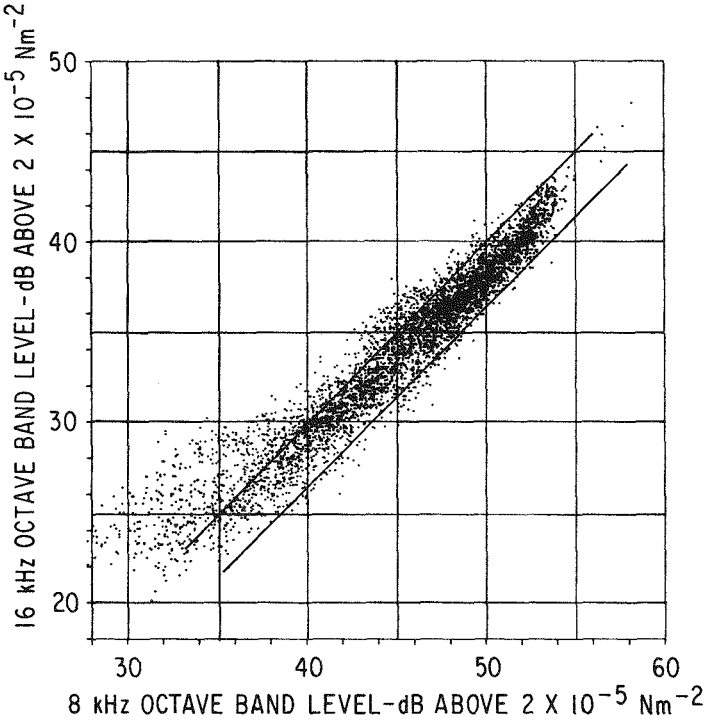


Figure B-2. Measured 16 kHz Octave Band Level Plotted Against 8 kHz Octave Band Level.

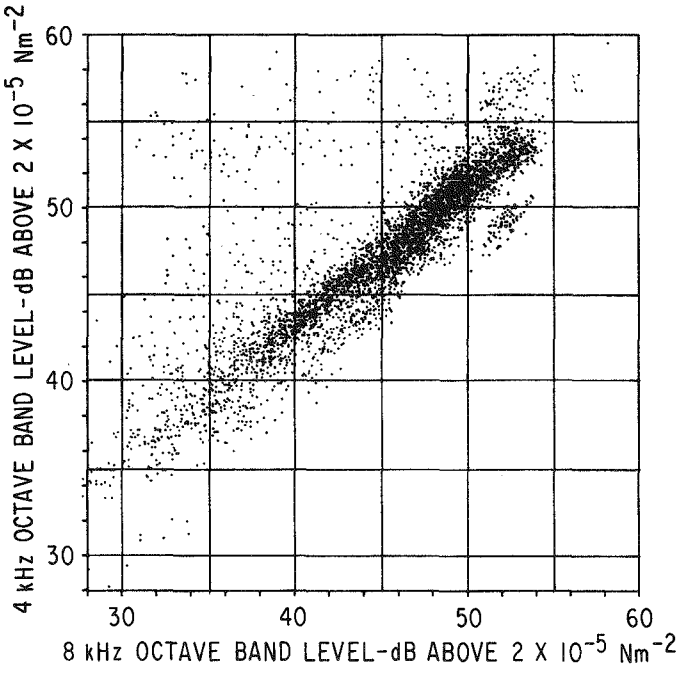


Figure B-3. Measured 4 kHz Octave Band Level Plotted Against 8 kHz Octave Band Level.

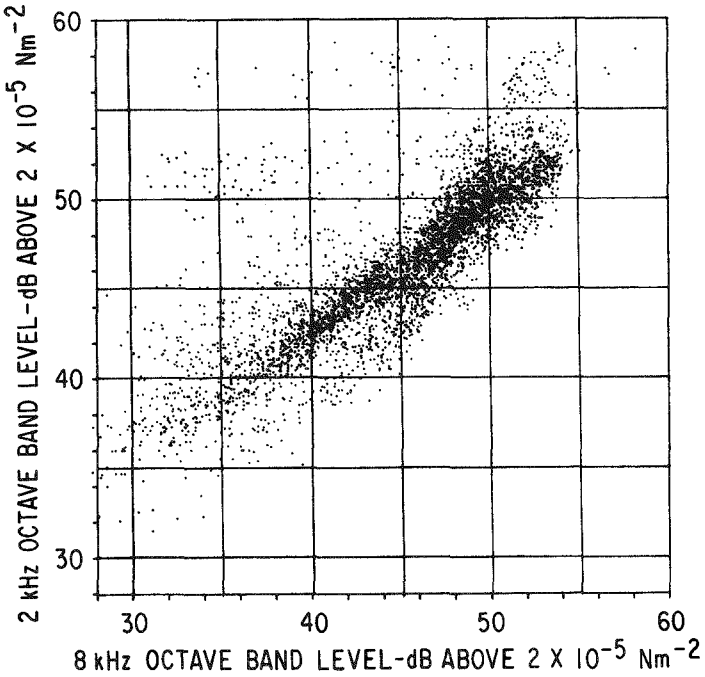


Figure B-4. Measured 2 kHz Octave Band Level Plotted Against 8 kHz Octave Band Level.

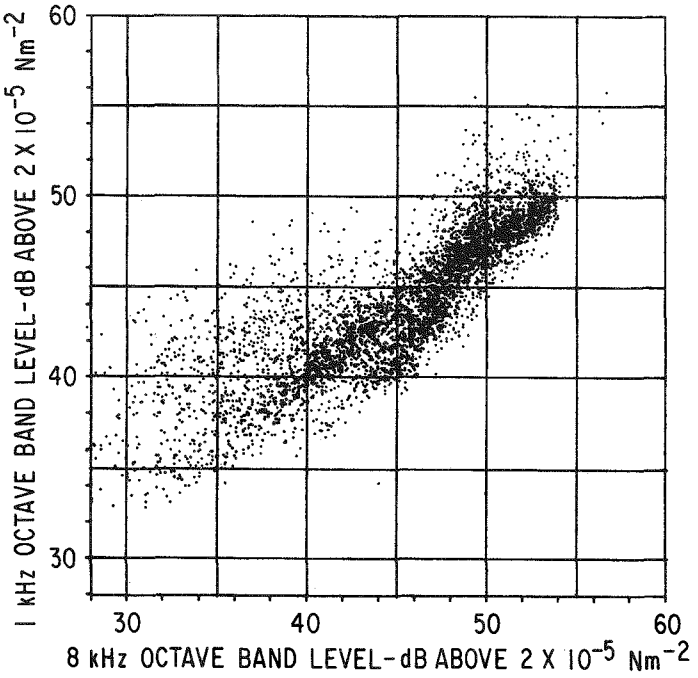


Figure B-5. Measured 1 kHz Octave Band Level Plotted Against 8 kHz Octave Band Level.

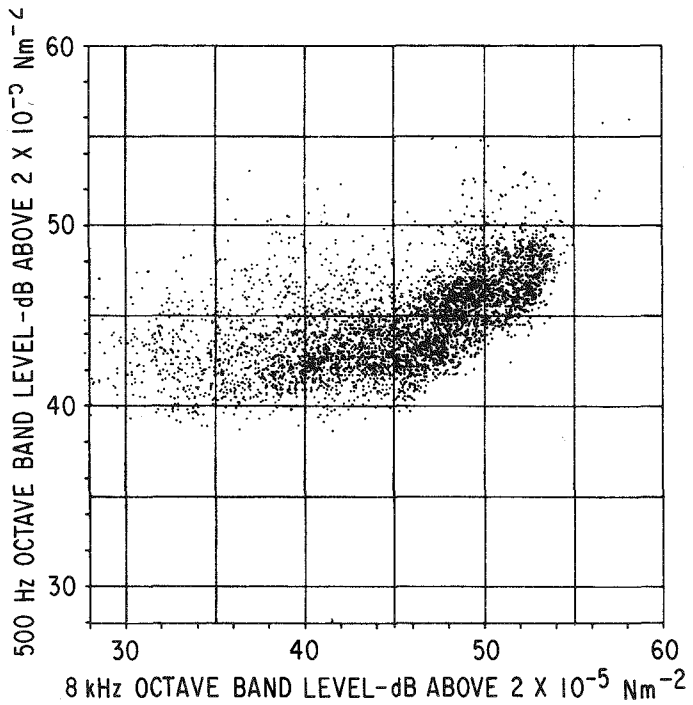


Figure B-6. Measured 500 Hz Octave Band Level Plotted Against 8 kHz Octave Band Level.

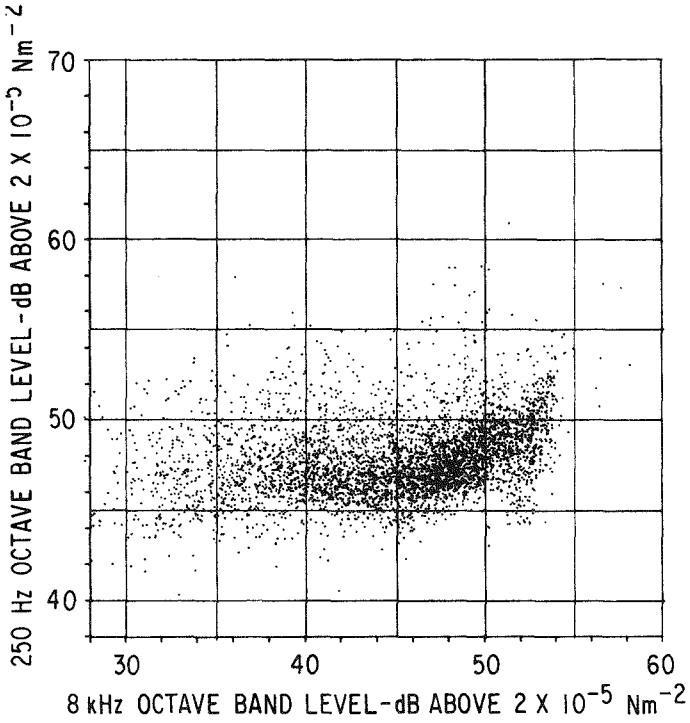


Figure B-7. Measured 250 Hz Octave Band Level Plotted Against 8 kHz Octave Band Level.

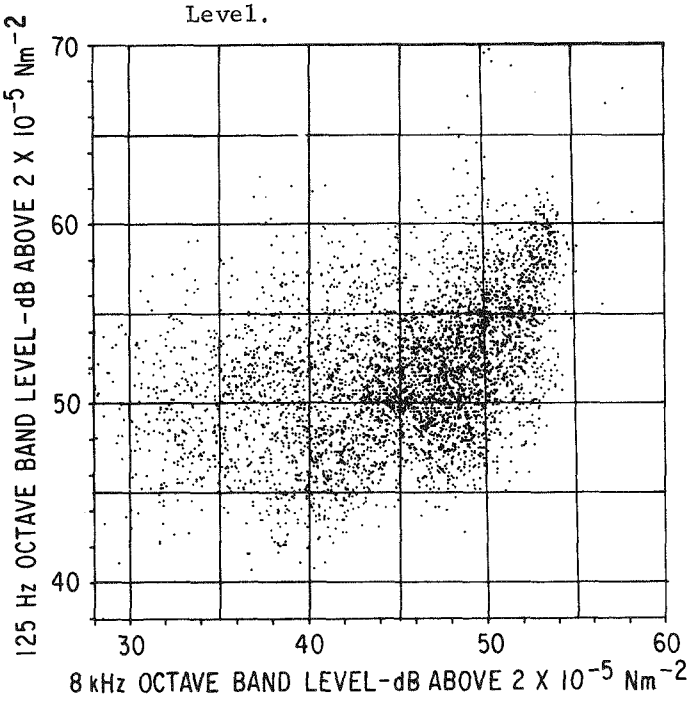


Figure B-8. Measured 125 Hz Octave Band Level Plotted Against 8 kHz Octave Band Level.

scale. That is, if 200 points of figure B-2 fell within the 8 kHz range of 45-46 dB, then the level which was exceeded by the dB(A) value of 100 of these points was found and plotted against an 8 kHz level of 45.5 dB in figure B-9. By drawing the best one-for-one straight line through the upper points in figure B-9, we find the following relationship,

$$dB(A)_{corr.} = dB(8000) + 7.0 \qquad \text{(B-1)}$$

where $dB(A)_{corr.}$ is the "corrected" dB(A) level for which the influence of ambient is removed, and dB(8000) is the measured 8 kHz octave band component of noise.

It should be noted that this relationship will be a function of both microphone characteristic and microphone location and should be determined on a case for case basis.

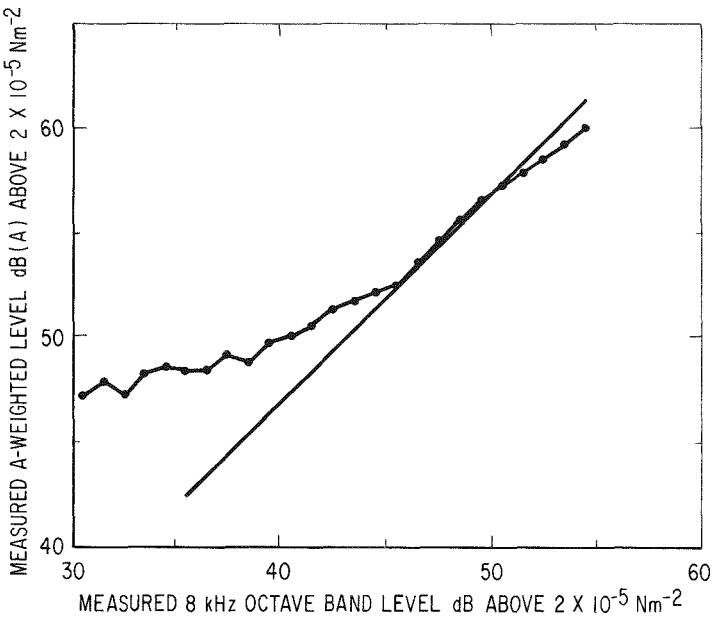


Figure B-9. Median dB(A) Noise Plotted Against 1 dB Increments of 8 kHz Octave Band Level (Base Data Taken From Figure B-1.

SECTION 4

INSULATION RESEARCH

CONTAMINATION PERFORMANCE OF LONG SUSPENSION INSULATOR STRINGS

Introduction

The electrical strength of long insulator strings in contaminated conditions may influence the design of future UHV transmission lines in areas where contamination is known to be a problem, either from previous experience with lower voltage lines in the same location or from other data on the site severity in regions where no prior operating lines exist. A fundamental question is whether insulator string lengths which have been adequate for lower voltage systems can be linearly extrapolated to the UHV range and still give comparable performance. For example, if 26 units of a certain type of insulator have been acceptable for a 550 kV system, will 57 units of the same insulator be sufficient at 1200 kV?

Previous data obtained at Project UHV have shown a pronounced nonlinearity in the contamination flashover strength as a function of string length for certain types of insulators such as "standard" units having dimensions of 146mm x 254mm (5 3/4 in x 10 in). [4-1] These results have received a great deal of interest because of the design requirements they imply. Furthermore, the nonlinearity of strength with string length has not been found in other laboratories, a fact attributed primarily to differences in test methods since most test facilities do not duplicate the slow wetting fog employed at Project UHV.

A major effort has been made to check the previous results and to update design rules based on the latest data. This effort included tests performed at higher voltages than previously possible and procedures which were intended to eliminate the influence of certain parameters which might bias the data in some manner.

For example, most of the earlier data on long strings were obtained on V-suspension configurations having a shape which resembled a "U" or a portion of a semi-circle. These shapes resulted from the fact that the test chamber structure could not support the amount of loading required to pull the strings into a "V". The tested

strings thus had some insulators which were horizontal, whereas others were inclined at approximately forty five degrees. Such insulator string geometries are not representative of configurations on actual lines, and the influence of different orientations within the same string on the flashover voltage is not known. Consequently, only vertical strings were used in the data reported here to evaluate flashover strength as a function of string length.

Other factors which may have affected the original results relate to differences in the EHV and UHV fog chambers in which the tests had previously been made. Data from both chambers had been used to draw the conclusions, although the fog generation, test circuits and proximity effects were somewhat different in the two facilities. All of these factors may have contributed to the degree of nonlinearity of insulation strength with string length which was reported. The influence of the above parameters was eliminated by making a new series of tests entirely within the same UHV test chamber.

Test Facilities for UHV Research

Fog Chamber with Plastic Window and Porcelain Bushings. Indoor contamination tests were made at UHV voltages in a fog chamber which is approximately cylindrical in shape with a diameter and height of 24.4m (80 ft), giving a total volume of 11.4 x $10^3 m^3$ (40 x 10^4 ft^3). The tests were made at constant voltage with a slow wetting clean fog. [4-1] The fog was produced by evaporating water from three large vats, each of which has a capacity of 760ℓ and contains 80 kW of electrical heating.

The transformers used for supplying the test voltages were located outside the contamination chamber. Prior to 1975, the highest level attainable inside the building was limited by the original plastic window bushing to about $1100/\sqrt{3}$ kV. In November, 1975, the construction of a much larger plastic window bushing was completed so that tests could be carried out at voltages up to $1500/\sqrt{3}$ kV. A diagram of the new window bushing is given in figure 4-1. The bushing consisted of two paralled polyethylene sheets recessed approximately 3.6m (12 ft) from the building wall. The plastic sheets each had dimensions 11.6m x 11.6m x 0.15mm (38 ft x 38 ft x 6 mil) and were stretched between two pairs of wood poles. Kerosene heaters with a total output of 249 kW (850 x 10^3BTU/hr) were used to heat the air in the 1.2m (4 ft) wide space between the sheets in order to prevent a reduction in electrical strength which would be caused by moisture accumulating

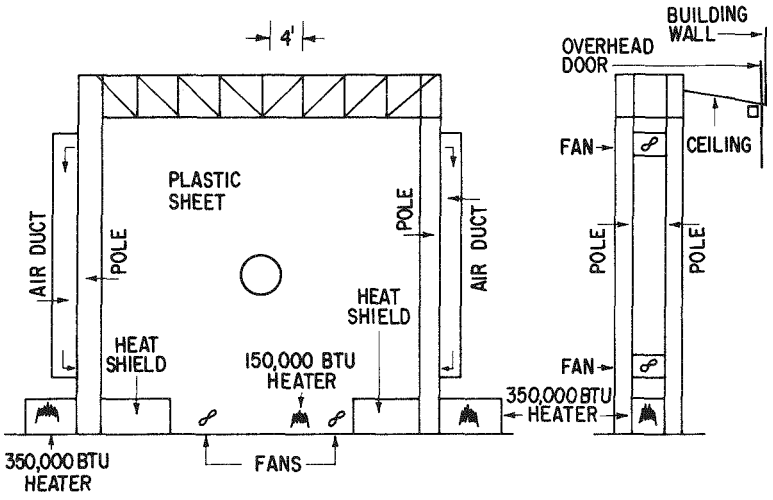


Figure 4-1. Outline of new 1500/√3 kV Plastic Sheet Window Bushing in the UHV Contamination Building.

on the plastic during the fog tests. The heated air was also circulated by a system of fans which were located in ducts on the sides of the window and on the floor between the sheets.

The test voltage was brought into the chamber on a thin wire which passed through a 7.3m x 11.6m (24 ft x 38 ft) opening in the building wall and 1.2m (4 ft) diameter holes located in the centers of the two plastic sheets as shown in figure 4-2. Some experimentation with the size of the holes indicated that although smaller holes reduced condensation on the sheets due to a decrease in the amount of cooler outside air flow, corona streamers would eventually cause a tearing of the plastic around the holes unless they had at least the above dimensions. A view of the entire window bushing from inside the chamber is given in figure 4-3, where the light area outlines the opening in the building wall.

It should be noted that the thin wire conductor previously had been found superior to large smooth pipes for bringing voltages through a plastic window bushing, since the ultracorona around the wire suppressed the large streamers which would occur on a smooth conductor having water drops on its surface. At the voltage levels achievable with the new plastic window bushing, there were streamers on the wire when the fog was present. An example of this type of corona activity is shown in figure 4-4, where streamers are visible during a fog test at 1450/√3 kV.

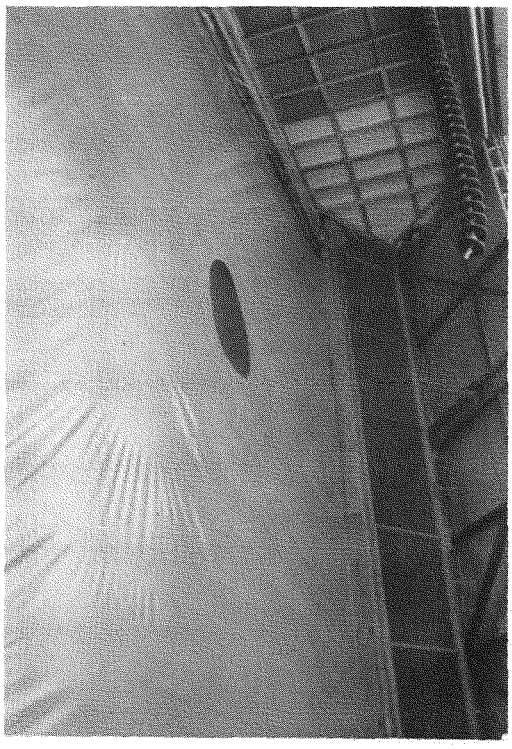


Figure 4-2. Outer Sheet of the Plastic Window Bushing. Feed Wire Passing Through Circular Opening in the Sheet.

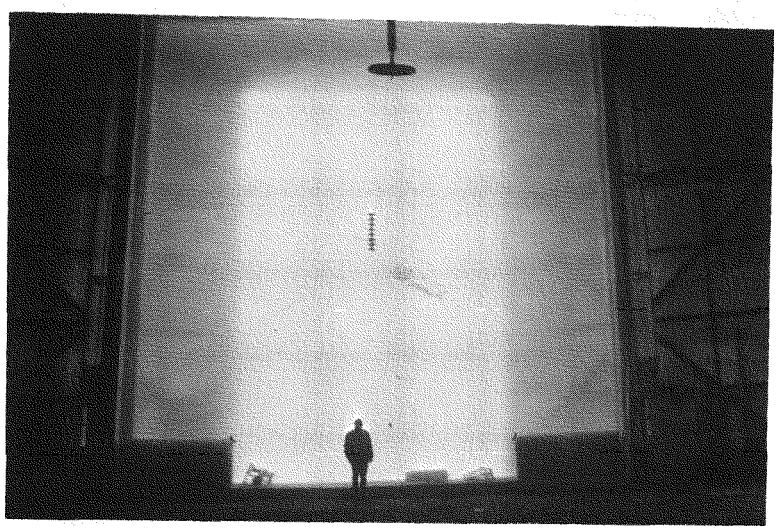


Figure 4-3. Plastic Window Bushing as seen from Inside the Contamination Chamber. Insulator String Shown in Figure 4-1 for Support of Feed Wire may also be seen here Through Circular Openings.

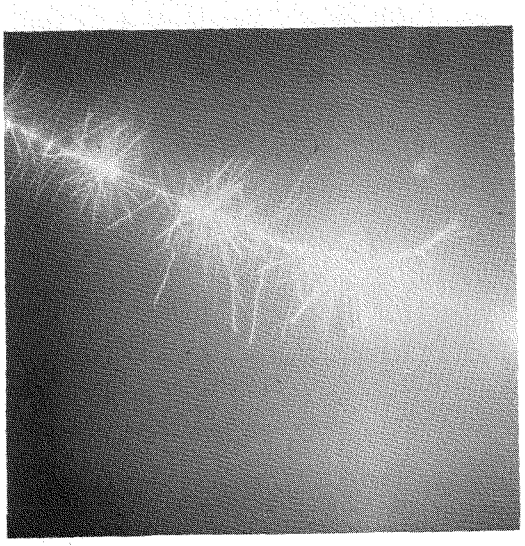


Figure 4-4. Corona Streamers on Feed Wire Inside UHV Contamination Chamber During Fog Test at $1450/\sqrt{3}$ kV.

In order to prevent damage to the plastic sheets of the window bushing by wind when tests were not in progress, the building was sealed by a two part vertical lift door after the wire was removed. The plastic window bushing as seen from outside the building is shown in figure 4-5, and in figure 4-6 the large door is shown closed.

The performance of the new plastic window bushing has been excellent. No replacement of the plastic was required at all during tests at $1350/\sqrt{3}$ kV. However, at the $1450/\sqrt{3}$ kV level, occasional flashovers occurred on the plastic sheets and the material was replaced several times during one test series.

In September, 1976, a porcelain bushing was installed in the UHV contamination building on the opposite side of the chamber from the new plastic window bushing. The porcelain bushing is shown during installation in figure 4-7 and in place inside the building in figure 4-8. This bushing has successfully passed the following tests before installation:

1) power frequency (dry) for six hours at voltages between $1560/\sqrt{3}$ kV and $1650/\sqrt{3}$ kV.
2) power frequency (wet) for 1 min at $1650/\sqrt{3}$ kV.
3) negative polarity dc for one hour at 1200 kV.

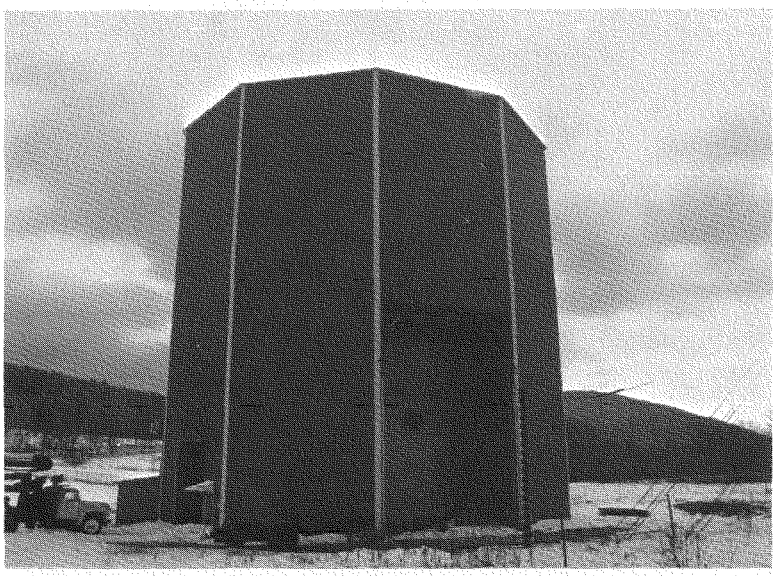


Figure 4-5. UHV Contamination Building with Plastic Window Bushing Overhead Door Open.

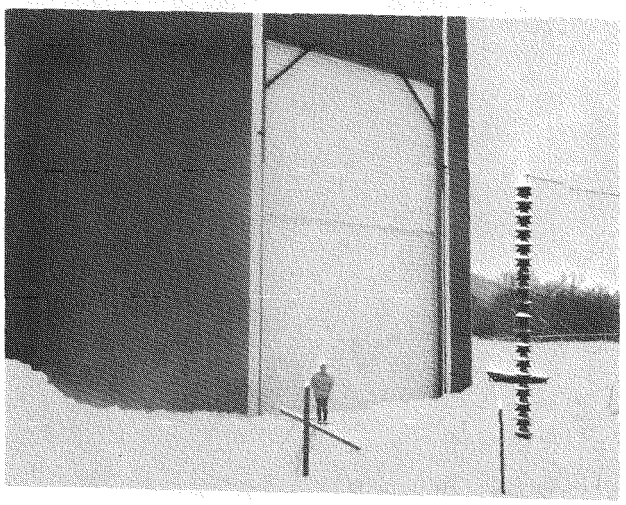


Figure 4-6. UHV Contamination Building with Protective Door for Plastic Sheet Window Bushing Closed.

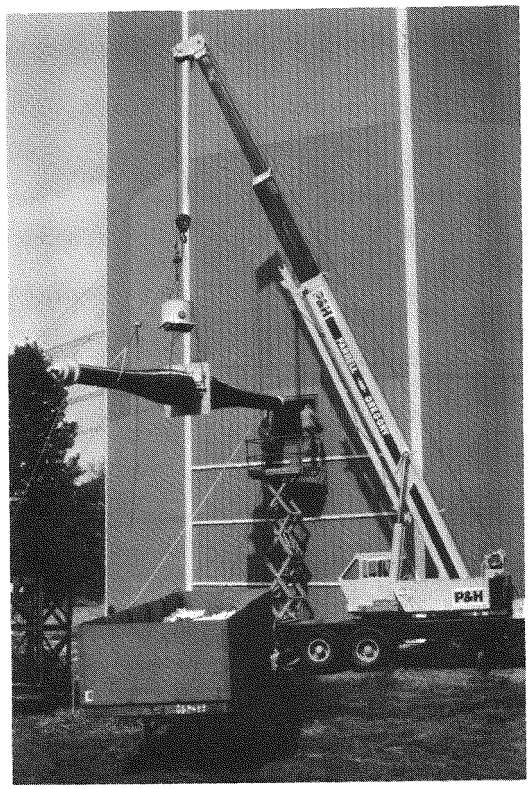


Figure 4-7. 1500/√3 kV Porcelain Bushing Being Installed in UHV Contamination Chamber on Wall Opposite Plastic Sheet Window Bushing.

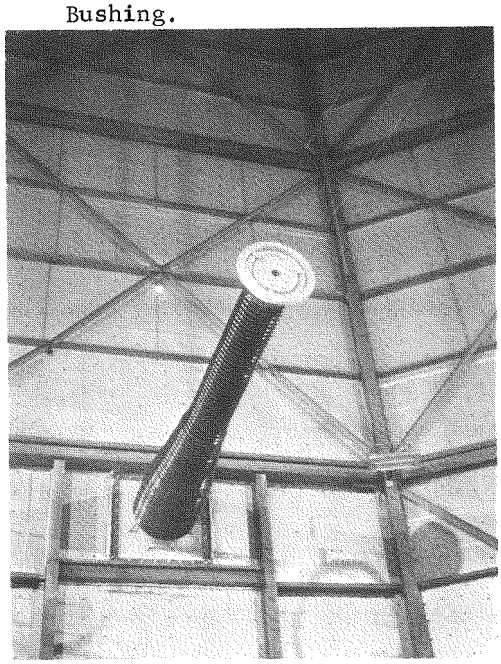


Figure 4-8. Porcelain Bushing Installed in UHV Contamination Chamber.

The porcelain bushing has made it possible to make tests more efficiently at UHV voltage levels and allows these tests to be conducted in darkness when the large plastic window door is closed. There are two additional advantages to having both the porcelain and plastic window bushings available. The presence of the two bushings allows tests at EHV and UHV levels to be performed simultaneously, and the two bushings allow phase-to-phase contamination tests to be conducted at voltages up to 1150 kV by using two of the UHV transformers.

Line Strings for Natural Humidity Tests. In principle, any of the insulator strings on the three phase UHV test line may be used for full scale natural humidity tests, in which the insulators are artificially contaminated and exposed to the natural fog, dew, mist or rain which occur frequently at the location of Project UHV. Late summer provides the greatest opportunity for tests in high humidity and fog which often is present on cool nights after warm days.

The use of the UHV test line insulators for such experiments provides an opportunity for checking the results obtained indoors with artificial fog. The insulator strings on the line are representative of the types which are suitable for prospective lines and in addition have hardware and conductor bundles which are similar to practical configurations on actual lines.

For the tests during this contract, the center phase suspension insulator string was chosen for all natural humidity experiments, since substantial indoor data were already available on this type of unit. The string, which contains 39 units per side of NGK 40 x 10^3kg (90 x 10^3 lb) insulators, is shown in figure 4-9. Tests were performed with all units at the higher voltages and also with part of the string shorted in order to check results at lower voltage levels.

Indoor Test Results

Standard and Antifog Vertical Single Strings. While the use of vertical insulator strings may not be feasible at UHV levels because of wind swing limitations, they allow the concept of nonlinearity of strength with string length to be checked in the fog chamber without the complications of improperly shaped V strings.

The standard and antifog insulators utilized in the indoor vertical string tests are shown in figure 4-10.

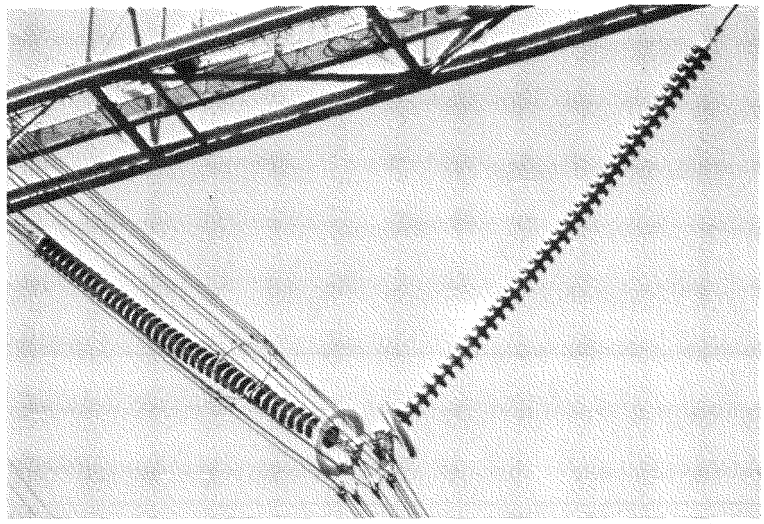
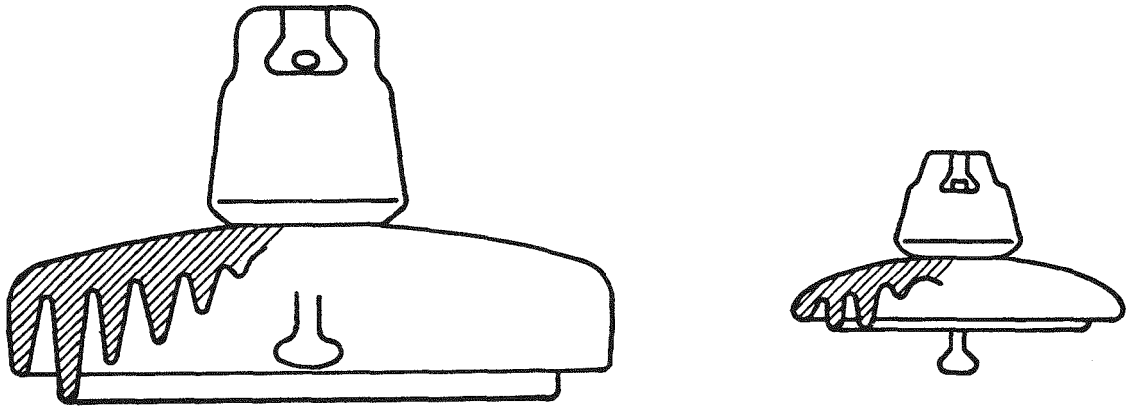


Figure 4-9. Center Phase Insulator String on Suspension Tower of UHV Test Line Contains 39 Units per Side (8.6m) of High Strength Antifog Units and was Used for Natural Humidity Contamination as well as Clean Wet Tests.



	Antifog	Standard
Spacing:	220mm ($8^{11}/16$ in)	146mm ($5^{3}/4$ in)
Diameter:	420mm ($16^{1}/2$ in)	254mm (10 in)
Leakage Distance:	740mm (29 in)	305mm (12 in)
Mech. Strength:	40,000 kg (90,000 lb)	7500 kg (15,000 lb)

Figure 4-10. Geometrical and Mechanical Characteristics of Standard and Antifog Insulators used in this Study.

The slow wetting steam fog developed previously at Project UHV was used for the tests. [4-1] In this procedure, the insulators are first contaminated with a water based solution containing fixed amounts of kaolin and sodium chloride. This mixture is sprayed onto the insulators until they are saturated. The insulators are then dried in warm ambient air and cooled before the test begins.

The kaolin in the mixture described above represents the inert component of surface contaminants generally found on insulators exposed to industrial or agricultural pollution. The amount and specific type of inert material is of course quite variable in service conditions. It is suggested that 40 grams of kaolin per liter of water in the artificial tests gives a surface deposit similar to a "light dust" or "thin layer" condition found in many areas of natural contamination. Consequently, this proportion of kaolin was used in the mixtures applied to the insulators for all the tests reported in this section. The amount of sodium chloride in the mixture was varied in the different test series. The nomenclature adopted for describing the mixtures is K/S, where K is the number of grams of kaolin and S the number of grams of sodium chloride per liter of water. Data were obtained using 5, 10, and 20 grams of NaCℓ per liter of water. These mixtures are referred to as 40/5, 40/10, and 40/20. They yield average surface salt deposit densities averaging 0.01, 0.02, and 0.04 mg/cm^2 on standard insulators. These levels of contamination represent very light to light degrees of severity.

For each test series of eight to ten tests in which the same contaminant mixture was used, the same voltage was also employed. The string lengths in successive tests in a series were increased or decreased depending on whether a test resulted in a flashover or a withstand. The resulting "up and down" sequence in string length allowed the determination of the "fifty percent string length," or string length corresponding to fifty percent probability of flashover. By varying the string length and maintaining a constant voltage in subsequent tests, it was possible to conduct a test series with more than one type of insulator string in the chamber at the same time. This is particularly useful if a new type of insulator is to be compared with another insulator such as a standard type which may be used as a reference. When more than one string is tested, connections to the strings may be made with fuse wires so that the tests may continue after a string flashes over. Alternatively, fuses may be used to insert additional clean insulators in series with each test string on flashover. The latter technique was used in the present tests.

An example of one test series in which both the standard and antifog insulators were evaluated simultaneously is shown in Table 4-1. The step size in string length corresponds in this example to about six percent in kV/unit at the fifty percent level. If short strings are used, the method of changing string length may lead to step sizes which are much larger and thus reduce the accuracy in the determined fifty percent flashover voltage. The fifty percent string lengths in Table 4-1 were determined by averaging the string lengths for individual tests. For example, for the antifog units, the average length of tests 1-11 is 15.9 units. For the standard units in Table 4-1, tests 4-11 are used, since tests 1-3 are preliminary and would incorrectly bias the outcome.

TABLE 4-1

TEST SERIES ON STANDARD AND ANTIFOG INSULATORS.
RESULTS ALIGNED IN SAME VERTICAL COLUMN WERE OBTAINED DURING THE SAME TEST PERIOD.
VOLTAGE 375 kV (ℓ-g)
"FIFTY PERCENT STRING LENGTH" = 32.3 STANDARD, 15.9 ANTIFOG UNITS.

X = Flashover 0 = Withstand											
Test #:	1	2	3	4	5	6	7	8	9	10	11
Number of standard units											
35					0				0		
33				X		0		X		0	
31			X				X				0
29		X									
27	X										
Number of antifog units											
17						0		0			
16	0		0		X		X		0		
15		X		X						X	

A summary of the results of tests made on standard insulators is given in Table 4-2. Data for the antifog units are presented in Table 4-3. The measured salt deposit densities on the antifog vertical units were about the same as on the standard insulators.

TABLE 4-2

FIFTY PERCENT STRING LENGTH, ℓ_{50}, AND CORRESPONDING FIFTY PERCENT FLASHOVER VOLTAGE IN kV/INSULATOR FOR THE STANDARD UNITS SHOWN IN FIGURE 4-10

ℓ_{50} (Number of Insulators)				Fifty Percent Flashover Voltage (kV/Insulator)		
Contaminant: (mixture)	40/5	40/10	40/20	40/5	40/10	40/20
Voltage (kVℓ-g)						
111	-	-	10.8	-	-	10.3
145	-	10.2	-	-	14.2	-
375	26.0	32.3	40.7	14.4	11.6	9.2
635	-	60.4	72.2	-	10.5	8.8
780	58.8	-	-	13.3	-	-
840	-	79.0	-	-	10.6	-

TABLE 4-3

QUANTITIES RELATED TO 50% FLASHOVER PROBABILITY, NAMELY, FIFTY PERCENT STRING LENGTH, ℓ_{50}, AND CORRESPONDING FIFTY PERCENT FLASHOVER VOLTAGE IN kV/INSULATOR FOR THE ANTIFOG UNITS SHOWN IN FIGURE 4-10

ℓ_{50} (Number of Insulators)			Fifty Percent Flashover Voltage (kV/Insulator)	
Contaminant: (mixture)	40/10	40/20	40/10	40/20
Voltage (kVℓ-g)				
111	-	5.2	-	21.4
145	5.9	-	24.6	-
375	15.9	18.5	23.4	20.3
635	29.0	35.0	21.9	18.1

These results are also plotted in figures 4-11 and 4-12.

The data at the voltages of 111 and 145 kV in Tables 4-2 and 4-3 were obtained with a special test setup in which parts of a long string were isolated and used for several short string tests at the same time. In addition, the short circuit currents were much higher than in the other tests.

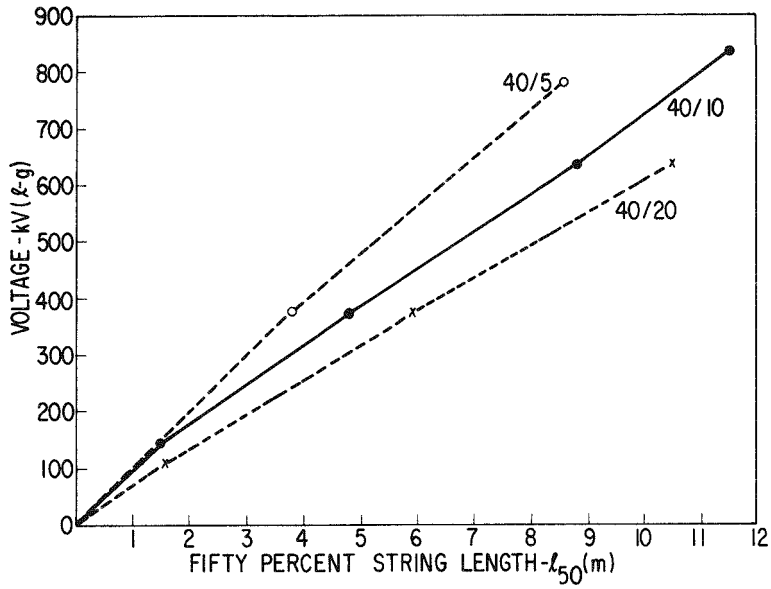


Figure 4-11. Voltage as a Function of Fifty Percent String Length for Vertical Strings of Standard Insulators.

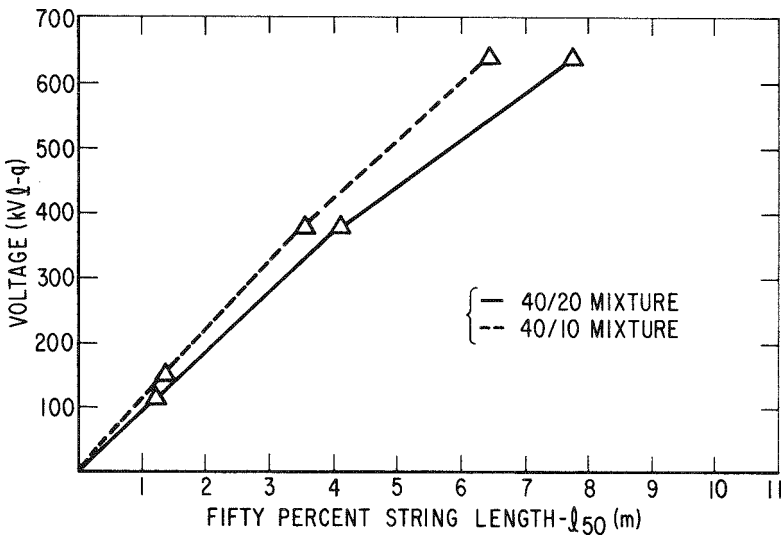


Figure 4-12. Voltage as a Function of Fifty Percent String Length for Vertical Strings of Antifog Insulators.

During the tests on the long vertical strings, scintillation activity began with blue arcs bridging the first few units of the string, with yellow scintillation discharges on other units gradually appearing as wetting progressed. This type of activity is illustrated in figures 4-13 and 4-14 which show scintillation on a string of standard units tested at 840 kV.

Multiple Strings. The mechanical loading imposed by UHV conductor bundles would require multiple insulator strings if conventional units were used. For this reason, it is of interest to learn whether the flashover voltage of multiple strings would be significantly different from that of single strings of the same type of insulator. If the individual strings were separated by a sufficient distance so that they did not physically interact, the effect on the flashover voltage may be calculated simply from statistics. Unfortunately, practical considerations limit the extent of the inter-string distances in a multiple string so that this assumption may not be valid.

Some tests were performed on a quadruple vertical string of standard insulators. The spacing between the individual strings was 46cm (18 inches), which corresponds to the same separation as exists on the quadruple dead end strings installed on the

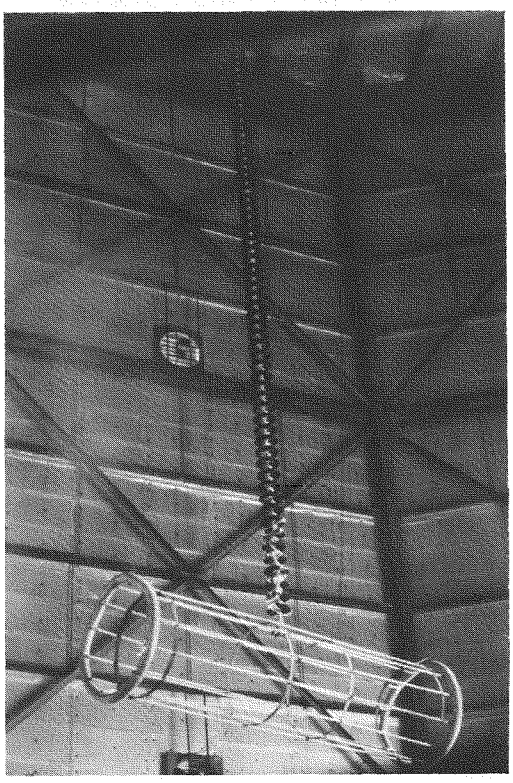


Figure 4-13. Time Exposure (~30 sec) Photograph of Scintillation Discharge Activity on Long Vertical String of Standard Units in Early Stage of Contamination Test at $1450/\sqrt{3}$ kV. Note arc in air Bridging First Three Insulators and Absence of Activity on Some Units.

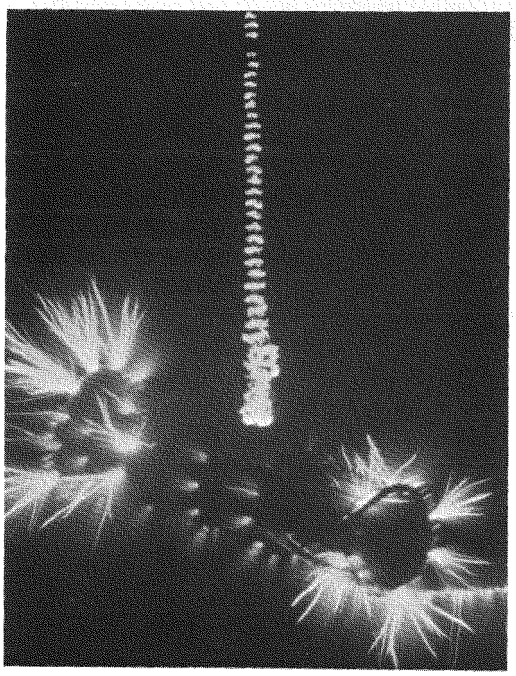


Figure 4-14. Time Exposure (~30 sec) Photograph of Scintillation Discharge Activity During Later State of Same Test as in Figure 4-13. Note Increased Intensity of Activity and Fewer Units on Which no Discharges Appear. Only a Portion of the String is Visible.

UHV test line. The string tested is shown in figure 4-15. The results for the fifty percent string length are given in Table 4-4, where calculated values are also listed. The calculated data were obtained from the single string results assuming that the standard deviation of the flashover voltage is 10% and that the four parallel strings comprising the quadruple may be treated as independent. [4-1]

TABLE 4-4

FLASHOVER TEST RESULTS ON A QUADRUPLE VERTICAL STRING OF STANDARD INSULATORS AND COMPARISON WITH SINGLE STRING DATA, EITHER FROM TABLE 4-2 (*), OR FROM TESTS MADE SIMULTANEOUSLY WITH A SINGLE STRING PRESENT. SPACING BETWEEN INDIVIDUAL STRINGS IN QUADRUPLE WAS 46cm (18 in).

Voltage (kV ℓ-g)	Contaminant	Single String ℓ_{50} (units)	Single String kV/unit	Quad String ℓ_{50} (units)	Quad String kV/unit	Quad Calc. ℓ_{50} (units)	Quad Calc. kV/unit
375	40/10	33.6	11.2	33.6	11.2	38.3	9.8
375	40/20	40.5*	9.2	41.5	9.0	46.2	8.1
577	40/10	52.2	11.0	57.5	10.0	59.6	9.7
635	40/20	72.2*	8.8	> 80	< 7.9	82	7.7

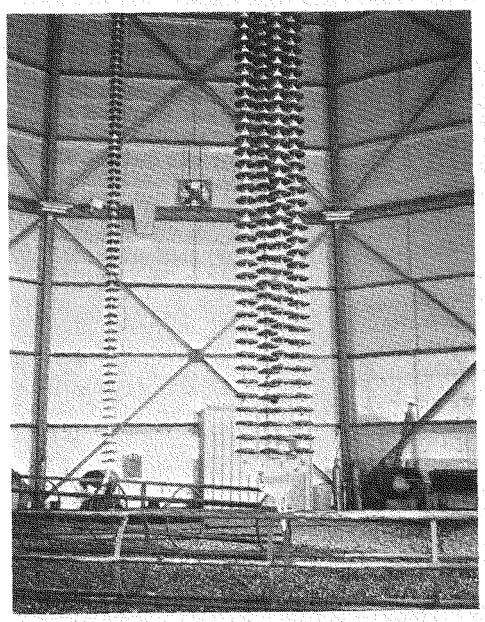


Figure 4-15. Quadruple Vertical String of Standard Insulators and Single String Which was Sometimes Tested in Parallel.

For both contaminants, the results at 375 kV indicate the performance of the single string and the quadruple are essentially the same, whereas the flashover voltages calculated assuming statistical independence predict a 12% lower kV/unit for the quadruple compared with the single string. At 577 kV, a 10% decrease in kV/unit was obtained for the quadruple, which is still less than the 12% theoretical estimate. Similarly at 635 kV, a substantial reduction in the kV/unit was observed for the quadruple string. However, at this voltage level with the 40/20 contaminant, it was not possible to complete the tests since more than 80 insulators could not be used for mechanical reasons.

During the contamination tests on the quadruple string, it became evident that the individual strings were not independent. The influence of the adjacent strings was particularly apparent during scintillation activity on the longer strings. Discharges would frequently extend along one string, bridge to a second string and continue along it to ground. In addition, scintillations which appeared to be simultaneous on several strings according to visual observations were noted.

This interaction of the individual strings of the quadruple suggests a possible explanation for the decrease in flashover voltage for the long strings. One such explanation is that as a discharge progresses part way along one string, it has the

possibility of jumping to one of the other three strings if conditions on the string along which it started do not allow it to continue there. Thus the probability of flashover is increased because of the multiple paths. Perhaps this mechanism also requires a certain string length before it may be effective. This might explain the close agreement between the quadruple and single string flashover voltages at 375 kV.

Outdoor Natural Humidity Tests

As mentioned earlier, the center phase V-string on the 3 phase test line with antifog insulators was used for the tests reported here. The geometrical and mechanical properties of these units are shown in figure 4-10.

Procedures. The test procedure consisted of contaminating the insulators in the early afternoon with the same type of slurry used in the indoor tests. Mixtures containing 40g per liter of kaolin and either 10 or 20g per liter of sodium chloride were used. The total length of each side of the string was 39 units. Different numbers of insulators on each side were contaminated in any one test, with the remaining clean units shorted by a fuse wire. This fuse allowed the test to be continued on the other side of the V-string after a flashover by inserting the remaining clean units in series and thus providing enough electrical strength for a withstand on the faulted side.

The application of the contaminant to the insulators proved to be a difficult and time consuming operation, due to the height of the insulator string above ground. For tests with short strings such as 17 units, it was sufficient to place an operator in the conductor bundle at the apex of the V and to contaminate the units from this fixed position. In the case of long strings such as 30 or more units, careful application of the contaminant required that the operator be in close proximity to all parts of the string. This was accomplished in two ways. During 1975, a large rental crane was used to hoist the operator to the string as shown in figures 4-16 and 4-17. The standard spray container was employed, with compressed gas supplied by a bottle located on the tower bridge. In 1976, a lineman holding the spray nozzle was lowered from the tower bridge in such a way as to remain near the insulators. This is illustrated in figure 4-18.

After the insulators were contaminated, they were allowed to dry in ambient air before voltage was applied. The string was usually energized at about four o'clock in the afternoon and generally remained under test at constant voltage in the

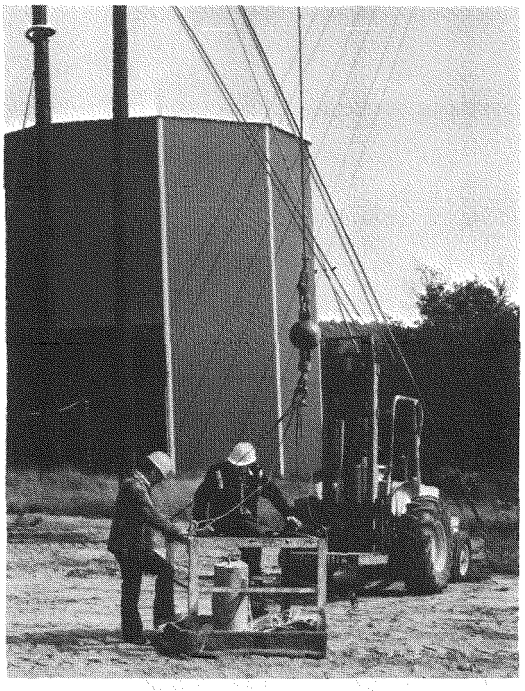


Figure 4-16. Crane Lifted Platform Used for Bringing Operators Near Insulator String During Contaminated Application in Natural Humidity.



Figure 4-17. Platform of Figure 4-16 Adjacent to Insulator String in Preparation for Natural Humidity Test.

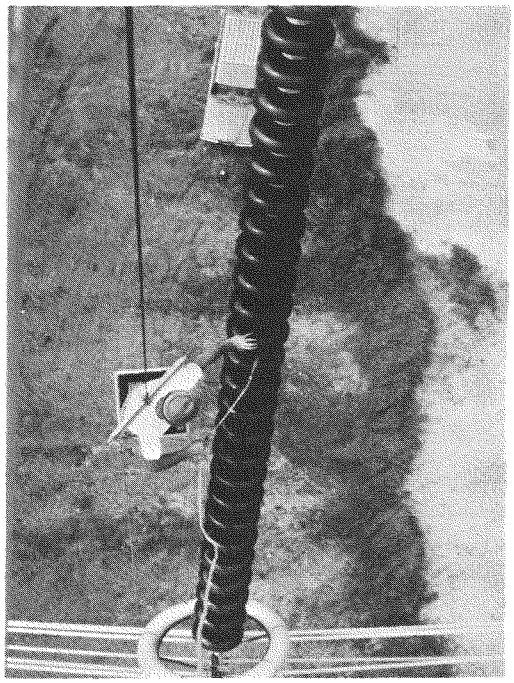


Figure 4-18. Lineman Applying Contaminant to Center Phase V-String Before Natural Humidity Test.

natural humidity until the following morning unless both sides flashed over. Voltage was supplied by the center phase UHV transformer, with the 172 Ω wire resistor connected between the 110 kV regulator and this transformer. The center phase conductor was energized directly from the output of the transformer without the normal high voltage card resistor, in order to eliminate the possibility of excessive TVI generation.

If a flashover occurred, the tap on the regulator was lowered to about one third its value at full test voltage before reclosing and then immediately increased to its previous level, thereby avoiding flashover on the reclosing transient.

On each day following one of these contamination tests, the insulator string was washed and dried before applying a new coating of contaminant for a subsequent test.

Test Results on the Antifog V-string. The results of the natural humidity tests performed during 1975 and 1976 are given in Table 4-5. As is shown in Table 4-5, two tests were performed in 1975 with 40/20 contaminant. The indoor data on vertical strings of the same type insulator were presented in Table 4-3 and gave a fifty percent string length of 18.5 units. Thus the outdoor results in fog with 40/20 show a slightly higher strength than the indoor data, although the number of outdoor

TABLE 4-5

NATURAL HUMIDITY TESTS ON CENTER PHASE V-STRING OF ANTIFOG INSULATORS ON UHV TEST LINE. ENTRIES FOR EACH TEST GIVE THE NUMBER OF INSULATORS ON EACH SIDE OF THE STRING

X = Flashover
0 = Withstand

Test Number	Voltage (kV ℓ-g)	Contaminant	Number of Units East side	Number of Units West side	Comments
1975:					
1	375	40/20	17(0)	16(X)	Fog
2	425/450*	40/20	16(X)	17(X)	Drizzle; 16(X) at 425, 17(X) at 450
3	837	40/10	39(0)	39(0)	Drizzle / heavy rain
4	837	40/10	39(0)	39(0)	Fog
5	837	40/10	39(0)	39(0)	Light fog
6	837	40/10	39(0)	39(0)	High humidity (> 90%)
7	837	40/10	39(0)	39(0)	Light rain
1976:					
8	780	40/10	29(0)	34(0)	Humidity not high enough
9	780	40/10	29(X)	34(0)	High humidity (> 90%)
10	780	40/10	29(X)	32(0)	Fog
11	780	40/10	32(X)	29(X)	High humidity
12	780	40/10	34(X)	32(0)	High humidity
13	375	40/10	14(X)	17(0)	Flashover after 30 min light rain and 3 min heavy rain

* Withstood for about 3 hours in light intermittent drizzle at 375 kV. Voltage then raised to these levels, followed by flashover in about 5 min.

tests is very small. In the second test of Table 4-5 which was carried out during drizzle, both the sixteen and seventeen units flashed over when the voltage was increased. It was not possible in the remaining 1975 tests with 40/10 to obtain a flashover, even though the wetting conditions were sufficient. In 1976, all tests were performed with 40/10 contaminant. In only one test, number (8), were the wetting conditions insufficient for adequate wetting. (The humidification rate will be discussed in a later section on the effect of fog parameters).

The data from the tests in Table 4-5 in which there was fog or high humidity are compared with the results of the indoor vertical fog tests in figure 4-19.

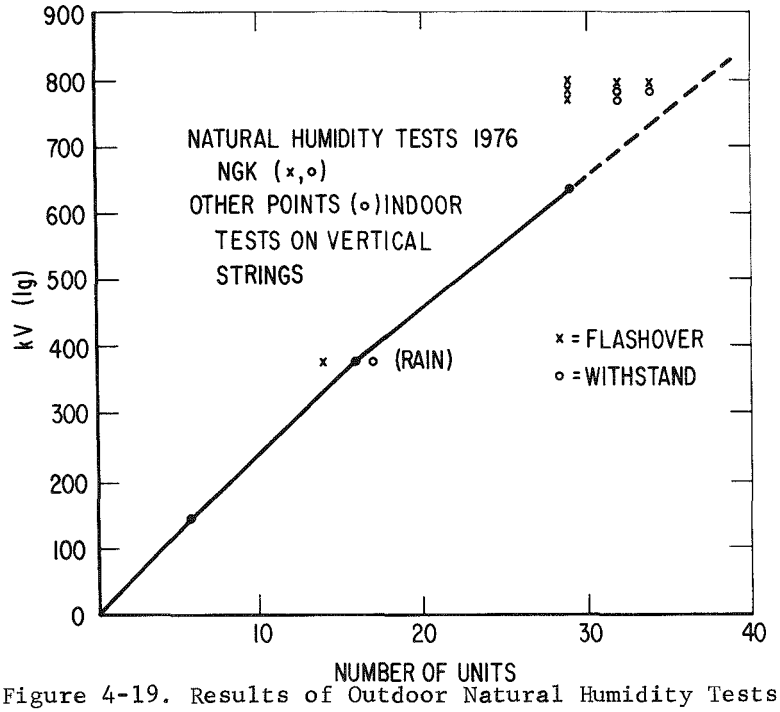


Figure 4-19. Results of Outdoor Natural Humidity Tests on V-Strings Compared with Results of Indoor Tests on Vertical Strings.

The results of the outdoor tests both at 780 kV and 837 kV indicate a higher strength than a linear extrapolation of the indoor vertical string data as shown in the figure. It should be noted however that earlier results for this type insulator indicated only a slight improvement for V- over vertical configurations. [4-1]

The tests in Table 4-5 referring to rain are quite interesting. Tests (3) and (7) in 1975 resulted in withstands, even though scintillation activity was heavy. In particular, during the heavy rain of test (3), scintillation activity was persistent and almost always of a heavy constant level. In test (4), in light rain, scintillation bursts were quite frequent. During the rain it seemed as if flashover were imminent. Finally, in test (13) of 1976, the 14 units flashed over and 17 withstood, which indicates a flashover voltage comparabile to that obtained in the indoor fog tests.

As a consequence of the natural humidity tests reported here, it is suggested that future tests be performed indoors with a true V-shaped string of the same insulators and that the onset of rain as a critical wetting condition for UHV be investigated.

The importance of the outdoor natural humidity tests should be stressed. Although time consuming, expensive, and difficult to perform, these tests provide an opportunity for a check on the data obtained indoors. The test line insulators, when subjected to artificial contamination and natural wetting conditions, serve as an excellent full scale demonstration and example of insulation behavior.

Design Rules Based on Latest Results and Comparison with Previous Results

As mentioned in the introduction, one of the primary concerns for the design of UHV lines in contaminated areas is whether or not a linear extrapolation of the performance at lower voltages may be made. A convenient method of assessing the degree of nonlinearity of strength with length involves the parameter known as long string efficiency, defined by

$$\text{long string efficiency } (\ell\text{se}) = \frac{\text{kV/insulator (at voltage of "interest")}}{\text{kV/insulator (at "low" voltage)}}$$

where the kV/insulator refers to the fifty percent flashover voltage divided by the number of units in the string. If the performance were linear, the long string efficiency would be 100%, regardless of the voltage chosen or the "low" voltage used for a reference. It is generally agreed that up to EHV levels of 362 kV and 550 kV the performance is linear, so in principle the "low" voltage used in the above formula could be any test level up to these voltages. However, small errors in kV/unit made in estimating the flashover voltage for very short strings, such as three or four standard discs, could lead to large errors in the long string efficiency. For this reason it is suggested that the "low" voltage should be somewhere in the EHV range mentioned above.

Using figure 4-11, the long string efficiency for vertical standard insulators has been calculated taking the "low" voltage as 318 kV (550 kV ℓ-ℓ). The results are plotted as a function of voltage in figure 4-20. If the earlier data were used in the same manner, the long string efficiency is somewhat lower but also tends to saturate at about 87%, as shown in figure 4-20. The curves imply a maximum deviation of about 10% from linearity up to the highest test voltage used, which is 840 kV (1450 kV ℓ-ℓ). It is suggested that the required insulator string length (L_{UHV}) for a UHV voltage V_{UHV} can be obtained from the formula:

$$L_{UHV} = L_{EHV} \frac{V_{UHV}}{V_{EHV}} \times \frac{1}{(\ell\text{se})}$$

where L_{EHV} refers to a string length which has been found acceptable for an EHV voltage V_{EHV} with the same contamination conditions and ℓse is the long string

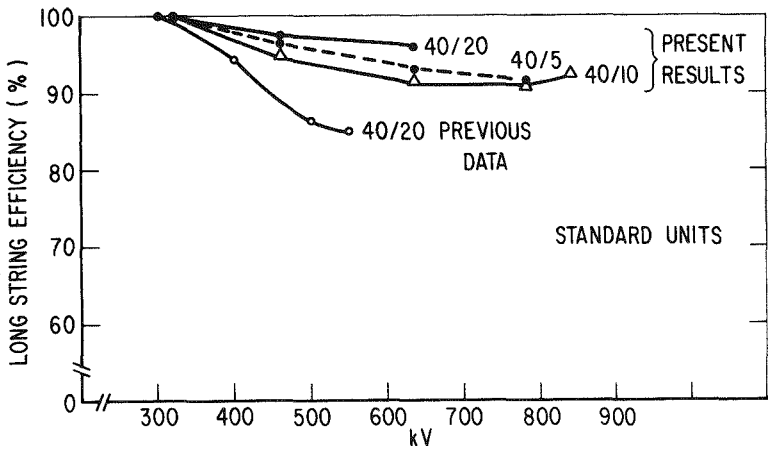


Figure 4-20. Long String Efficiency for Vertical Standard Insulators Using Present Results Compared with Previous Results.

efficiency. For the standard vertical strings, a conservative design would be given by using a ℓse of 0.9.

Similar design rules apply to the antifog units, using the long string efficiency for these insulators shown in figure 4-21.

Future Work Required

V-Strings With Straight Arms. Indoor contamination tests reported here are confined to vertical insulator strings. It is very likely that the first UHV lines to be built will make use of V-strings if current tower design technology is employed. Consequently, data should be obtained on V-strings of different insulator types, including multiple strings, with the string straight as it would be on an actual line. This requires a chamber in which sufficient mechanical strength is availab.e

At Project UHV, these tests will be performed as part of the next phase of the UHV research program, and the outdoor natural humidity data reported here will be used as a check on the indoor results.

Double Strings. In light of the results on multiple (quadruple) vertical strings described previously, tests are required with double V-strings. It is possible

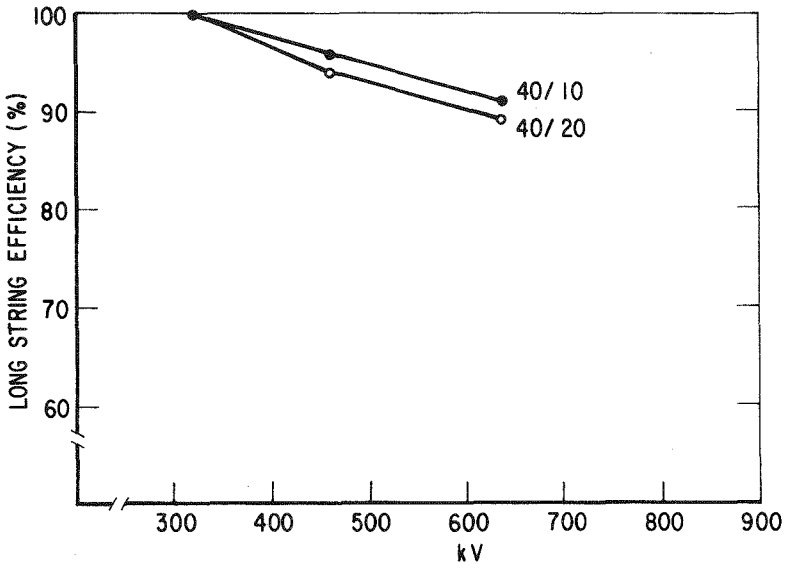


Figure 4-21. Long String Efficiency Vs kV for 40/10 and 40/20 Contaminants.

that even if single units can be made with adequate strength, the designer may ask for the redundancy of a double string for additional safety. The influence of a second string in close proximity should be investigated by making contamination tests on double strings with practical spacings.

Other Weather Conditions. Some of the outdoor natural humidity tests have indicated that the onset of rain may be as critical a wetting condition as fog or dew condensation. These tests should be made indoors with the same contamination method and a cold spray to simulate rain. The duration of these tests would be much less than the fog tests since washing would occur much more rapidly.

Other Operating Conditions. Contamination performance on switching surges after reclosure and also during temporary overvoltages should be investigated. For example, a question of interest is whether, at UHV, a successful reclosure can be obtained after a contamination flashover. General experience at lower voltages is that such outages are permanent, at least until weather conditions change or the insulators can be cleaned.

Grading Shield Influence. It is possible that UHV insulator strings will require shielding electrodes in order to limit corona. The effect of such rings on the contamination flashover voltage should be studied.

NEW INSULATOR TECHNOLOGIES

Introduction

The length of insulator strings required for withstanding even light contamination on UHV lines has provided a great incentive for the development of new technologies. Long strings of cap and pin type units have disadvantages both electrically and mechanically. For example, in dry conditions, the nonuniform voltage distribution along a string will stress several units so that they are in corona at normal operating voltage. The weight of high mechanical strength units used in a single string, or the total number of units required when lower strength units are paralleled, may amount to a significant factor in the vertical loading on the towers.

For these reasons, several new insulator technologies have been developed and investigated. Some of the principles involved and presently available alternatives to conventional designs will be discussed.

Electrical Considerations for UHV Insulators

Voltage Distribution on Cap and Pin Strings. In dry conditions, the voltage distribution on an insulator string is determined by the self capacitance between the cap and pin of each unit and the stray capacitances between each electrode (i.e. the pins) and all the other electrodes. As an example of the voltage distribution, a calculation has been made for a string containing 30 fog type units considering only stray capacitances to ground and to the transmission line conductor. The parameters used and the results are illustrated in figure 4-22. Note that the insulator nearest the conductor has a voltage across it which is 4.6 times the average voltage. For 1200 kV system, this implies that the voltage across the first insulator is 106 kV! Of course, this insulator would be in corona and hence these simple calculations are no longer valid since the corona would modify the voltage distribution. Nevertheless, this example emphasizes the very nonuniform voltage distribution on long strings of cap and pin insulators. Actual measurements on insulator strings at low voltage have also verified the degree of nonuniformity of these distributions, and these will be described later.

The consequences of the high stress in dry conditions are mainly corona generation. Provided the corona is of the glow type, it will likely affect neither the life of the insulators nor the radio noise generation of the line. However, if sparking occurs, there could be damage to the insulator as well as unacceptable radio noise. The presence of such sparking may require the installation of shield rings to obtain a better voltage distribution.

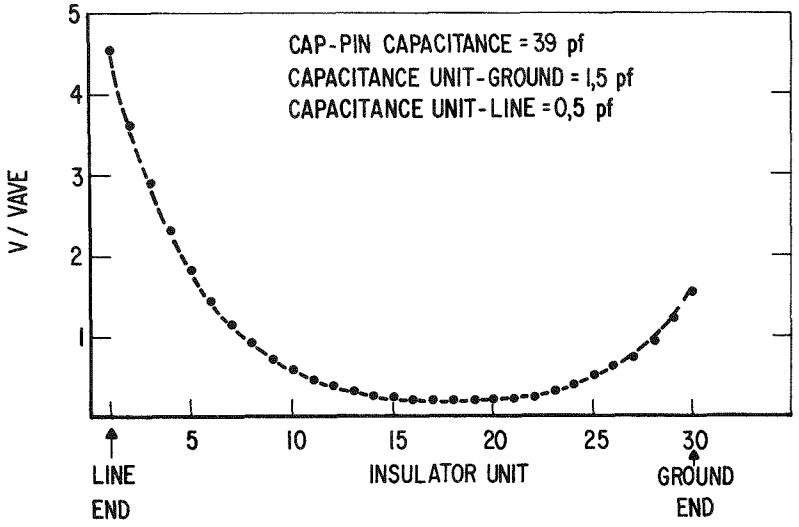


Figure 4-22. Voltage Distribution on 30 Unit Insulator String.

In clean wet conditions, or in contaminated conditions with moisture on the insulators, sparking may again occur as a result of the highly nonuniform voltage distribution. It would therefore be desirable to improve the voltage distribution on insulator strings for UHV.

Voltage Grading and Contamination Performance

High Capacitance Insulators. Earlier studies at Project UHV on the nonlinearity of insulation strength as a function of contaminated insulator string length had attributed this phenomenon in part to the initial nonuniform voltage distribution on long strings and its influence on wetting and the development of discharges. The voltage distribution depends on the relative magnitudes of the self and stray capacitances of the insulators. On standard 146mm x 254mm (5 3/4 in x 10 in) insulators, for example, the self capacitance is approximately 25 pF, and the stray capacitances to ground and to the line conductor are on the order of 0.5 to 5 pF.

Special insulators identical in shape to standard units and having a capacitance between cap and pin of about 1600 pF at operating voltage were developed in order to provide a uniform voltage distribution on long strings by means of the high self capacitance. These special units were fabricated by inserting a high dielectric constrant capacitor between the cap and pin of a standard insulator. A cross-

sectional view of the specially developed high-capacitance insulator is shown in figure 4-23. The insulators were fabricated by the Ceramic Laboratory of GTRO (Group Technical Resources Operation of General Electric).

The high dielectric constant capacitors which were inserted in the standard insulators exhibit a voltage-dependent dielectric constant, in which dielectric constant increases with increasing voltage. Measurements on 27 assembled individual high-capacitance units showed an average capacitance of 1635 pF with 1% standard deviation at 6 kV per unit, and 1800 pF with 1.4% standard deviation at 12 kV per unit. The rising capacitance-voltage characteristic of these insulators should also help to maintain the uniform voltage distribution under dynamic conditions.

Before making contamination tests, 3 strings containing 8 clean and dry units each of the high capacitance insulators were subjected to a stress of 128 kV (ℓ-g), or 16 kV/insulator, for a period of 2 hours. This was done to insure that none of the insulators were susceptible to internal failures at the highest planned voltage to be applied during contamination tests.

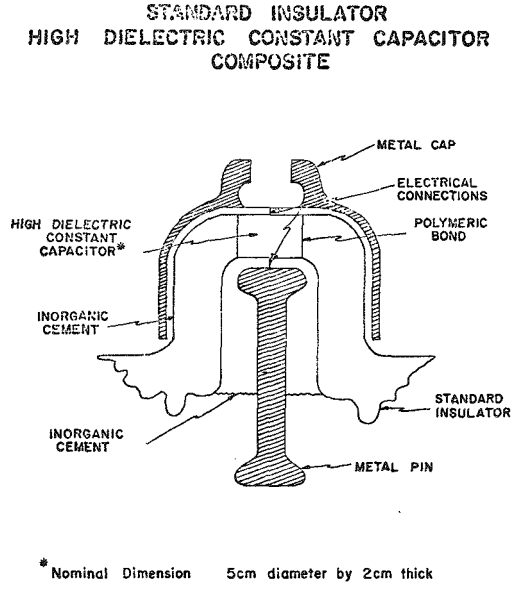


Figure 4-23. Cross-Sectional View of the High-Capacitance Insulator.

The static voltage distribution on a 25 unit string of high capacitance insulators shown in figure 4-24 was measured using a 23-kV source. For comparison, measurements made on a string of similar length but composed of standard insulators are given in figure 4-25. During contamination tests, the voltage stress per unit would be an order of magnitude higher; because of the increasing capacitance-voltage characteristic, the distribution is therefore expected to be even more uniform during actual test conditions. A comparison of figures 4-24 and 4-25 shows a dramatic reduction of the non-uniformity in the voltage distribution for the high capacitance units over standard insulators.

The contamination performance of the high capacitance insulators was evaluated by means of the regular indoor steam fog test. [4-1] The procedure consisted of simultaneously energizing two contaminated insulator strings in parallel. One of these contained a variable number of high capacitance units, while the other contained 27 standard insulators. For the first test, 25 high capacitance units subjected to an average stress of 13 kV/insulator were compared with 27 standard units at 12 kV/insulator. After each test in which the standard units flashed over, the high capacitance string was shortened. This initial test series led to to the conclusion that the flashover voltage of 17 high capacitance units is higher

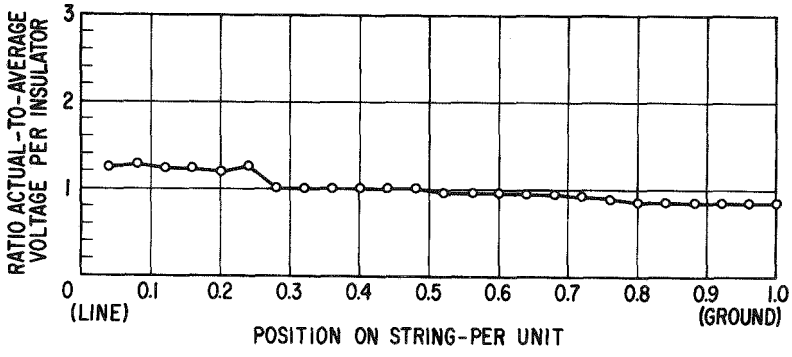


Figure 4-24. Voltage Distribution on a 25-Unit String of High-Capacitance Insulators.

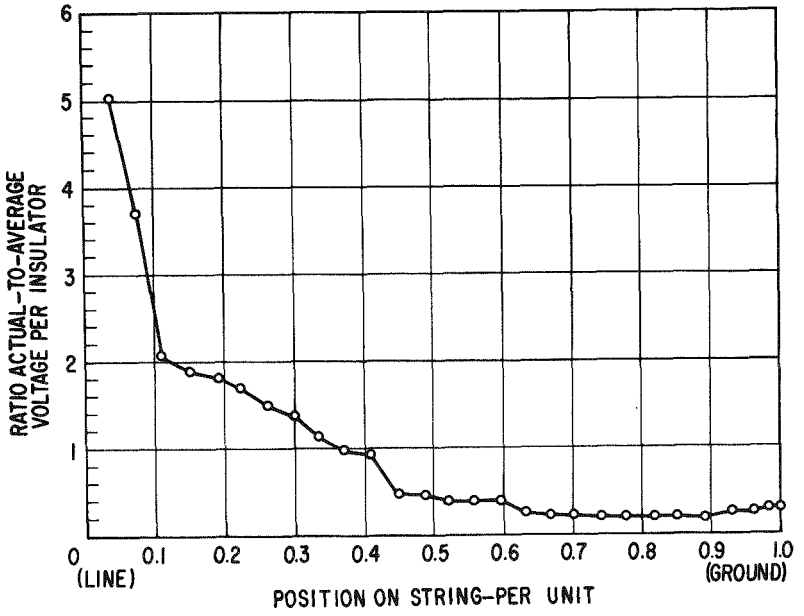


Figure 4-25. Voltage Distribution on a 27-Unit String of Standard Insulators.

than that of 27 standard units contaminated with 40/20. During the flashover tests, occasional light scintillation activity was observed on the high capacitance units. The scintillations were not localized near the line conductor, as was the case for the standard units which exhibited intense discharges.

The excellent contamination performance of the special high capacitance insulators was even better than expected from a linear extrapolation of short string data for standard units. It was therefore suspected that the high capacitance units had a very high strength in short strings also. Tests on short strings revealed that with 40/40 contaminant (0.1 mg/cm^2 equivalent salt deposit density), the high capacitance units could withstand 18 kV/unit, in contrast to standard units which flashed over at 15 kV/unit.

The reason for the superior performance in these short strings was thus not related to the improved voltage distributions on long strings but rather to the following phenomenon. The high dielectric constant capacitors which were inserted into standard insulator shells to make high capacitance units had dissipation factors on the order of 7% at 12 kV, implying a resistive loss of about 7 watts per unit. Due to the increasing dissipation factor and capacitance with increasing voltage, the resistive loss at 18 kV would be about 25 watts. It was observed during the

tests reported here that the high capacitance insulator caps were warm after the tests were performed. This heating inhibited the condensation of moisture on the insulator surfaces, especially on the adjacent skirts of the next unit above each cap, and thus was responsible for the high flashover voltage.

The combination of heat dissipation and linearity of voltage distribution on long strings thus explains the improvement in performance of these insulators compared with long strings of standard units. The fact that the voltage distribution in a long string of the high capacitance units is quite uniform allows an extrapolation of the behavior from short to long strings. The question still remained as to whether long string contamination performance of insulators could be improved without the additional physical mechanism of heat dissipation.

External Grading. In order to examine the possibility of improving long string contamination performance by means of a more uniform voltage distribution, two types of special tests were performed. In the first set of experiments, a string of 27 standard insulators was tested in parallel with a second standard unit string which was externally graded by high capacitance insulators. Both strings of standard type insulators were contaminated, whereas the high capacitance units themselves were left clean. The combination standard - high capacitance strings were varied in length and compared with the single, 27-unit standard string.

For the initial flashover tests, a wire was connected between each standard unit and the corresponding high capacitance insulator to accomplish the external grading. The static voltage distribution on such an externally graded standard string of 25 insulators is shown in figure 4-26. This distribution is almost as uniform as the voltage distribution on the high capacitance insulators shown previously in figure 4-24.

Results of flashover tests showed that 25 graded units had higher strength than a 27-unit standard string, but 23 graded units were weaker than 27 standard insulators.

One possible explanation for the poor performance of the graded string compared to a string of high capacitance insulators is that the presence of the connecting wires severely distorted the field near the units. The influence of the connecting wires was examined by removing every two out of three connections and making additional contamination tests. In this case it was again demonstrated that a 23 graded unit string was weaker than a string of standard insulators 27 units long.

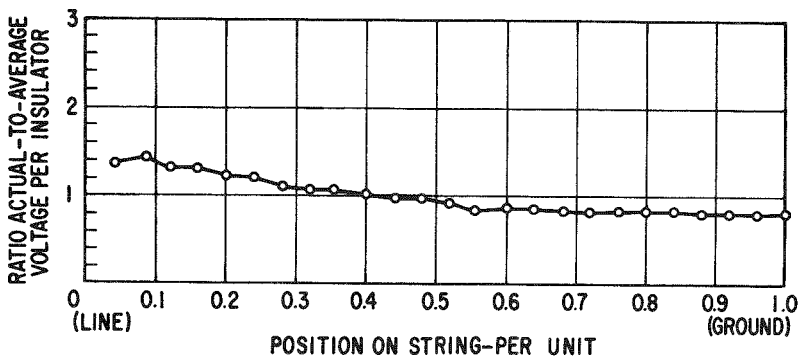


Figure 4-26. Voltage Distribution on an Externally Graded String of 25 Standard Insulators.

Further tests were made to check the influence of the connecting wires for the external grading tests.

First, three parallel strings of standard insulators containing 27 units each were suspended adjacent to each other. Two of the strings were connected by wires between corresponding caps of each unit, in effect "grading" a standard insulator string with another standard insulator string using wired connections. The wires were placed carefully, so that they were not too close to adjacent insulator skirts and were parallel. Only one of these two strings was contaminated. The contamination performance of the "graded" string was checked by making comparison tests in which the third 27-unit standard string was also contaminated. The purpose of the tests was to determine whether the presence of the grading wires would cause a deterioration in the graded standard string behavior. A total of 10 steam-fog tests were made. During most tests scintillation activity occurred on both the graded string and the single string. Frequently, there were small discharges near the pins of the contaminated units along with a buzzing sound. On the basis of these tests, it was concluded that the presence of grading wires did not cause a decrease in insulation strength. In fact, although scintillation activity was more or less evenly distributed between the graded and single strings, with only one exception did the graded string flash over first.

Since the wired connections were not made with a uniform distance between parallel wires in the above experiments, it was decided to repeat the grading of standard insulators using high capacitance units in a slightly different arrangement. Twenty-two units of high capacitance insulators were utilized to externally grade the voltage distribution on 22 standard insulators, but an intermediate string of standard units was used so that connections could be made as they were in the tests reported above. The experimental setup is shown in figure 4-27. The intermediate string of standard insulators was required because the high capacitance units had a slightly longer connection length than standard insulators; as may be seen in figure 4-27, the wires could not be paralled between the high capacitance and standard strings. The intermediate string is, however, connected with parallel, uniformly spaced wires to the contaminated string under test. Unfortunately, the result of this experiment was a flashover of the graded string at 11 kV/insulator, well below the minimum flashover voltage of 12.8 kV for individual units. In other words, linear performance of the 22-unit string was not achieved.

An attempt was made to improve the contamination flashover performance of standard insulators by grading the voltage distribution on a long string without any wired connections, i.e. by shaping the electric field in the vicinity of the insulator string. The electrodes used for these experiments are shown in figure 4-28. The

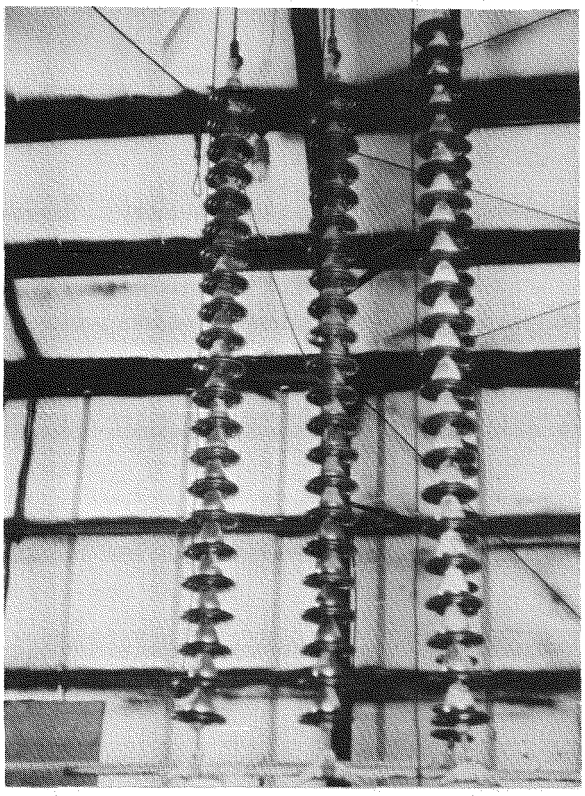


Figure 4-27. Experimental Test Setup for External Capacitive Grading Using Wired Connections to High Capacitance Insulators. String on Right Contains 22 High Capacitance Units, While Other Two Strings Contain 22 Standard Insulators Each. Only the String on the Left was Contaminated. The Purpose of the String in the Center was to Insure that the Wires to the Contaminated String Would be Parallel and Uniformly Spaced.

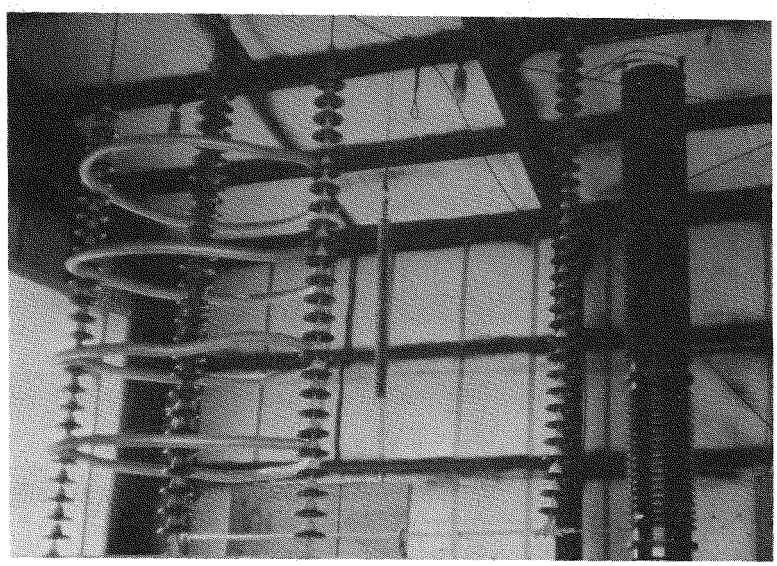


Figure 4-28. Experimental Test Setup for External Field Grading of an Insulator String. The 25-Unit Insulators in the Center of the 4 Rings were Contaminated. The Voltage on the Rings was Controlled by Connections to the Capacitor-Divider Stack on the Right.

capacitor stack shown in the foreground contained five sections of 6000 μF capacitors. Connections were made from this stack to the 203cm (80 in) diameter rings which were composed of 10cm (4 in) tubing and surround the insulator string to be graded, but no physical connection between the rings and the insulators under test was made. In figure 4-28, four rings are shown at the positions of the 5, 10, 15 and 20th insulators of a 25-unit test string in the center of the rings. Some tests were also made with two additional rings, one on the high voltage conductor and another at the ground end of the string, as illustrated in figure 4-29. The voltage distribution on the string in the center of the rings is shown in figure 4-30 for both the case of four grading rings illustrated in figure 4-28 and the situation in which additional rings are added on the ground and high voltage ends, shown in figure 4-29. As may be seen in figure 4-30, the voltage distribution is made somewhat more uniform when the additional rings are employed.

In the tests performed with the graded string, the flashover voltage was the same as that of an ungraded string of the same length. The conclusion was that external grading without connections was also ineffective in improving insulation strength of long strings. In other words, a voltage distribution on the string such as that shown in figure 4-30, produced by external grading, does not necessarily result in an increase in insulation strength above that which exists for a string without

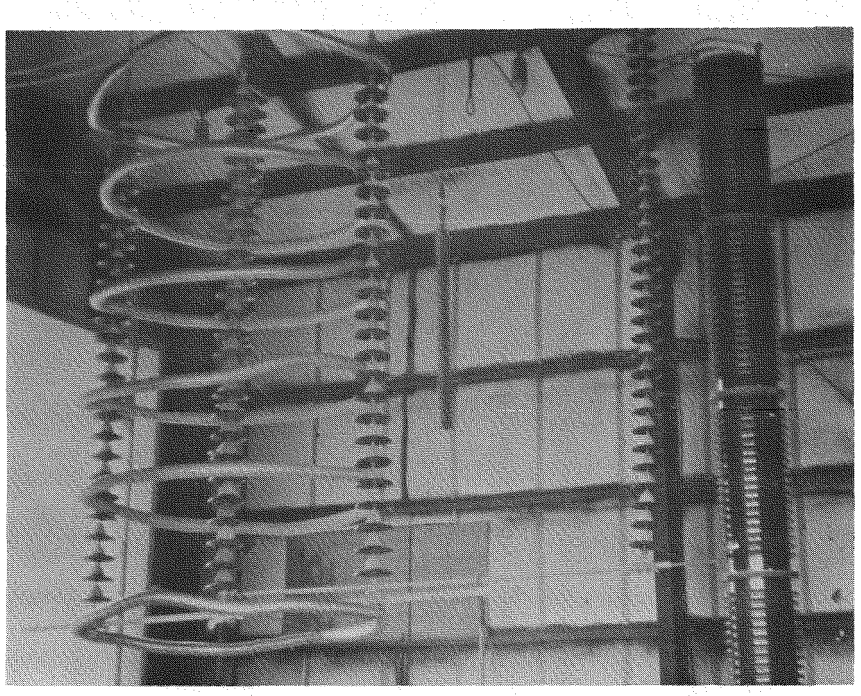


Figure 4-29. External Field Grading with 2 Additional Rings to Improve the Voltage Distribution Obtained with the Apparatus in Figure 4-28.

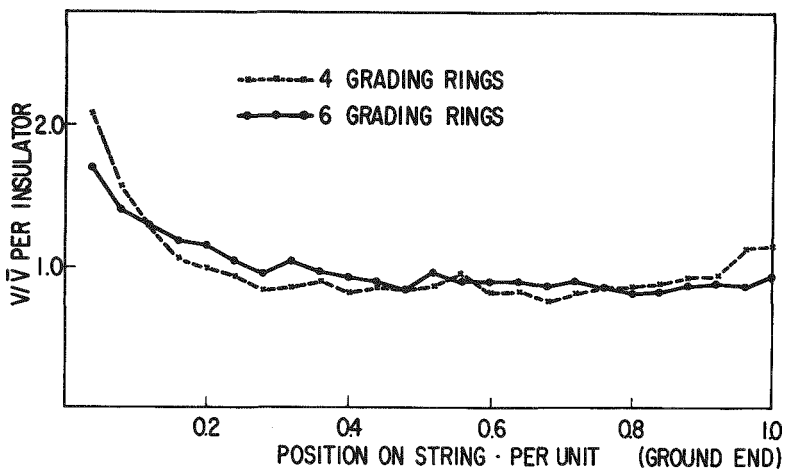


Figure 4-30. Voltage Distribution on Field Graded Insulator Strings for the Case of 4 Rings (Figure 4-28) and 6 Rings (Figure 4-29).

grading. The scintillation activity during these tests was somewhat unusual in that widely separated parts of the string were observed to be bridged by partial discharges, with "quiet" units between the "active" areas.

In order to confirm the hypothesis that an extremely nonuniform voltage distribution would further decrease the insulation strength of a long string, the external grading arrangement shown in figure 4-31 was tested. The top three rings in that setup are shorted to ground, while the lower two are left floating electrically. This results in the voltage distribution on the test string as shown in figure 4-32. The 25-unit string in the center of those rings had a flashover voltage 12% lower than an ungraded string.

It was thus concluded that while the flashover voltage could be lowered slightly by imposing a voltage distribution which is worse than that of the string by itself, no improvement could be obtained by making the voltage distribution more uniform than that which exists when the string is not externally graded.

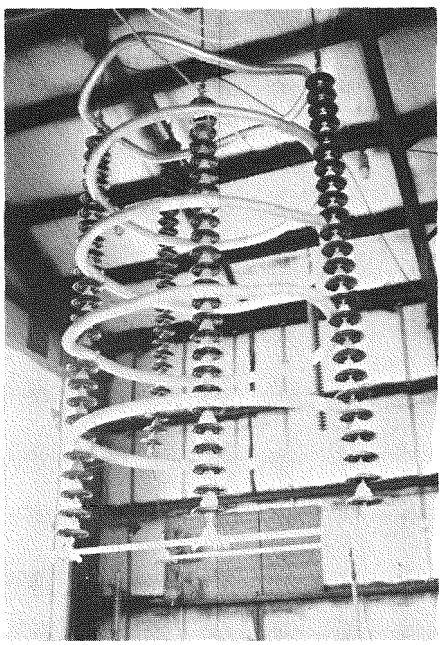


Figure 4-31. Experimental Setup Used to Obtain Nonuniform Voltage Distribution with External Field Grading. Top Three Rings Grounded, Other Two Electrically Floating.

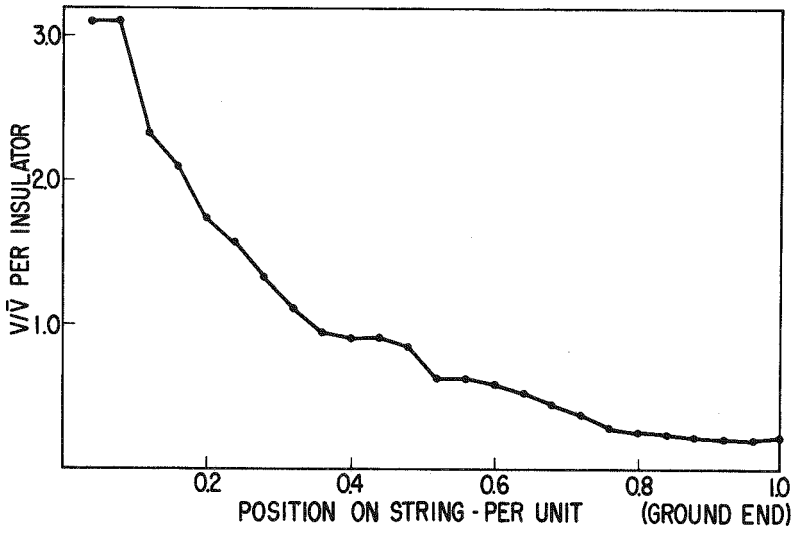


Figure 4-32. Nonuniform Voltage Distribution Obtained by External Field Grading Setup of Figure 4-31.

Semiconducting Glaze Insulators

Introduction. Insulators with semiconducting glaze have been available for some time. The use of resistive coatings has been found effective both in suspension and post type insulators as a solution for insulation design in heavily contaminated areas. The basic principle involves the continuous flow of current on the order of one milliampere as a means for providing enough heat on the surface of the insulators so that they cannot become wet in dew or fog. There have been some difficulties with the fabrication and field life of these insulators in the past, but significant technological improvements have been made and substantial service experience exists so that their use should be considered in the contamination design of UHV transmission lines.

Design Considerations. The contamination performance of semiconducting glaze insulators was checked by making tests on suspension units with a predeposited contaminant and a clean fog as for other regular tests described previously. The insulators were of the standard shape (146mm x 254mm) and were intended for energization at 11 kV/unit and a nominal resistive current of 1 mA. Short strings containing five units of these insulators were contaminated with 40/100 mixture corresponding to a salt deposit density of about 0.25 mg/cm^2, which is a very high

level of severity. Theinsulators were energized at a constant voltage of 11 kV/unit and exposed to the clean fog. The heat dissipation of 11 watts/insulator kept the surfaces dry and no flashovers occurred. It was thus verified that this type of insulator is effective for heavy contamination in areas where wetting normally occurs by fog.

Three factors would influence the application of semiconducting glaze units for UHV lines. First, if the normal operating voltage per insulator were constrained to be on the order of 11 kV/unit, long insulator strings would still be required. For example, on a 1200-kV system, 63 units of the standard type tested would be needed to achieve the proper working voltage for each insulator. Second, there is a question as to the voltage distribution on long strings and the importance of other factors such as thermal stability on performance. Finally, there is the economic consideration of the acceptability of a constant power loss due to resistive heating.

In regard to the question of the working voltage per insulator, prototype units of standard shape but designed for nominal 15 kV, 1 mA operation were delivered to Project UHV for the tests to evaluate cold switch-on performance. It appears that such insulators would be attractive for UHV. On a 1200-kV system, 46 of the standard shape insulators would be required. This would mean a shorter string length than the 55 conventional units of standard shape otherwise necessary for even light contamination.

The voltage distribution on a long string of semiconductive glaze insulators will be more uniform than a conventional string as a result of the resistance of each unit. [4-2] It is therefore reasonable to expect that the test results obtained with short strings will also apply to the long strings required for UHV, since the primary mechanism involves the heating of the surfaces of each insulator. The thermal stability of a long string should also be better than that of short strings. The reason for the improvement in stability in long strings is due to the fact that overheating in one unit, due either to a higher voltage per unit or external sources such as sunlight would create a smaller increase in current because of the larger number of impedances in series with the unit in question.

Finally, the issue of constant dissipation and its economic penalty should be considered in any widespread application of the semiconducting glaze insulators. As an example, consider the possible use of these units for 1200 kV transmission.

With 1 mA resistive current, each leg of a semiconducting glaze string would dissipate 692 watts. Assuming a double V-string for each phase, the dissipation per tower would be 8.3 kW. With four towers per mile, the constant loss due to these insulators would be 33.2 kW per mile. For a typical 1200 kV design, the expected total average yearly I^2R and corona loss would amount to 110 kW/mi. This implies the insulator losses are 30% of these other losses, and thus a factor which would contribute significantly to operating costs.

Cold Switch-on Performance. It was shown in above that if semiconductive glaze units with sufficiently high working voltage were available, it would be possible to compact lines and drastically reduce string lengths in areas with contamination. However, the resulting increased stress per unit in this case has focused attention on the insulation strength during the energization of strings which are contaminated and wet, a condition which is known as "cold switch-in." This situation would occur on lines which have been unenergized for a period of time long enough so that the heating, which results from the semiconducting glaze while the units are energized, is no longer effective in preventing the accumulation of moisture on the insulator surfaces.

Some data on the cold switch-on strength of semiconducting glaze insulators are available [4-3] However, those results were obtained with relatively short strings containing ten units (1.5 meters) or less. The purpose of the tests reported here is to extend those data to strings which would be suitable for UHV transmission systems and to make a direct comparison to the cold switch-on strength of conventional insulators which have a similar shape. In addition, it was desirable to obtain data with the same type of contaminant which has been used to evaluate the strength of contaminated insulators under constant voltage in regular steam fog tests at Project UHV.

The test method used to determine cold switch-on strength is similar in principle to that of the wet contaminant test, with several notable exceptions.

First, the contaminant was composed only of kaolin, sodium chloride, and water. This solution was applied to the insulator strings, as in the regular constant voltage tests [4-1] The insulator strings were dried by heating the air in the chamber, and then cooled to the outdoor ambient temperature. It was found that bypassing the drying and cooling periods gave unsatisfactory results, since the contaminant was frequently removed from the insulators due to excessive dripping during the subsequent application of fog.

After drying and cooling, the fog generation was initiated by turning on the electrically heated water containers which produce the clean fog. The cold switch-on test voltage was not applied to the insulator strings until they were thoroughly wet. The time at which the cold switch-on tests began was determined by measuring the impedance of either the strings to be tested or an auxiliary monitor string which was prepared in an identical manner to the test strings. In order to find the impedance, a maximum voltage of 1 kV/unit was applied to the insulators every five minutes for a duration which was only long enough to measure the current, generally 0.5 sec. or less. When the resistance reached its minimum value and was stabilized, the test series was started.

For the results reported here, two vertical insulator strings (one conventional and the other semiconducting glaze) were always tested essentially in parallel. This was accomplished by applying the full test voltage alternately to the conventional string for a maximum duration of 30 secs. and to the semiconducting glaze units for 5 secs., with another application of voltage on each string every ten minutes. The fifty percent flashover voltage was determined by an "up-and-down" technique, in which the voltage in consecutive shots was raised or lowered by $\sim$ 10%, depending on whether a withstand or flashover occurred. The total time of the test series was about 2-3 hours, so that results of between 10-15 voltage applications on each string were used to determine the 50% flashover voltage for a given string length and contaminant.

The justification for this test procedure is as follows. First, with respect to the duration of the applied voltage, it was found that flashovers occurred on the conventional units in less than 30 secs. after energization, and in less than 5 secs. on the semiconducting glaze insulators. Furthermore, an investigation was made in order to find the appropriate time interval between consecutive voltage applications. This involved applying voltage for different durations and measuring the resistance of the string as a function of time afterwards. The results are shown in figure 4-33, where the resistance is given for standard and semiconducting glaze insulators after voltage was applied for different lengths of time. For the data shown in figure 4-33, withstand voltage levels were used, since it was determined from other measurements that the resistance recovers more rapidly after a flashover than after the scintillation activity of several seconds. It may be seen in figure 4-33 that ten minutes is a sufficient time interval between tests if voltage is applied for 30 secs. to conventional units, whereas only 5 secs. should be used for the semiconducting glaze insulators if another shot is to be made in 10 minutes.

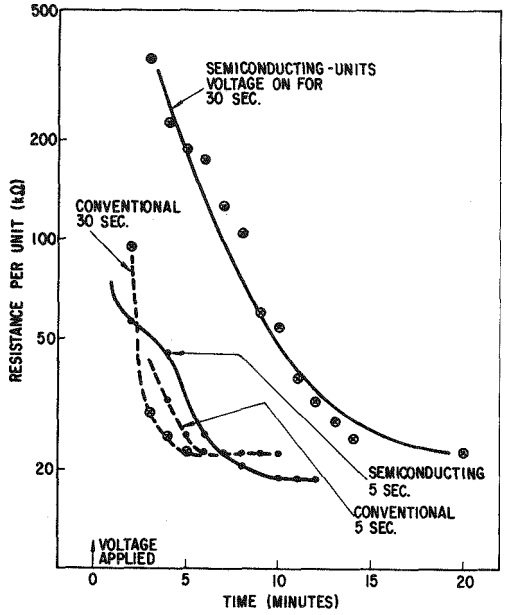


Figure 4-33. Resistance of Insulator String as a Function of Time for Different Lengths of Application of Voltage.

Another characteristic of the test procedure which requires justification is the fact that the insulators were only contaminated once for the entire 2-3 hour test series, in contrast to the wet contaminant test which requires cleaning and contamination before each application of voltage. If the amount of contaminant were substantially reduced during the time of the test, it should become apparent by observing(1) a decrease in the salt deposit density and/or(2) a tendency of the 50% flashover voltage to increase as the test sequence progressed. Measurements of the salt deposit density on units in the tested strings after the normal 2-3 hour period of fog and voltage applications indicated that the maximum change was a decrease of 10%. The up-and-down sequence also showed no tendency to migrate upward in voltage, as shown by typical results in Table 4-6. These facts led to the conclusion that the test procedure described above is suitable for determining the cold switch-on performance of insulator strings contaminated with a kaolin-sodium chloride and water solution.

The shape of the semiconducting glaze units tested was the same as that of the standard insulators shown in figure 4-10. The only difference was that the hardware of the semiconducting units was slightly larger than that of the standard insulators illustrated there. The semiconducting glaze insulators were designed for a nominal operating voltage of 15 kV/unit and a steady resistive current of 1 mA.

TABLE 4-6

COLD SWITCH-ON TEST SERIES PERFORMED ON CONVENTIONAL AND SEMICONDUCTING GLAZE UNITS. INSULATORS CONTAMINATED ONLY BEFORE BEGINNING OF TEST SERIES. TOTAL TIME OF TEST: 2 HOURS

X = Flashover
0 = Withstand

Test #:	1	2	3	4	5	6	7	8	9	10	11	12
kV (ℓ-g)												
690		X										
640	0		X		X							
590				0		X		X		X		X
540							0		0		0	

56 Conventional Insulators

690				X								
640	X		0		X		X		X			
590		0				0		0		X		0
540											0	

56 Semiconducting Insulators

TABLE 4-7

FIFTY PERCENT COLD SWITCH-ON FLASHOVER VOLTAGE OF CONVENTIONAL AND SEMICONDUCTING GLAZE INSULATORS.*

Number of Units	Average Salt Deposit Density (mg/cm^2)	50% Flashover Voltage (kV)	kV/Unit
15		143 Conv.	9.53 Conv.
		173 S.C.	11.5 S.C.
31	0.04 (40/20)	283 Conv.	9.12 Conv.
		305 S.C.	9.84 S.C.
56		525 Conv.	9.38 Conv.
		525 S.C.	9.38 S.C.
64		573 Conv.	8.95 Conv.
		618 S.C.	9.66 S.C.
14		158 Conv.	11.3 Conv.
		155 S.C.	11.1 S.C.
25	0.02 (40/10)	275 Conv.	11.0 Conv.
		286 S.C.	11.4 S.C.
56		594 Conv.	10.6 Conv.
		617 S.C.	11.0 S.C.

* Voltage applied for maximum duration of 30 secs. on conventional insulator & 5 secs. for semiconducting glaze units.

The data on cold switch-on strength is presented in Table 4-7 for these two types of insulators and two different contaminants, as noted by the equivalent salt deposit density. The results showing fifty percent flashover strength as a function of string length are given in figure 4-34, whereas the 50% flashover voltages expressed as kV/insulator are shown in figure 4-35 as a function of the number of insulators in the string.

The curves in figures 4-34 and 4-35 indicate that the cold switch-on strength of the semiconducting glaze insulators is equal to or slightly greater than that of the conventional units. Even for long strings, the strength is almost a linear function of string length, showing only a slight nonlinearity or saturation.

The scintillation activity during cold switch-on on the two types of insulators was markedly different. On the semiconducting glaze insulators, scintillations extinguished in a few seconds after application of voltage, whereas on the conventional insulators scintillation activity often persisted for much longer times. This supports the idea that the heating of the semiconducting insulators becomes effective in a short time. [4-3] Flashovers never occurred on the switching surge resulting from sudden energization, but generally took place after a few cycles at the earliest.

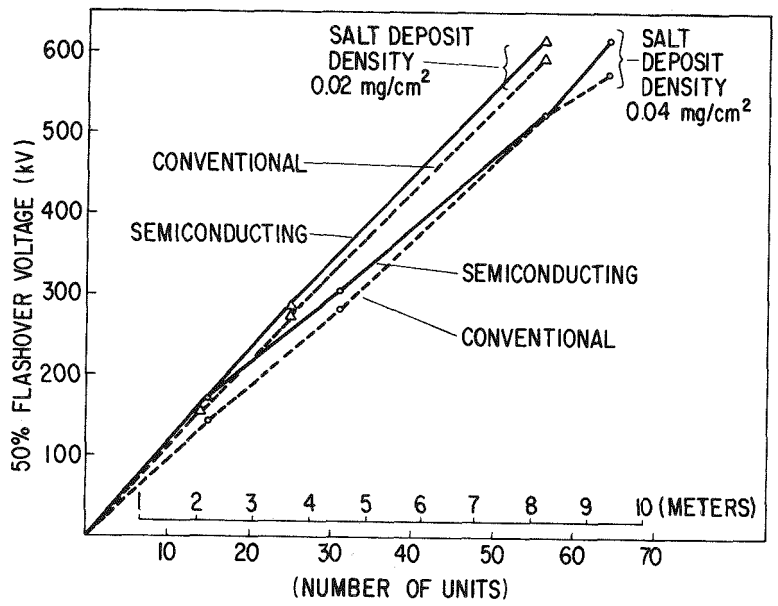


Figure 4-34. Fifty Percent Flashover Strength as a Function of String Length.

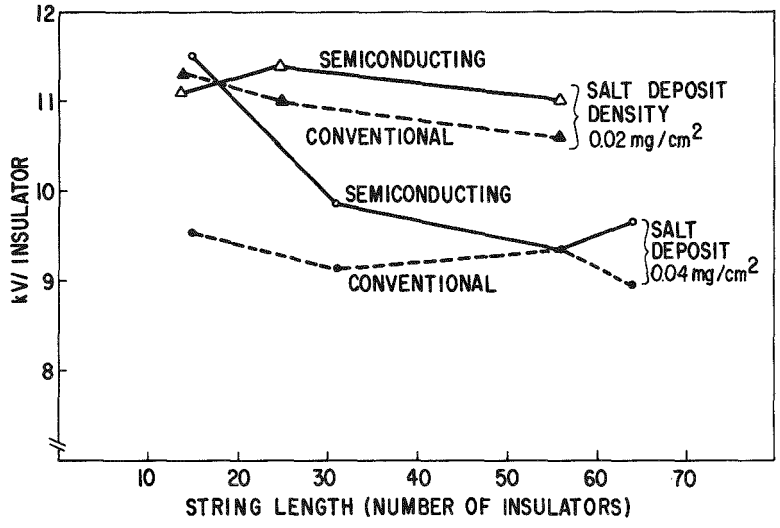


Figure 4-35. Fifty Percent Flashover Voltage Expressed as kV/Insulator.

Since the semiconducting glaze units on which the cold switch-on tests were performed had a nominal operating voltage of 15 kV/unit and 1 mA resistive current under continuous voltage, they could be used to compact insulator strings and significantly reduce required clearances. On a 1200-kV system, 46 units would be required, corresponding to a string length of 6.7 meters. This leads to an air gap which may not be sufficient to withstand switching surges. In addition, the data in Table 4-7 and figures 4-34 and 4-35 indicate that the cold switch-on strength under continuous voltage. For example, in a string 6.7 meters in length, the fifty percent flashover voltage would be 500 kV in cold switch-on with 40/10. This is far less than the operating level of 693 kV for a 1200 kV system and thus cold switch-on might be an important consideration in the design.

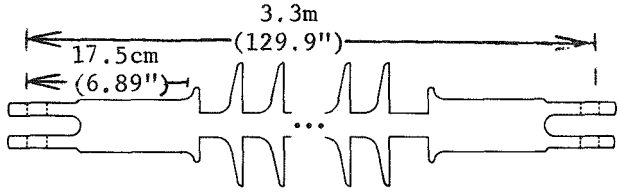
Non-Ceramic Insulators

Concepts. Another new insulator technology which has recently come to the attention of the utility industry involves the use of organic materials everywhere except at the end fittings. These insulators employ a fiberglass rod for mechanical strength and a weather shed on the surface using some type of polymer for sufficient electrical leakage distance. The mechanical strength can be far in excess of the highest strength 55 kg (120,000 lb) ceramic units which are presently available. In principle any length of fiberglass rod can be manufactured and thus single pieces would

even be available for UHV line insulation. However, transportation facilities may make single section lengths over 6m (20 ft) impractical.

There are two distinct advantages to these insulators apart from electrical performance. First, their weight is only a fraction (usually about 10%) of a conventional insulator string with the equivalent load characteristics. Vertical tower loading for UHV lines could be substantially reduced by using these units. Second, their single or several piece construction makes installation more simple since cap and pin type string assembly is unnecessary.

Contamination Performance/Linearity. The contamination performance of one type of plastic insulator has been evaluated in indoor fog chamber tests. The units tested had sheds made of silicone rubber over the fiberglass rod core. The shed shape is illustrated in figure 4-36. The total length of each piece was 3.3m (130 in) which corresponds to the length of a 23 unit string of standard cap and pin suspension insulators. These single sections were intended for insulating a 550 kV system, where 24 conventional units are commonly used in clean areas.



64 SHEDS

Shed outer diameter:	13cm (5.12")
Core diameter:	2.5cm (0.98")
Shed spacing:	4.5cm (1.77")
Leakage distance:	8.7m (342.9")
Leakage/connection length=	2.64

Figure 4-36. Shape and Dimensions of a Single Unit Silicone Rubber, Glass-Fiber Reinforced Long-Rod Insulator.

In order to assess the flashover strength of these nonceramic insulators in contaminated conditions, tests were made with different levels of contamination severity on single unit vertical and V-configurations for EHV and on similar double unit configurations for UHV. These latter data also provide information on the linearity of insulation strength with length for this type of insulator.

Mechanical Loading Considerations

Insulators for transmission lines must have sufficient mechanical strength to withstand the maximum expected loading conditions imposed by wind forces and ice on the conductors. For a given voltage level in a UHV system, a large variety of conductor bundle configurations may be acceptable for the purpose of satisfying other design criteria such as audible noise performance or electric field at ground level. The choice of a particular bundle design may then be influenced by other factors, one of which is the magnitude of mechanical stresses applied to insulator string.

A detailed analysis has shown that for a given voltage class, as the number of subconductors in a bundle increases, the insulator string weight may become a substantial percentage of the maximum vertical load on a tower. For available ceramic insulators, this percentage may reach 20% for a 1200 kV system. In addition, for any given bundle, the total string weight is relatively independent of the string design. In other words, the total weight of single strings of high strength units is roughly the same as the weight of multiple strings of lower strength insulators. This is due to the fact that the high strength units have greater weight but also larger connection lengths.

The regular fog test procedure was utilized for all the results presented here, with single units evaluated in the EHV chamber and double units in the UHV contamination building. An up and down sequence in voltage was used to determine the 50% flashover voltage (CFO) for each level of contamination severity.

An important preparatory step, which was performed before each insulator was tested included a careful scrubbing with kaolin (clay power) in order to remove any excess surface grease which may have been present from the manufacturing process. This has been standard practice for all other types of new insulators tested at Project UHV. In addition, some long rod units were contaminated with the normal contaminant mixture and washed several times before testing, since initial units on which this was not done showed a visual aging effect with respect to the appearance of the

surface after the first few tests, as well as an increase in salt density with the same contaminant mixture.

An example of the appearance of the long rod insulator shed surfaces after being contaminated is shown in figure 4-37. The contamination severity was evaluated by washing both top and bottom surfaces of two complete sheds on a sample insulator which was contaminated and dried in a manner similar to the insulators under test. In cases where the test units were placed in a V-configuration, the sample insulator was also inclined at approximately the same angle as the insulators being tested.

The EHV contamination chamber was used for tests on single sections of these plastic insulators. The setup for vertical and V-configurations of single units is illustrated in figures 4-38 and 4-39. During the first set of tests on the vertical configuration, a long up and down sequence of about 25 tests showed a decrease of about 14% in the flashover level, in addition to an increase of 20% in the salt deposit density, indicating an aging effect.

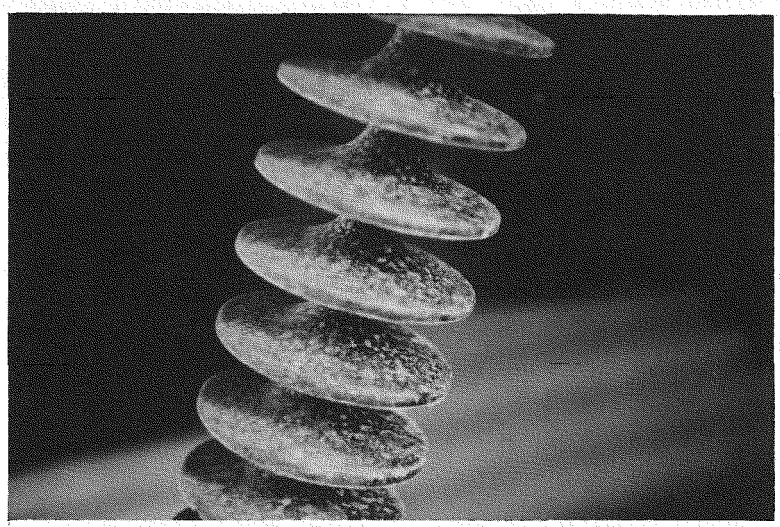


Figure 4-37. Shed Surfaces of Long-Rod Insulators After Being Contaminated and Dried.

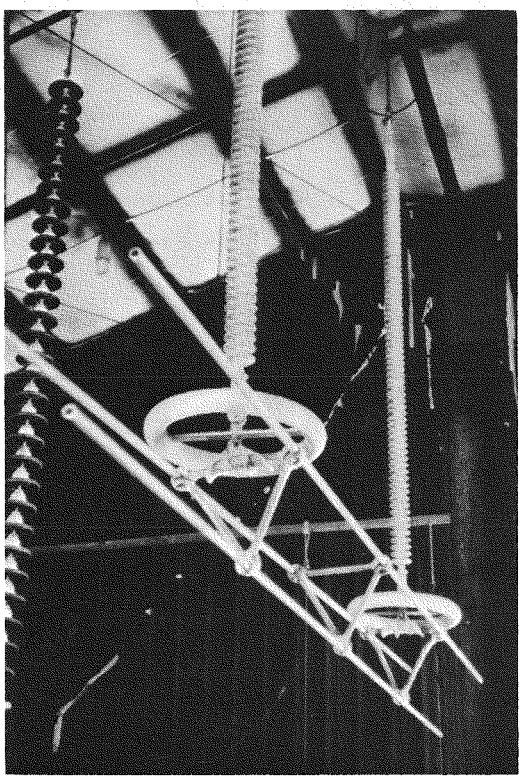


Figure 4-38. Experimental Test Setup for EHV Contamination Tests on the Single Unit Vertical Configuration.

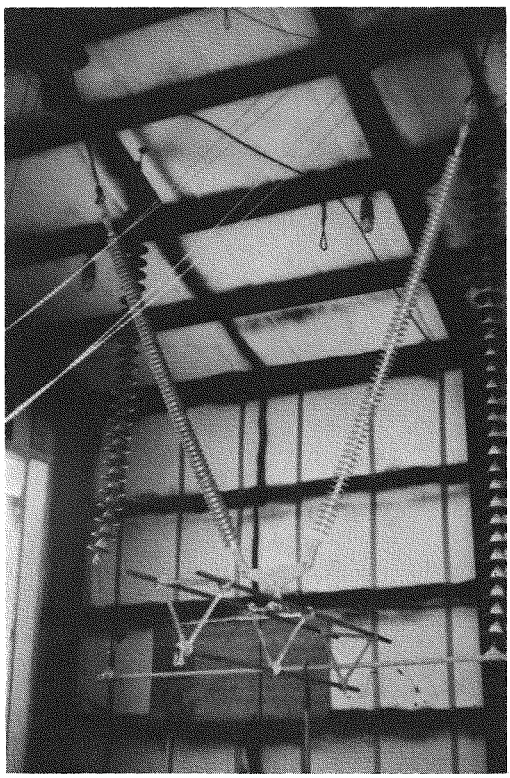


Figure 4-39. Experimental Test Setup for EHV Contamination Tests on a Single Unit V-Configuration.

It was because of these results that repeated pre-contamination and washing were performed on other new insulators tested, as discussed above in the section on test procedure.

The UHV tests on double units of these long rod insulators were also made in both vertical and V-geometries. An example of the V-string is shown in figure 4-40.

Data for all the EHV and UHV tests are summarized in Table 4-8. Note that the CFO for the vertical configurations has been corrected to the equivalent of a single string, since two vertical strings were always tested in parallel. The correction amounts to 8% if a standard deviation of 10% for single insulators is assumed. In the case of V-strings, the insulators comprising the V were treated as one insulation, and no corrections were made. Also shown in Table 4-8 is the insulation strength in kV/m, which was calculated by dividing the CFO by the total connection length of the particular insulators being considered.

A plot of insulation strength as a function of salt deposit density for the plastic insulators is given in figure 4-41, where some results for standard cap and pin (146mm x 254mm) units are also plotted for comparison. There are several observa-

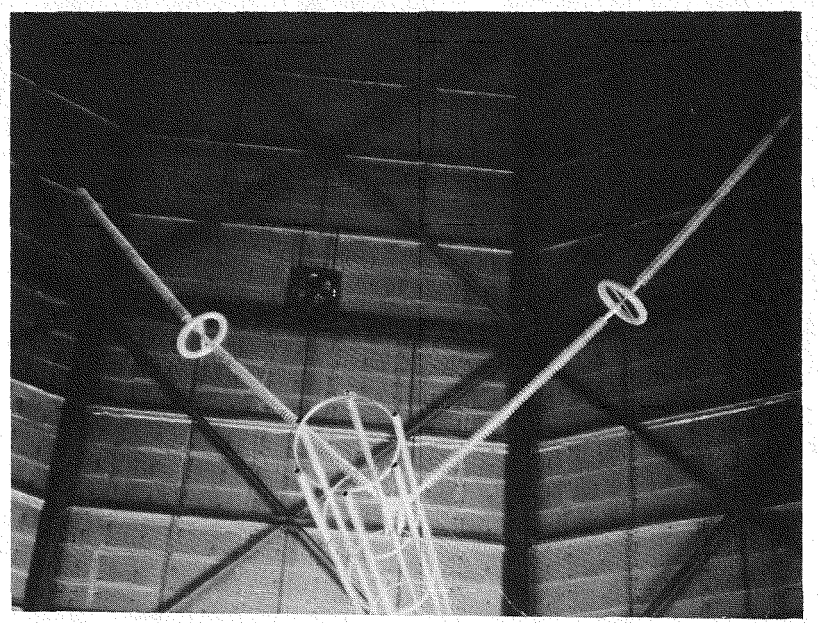


Figure 4-40. Experimental Test Setup for UHV Contamination Tests on a Double Unit V-String.

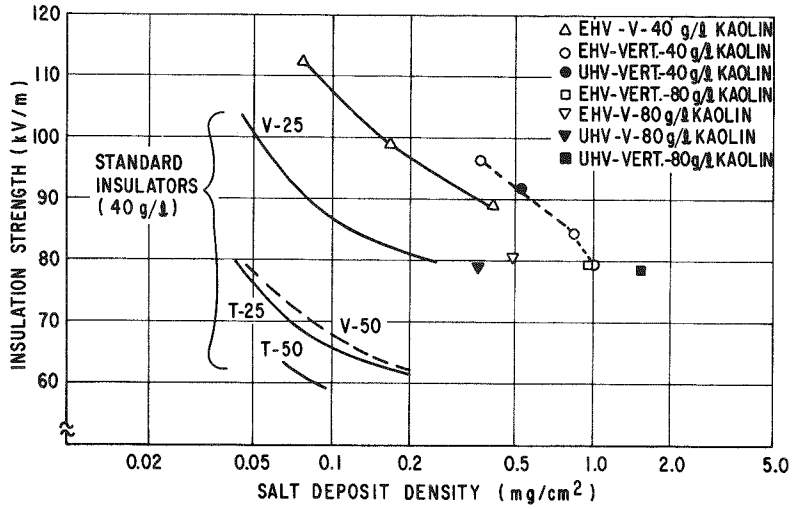


Figure 4-41. Contamination Performance of Silicone Rubber, Glass-Fiber Reinforced Long-Rod Insulators. The Curves Marked T-25, T-50, V-25, and V-50 Represent the Performance of Standard Cap and Pin Insulators in Vertical (T) and V-Configurations Having Lengths of 25 and 50 Units.

tions to be made on the data given in this figure. First, in EHV tests with 40 g/1 kaolin, performance of the V-configuration is slightly lower than a vertical arrangement. However, if the V-configuration results were converted to single insulator values by increasing the strength 8%, the data would be directly in line with the vertical configuration strengths. The second point is that the amount of kaolin in the mixture does not have as much effect on insulation strength for these insulators as it does for standard insulators. For example, in the case of these long rod units, the most variation is for V-configuration, where a decrease of 10% in strength is observed when increasing the kaolin from 40 g/1 to 80 g/1. For EHV vertical units, no change in strength was found. In contrast, for standard insulators, a decrease of 20% in insulation strength has been found when increasing kaolin from 40 g/1 to 80 g/1 for vertical strings. [4-1] These effects are a result of the differences in the manner in which the mixture adheres to the porcelain and silicone rubber surfaces. The third observation to be made in figure 4-41 is that a comparison of EHV and UHV data on these long rod units does not show the drastic nonlinearity in insulation strength with length which has been found for standard insulators. In fact, double unit performance is essentially twice that of single units. Finally, the long rod data in figure 4-41 show that the contamination performance of silicone rubber long rod insulators is substantially better than that of standard insulators in both vertical and V-configurations.

TABLE 4-8

SUMMARY OF CONTAMINATION TEST RESULTS ON PLASTIC INSULATORS.*

Test		SDD (mg/cm^2)	CFO (kV)	CFO for Single Unit (kV)	kV/m (Single Unit)
1.	(EHV-Vert.) (40/40)	0.37	294	318	96.4
II.	(EHV-Vert.) (40/80)	1.01	242	261	79.1
III.	(EHV-Vert.) (40/100)	0.86	258	279	84.6
IV.	(EHV-Vert.) (80-100)	0.99	242	261	79.1
V.	(EHV-V) (40/20)	0.079	371	371	112
VI.	(EHV-V) (40/40)	0.17	325	325	98.5
VII.	(EHV-V) (40/80)	0.42	294	294	89.1
VIII.	(EHV-V) (80/100)	0.50	266	266	80.6
IX.	(UHV-Vert.) (40-80)	0.53	559	604	91.5
X.	(UHV-Vert.) (80/100)	1.54	452	488	73.9
XI.	(UHV-V) (80/100)	0.37	523	523	79.2

*CFO = fifty percent flashover voltage

During contamination tests, scintillation activity at both the EHV and UHV levels was uniformly distributed along the insulator units. This is in contrast to the partial discharges which occur on long standard insulator strings near the line conductor when scintillation activity first begins.

Several remarks about the salt deposit density are in order. For a given contaminant mixture, the plastic insulators retain considerably more salt than standard insulators. With 40 g/l salt and 40 g/l kaolin, the salt deposit density on standard insulators is normally about 0.10 mg/cm^2. On the long rod units, however, an average value of 0.37 was obtained for this mixture. Even if a comparison is made with standard insulators on the basis of the same mixture and not salt deposit density, the long rod insulators still show a superior performance.

Finally, there is the most important question of the long-term aging of the plastic materials. No time or facility for evaluating this effect was available. It is possible that some techniques of artificially accelerating the aging effect may be valid, but a more reliable technique would consist of placing units in test on a field trial basis.

Examples of Full Scale Plastic Insulators on the UHV Test Line. Two types of plastic insulators have been installed on the UHV test line. One configuration is composed of Rosenthal RODURFLEX units and was installed during October, 1975. This V-string is illustrated in figure 4-42. The other configuration is composed of Ohio Brass HI-LITE units, installed during February, 1976 and shown in figure 4-43. As may be seen in figures 4-42 and 4-43, both strings employ two single section units in each leg of the V. The mechanical characteristics of these plastic insulator strings are listed in Table 4-9.

TABLE 4-9

PLASTIC INSULATORS INSTALLED ON THE UHV TEST LINE

Type	Total Length	Leakage/ Spacing	Mechanical Strength	Weight
Rosenthal RODURFLEX	11m (36 ft) (two equal sections 5.5m each)	2.61	Perm. Admissible Load: 25 x 10^3 lb Min. Failing load: 90 x 10^3 lb	248 kg (540 lb)
Ohio Brass Hi-LITE	9m (30 ft) (one 3m and one 6m section)	2.54	Max. working load: 80 x 10^3 lb	277 kg (609 lb)

The purpose of installing these insulators on the UHV test line was to demonstrate available insulator stringing technology, as is the case for the other strings on the line, and in addition to gain some experience with operating such units at voltages up to 1500 kV system levels.

Future Work

Two additional new types of insulators on which service experience already exists at lower voltages are semiconducting glaze units with special shapes and composite insulators with porcelain sheds and fiberglass cores.

The semiconducting glaze insulators with a bell shaped smooth shed have been used to upgrade an existing 115 kV system to 230 kV using the same towers. (4-5) The

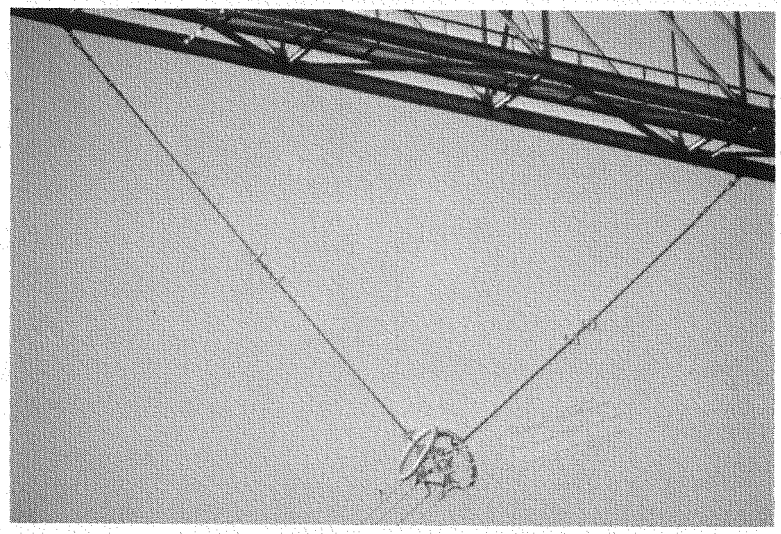


Figure 4-42. V-String on East Phase of the UHV Test Line, Tower 2, Consisting of Rosenthal RODURFLEX Units, Installed in October 1975.



Figure 4-43. V-String on East Phase of the UHV Test Line, Tower 3, Consisting of Ohio Brass HI-LITE Units, Installed in February 1976.

performance of this insulator at UHV in various weather conditions should be investigated.

The composite insulators having fiberglass cores for mechanical strength and porcelain sheds are similar to the plastic units described above. They also can be manufactured in long single sections, but do not have as much advantage in weight because of the presence of the porcelain. On the other hand, the long term behavior of porcelain is well known and offers more confidence with respect to aging than some of the newer materials. The use of such insulators at UHV should also be explored.

Finally, the contamination tests reported here on non-ceramic insulators should be extended to the 1500 kV level in order to determine the relationship between strength and string length.

INFLUENCE OF THE TEST PARAMETERS

Introduction

The results of contamination tests are determined to some extent by the nature of the circuit used in the investigation. The influence of circuit parameters on 60 Hz flashover voltage has recently been demonstrated for the salt fog test at a voltage level of 84 kV. [4-6] For higher voltages, the characteristics of the test circuit may affect not only the results at a given voltage, but may also determine whether linearity or nonlinearity of insulation strength with length is found when tests are made at different voltage levels.

The purpose of this section is to present the characteristics of the equipment used at Project UHV for indoor and outdoor artificial contamination tests and to give results which show the importance of the circuit constants up to ultrahigh voltages.

Description of Available Circuits

Four types of transformers are available for contamination tests at Project UHV and the pertinent data for this equipment are given in Table 4-10. As noted in the Table, two of these are regulators which can be used by themselves or to supply either the EHV or UHV power transformers, depending on the output voltage desired. The UHV transformer is a single phase unit, whereas the EHV transformer is three phase and allows a variety of special connections. For example, by connecting two

output windings together and feeding the third low side winding, voltages of half the values listed in the table may be obtained since the transformer contains an internally delta connected tertiary. The EHV transformer may also be connected to provide additional reactance when the UHV transformer is being employed as the main supply unit. The UHV transformer has an externally accessible tertiary which provides an alternate turns ratio and a different reactive impedance for tests at UHV voltage levels.

TABLE 4-10

CIRCUIT PARAMETERS FOR CONTAMINATION TEST EQUIPMENT AT PROJECT UHV

Transformer Equivalent Circuit: 1 : N Z



Supply Ststems	Bus Impedance
110 kV	0.866 + j5.18 Ω
23 kV	2.6 + j4.23 Ω

REGULATING TRANSFORMER	RATING (kVA)	TAPS	TURNS RATIO "N"	EFFECTIVE SERIES IMPEDANCE (OUTPUT SIDE)
110 kV (x 1/√3)	40,000 (3 phase)	73 (TAPS 1-73)	N=1+.0083 x (TAP-37)	Z=j[13.79+.010085x(TAP-37)]Ω
23 kV (x 1/√3)	5,000 (3 phase)	33 (TAPS 0-32)	N=.5567+.01508 x (TAP)	TAP 0 Z = j3.13 Ω TAP 13 Z = j0.96 Ω TAP 23 Z = j0.81 Ω TAP 32 Z = j1.42 Ω

POWER TRANSFORMER	VOLTAGE CLASS (SYSTEM VOLTAGE)	RATING (BASE kVA)	TURNS RATIO "N"	IMPEDANCE (PERCENT)	WATTS LOSS (RATED CURRENT)	EFFECTIVE SERIES IMPEDANCE (OUTPUT SIDE)
UHV (Single Phase)						
Tap 1	143kV/1500 kV	33,000	10.49	16.46	107,100	73.8 + j3741 Ω
Tap 2	143kV/1111.5kV	25,000	7.77	19.9	106,100	69.9 + j3278 Ω
Tertiary	23.9kV/1500 kV	11,500	62.76	7.4	20,130	114 + j4826 Ω
EHV (Three Phase)	134 kV/650 kV	40,000	4.85	17.80	275,670	72.8 + j1880 Ω

Three types of resistances are available for different circuit connections. The first consists of a nichrome wire structure having four sections of 43 ohms each. These sections may be used in series or parallel on the low voltage sides of the power transformers or on either side of the regulators. The second type of resistance is composed of twenty wire wound cards of 10 ohms each which may be connected on the high voltage side of the transformers. A third resistor is also designed for use on the high voltage side of the transformer and is liquid filled with a nominal value of 6000 - 12000 ohms depending on the concentration of the conducting agent and the temperature.

To illustrate the range of circuit parameters available during regular contamination tests, the equivalent series R and reactance X have been used to calculate the ratio R/X and the short circuit current with both the EHV and UHV transformers. The results are plotted in figure 4-44, where the output voltages are also indicated. The data in figure 4-44 include the bus impedance and assume that resistors of the values shown are in place. In the case of the EHV tests, the shaded region shows the range of parameters which results from different values of the liquid resistance. Many other combinations of resistance and reactance are possible and some of these have been employed for the tests described below.

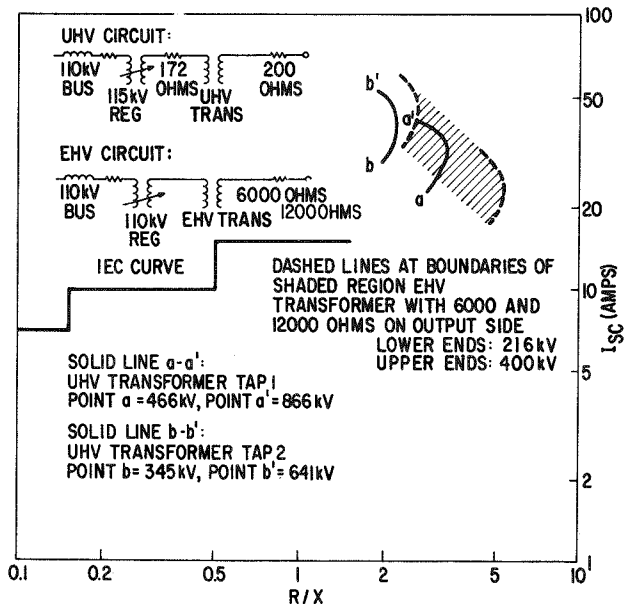


Figure 4-44. Short Circuit Strength and R/X Characteristics of the Power Supplies Available at Project UHV.

Test Results with Different Circuits

Flashover Voltages. The influence of the circuit was investigated by conducting a series of flashover tests. The tests reported here were all conducted in the UHV contamination chamber. Contamination severity was .01 mg/cm^2, produced by a slurry containing 40 g/ℓ kaolin and 5 g/ℓ sodium chloride. The test objects were standard suspension insulators having a spacing of 146mm, diameter of 254mm, and leakage distance of 305mm. Only vertical string configurations were tested.

The procedure for determining the flashover voltage consisted of a series of tests in which the voltage was held constant and the string length adjusted on subsequent tests in accordance with an up-and-down method. Using this approach, the short circuit current and equivalent R/X remained unchanged for a given test series.

Two voltage levels were employed in this investigation, one at approximately 250 kV and the other at 780 kV line to ground. The data in Table 4-11 show the results expressed in terms of the "fifty percent string length" for each circuit and the corresponding flashover voltage in kV/insulator.

For the tests made in the 250 kV range, Table 4-11 indicates a 17% decrease in flashover voltage in passing from the circuit (1) to circuit (2). Note that both of these circuits have a large resistive component. However, in circuit (3), which is essentially reactive, the flashover voltage is comparable to the previous case (2).

At 780 kV, a progressive decrease of 5% in flashover voltage was observed as the short circuit current increased in currents (4) - (6) from 4.6 to 95 amperes. It should be noted that R/X was only 0.76 for the test with the highest short circuit current. The 5% differences between circuits are within the expected range of experimental accuracy. However, the fact that the flashover voltage consistently decreased with increasing short circuit current seems to indicate a trend. The last test series (7) was performed after the high current tests in order to verify that the insulators had not been electrically damaged in those tests. As may be seen in Table 4-11, the flashover voltage was unchanged from the first series at 780 kV with the same circuit parameters.

The range of R/X and I_{sc} values for the tests of Table 4-11 are illustrated in figure 4-45. The circuits used at 250 kV with R/X $\approx$ 1.7 (1 and 2) are widely separated in I_{sc} above and below the IEC curve which supposedly gives minimum

TABLE 4-11

"FIFTY PERCENT" STRING LENGTHS AND FLASHOVER VOLTAGES IN kV/INSULATOR FOR DIFFERENT TEST CIRCUITS

Test (Circuit)	Voltage (kV line to ground)	Short Circuit Current (amperes)	R/X	Fifty Percent String Length (# of Units)	Flashover Voltage (kV/Insulator)
1	250	2.4	1.60	15.1	16.6
2	250	53.0	1.81	18.2	13.7
3	280	5.0	.02	20.8	13.4
4	780	38.2	2.98	58.8	13.3
5	780	4.6	7.36	56.0	13.9
6	780	95	.76	61.7	12.6
7	780	38.2	2.98	58.4	13.4

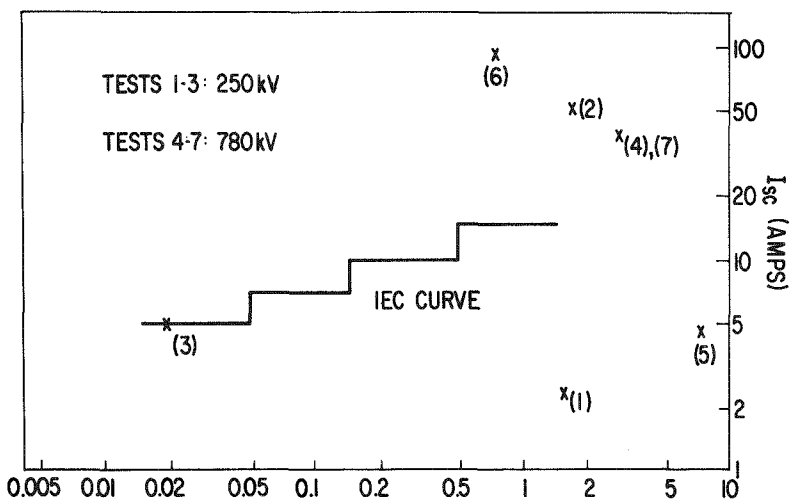


Figure 4-45. The Range of R/X and I_{sc} Values for the Test of Table 4-11.

circuit requirements. The influence of the short circuit current on the flashover voltage is apparent for these cases in Table 4-11. However, the other test (3) at this voltage level with small R/X on the other side of the diagram also produced the same flashover voltage as test (2) with $I_{sc} \approx 50$.

It has also been verified that at UHV voltages the flashover voltage depends on the circuit as shown by tests (5) and (4), which are widely separated in I_{sc}. However, tests (4) and (6) are both above the IEC curve and yet a further decrease in kV/unit was observed.

The analysis of test circuits described here may be used to describe the parameters used in the fog chamber tests on long strings described previously for the purpose of studying flashover voltage as a function of string length. The test circuit parameters for those studies are illustrated in figure 4-46. The region of the R/X - I_{sc} diagram occupied by the tests of figure 4-46 is shown in figure 4-47. Of particular interest is the fact that the circuits used at 375 kV and above are fairly close to one another in this diagram and yet some nonlinearity of strength with length was observed. These results show that the nonlinearity was not a consequence of differences in test circuits. This is substantiated also by the fact that the

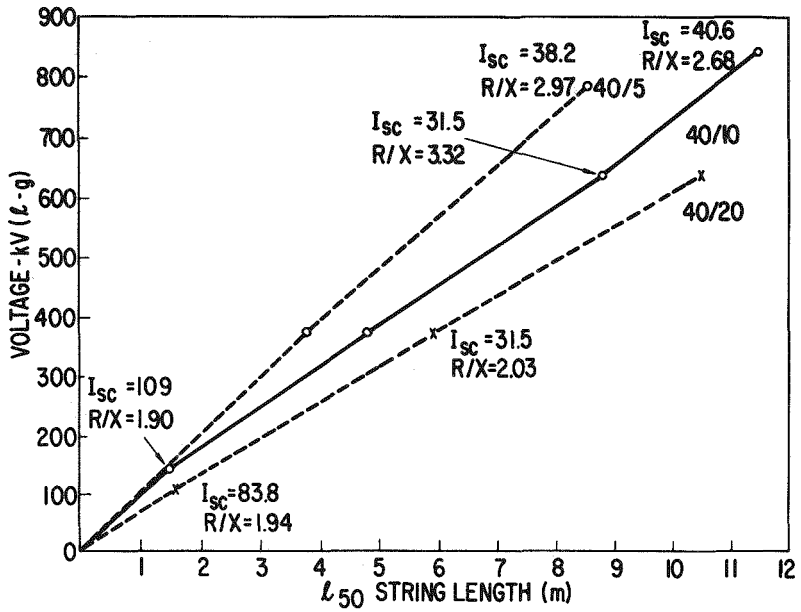


Figure 4-46. Test Results Showing Characteristics of Test Circuit.

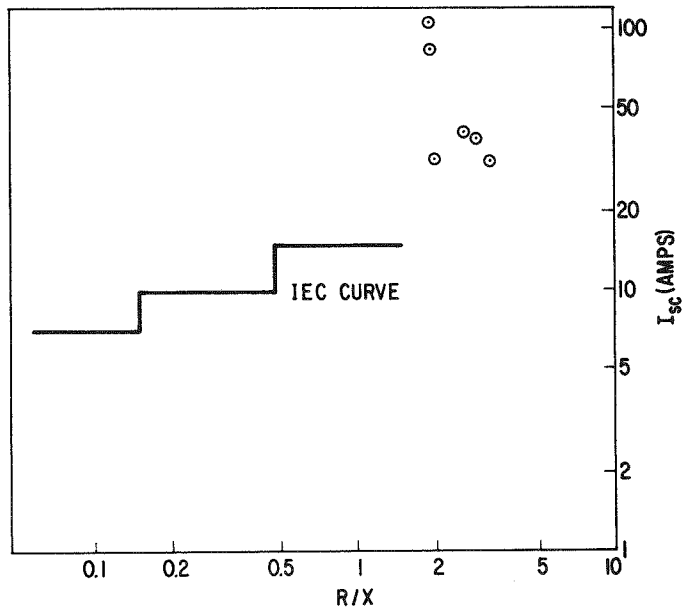


Figure 4-47. Region of R/X-I_{sc} Diagram Occupied by Tests of Figure 4-46.

peak leakage current surges (I_p) recorded during scintillation discharges were about the same for the voltage levels of 375 kV and 635 kV, namely 900 mA for standard insulators and 40/20 contaminant. This implies a maximum percentage voltage drop on the order of $Ip/\sqrt{2}/I_{sc}$, or 2%. The details of these voltage drops for a variety of circuits are discussed in the following section.

Voltage and Current During Scintillation and Before Flashover. The test circuits described above were also used for investigating the detailed behavior of the voltage and current during discharge activity before flashover on the contaminated insulator strings. Voltage was measured on the high voltage bushing of the UHV transformer, which was always energized by means of the UHV strain bus even when not being used as the test source. The current was measured by means of a 10 Ω resistive shunt placed on the ground end of one insulator string.

Test circuit (4) in Table 4-11 is the usual circuit employed for UHV contamination tests. The voltage and current during a typical scintillation burst at 780 kV are shown in figure 4-48, and just before flashover in figure 4-49. The peak current during the burst in figure 4-48 is about 800 mA, with an estimated voltage drop of about 2%. Assuming a sinusoidal leakage current, the percentage drop in voltage for a purely resistive circuit would be given by $(I_p/\sqrt{2})/I_{sc}$, where I_p is the peak

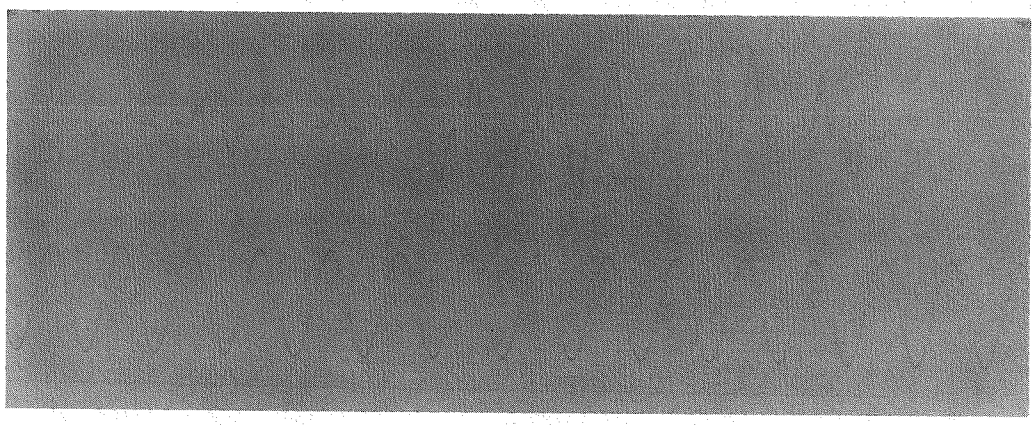


Figure 4-48. Current (top) and Voltage During a Typical Scintillation Burst at 780 kV.

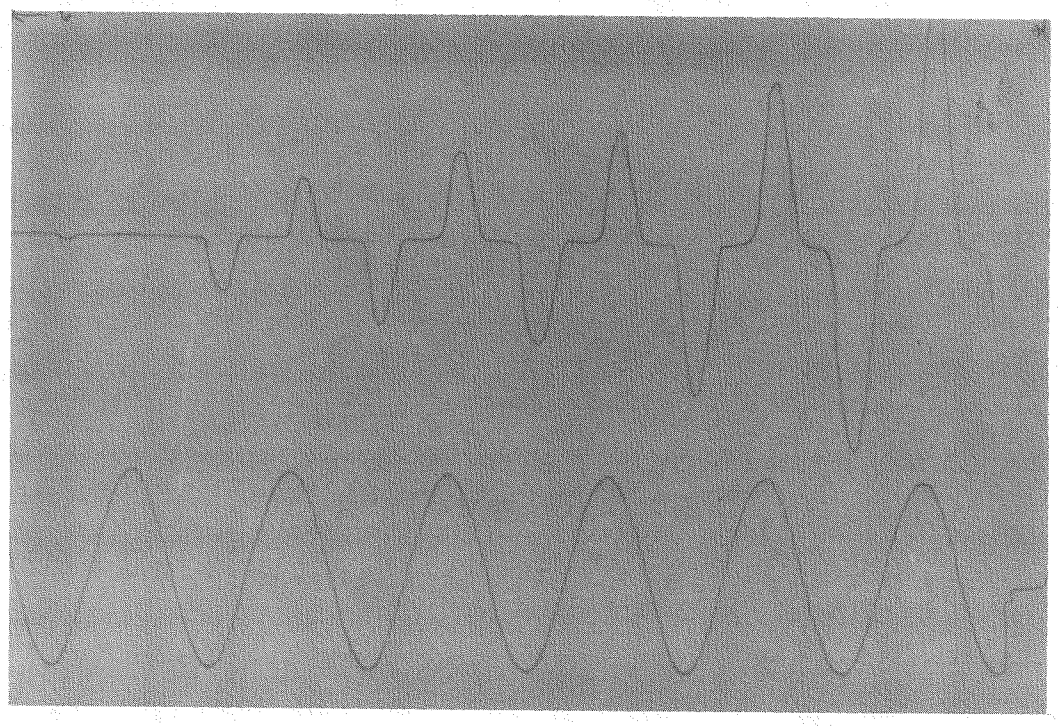


Figure 4-49. Current and Voltage Just Prior to Flashover at 780 kV.

current and I_{sc} the rms short circuit current. The estimate in this case would be 1.5%, which is in good agreement and within the accuracy obtainable from reading figure 4-48. In figure 4-49, the peak current in the last half cycle before flashover is about 1 ampere, with a similarly small voltage drop and virtually no distortion in the voltage waveshape.

In contrast to this test circuit, consider test circuit (5) for UHV voltages which has a high resistive component but low short circuit current. For example, figure 4-50 shows a scintillation burst with a peak current of 470 mA. The voltage during this burst dropped about 5.6% and the calculated estimate would be 7%. Figure 4-51 shows the discharges before a complete breakdown of the string. The current reached 1.4 amperes in the half cycle before the voltage distorted. Up to and including this time, the drop in peak voltage was still only about 5%. However, the voltage waveshape was quite distorted. Note that the voltage collapses after the largest burst, but the string recovers and the breaker does not operate. These phenomena should receive further attention in future research.

For the tests in the 250 kV range, circuit (2) was resistively limited with a high short circuit current. A scintillation burst is shown in figure 4-52 and a flash-

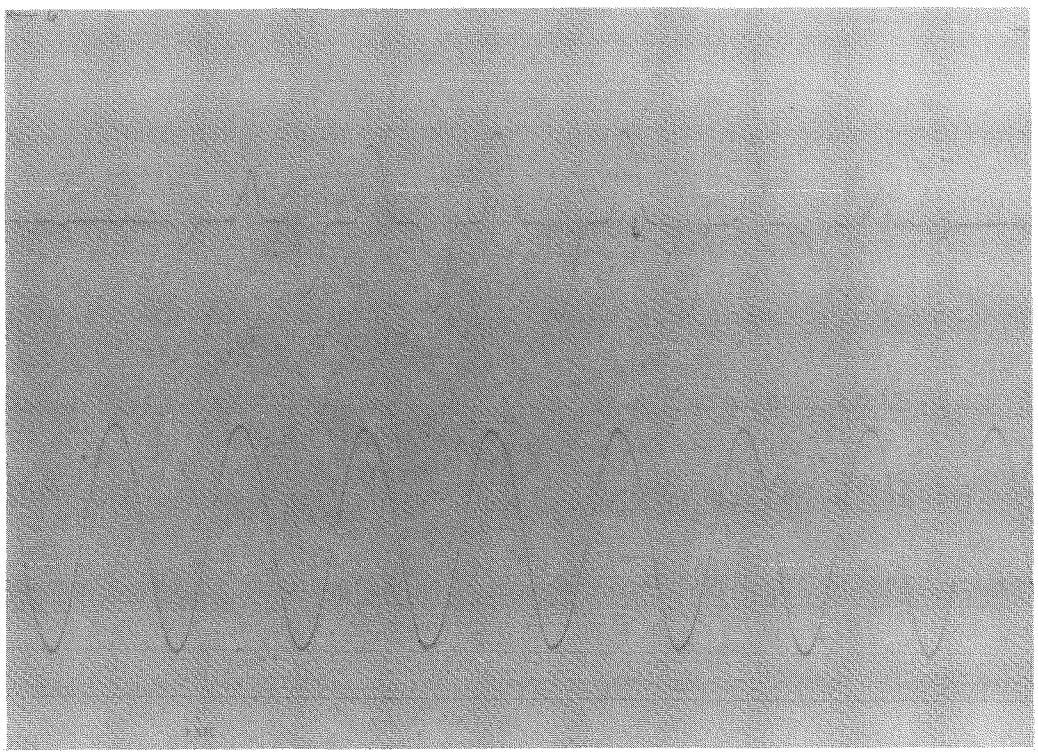


Figure 4-50. Current and Voltage During a Scintillation Burst of 470 mA Showing a 5-6% Voltage Drop.

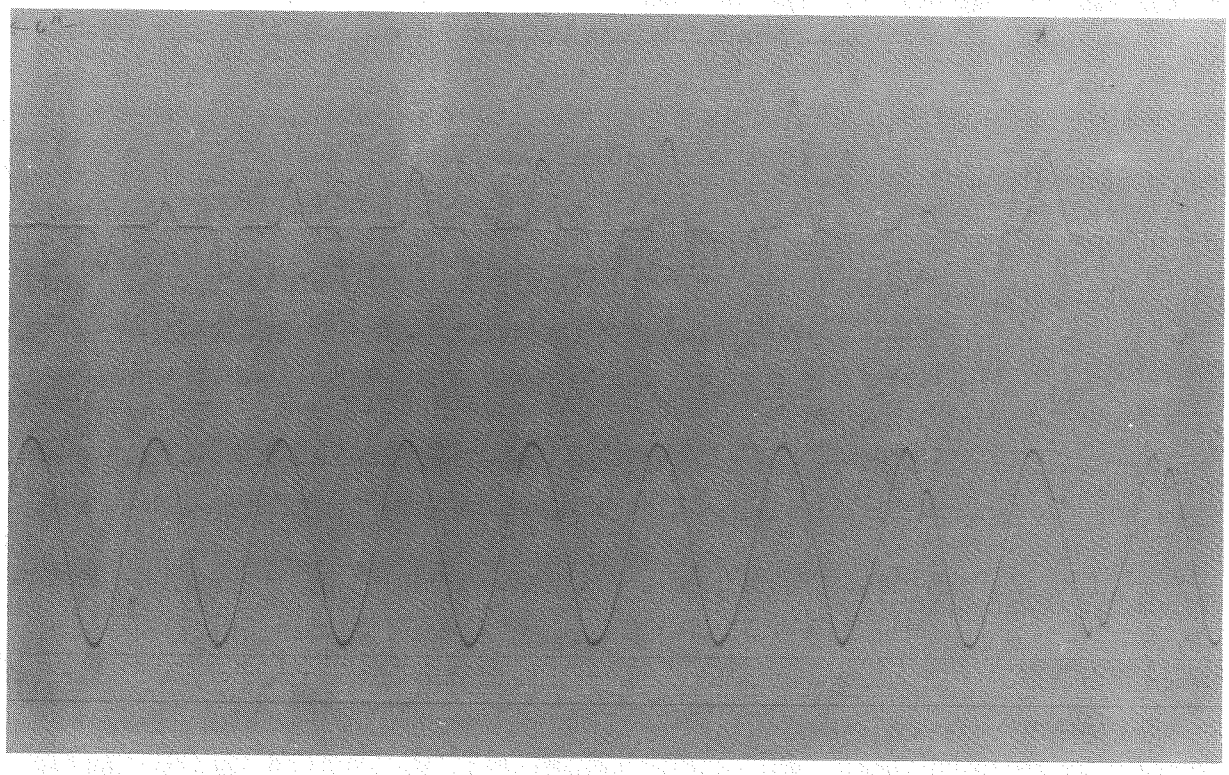


Figure 4-51. Current and Voltage Prior to Flashover.
Note no Measurable Voltage Drop.

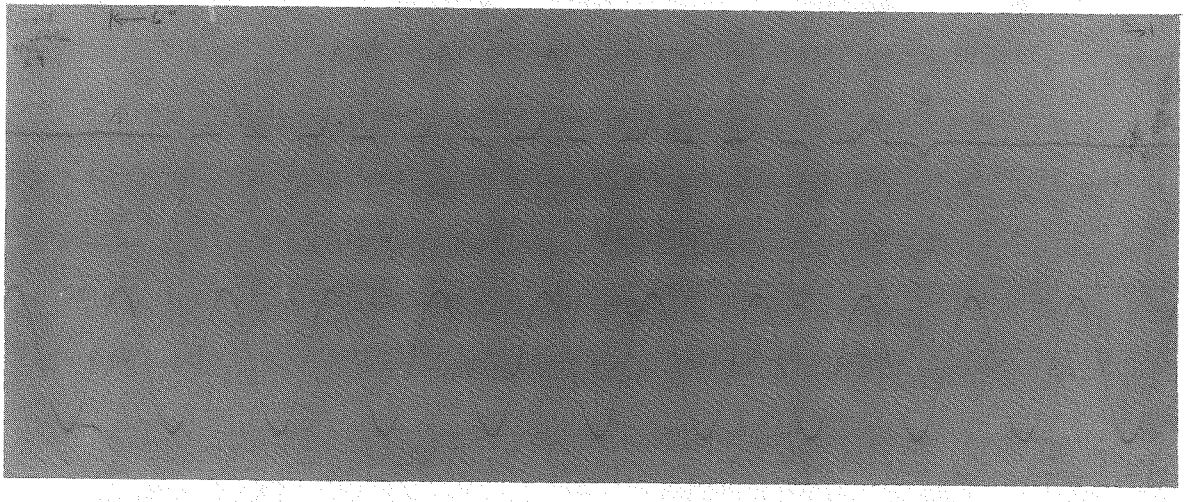


Figure 4-52. Current and Voltage During Scintillation.
Note no Measurable Voltage Drop.

over in figure 4-53. In figure 4-52 the surges reached about 660 mA peak with no measurable voltage drop. The theoretical estimate would be 1%. For this circuit, no measurable voltage drop was observed, even in the last half cycle before flashover, as shown in figure 4-53.

When the short circuit current was reduced as in circuit (1), maintaining a high resistive component, the waveshapes became distorted as shown in figure 4-54 during scintillation. The voltage drop for the 440 mA peak surge was only about 2%, whereas 13% would be predicted from the simple calculation technique described above.

Finally, for the reactive circuit (3), the current waveshape before breakdown is given in figure 4-55. The current was in excess of one ampere before breakdown, causing a severe distortion in the voltage waveshape. Nevertheless, the peak voltage drop was only a few percent. In this circuit, also, the string recovered without the breaker opening.

The conclusion of this study is that although the flashover voltage is a function of the test circuit, the parameter which controls the flashover voltage is not the voltage drop alone. This finding requires further investigation, possibly by a

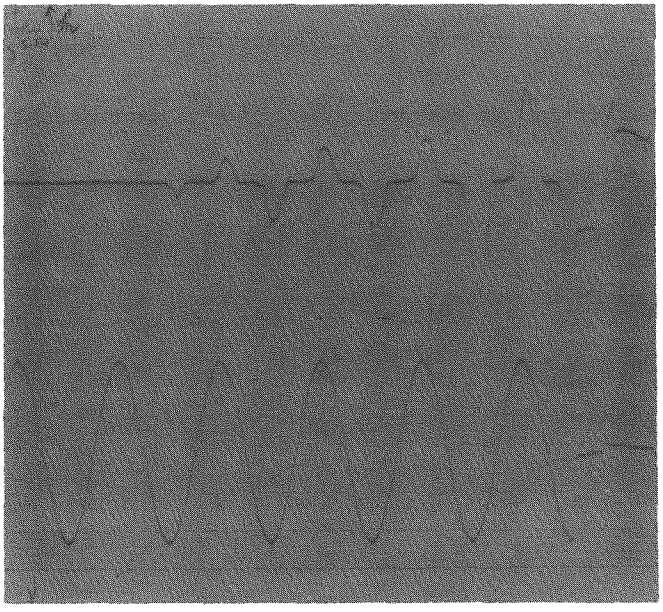


Figure 4-53. Current and Voltage Just Prior to Flashover with same Circuit as in 4-52. Here Again there is no Measurable Voltage Drop.

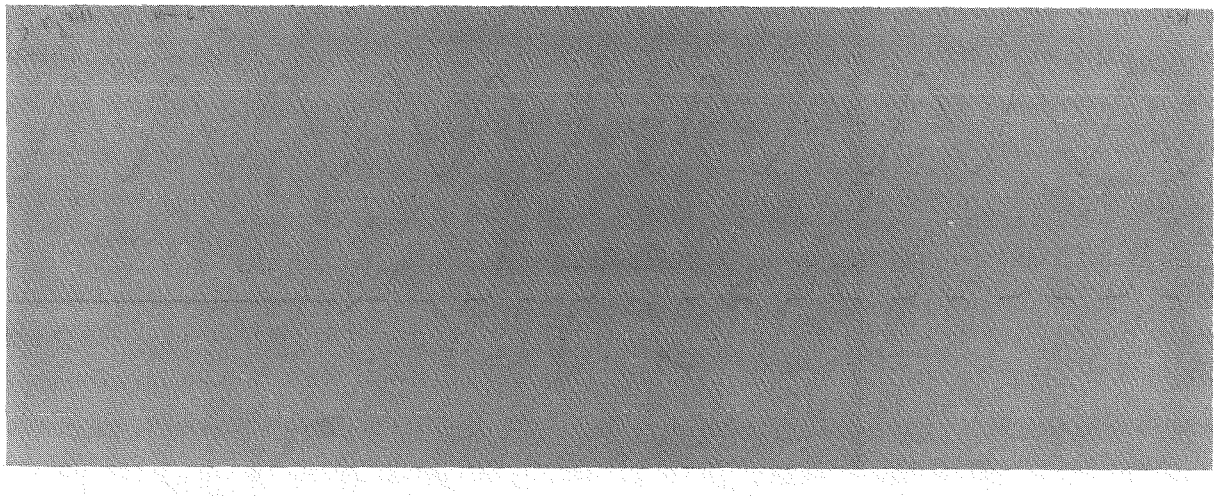


Figure 4-54. Voltage and Current During Scintillation with a Highly Resistive Circuit. Note Voltage Distortions.

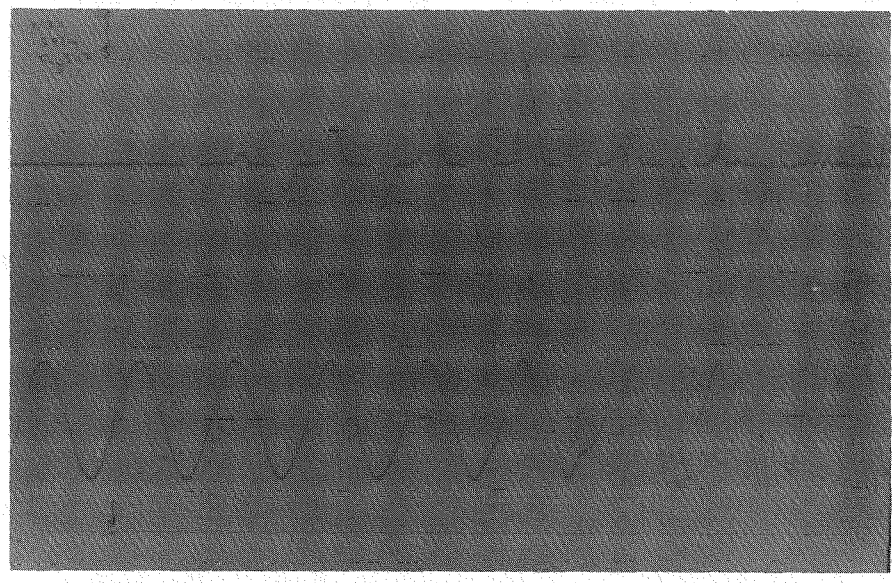


Figure 4-55. Current and Voltage During Scintillation Leading to Flashover with a Reactive Circuit. Note Distorted Voltage Shape.

study of the voltage and current cycle by cycle to determine the manner in which physical circuit parameters affect contamination flashover voltage.

Influence of Wetting Conditions

Critical Wetting in Outdoor Natural Humidity Tests. The outdoor contamination tests provided an opportunity for continuing a study of the conditions under which wetting is sufficient to cause flashover. For the longer strings, the most interesting results are those obtained in 1976 because both withstands and flashovers occurred.

Dew condensation wetting is an important condition which may lead to flashover. In several of the outdoor tests made at Project UHV, flashovers took place before the appearance of visible fog. The relative humidity as a function of time for tests 9-12 of Table 4-5 is shown in figure 4-56. The flashover times varied from as early as 21:35 for test (12) to as late as 2:30 (a.m.) for test (9). Note that in all these cases the relative humidity was already above 90% before midnight. The beginning of scintillation discharges occurred at the times indicated by the arrows in figure 4-56. This activity generally required humidity in excess of 85-90% for a period of one hour before it began. For test (8), in which the same

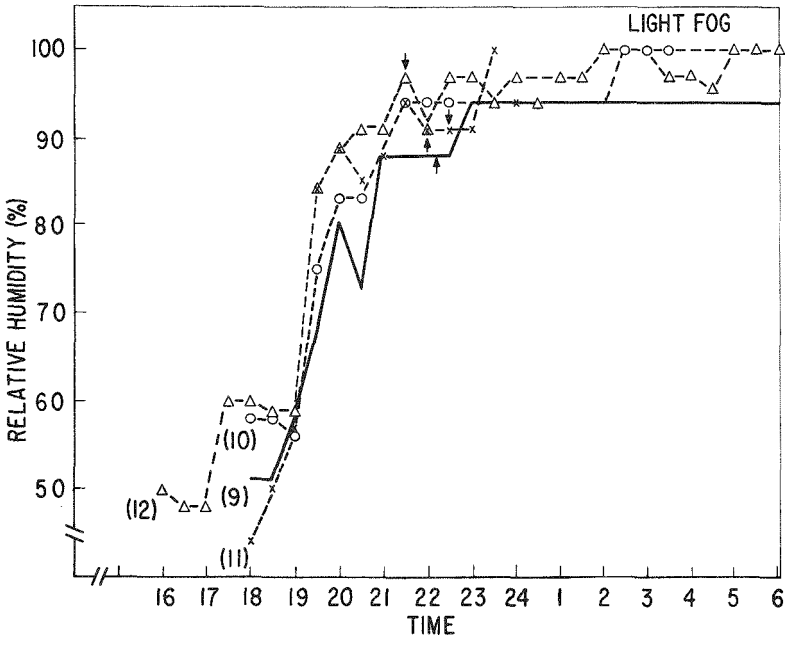


Figure 4-56. Relative Humidity as a Function of Time for Test 2-5. Arrows Indicate Times at Which Scintillation Activity Began.

string lengths were used as in test (9), the result was a withstand. However, as may be seen in figure 4-57, the relative humidity reached a maximum of 90% only for a short time around 22:00 and then again after 3:00 (a.m.). Although some scintillation discharges did occur briefly at these time, the period of high humidity after 3:00 was so late that the insulator and ambient temperatures were probably almost equal. In this condition, wetting by condensation can no longer occur. For condensation wetting, it is therefore concluded that the humidity must increase more rapidly, as in figure 4-56, to provide enough moisture for flashover of the insulators.

For reference, the relative humidity during the 1975 tests [4-6] is plotted in figure 4-58. All these tests resulted in withstands, even though the humidity variation with time was similar to that shown in figure 4-56 where the insulators on at least one side of the V-string flashed over during each test. Consequently, the results of tests 4-6 are considered valid data points.

Other Wetting Conditions. It is possible for insulators to become wetted sufficiently for flashover by mechanisms other than dew condensation. Impingement of water drops in fog is one example of these other mechanisms. However, with the

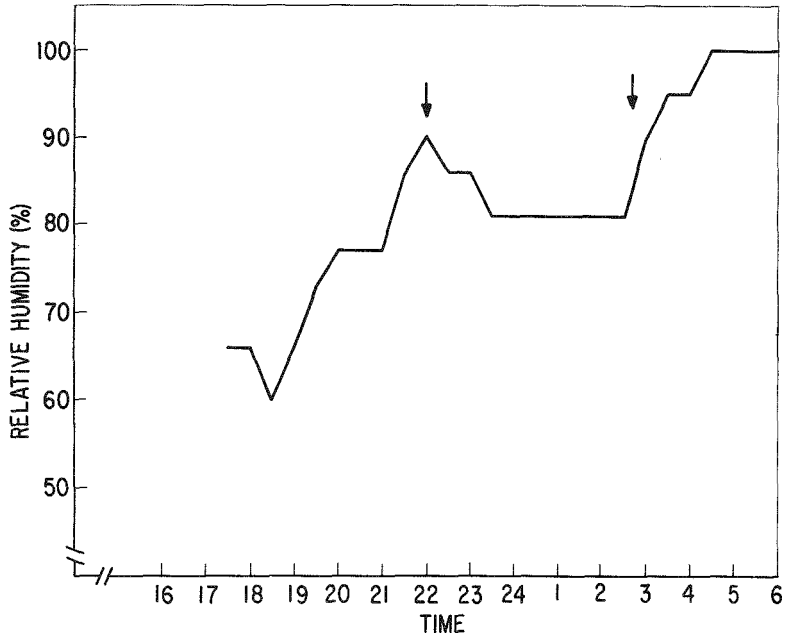


Figure 4-57. Relative Humidity as a Function of Time for Test 1. Arrows Indicate Times at Which Scintillation Activity was Observed.

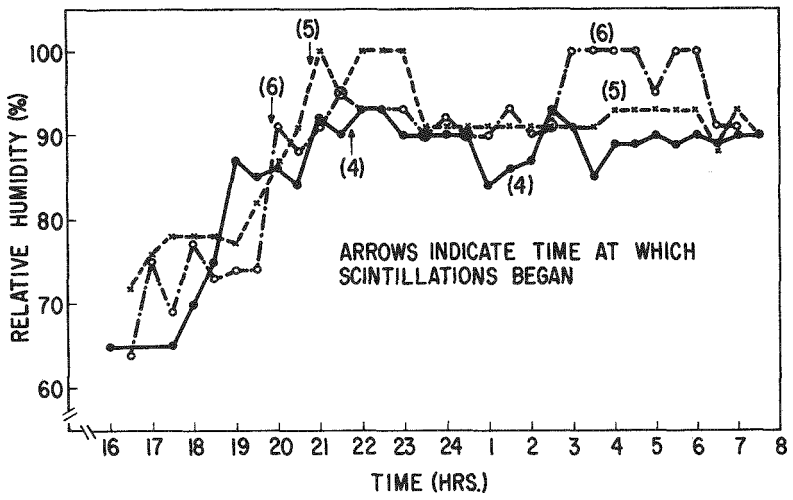


Figure 4-58. Relative Humidity During 1975 Tests.

exception of coastal areas, fog usually occurs during periods of low wind velocity. In such calm conditions, the impingement of water droplets probably cannot provide enough moisture on the insulator surfaces to cause flashover.

The onset of rain after a long dry period in which the insulators have become contaminated is another wetting condition which should be considered. As noted before, tests in natural rain did lead to flashover at about the same voltage as would be predicted from artificial fog tests. It is suggested that a series of artificial tests be conducted to investigate such wetting conditions.

CONTAMINATION PERFORMANCE OF STATION POST INSULATORS

Introduction

The contamination performance of station apparatus is of concern for the designer, since levels of severity are frequently high in locations where stations are constructed. Recently, a report has been made on the 60 Hz flashover characteristics of station posts in naturally contaminated conditions at EHV voltage levels. [4-7] However, few data are available on the behavior of posts in artificial contamination tests made either in natural conditions or with clean fog, especially in reference to the influence of various parameters such as column diameter and length

on the flashover voltage. For example, it has been suggested that the flashover voltage should decrease with increasing post diameter, since many effective "paths" are in parallel and the probability of flashover should increase.

Some tests were made on single section short posts in order to determine if diameter influenced the flashover voltage. These posts were specially manufactured and had different diameters but the same shed shapes and leakage distances. The geometrical parameters of the posts used for single section tests are listed in Table 4-12 and are illustrated in figure 4-59. The posts described in Table 4-12 had eleven sheds and a difference between inner and outer diameter of 13cm (5 in).

TABLE 4-12

POSTS USED TO INVESTIGATE EFFECT OF DIAMETER IN TESTS AT LOW VOLTAGE
CONNECTION LENGTH 76cm (30 in)

POST TYPE	OUTER DIAMETER		LEAKAGE DISTANCE	
	cm	in	cm	in
L	36	14	173	76
M	30	12	193	76
S	25	10	193	76

The tests on these posts were made in the EHV contamination chamber. The test circuit consisted of the 23-kV regulating transformer and the EHV transformer, with output voltages in the range of 45-70 kV and short circuit currents between 17 and 26 amperes.

Since the range of diameters in the above tests was confined to the ratio of 1:1.4, additional data were obtained on several sections of very large diameter porcelain shells connected to make a long column. In those tests, a long column of insulators similar to those shown in figure 4-59 was also tested in parallel with the large diameter posts. The two post insulators which were energized by means of fuses in the UHV contamination chamber are shown in figure 4-60, where the bases on which the columns were mounted may also be seen. As noted in Table 4-13, the large diameter post was composed of three identical hollow porcelain sections on top of which a fourth hollow shell was placed. This last porcelain was tapered, with a diameter varying from approximately the same value as the other three at the lower end and decreasing to a smaller value at the top end. The small diameter stack contained ten units of conventional posts of two diameters and approximately the same lengths.

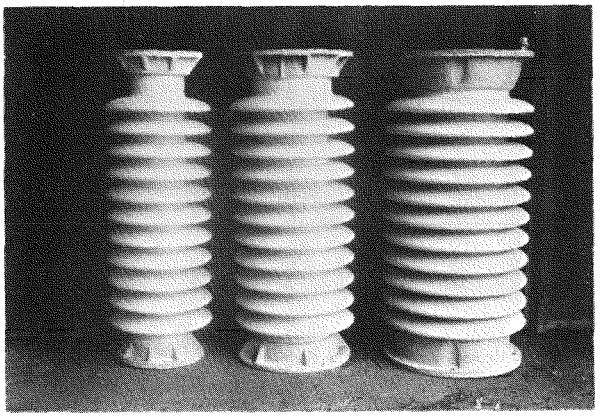


Figure 4-59. Single Sections of Post Which Have Identical Shed Design and Leakage Distance but Different Diameters.

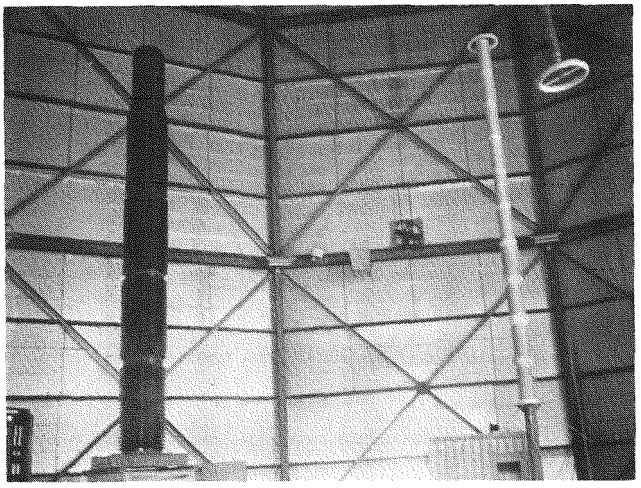


Figure 4-60. Large and Small Diameter Insulator Columns in UHV Test Chamber. Insulator in Upper Right Corner was Used to Support Connection Wires.

TABLE 4-13

GEOMETRICAL CHARACTERISTICS OF LONG INSULATOR COLUMNS

Post Column Type	Mounting Base	# of Sheds/ Section	Shed Spacing	Total Leakage/ Section	Shed Depth	Section Length	Diameter	Outer Diameter
	Framework dimensions:	lower 3 pieces:	6.03cm	442cm	7.3cm	152cm	68.6cm	83.2cm
Large diameter	1.27 x	23						
	2.13m	upper piece:						
	with 0.2m	20 on large	8.3cm	403cm	7.3cm	157cm	62.4cm	77.0cm
	I-beams on top	17 on small (includes transition)	7.9cm	334cm	5.9cm	145cm	47.5cm	59.3cm
	single	four						
	0.22m	lower						
	diameter	pieces:	5.4cm	180cm	5.9cm	81.3cm	23.3cm	35.1cm
Small diameter	vertical	11						
	tube	six upper						
	2.90m	pieces:	5.7cm	180cm	5.9cm	76.2cm	17.0cm	28.8cm
	in length	11						

The hardware on the small diameter post was similar to that shown on the posts in figure 4-59. On the large diameter column, the four hollow shell units had no attached end hardware and were sealed at the intermediate points by rubber gaskets. Metal plates were used to seal the high voltage and ground ends of the column. In this manner, the post simulated an equipment insulator on which intermediate hardware is often absent.

Initially, a Permalli rod located in the center of the large column and extending from the top plate to the bottom plate was installed for mechanical stability. This support failed electrically, as explained below, so that later tests were made with a free standing column. An attempt was made to increase the internal flashover strength with insulating gas, but all the tests reported here were conducted with air at standard pressure. The porcelain column was heated to remove moisture before the end cap was put in place.

The tests were made with the UHV transformer, energized by the 110-kV regulator through the wire current limiting resistor, or by a special connection obtained by first energizing the low voltage side of the EHV transformer in a half voltage connection. The latter circuit allowed the energization of the UHV chamber with voltages of one half the range normally available from the UHV transformer. At these voltages, three sections of the wire resistor were used in order to achieve sufficient short circuit currents.

Effect of Diameter

For the tests on single section posts, the contaminant used was 40/40, which gives an average salt deposit density on standard suspension insulators of about 0.1 mg/cm^2. Measured salt deposit densities on two complete sheds of sample post insulators also gave an average value of 0.1 mg/cm^2. In some tests on single sections, two posts of each type were energized in parallel, but in the tests during which standard insulators were used, only one of post type M was present. Care was taken in preparation of the tests to insure a longer cooling period than generally utilized for suspension insulators. The tests were begun only after the posts had cooled to ambient temperature.

In the data reported here, only those individual tests which resulted in sufficient wetting of the insulators have been listed. The tests discarded were selected on the basis of visual observations of the fog and surface conditions of the posts as well as by periodic measurements of the current on an otherwise unenergized contaminated post in the fog chamber.

The individual test results are given in Table 4-14, where the order of occurrence of flashovers for the various types of insulators is shown. All tests except numbers 1, 2, 5, 6, and 7 included a short string of standard insulators four units in length. In test 2, the standard unit string was six units in length. A larger number of tests was performed at 50-kV since it was decided that at higher voltages the insulators were overstressed. From Table 4-14, it appears that no order of merit may be assigned to different post diameters based on the order of flashover.

Assuming all posts are equivalent, that is diameter does not affect flashover voltage, the total number of test objects at each voltage becomes much larger. Flashover probabilities computed on this basis are shown at the bottom of Table 4-15. These probabilities are plotted in figure 4-61 on normal probability paper. An estimate of the standard deviation, obtained by the straight line drawn through two of the data points, gives a value equal to 30% of the fifty percent flashover voltage. The two points chosen for this estimate correspond to the two voltages in Table 4-15 for which the total number of samples is greatest. Other attempts at a best fit through all the data points in figure 4-61 would lead to an even larger standard deviation.

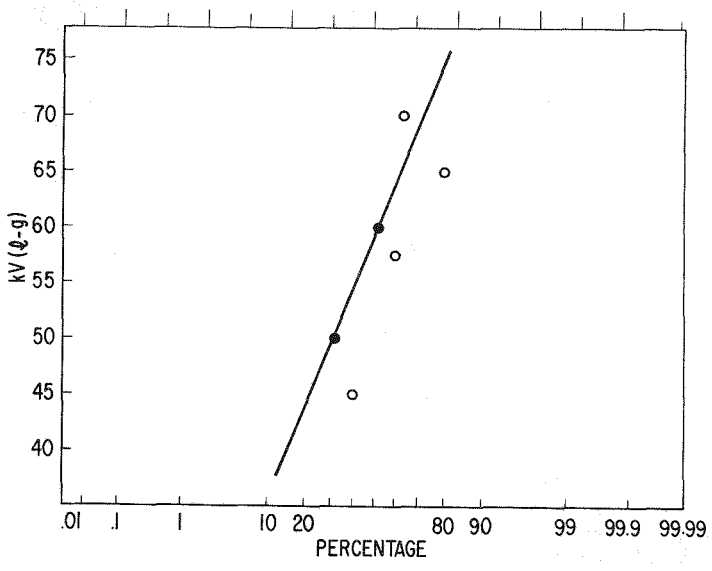


Figure 4-61. Flashover Voltage Probability Distribution from Table 4-15, Assuming all Posts Identical.

The fifty percent flashover voltage estimated from figure 4-61 for the single section posts is 58 kV, assuming flashover voltage to be independent of diameter for the range of diameters in Table 4-12. This corresponds to about .76 kV/cm (1.93 kV/in) of connection length compared with .84 kV/cm (2.13 kV/in) for standard suspension insulators and the same contaminant.

Consequently, two conclusions have been reached concerning the contamination flashover performance of the single section posts. First, over the range of diameters investigated, diameter has no influence on flashover voltage. Second, the dispersion in the flashover voltage is much higher for post insulators than for suspension insulator strings.

Scintillation discharges on the single section post insulators were quite different from that seen on suspension units. For example, partial arcs were observed bridging a few sheds at different positions along the length of the porcelain column. Entire groups of sheds were observed to be dry, corresponding to the dry bands which always appear first on suspension units near the pins where the current concentration is highest. In contrast, the surface current on post insulators is uniform, and the pre-flashover discharges somewhat different. An example of these discharges is given in figure 4-62.

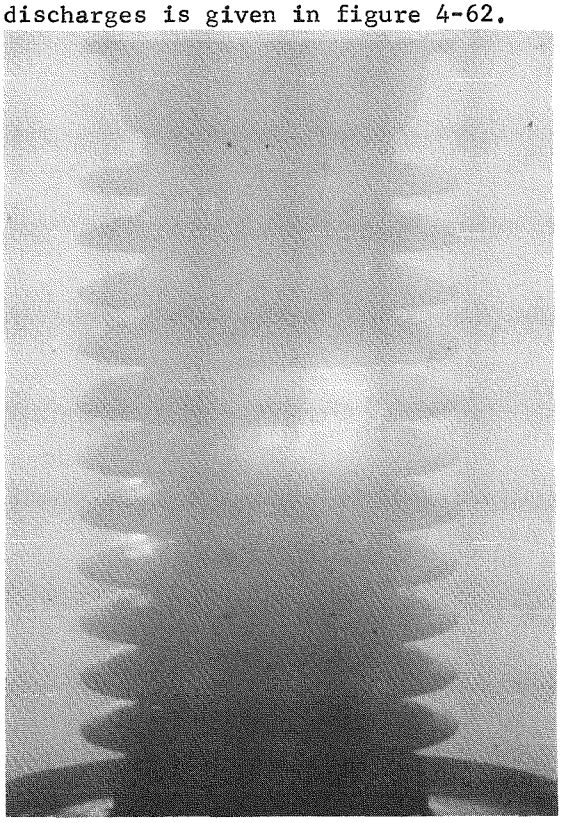


Figure 4-62. Scintillation Discharges on Post Insulator.

TABLE 4-14

RESULTS OF CONTAMINATION TESTS ON SINGLE UNIT (30 in) POSTS. SYMBOLS DENOTE POST TYPES (S, M, L) AND THE ORDER IN WHICH FLASHOVERS OCCURRED. NUMBERS INDICATE STANDARD UNITS WHICH FLASHED OVER. ASTERISKS INDICATE TESTS IN WHICH SIX POSTS WERE PRESENT (NO STANDARD UNITS). (W) INDICATES ALL INSULATORS WITHSTOOD.

Voltage (kV ℓ-g) Test #:	1	2	3	4	5	6	7	8	9	10	11	12	13	14	15	16	17	18	19	20	21	22	23
	*				*	*	*																
70	S	S S L L	4 S L L S M																				
65				4 L M L S																			
60					L M S L S	S	S	4 L S M S L															
55									S M 4 L														
50										4 M L	4 M S	L S 4 L S	W	S	L	S	W	L S S	L S				
45																				W	L S M	L	L L S S

TABLE 4-15

CALCULATION OF FLASHOVER PROBABILITY FOR EACH VOLTAGE LEVEL. NUMBERS OF FLASHOVERS (FO) AND WITHSTANDS (WS) FOR EACH INSULATOR TYPES AT DIFFERENT VOLTAGE LEVELS ARE SHOWN.

Insulator Type / Voltage: (kV)	45	50	55	60	65	70
L	4 FO 4 WS (.5)	6 FO 14 WS (.3)	1 FO 1 WS (.5)	4 FO 4 WS (.5)	2 FO 0 WS (1.0)	4 FO 2 WS (.67)
M	1 FO 3 WS (.25)	2 FO 8 WS (.2)	1 FO 0 WS (1.0)	2 FO 5 WS (.29)	1 FO 0 WS (1.0)	1 FO 3 WS (.25)
S	3 FO 5 WS (.38)	8 FO 12 WS (.4)	1 FO 1 WS (.5)	6 FO 2 WS (.75)	1 FO 1 WS (.5)	5 FO 1 WS (.83)
Total Number of tests (at each voltage)	20	50	5	23	5	16
Flashover Probability at each voltage (assuming diameter does not affect performance)	.40	.32	.60	.52	.80	.63

For the tests made in the UHV chamber on the long columns described in Table 4-13 40/5 and 40/40 contaminants were used. The 40/5 mixture represents very light contamination severity. The 40/40 mixture corresponds to a moderate-heavy degree of contamination, and has been used as it was for single section posts to illustrate a more severe condition for station design.

The test series conducted with 40/5 contaminant on the long column is shown in Table 4-16. No data are given for the large diameter column since this column had only internal flashovers with 40/5 at the voltages shown in Table 4-16.

TABLE 4-16

40/5 MIXTURE
TESTS ON SMALL DIAMETER POST 7.82m (25.7 ft) IN LENGTH.

Voltage (kV ℓ-g)					
635	X				
550		X	X	X	
490		O	O		(X/O)

Note: X = Flashover
0 = Withstand

V_{50} = 520 kV

Avg. salt deposit density = .01 mg/cm^2

The results with 40/40 mixture and the long columns are given in Table 4-17. These data were obtained after the large diameter column was dismantled, cleaned, and reassembled. With 40/40 contaminant and the voltages shown in Table 4-17, all flashovers on the large diameter post were on the outer surface of the porcelain. It appears from Table 4-17 that the large diameter porcelain column has a fifty percent flashover voltage which is 27% lower than that of the small diameter posts.

The data on the performance of the large column in Table 4-17 suggest that when the diameter becomes sufficiently large, it does affect the flashover voltage.

Scintillation activity on the small diameter posts usually began on the extremeties of the column and eventually encompassed the entire column. However, a few sections in the central portion were sometimes free of discharge activity even up to flashover.

TABLE 4-17

40/40 MIXTURE. TESTS ON LARGE AND SMALL DIAMETER COLUMN 7.6m (25 ft) IN LENGTH. X = FLASHOVER, O = WITHSTAND. AVG. SALT DEPOSIT DENSITY - 0.1 mg/cm^2. TESTS IN THE SAME COLUMN WERE PERFORMED SIMULTANEOUSLY.

Large diameter																				
Voltage (kV ℓ-g)																				
300		X																		
270			X															V_{50} = 225 kV		
240				X		X		X												
210					O		O													
Small diameter																				
360		X											X	X						
330											O					X		V_{50} = 310 kV		
300		X													X					
270			O																	
240				O		O		O												
210					O		O													

On the large diameter post, dry bands several sheds in length were observed forming on the uppermost (narrower) section of the column. These dry bands were subsequently bridged by discharges before activity was observed on any other regions of the column. The third section (from the bottom) was most often free of scintillation long after discharges occurred elsewhere. Examples of the type of scintillation seen on the large diameter post are given in figures 4-63 and 4-64.

Another aspect of station insulator contamination behavior is the effect of non-uniformity of contaminant around the circumference of a post on the flashover voltage. This problem may be of practical importance when the contaminant is deposited on large diameter posts by winds blowing predominantly in one direction. It is also of interest from a theoretical point of view, since a reduction in the size of the contaminated surface area would essentially decrease the number of effective "paths" which have been suggested as statistically influencing the flashover voltage of large diameter posts.

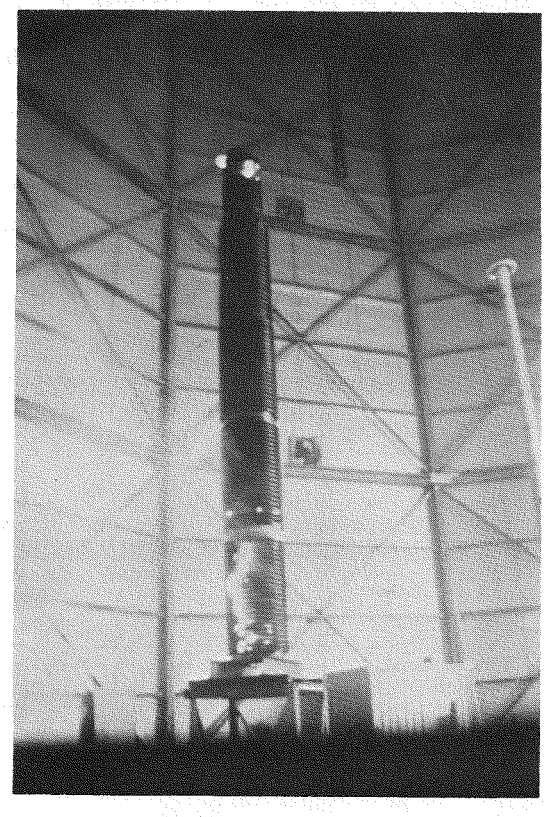


Figure 4-63. Scintillation on the Large Diameter Post.

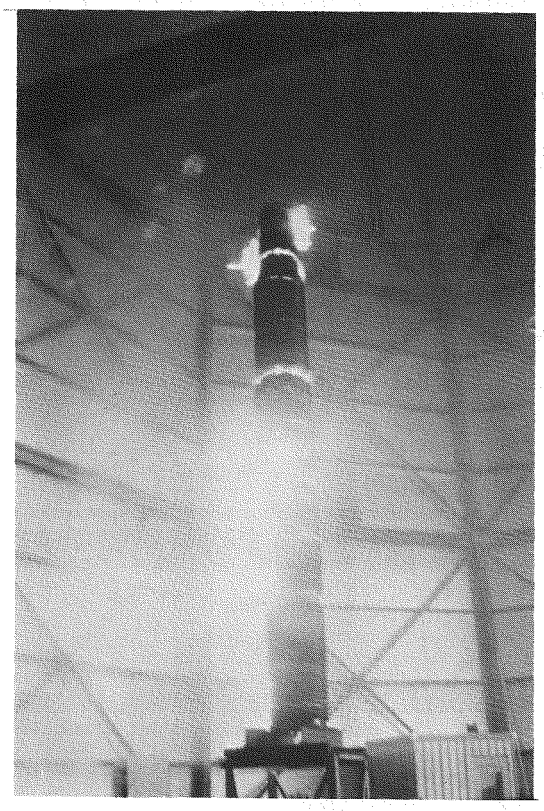


Figure 4-64. Scintillation on the Large Diameter Post.

To investigate the performance of nonuniformly contaminated columns, a set of special tests was conducted with only one strip of the large diameter column contaminated. The results for different strip widths are given in Table 4-18. It should be noted that the fifty percent flashover voltage with the entire porcelain contaminated was 225 kV using 40/40 mixture. The tests show that non-uniformity distributed contaminant on such a large diameter post may significantly affect the flashover voltage. For example, when approximately one half is contaminated and the remainder clean, the fifty percent level is on the order of 315 kV, or 40% higher than a uniformly contaminated column. With a narrower strip, such as 30-46cm, the flashover voltage is above 360 kV. Thus, in station locations where wind borne contaminants arrive on column surfaces from mainly one direction, the flashover voltage may be considerably higher than indicated by the fog chamber tests of Tables 4-16 and 4-17 where the entire post was uniformly contaminated.

It is also interesting to note that when the strip width on the large diameter column is on the order of the circumference of the small diameter posts, the flashover voltages are approximately equal.

TABLE 4-18

TESTS ON LARGE DIAMETER COLUMN WITH VERTICAL STRIPS OF VARIOUS WIDTHS CONTAMINATED WITH 40/40. NUMBERS IN PARENTHESIS BELOW EACH TEST INDICATE WIDTH OF CONTAMINATED STRIP (LOWER SECTIONS). ENTIRE CIRCUMFERENCE OF COLUMN IS APPROXIMATELY 250cm

Voltage					
360		0 (30-46cm)	X (127cm)		
330	0 (30-46cm)			X (127cm)	
300					0 (127cm)

Effect of Length

The decrease in flashover voltage of the large diameter long column was discussed above. However, the flashover voltage of the small post (Table 4-16) is already low enough so that station design for contamination of this severity becomes impractical.

A comparison of the flashover voltages for the small diameter column given in Tables 4-16 and 4-17 with data obtained on short post stacks is shown below in Table 4-19.

TABLE 4-19

COMPARISON OF FLASHOVER VOLTAGES OF SMALL DIAMETER POSTS IN LONG STACKS (7.82m) WITH DATA OBTAINED IN SHORT (1-3 section) COLUMNS.

Contaminant	V_{50} (Short Stack)		V_{50} (Long Stack)		Long Stack* Efficiency
	kV	kV/cm	kV	kV/cm	
40/5	88	1.15	520	.66	57%
40/40	58	.76	310	.40	53%

* Long stack efficiency = (kV/m) long stack/ (kV/m) short stack

The data for single post sections with 40/40 were taken from figure 4-61, whereas the 40/5 data on short stacks are estimated from an extrapolation of published curves [4-1] assuming a salt deposit density of 0.01 mg/cm^2. The results in Table 4-19 indicate that there is a strong nonlinearity of insulation strength with length for these post insulators. In fact, for very light contamination (40/5), the small column has a fifty percent flashover voltage corresponding to 900 kV system voltage, whereas with 40/40 the fifty percent flashover voltage corresponds to a system level of 540 kV.

Since the flashover voltage of long stacks showed a severe nonlinearity of strength with length and the large diameter post had a much lower flashover voltage compared with the smaller column, another series of special tests was conducted.

These tests were designed to determine whether the voltage distribution on the posts would significantly affect the flashover strength, since the contamination chamber experiments gave different results from earlier outdoor tests. The voltage distribution on the two columns in the UHV chamber was modified by energizing a large 12-conductor bus located at about one half the column height and between the posts as shown in figure 4-65. In addition, hipot wire was connected at this height to an insulator string on the other side of the small diameter post. Both the bus and hipot wire were energized at the full test voltage.

The modification of the voltage distribution on the small and large diameter columns due to the proximity of these additional electrodes is shown in figures 4-66 and 4-67 respectively. Note in figure 4-66 that the distribution on the small diameter column in the absence of the additional electrodes was obtained by the conventional neon bulb method in use at Project UHV and by means of the recently

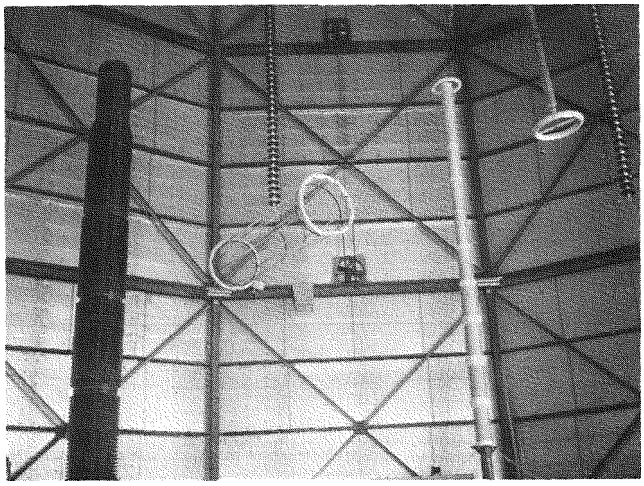


Figure 4-65. Energized 12-Conductor Bus Placed Between Posts to Modify Voltage Distribution. Hipot Wire also Extends to Conventional Insulators at far Right.

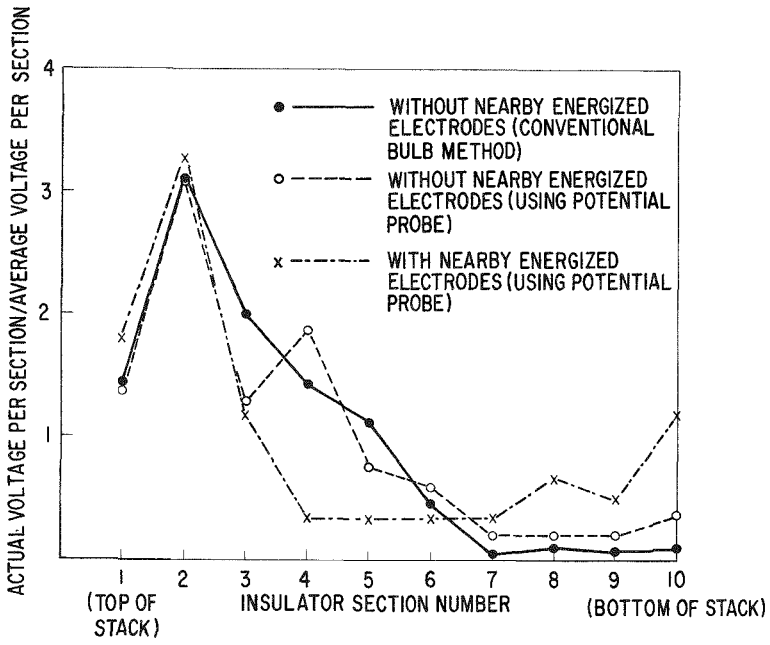


Figure 4-66. Voltage Distribution on Small Diameter Column with and without Nearby Energized Electrodes. Measurements in Absence of Electrodes was made with Conventional Technique and with Space Potential Probe.

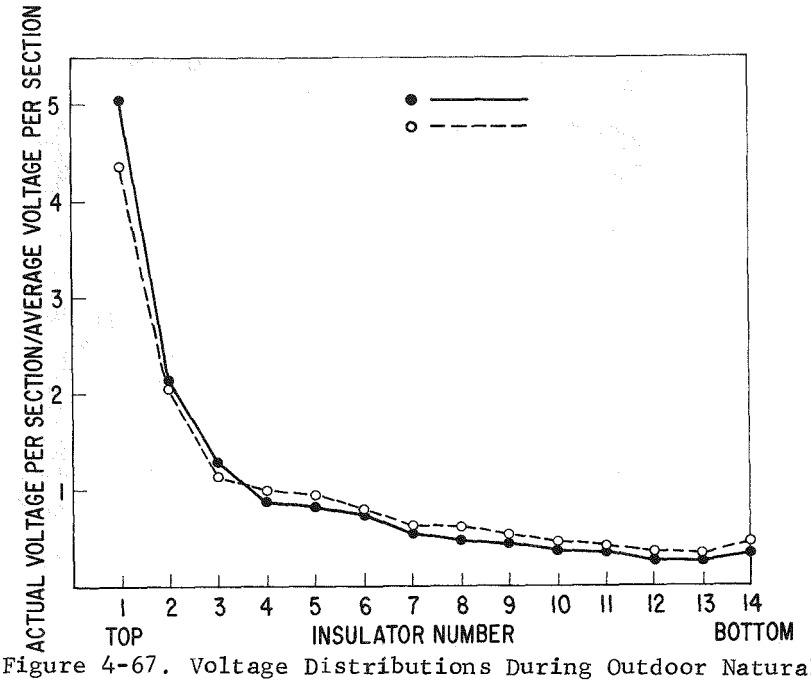


Figure 4-67. Voltage Distributions During Outdoor Natural Humidity Tests on Two Small Diameter Columns Having 14 Sections.

developed potential probe. [4-8] The data from the two methods are in relatively good agreement. Only the probe was used with the additional electrodes present, since these structures limited the accessibility of the operator. In figure 4-67, the probe was used exclusively because the conventional technique is most easily applied when metallic hardware exists for connection purposes.

Two interesting aspects of figures 4-66 and 4-67 are the shape of the distributions themselves and the influence of the energized electrodes. First, it appears that the highest voltage stress occurs not on the section closest to the electrode, but one or more sections below it. This may be a consequence of the fact that no large shielding rings were employed on either column. Second, the modification of the voltage distribution was mainly confined to central and lower region of the small column. On the large column, there was a substantial reduction on the most highly stressed region. For comparative purposes, the voltage distributions obtained in the outdoor test setup for two columns similar to the small diameter posts but of greater length are given in figure 4-68. These columns had an electrode consisting of a 4-conductor bundle of 8.9cm conductors spaced 76cm apart. Note that the uppermost units were most highly stressed in this case.

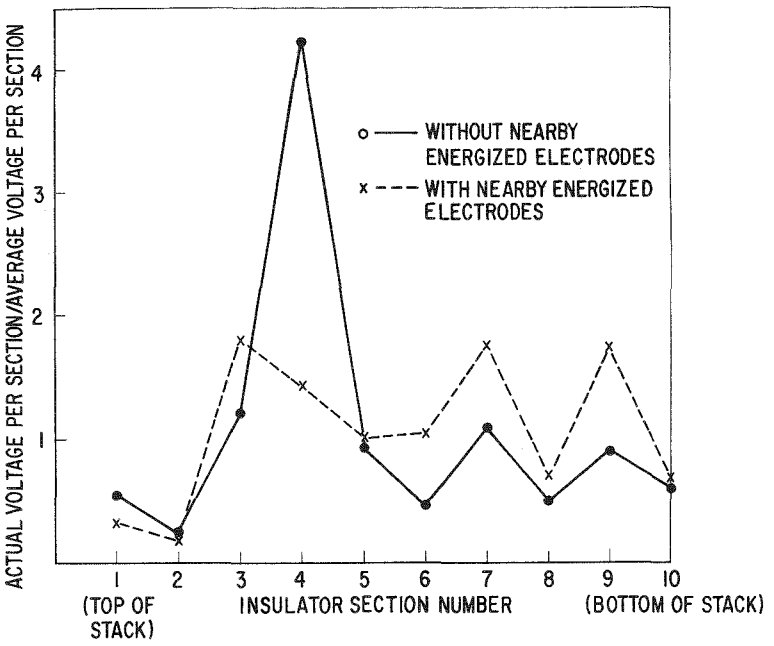


Figure 4-68. Voltage Distributions on Large Diameter Column with and without Nearby Energized Electrodes. Measurements made with Space Potential Probe. "Section" Corresponds to a Length of About 5 ft.

The test voltage used for determining the effect of the additional energized electrodes was 300 kV. The results are shown in Table 4-20.

TABLE 4-20

CONTAMINATION TESTS ON LARGE AND SMALL DIAMETER POSTS WITH MODIFIED VOLTAGE DISTRIBUTION. VOLTAGE 300 kV.

Test:	1	2	3	4
Large post	x	x	x	-
Small post	x	0	0	x

Based on the limited number of tests in Table 4-20, it may be concluded that for the small diameter column, the fifty percent flashover voltage is 300 kV, or about the same as it was in the original series of Table 4-17, where no grading electrodes were present. For the large diameter column, only flashovers occurred at 300 kV. Consequently, the only conclusion is that the fifty percent flashover voltage is still below this level.

Design Considerations

The contamination design of a UHV station using posts would lead to extremely long columns. For example, assuming the long stack flashover voltages in kV/cm apply to even longer columns, consider the requirements for a 1200 kV station. If a standard deviation of 10% is assumed for long posts, a 3σ withstand criterion would imply a fifty percent flashover voltage of 990 kV to ground. According to Table 4-17, the necessary post length would then be 15 meters (49 ft) for 40/5 and 25 meters (82 ft) for 40/40. This implies that periodic washing of long post columns would be required in order to avoid such impractical insulator lengths. The situation is even more critical for large diameter columns, as may be seen from Table 4-17.

ICE FLASHOVER PERFORMANCE

Introduction

In the design of overhead transmission lines for geographical regions in which ice storms may occur, the effect of ice accumulation is normally taken into account in the determination of the required mechanical strengths of insulator strings and towers which must support spans of ice-coated conductors. However, ice-bridging of insulator strings may also cause a substantial reduction in electrical insulation strength, and has been known to be responsible for flashovers and consequent outages. Unfortunately, very few first-hand observations of such flashovers have been made on lines in service, due mainly to the remote locations and inclement weather in which icing conditions often occur. As a result, there is a lack of precise information on the meteorological conditions which prevail at the time of ice-coated insulator flashover.

One example of the appearance of insulator strings which have become covered with ice on an operating line is shown in figures 4-69 and 4-70. These figures illustrate two views of one tower which is part of a double-circuit 230 kV line in the Ontario Hydro system. It is not known whether any of the insulator strings shown in these photographs experienced flashovers, but there are three characteristics of the icing which should be noted because of their similarity to some phenomena which have been found in the artificial tests presented here.

First, in figure 4-69, it may be seen that the ice forms a continuous bridge along the insulator strings, with ice between adjacent skirts in the form of thin "icicles". Second, on several of the six strings shown in the photographs, the insulators closest to the line conductor are free of ice and hence are not part of the

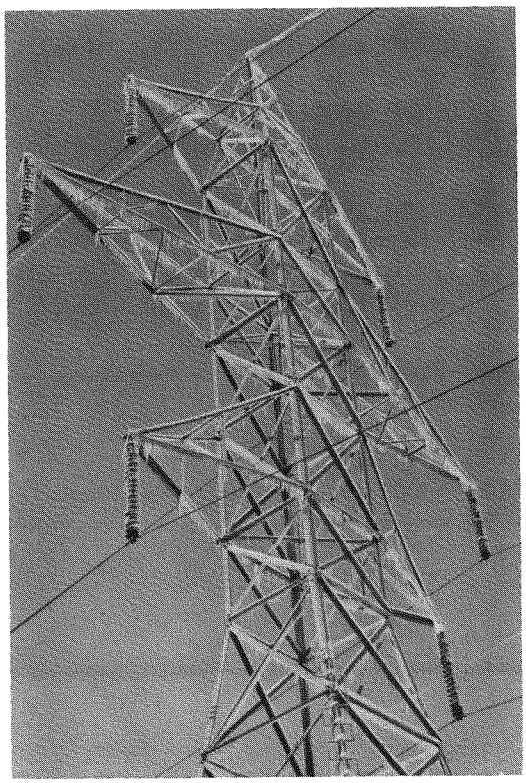


Figure 4-69. Ice Accumulation on Insulators and Tower in the Ontario Hydro 230-kV System.

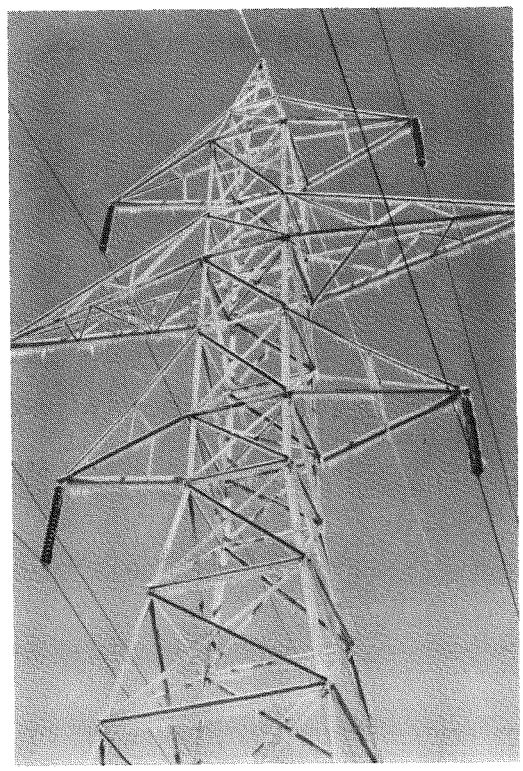


Figure 4-70. Alternate View of the Same Tower Shown in Figure 4-69.

ice-bridge. Finally, the opposit view of the tower as shown in figure 4-70 indicates that one side of all the insulator strings is ice-free. This inhomogeneous distribution of the ice coating around the insulator is an indication of the wind direction during ice accumulation.

In a previous report, several aspects of the mechanism of ice flashover of insulators were discussed. [4-9] One conclusion which was reached in that paper was that the presence of water is required to initiate ice-coated insulator flashover. This may occur in nature in at least two ways. One of these is associated with the period in which ice accumulates on insulator strings. During this time, the rain or mist which accompanies the ice storm may provide the necessary water for the flashover process to begin. A second possibility is that ice may be formed at very low temperatures during the night, in which case the moisture may freeze on contact with the insulator surfaces. Radiation from the sun and/or the increase in ambient air temperature on some subsequent morning may be sufficient to trigger melting and thus lead to flashover. The tests reported here were made by means of a technique which simulates both of these mechanisms to some extent. Nevertheless, it should be noted that the validity of any artificial test method for evaluating the flashover characteristics of ice-coated insulators may be subject to some doubt, and until more field data are available, each testing technique must be examined on its own merit with regard to the simulation of natural conditions.

Test Procedure with Ice Thickness as a Severity Parameter

All tests reported here were made in the EHV poleyard. For the tests on suspension insulators, voltages in the range of 220-400 kV (ℓ-g) were available by energizing the EHV transformer with the 110 kV regulator. A 12 k Ω resistor connected in series with the test objects at the output of the EHV transformer limited the short circuit current to between 18 and 33 amperes. For the low voltage tests on post insulators, the EHV transformer was fed by the 23 kV regulating transformer, with test voltages between 35 and 65 kV. A special series parallel connection of the liquid resistor of 2.7k Ω at the EHV transformer output limited flashover currents to the range of 13-31 amperes.

Since it was previously determined that ice which is formed while insulators are unenergized is quite different from ice which is made while voltage is applied, all tests were formed by creating ice while the insulators were energized in order to simulate conditions occurring on energized lines in service. [4-9] The ice was applied to the insulators by spraying tap water having resistivity of approximately

35kΩ-cm on the various configurations generally during evenings when the temperature was below 0°C (32°F). For the tests on suspension insulators, the water spray was in the form of a fine mist, generated by a fog-type nozzle mounted on the bucket end of a boom truck, as shown in figure 4-71. The boom on the truck was operated by a man on the truck platform, which allowed flexibility for making ice even when wind speed and direction changed. For the tests on post insulators (below 100 kV), the water spray was derived from a spray nozzle on a garden hose.

The test procedure in all cases, except where noted in the sections below, consisted of applying a fixed voltage to the insulators and creating ice by means of the water spray until a flashover occurred. The severity of the icing was determined by measuring ice thickness after a flashover or at the end of a test in two ways. First, the thickness of the ice layer formed on a 2.5-cm (1-inch) diameter copper pipe, placed so that it received the same water spray as the insulators, was recorded. An example of such a monitoring device is shown in figure 4-72. This scheme has been used for some time in standards for ice tests on switches. [4-10] Although the ice deposited on such an unenergized object provides only an approximate index of severity for ice on the energized string itself, it will be seen that it is a useful parameter for analyzing test results. In addition, it is

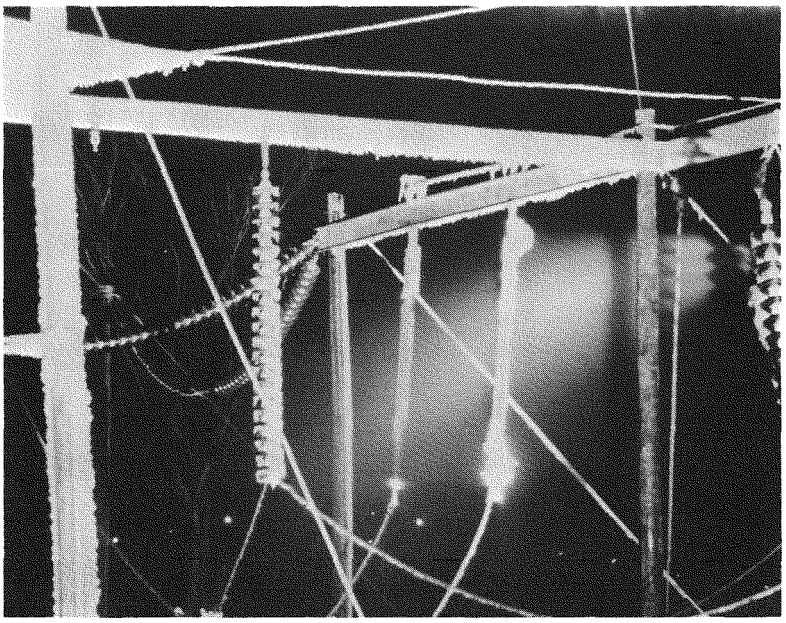


Figure 4-71. EHV Poleyard Showing Boom of Truck From Which Water was Sprayed on Insulators.

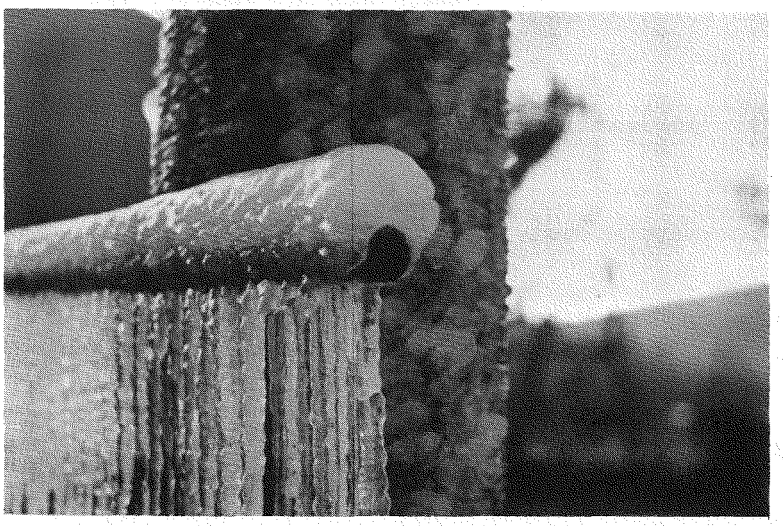


Figure 4-72. Copper Pipe Ice Monitor. Ice Thickness Measured on Top Surface.

suggested that this type of ice severity monitor might be a practical method for recording icing on existing transmission lines. A second method of measuring ice build-up involved measuring the actual thickness of ice on the insulators after the test was completed. This is also a very approximate technique, since ice thickness sometimes varied considerably along the string. In such cases, the maximum value of the ice thickness was employed as a parameter.

The duration of a single test was normally several hours. If no flashover occurred after a period of four hours, the result was considered a withstand.

Standard Insulators

One of the main purposes of the tests reported here was to evaluate the insulation strength of ice-coated vertical strings of standard insulators as a function of string length, using thickness as a severity parameter.

In order to determine the ice flashover performance of the standard insulators shown in figure 4-5, four vertical strings containing different numbers of these units were tested. These consisted of two strings containing 27 insulators, one string having 24 units, and one with 30 units. A V-string containing 24 units on a side was also tested. Under constant voltage, all strings were connected in

parallel, but water was sprayed generally on only one string at a time to develop an ice coating. After flashover occurred, the ice thickness on the monitor pipe was recorded and the string which flashed over was disconnected from the circuit. The icing procedure was then repeated on another insulator string. The four vertical strings in the poleyard on a morning after such a test series was performed are shown in figure 4-73. The ice thickness on the insulator strings was usually measured in the morning after a test.

The details of the ice flashover tests are given in Table 4-21. As may be seen in that table, two voltage levels were applied: 288 kV (500 kV ℓ-ℓ) and 318 kV (550 kV ℓ-ℓ). The data for flashover tests made during the application of ice to the insulators (tests 1-5) are plotted in figure 4-74 for monitoring pipe ice thickness and in figure 4-75 for the radial ice thickness on the insulator strings. Most data points shown are for tests where flashovers took place. However, the results of test 5, a withstand, are shown with arrows in figure 4-74 in order to indicate that a flashover might have occurred with more ice. A similar representation was used for the withstand of test 3 in figure 4-75. The general trend which may be seen in figures 4-74 and 4-75 is that the flashover voltage increases as the string length changes from 24 to 30 units.

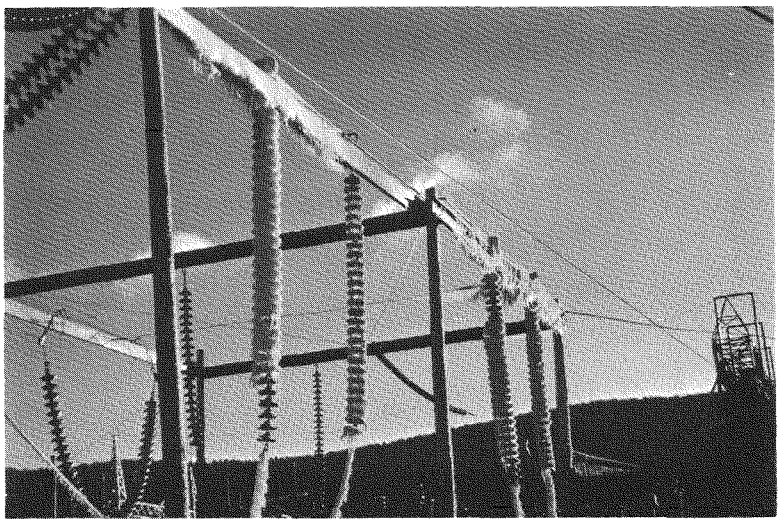


Figure 4-73. Experimental Setup for Effect of Length on Ice Flashover Strength. Standard Unit Strings of 30, 27, 27 and 24 Units are Shown.

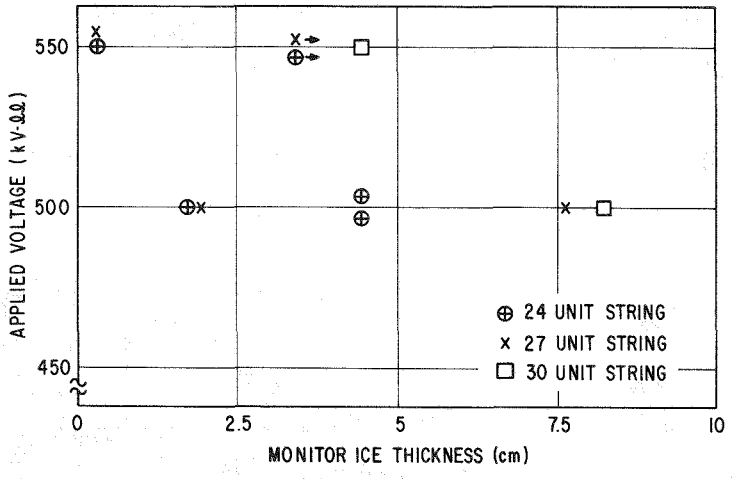


Figure 4-74. Flashover Voltage as a Function of Ice Thickness Measured on Pipe Monitor for Vertical Strings of Standard Insulators with Different Lengths.

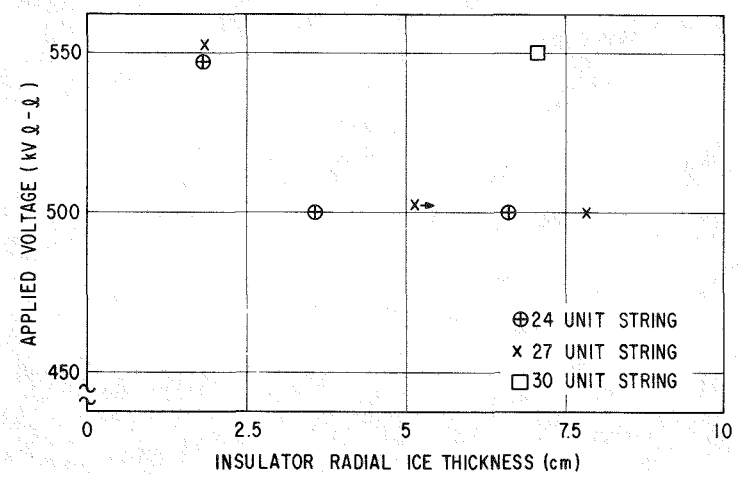


Figure 4-75. Flashover Voltage as a Function of Radial Ice Thickness Measured on Insulator Strings on Morning After Tests.

The result of test 7 on a V-string of 24 units is significant for the design of insulator strings for regions where icing may occur. Although the ice accumulation during test 7 was 70% higher than that of the average of 24-unit vertical strings, no flashover occurred. This indicates that V-strings offer a substantial improvement over vertical strings on ice flashover strength, since water does not cascade down the string but instead drips from each insulator directly to ground. Consequently, the formation of a continuous ice bridge along the string is inhibited. Earlier tests indicated that this effect was even more pronounced on horizontal strings. [4-9]

An interesting comparison between two test methods may be made by examining tests 5 and 6 in Table 4-21. In test 5, ice was made under voltage at night, but no flashover occurred. Note that the temperature was rather high compared with other tests in the table. The next morning, sun-induced melting of the ice occurred, but no flashover took place in this case either. For these tests, the conclusion is that water due to sun-induced melting is no more severe in reducing insulation strength than the presence of water which accompanies the formation of ice.

The physical appearance of the discharges preceding flashover were similar to those reported previously.[4-9] Scintillations were observed both near the ground and high-voltage ends of the string before flashover took place. Frequently, large sections of ice would fall off the strings during bursts of scintillation.

The characteristics of the ice deposited on the insulator strings after one of these artificial ice tests may be compared with that found in natural conditions as illustrated in figures 4-69 and 4-70. For this purpose, the closeup details of the ice on the 27-unit vertical test string is shown in figure 4-76. Note that several insulators near the high-voltage electrode are relatively free of ice. This was also observed to occur in natural conditions (figures 4-69 and 4-70), and is a consequence of the nonlinear distribution of voltage along the string. The first few units receive a larger share of the total voltage and consequently ice does not readily form there. Second, the ice between skirts is in the form of icicles, as is also the case for naturally iced insulators. Although not apparent in figure 4-76, it was frequently observed that the icing is nonuniformly distributed around the insulators because of the wind.

TABLE 4-21

ICE FLASHOVER TESTS ON VERTICAL AND V-STRINGS OF STANDARD INSULATORS
NOTE: TESTS 1-6, VERTICAL; 7 V-STRING

Test	Voltage (kV)	Temperature °C	Temperature (°F)	String Length (units)	Monitor Ice Thickness cm	Monitor Ice Thickness (in)	Insulator Radial Ice cm	Insulator Radial Ice (in)	Result
1	288	-6.7 - -5	(20-23)	24	1.8	(0.7)	-		Flashover
	[500 (ℓ-ℓ)]			27	1.8	(0.7)	-		Flashover
2	288	-12.8	(9)	24	4.6	(1.8)	6.6	(2.6)	Flashover
				27	7.6	(3.0)	7.8	(3.1)	Flashover
				30	8.4	(3.3)	-		Flashover
3	288	-7.8	(18)	24	4.6	(1.8)	3.6	(1.4)	Flashover
				27	-	-	5.1	(2.0)	Withstand
4	318	-10.6	(13)	24	0.3	(0.12)	1.8	(0.73)	Flashover
	[550 (ℓ-ℓ)]			27	0.3	(0.12)	1.8	(0.73)	Flashover
				30	4.6	(1.8)	7.1	(2.8)	Flashover
5	318	-3.3	(26)	24	3.8	(1.5)	-		Withstand
				27	3.8	(1.5)	-		Withstand
6	318	-		24	3.8	(1.5)	-		Withstand*
		-		27	3.8	(1.5)	-		Withstand*
====									
7 (V-String)	288	-4.4	(24)	24	6.4	(2.5)	-		Withstand

*Tests made during sun melting of ice formed in test 5

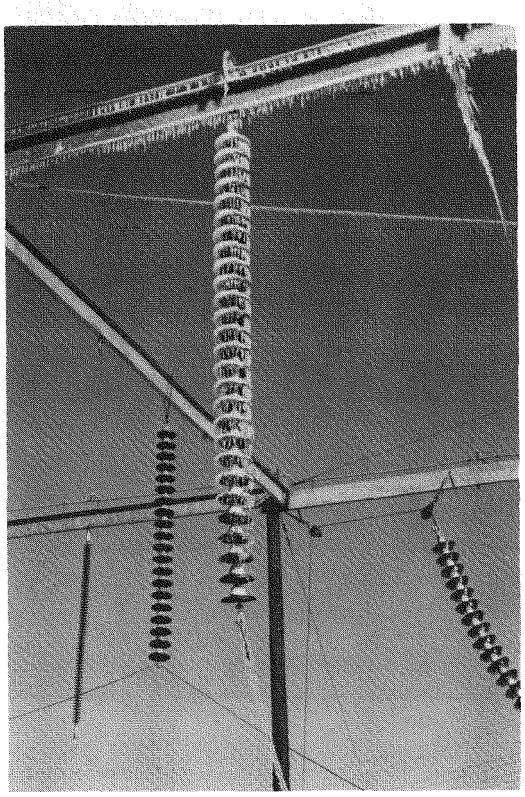


Figure 4-76. Typical Appearance of Vertical Insulator String After Ice Test.

Plastic Insulators

Ice tests were also made on several types of plastic long rod insulators. A generalized sketch of these insulators is given in figure 4-77 and the details of the units tested are listed in Table 4-22.

Two different test periods were used for the evaluation of the ice flashover of plastic insulators. During the first test period, only type R1 was available.

The results of the individual ice tests during this first test period on two vertical units ("a" and "b") and one V-string of type R1 insulators are given in Table 4-23. In the case of the vertical configurations, tests 1-4, the performance was somewhat inferior to that found for similar length vertical strings of standard units. For example, a flashover occurred at 210 kV with only 1.0cm of ice. Ice buildup in the tests was relatively fast for this type of insulator design, due to the short distance between adjacent sheds. The close proximity of the sheds to each other allows ice bridging to take place rather easily, when compared with standard suspension insulators.

TABLE 4-22

CHARACTERISTICS OF PLASTIC LONG ROD INSULATORS USED FOR ICE TESTS

Type	Connection Length	Spacing	Outer Diameter	Inner Diameter	Leakage dist./ Connection Length	Remarks
	cm (in.)	cm (in.)	cm (in.)	cm (in.)		
R1	329 (130)	4.5 (1.8)	13 (5.1)	2.5 (1.0)	2.64	Tested Previously
R2	330 (130)	11.0 (4.3)	13 (5.1)	2.5 (1.0)	1.59	-
R3	330 (130)	8.7 (3.4)	11 (4.3)	2.5 (1.0)	1.59	-
R4	330 (130)	4.5 (1.8)	16 (6.3)	2.5 (1.0)	2.69	6 Groups 14cm gaps

This suggests that an important parameter in the design of such units for good insulation strength in icing conditions is the spacing between sheds. For example, the performance of vertical configurations may improve if the insulators were constructed with alternating large and small diameter sheds in order to inhibit ice bridging.

TABLE 4-23

ICE TESTS ON PLASTIC INSULATORS OF TYPE R1 DURING FIRST TEST PERIOD

Test	Configuration	Voltage (kV)	Temperature °C (°F)		Monitor Ice Thickness cm (in)		Insulator Radial Ice cm (in)		Remarks
1	Vertical	288	-15 (5)	a	1.5 (0.6)		4.8 (1.9)		Flashover
		[500 (ℓ-ℓ)]		b	1.5 (0.6)		-		Flashover
2	Vertical	210	-6.7 (20)	a	1.0 (0.38)		4.3 (1.7)		Flashover
		[364 (ℓ-ℓ)]		b	1.3 (0.5)		-		Flashover
3	Vertical	232	-8.9 (16)	a	-		4.1 (1.6)		Flashover
		[402 (ℓ-ℓ)]		b	-		4.8 (1.9)		Flashover
4	V	232	-3.3 (26)		4.4 (1.75)		-		Withstand

An example of the ice accumulation on the morning after a test is given in figure 4-78. The appearance of pre-flashover partial discharges on these units was quite similar to that observed in the case of standard units. Bluish-white arcs were

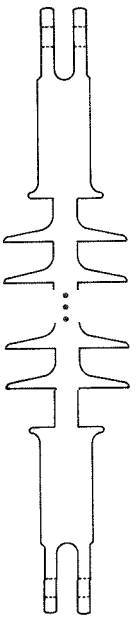


Figure 4-77. Generalized Sketch of Sheds and Hardware on Synthetic Long Rod Insulators R1-R4.

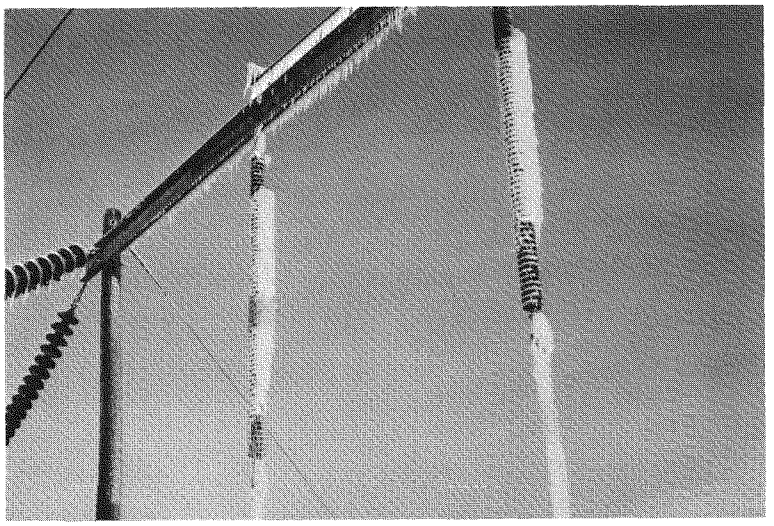


Figure 4-78. Ice Accumulation on Vertical Configuration of Long-Rod Insulators.

observed to bridge the ice-free sections at the ground and high voltage ends of the insulators.

Only one test, number 4, was made with the single units connected in a V-configuration. As may be seen from Table 4-23, however, the units did not flash over even with an extremely large ice buildup on the monitor. The improvement in performance compared with vertical configurations may be attributed to the inclination of the sheds, which allows flowing water to drip from them, instead of cascading down the entire length of the unit.

The relationship between flashover voltage and icing severity for vertical configurations of standard and plastic insulators of type RI obtained from the first test period is shown in figure 4-79. These results show the insulation strength in kV/unit and kV/m as a function of ice thickness on the pipe monitor. It may be seen that for standard units with light ice accumulation (0.3cm), the strength is in the range of 12-13 kV/unit. For heavy icing (8cm), the strength is reduced to about 10 kV/unit. The data in figure 4-79 also indicate the range of dispersion in the test results, which may in part be attributed to the difference in temperatures occurring during the various tests. For long-rod insulators, the dispersion in the experimental results is higher than for standard units.

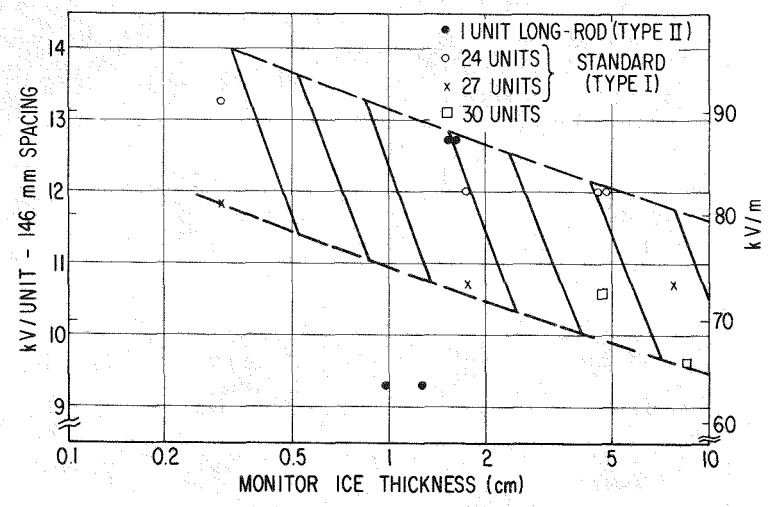


Figure 4-79. Flashover Voltage per Unit and Per-Unit Length of Ice-Coated Standard and Long-Rod Insulators as a Function of Monitor Ice Thickness. Shaded Band Indicates Range of Insulation Strength for Standard Units.

Because of the relative ease with which the sheds of insulator type RI became ice bridged, a second period of tests was performed. In addition to insulator type R1, the additional types R2-R4 were used. The individual shed design on R2 is identical to that on R1 except for increased shed spacing which results in fewer sheds and reduced leakage distance. Type R3 has shed spacing which is intermediate between R1 and R2, but a smaller outer diameter such that the leakage distance is equal to that of R2. The long rod type R4 has a radically different configuration, with five gaps of 14cm between six groups of sheds as shown in figure 4-80. Its total leakage and shed spacing is the same as the original unit (R1), which was accomplished by using larger shed diameter.

The results of the ice tests on these insulators are given in Table 4-24. As indicated in the table, the two tests involving R1-R4 consisted of energizing the four units in parallel, with icing (water spray) mostly confined to one insulator at a time.

Although the data available from these tests is very limited, a relative comparison of the results in Table 4-24 for insulators R1-R4 indicates that type R4, with isolated groups of sheds, is superior to others. This fact was also apparent during

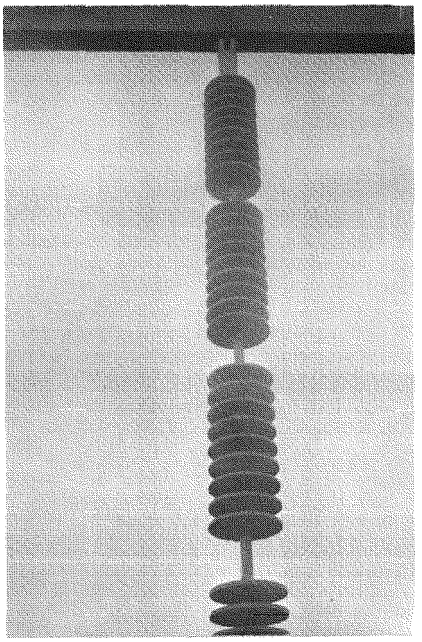


Figure 4-80. Synthetic Long Rod Insulator Type R4 Having 6 Groups of Sheds Separated by a Gap of 14cm.

TABLE 4-24

ICE TESTS ON PLASTIC INSULATORS DURING SECOND TEST PERIOD

Test	Voltage	Temperature		Insulator	Monitor Ice Thickness		Insulator Radial Ice		Result
	(kV ℓ-g)	°C	(°F)		cm	(in.)	cm	(in.)	
1	288	(-8)	17	R1	(1.4)	.56	-		Flashover
			(start)	R2	(2.5)	1.0	-		Flashover
		(-11)	12	R3	-		(2.8)	1.1	Flashover
			(end)	R4	-		(4.7)	1.85	Flashover
2	320	(-8)	18	R1	(2.0)	.8	(2.45)	.96	Flashover
			(start)	R2	(2.1)	.8	(2.79)	1.1	Flashover
		(-12)	11	R3	-		(1.85)	.73	Flashover
			(end)	R4	-		(3.35)	1.3	Flashover

the tests, as noted by the difficulty in bridging the gaps between the groups of sheds. In test 2, it also seems that type R3 having the smallest outer diameter is even weaker than the original insulator R1. Again, during the icing, bridging occurred rather easily on this type insulator. At this time, the best qualitative assessment of the relative performance which can be made from these tests is that type R4, with isolated groups, is advantageous in icing conditions. It should also be noted that quantitative comparisons using ice thickness between Table 4-24 and Tables 4-21 or Tables 4-23 should not be made, since the ice monitors were in different locations in the two test periods.

The appearance of these four types (R1-R4) of insulators after an ice test is shown in figures 4-81 - 4-84. Figure 4-86 shows all four insulators together, whereas the individual characteristics are given in figures 4-82 - 4-84. Note that the most evident prevention of continuous ice bridging occurs for R4 as seen in figure 4-84, where no ice bridges the gaps between groups of sheds.

Scintillation activity on units R1-R3 consisted of initial white-blue arcs bridging sections of the insulators at both the ground and energized ends of the long rod. This activity was observed previously on both long strings of standard units and the original type long rod, R1. An example of such discharges is illustrated in figure 4-85, which shows scintillation on insulator R3.

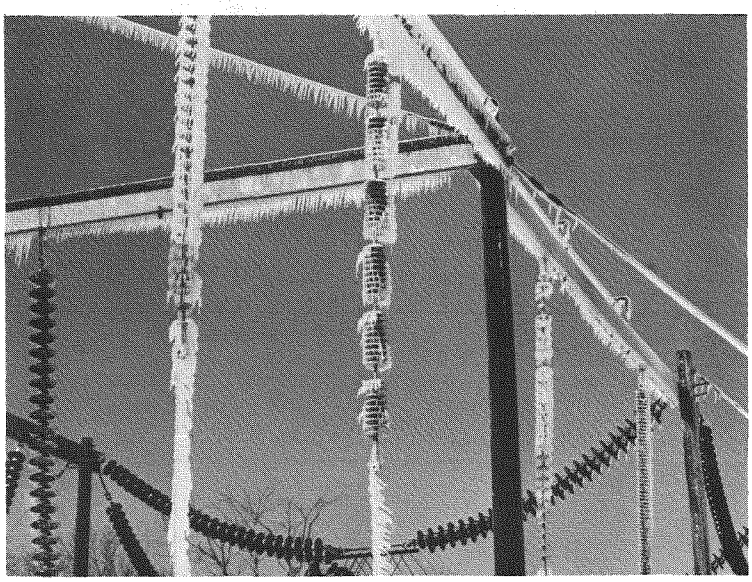


Figure 4-81. Synthetic Long-Rod Insulators After Ice Test. From Left Types are R3, R4, R2, R1.

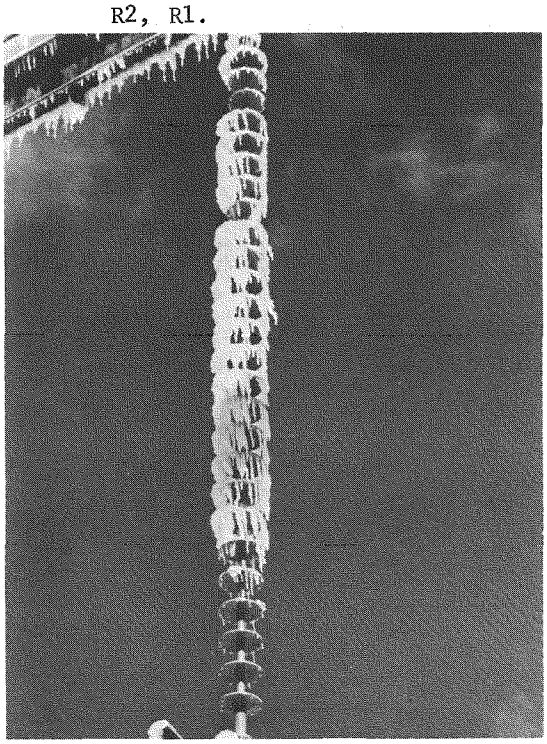


Figure 4-82. Ice Accumulation on Insulator Type R2 After Test.

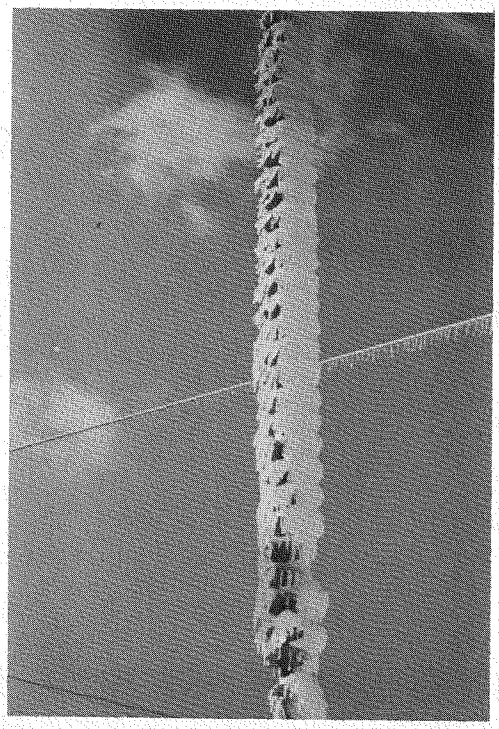


Figure 4-83. Ice Accumulation on Insulator Type R3 After Test.

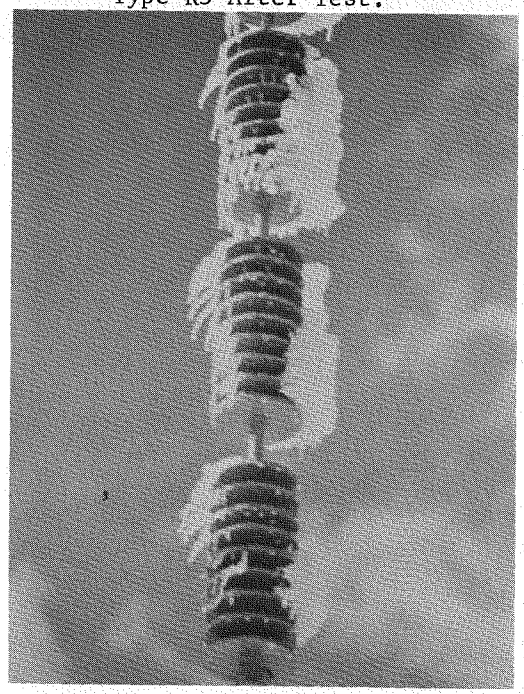


Figure 4-84. Ice Distribution on Long Rod Insulator Type R4. Note That Large Gaps Between Groups of Sheds Remain Free of Ice Bridging.

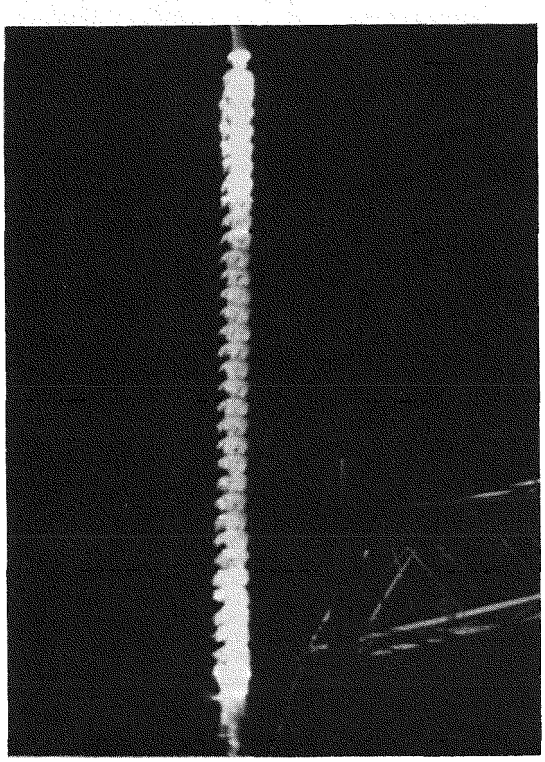


Figure 4-85. Pre-Flashover Scintillation Activity on Insulator Type R3 During Ice Test. Note Partial Arcs at Both Ground and Energized Ends of the Unit.

The pre-flashover discharges on insulator R4 which has isolated groups of sheds had interesting characteristics. The gaps between groups of sheds, which remained free of a continuous ice bridge, became the sites of arcs connecting the adjacent ice coated groups of sheds. Initially, these discharges were glow type corona confined mainly to the energized end of the unit, as shown in figure 4-86. As icing continued, all the gaps contained white arcs as in figure 4-87.

Results on Antifog Units and EHV/UHV Comparison

Large-disc antifog units were employed earlier for ice tests on long UHV strings containing as many as 40 units. (4-11) Such tests are extremely difficult to perform because of the lengths of strings involved. It was therefore of interest to determine if long-string results could be predicted from tests which are made at lower voltages on short strings, where the complexity of carrying out experiments is somewhat less. Data on 20-unit strings of these insulators are presented here and compared with the previous long-string results. The characteristics of the antifog glass insulators used for the EHV and UHV tests are shown in figure 4-88.

The results of the earlier UHV tests were that a 40-unit string flashed over at 650 kV, while a 35-unit string flashed over at 575 kV. In order to make a comparison

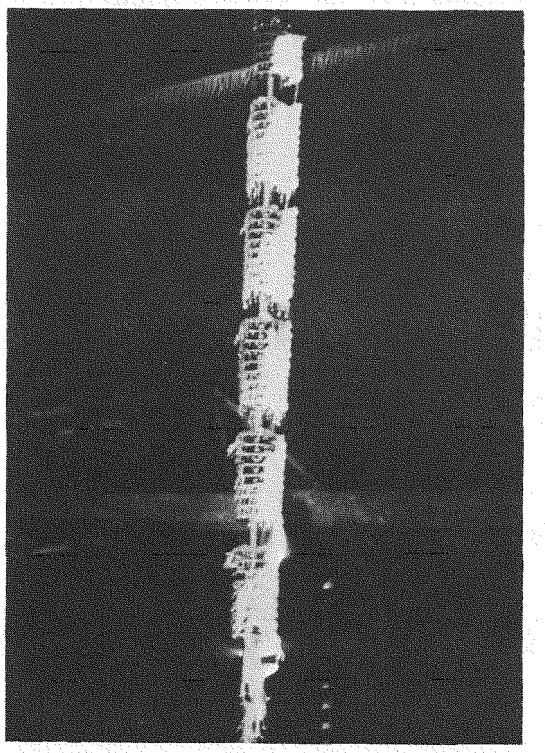


Figure 4-86. Partial Arcs on Type R4 Insulator. Corona Type Glow may be seen at Energized End and Across Gap Between First Two Shed Groups.

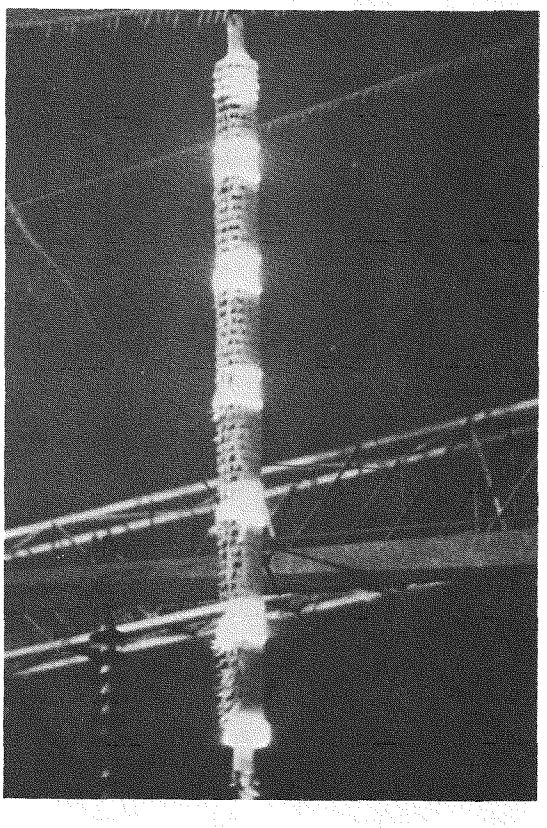
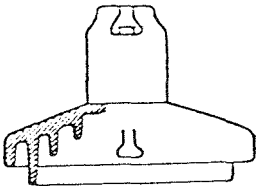


Figure 4-87. Heavy Scintillation Activity Across All Gaps and Some Sheds of Type R4 Insulator.



(ANTI-FOG)

Spacing:	184mm ($7\frac{1}{4}$ in)
Diameter:	330mm (13 in)
Mech. Strength:	30,000 kg (66,000 lb)

Figure 4-88. Characteristics of the Antifog Glass Insulator.

of this data with tests at EHV voltage levels, a 20-unit string of these insulators was selected. A linear extrapolation of the UHV results indicates that a 20-unit string should flash over at 325 kV. The data obtained in the EHV tests are given in Table 4-25, where it is shown that a 20-unit string flashed over at a voltage as low as 288 kV. This result, in addition to the others given in Table 4-25, indicates that ice flashover strength is at least linear with insulation length. In fact, the performance for long strings may even improve more than linearly over short string results, since the increasing nonlinearity of voltage distribution on the string may retard the complete ice bridging on very long strings.

The appearance of the 20-unit V-string after an ice test is shown in figure 4-89. Note that there is a tendency for the icicles to hang vertically without bridging adjacent units as would take place in a vertical string. In fact, due to the light mechanical loading of the string in figure 4-89, the units on the bottom are almost horizontal and might be more representative of a strain-string configuration.

Tests 4 and 5 in Table 4-25 are of interest again in considering the question of whether flashover during precipitation or after is more critical. In test 4, the flashover during precipitation or after is more critical. In test 4, the flashover

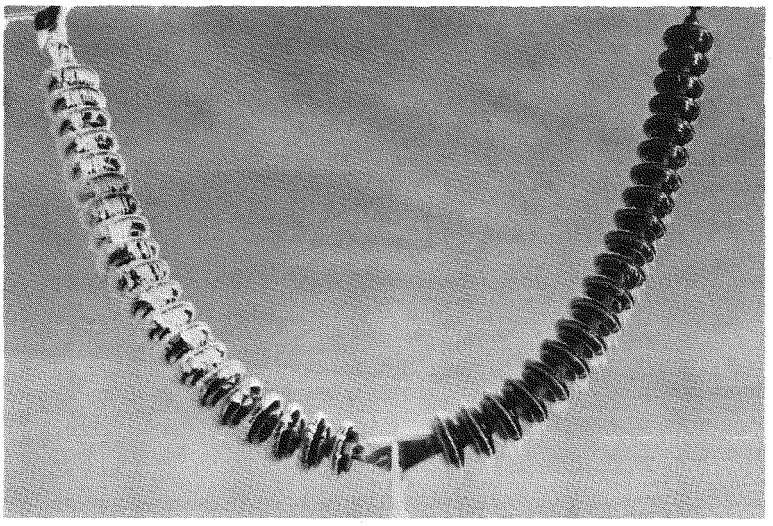


Figure 4-89. Ice on a 20-Unit V-String of 66,000-lb Glass Insulators Used to Compare EHV and UHV Performance.

occurred while ice was being applied to the insulators. The string was de-energized during the remainder of the night and energized again in the morning without the application of additional water spray. Ice melting took place during test 16 because of electrical heating and sun melting. The fact that a flashover occurred only after melting began agrees with previous experience during such tests, regarding the necessity of the presence of water. [4-10] Since a flashover took place, it appears that in this case the sun-induced melting may also produce flashover.

TABLE 4-25

ICE TESTS ON A 20-UNIT GLASS V-STRING OF ANTIFOG INSULATORS

Type	Voltage (kV)	Temperature °C	(°F)	Monitor Ice Thickness cm	(in)	Insulator Radial Ice cm	(in)	Remarks
1	288	-15	(5)	7.6	(3.0)	-		Flashover
2	260	-6.7	(20)	2.3	(0.9)	-		Withstand
3	317	-8.9	(16)	0.8	(0.3)	6.1	(2.4)	Flashover
4	300	-16.1	(3)	-		-		Flashover
5	300	-17.8	(0)	-		-		Flashover
						Test on Morning After #15		

Post Insulators

Station equipment is also subject to icing, as is well known from existing requirements on the mechanical performance of disconnect switches in such conditions. Tests were made on single unit post insulators in order to determine whether ice bridging of column type insulation would be a significant design consideration for UHV stations.

During ice tests on post insulators, four single section units approximately 76cm (30 in) in height were energized in parallel. All four units had different diameters and shapes, as shown by the geometrical characteristics in Table 4-26. The posts were mounted on grounded 55 gallon barrels to simulate a column insulator base support. The unenergized pipes used for monitoring ice thickness were installed at the base of each post insulator on the top surfaces of these barrels.

TABLE 4-26

GEOMETRICAL CHARACTERISTICS OF POST INSULATORS USED IN ICE TESTS

Post Type	Connection Length		Max. Diameter		Min. Diameter		Number of Sheds
	cm	(in)	cm	(in)	cm	(in)	
A (West end)	76.2	30	(30.5)	12.3	(19.8)	7.8	11
B	76.2	30	(23.1)	9.1	(13.5)	5.3	13
C	76.2	30	(15.2)	6.0	(7.6)	3.0	17
D (East end)	76.2	30	(11)	27.9	(7.0)	17.8	11

The results of the post insulator ice tests are given in Table 4-27. An interesting comparison of the post insulator ice flashover strength with that previously obtained for standard insulators is given in figure 4-90, where the voltage stress is plotted in kV/m of connection length as a function of the monitor ice thickness.

From the limited test data available, it appears that the post insulators have a somewhat higher flashover voltage than an equivalent connection length of standard suspension insulators for the same severity of icing as measured on the pipe monitor. However, as may be seen in figure 4-90, the difference between the post and standard insulators is more pronounced when the icing severity increases beyond 5cm deposition on the monitor. Such levels correspond to rather severe conditions and would probably not be encountered in practice.

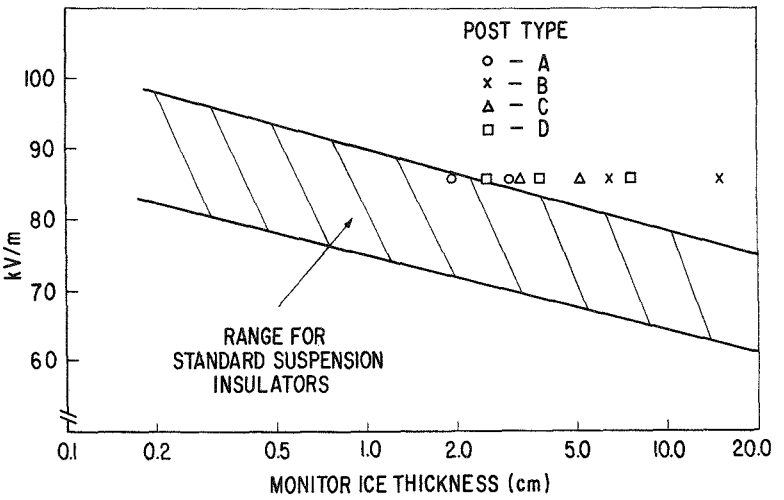


Figure 4-90. Comparison of Ice Flashover Voltages Expressed in Voltage/Connection Length as a Function of Icing Severity for Standard Suspension Units and Post Insulators.

TABLE 4-27

ICE TESTS ON POST INSULATORS

Test	Voltage	Temperature		Post Type	Monitor Ice Thickness		Result
	(kV ℓ-g)	°C	(°F)		cm	(in)	
1	65	(-0.5)	31 (start)	A	(.64)	.25	Withstand
				B	(.79)	.31	Withstand
		(-5.6)	22 (end)	C	(.79)	.31	Withstand
				D	(.79)	.31	Withstand
2	65	(-17.8)	0 (start)	A	(1.9)	.75	Flashover
				B	(15.2)	6.0	Flashover
		(-15.6)	4 (end)	C	(5.1)	2.0	Flashover
				D	(7.6)	3.0	Flashover
3	65	(-7.8)	18 (start)	A	(3.2)	1.25	Flashover
				B	(6.4)	2.5	Flashover
		(-13.3)	8 (end)	C	(3.2)	1.25	Flashover
				D	(3.8)	1.5	Flashover
4	65	(-2.2)	28 (start)	A	(12.1)	4.8	Withstand
				B	(12.1)	4.8	Withstand
		(-7.2)	19 (end)	C	(12.1)	4.8	Withstand
				D	(2.5)	1.0	Flashover

The appearance of the ice coating on the post insulators on the morning after a test is illustrated in figures 4-91 - 4-93. In figure 4-91, the sheds of the post are completely bridged by a layer of ice and icicles. The coating obtained is quite non-uniform around the circumference of the posts, even for units having a small diameter such as that shown in figure 4-92. This non-uniformity is a consequence of spraying water from only one side, but it also occurs on naturally iced insulators in service conditions. It is interesting to note in figure 4-92 that the three sheds on the energized (top) end of the post are not bridged by ice. Generally, this lack of ice is a result of scintillation discharges during which the ice shedding occurs. This phenomenon has also been seen on the ground end of some posts such as that in figure 4-93. These effects are similar to the lack of ice at the ends of vertical strings of standard insulators in ice tests and also on actual transmission lines after ice storms. Another interesting observation is related to "whisker" type icicles which sometimes extended outward from the top of a post without bridging insulator sheds. A few of these ice formations may be seen in figure 4-92. Partial arcs often originated on the tips of such icicles and reached to a shed located farther down the column. This phenomenon may not occur in a practical full-scale setup where posts are stacked in series since the cap region would not be free and thus the "whisker" formation may be inhibited.

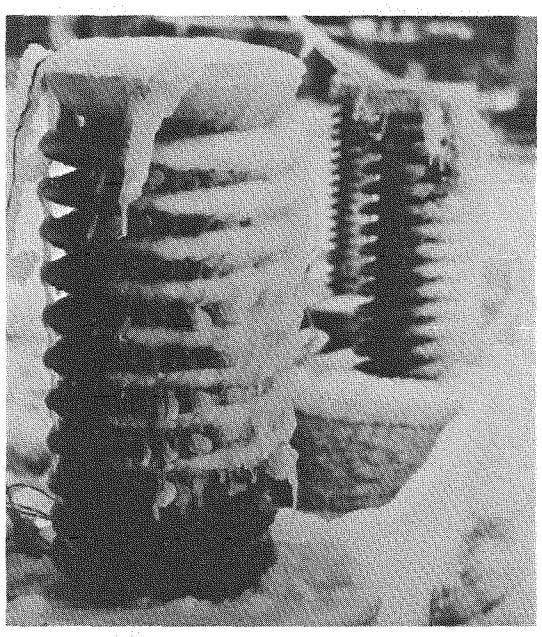


Figure 4-91. Ice on Post Type A After Test. Sheds at Bottom (Ground End) no Longer Bridged. Large "Whisker" in Center of Hardware on Which Partial Discharges were seen are Also Present in Figure 4-92.

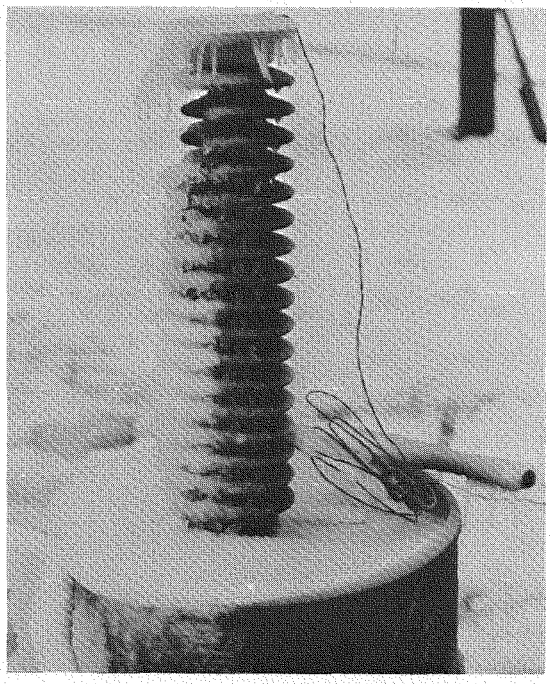


Figure 4-92. Ice on Post Insulator Type C After Test. Note Nonuniform Distribution of Ice Around Column. Sheds at Top (Energized End) Lost Ice During Scintillation.

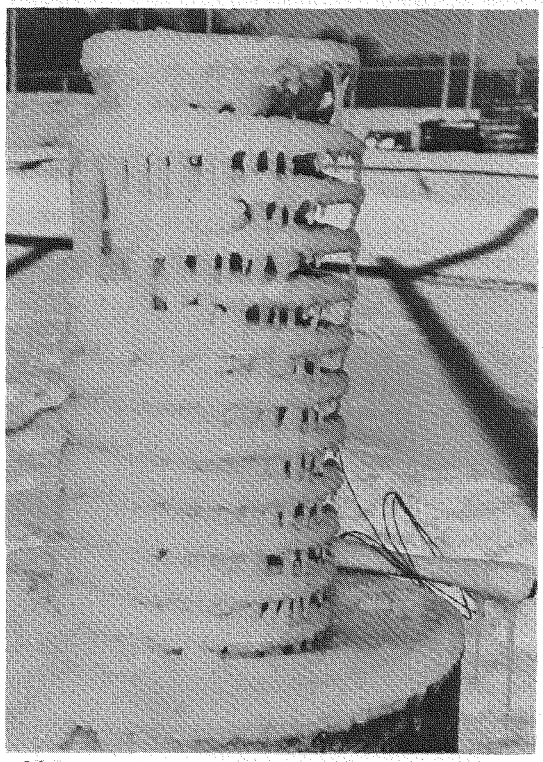


Figure 4-93. Ice Accumulation on Post Type D After Test. Pipe Monitor in Lower Right Hand Corner.

Since arcing from these icicles would only tend to lower the insulation strength, the basic conclusion from figure 4-90, namely that for the same connection length posts have a higher flashover voltage, would not be altered.

UHV INSULATOR DESIGN FOR CLEAN AREAS

Introduction

For UHV transmission lines constructed in clean areas, the power frequency insulation design would be limited by the performance of the insulators in rain. It is expected that string lengths required to withstand power frequency voltage in clean wet conditions will be much shorter than other constraints such as switching surge clearances. Full scale tests were made at UHV levels to verify the performance of insulators in clean conditions.

Full Scale Tests in Artificial Rain

The clean wet tests were made on the same string of insulators on the UHV test line which had been used for natural humidity contamination tests. This center phase V-string contained 39 units on each side of the antifog units shown in figure 4-6.

A rain spray system was installed on the tower bridge above the string. This system produces a rain rate of approximately 1.3mm/min (.05 in/min) with a water resistivity of about 22 kΩ cm. The rain rate thus is much heavier than that of most natural rains, corresponding to what might be described in nature as a downpour. The spray produced by the rain apparatus is shown in figure 4-94. The tests reported here were performed on a relatively calm day, but even a very light wind would divert the water spray from the insulators and would generally result in a withstand.

The test procedure consisted of using the same circuit as in the natural humidity tests and a "one minute withstand" technique of consecutive voltage applications, wherein a withstand was assumed if no flashover occurred in one minute. An up and down method, with voltage steps of 5%, was used to determine the fifty percent flashover voltages.

Three different string lengths were employed for the tests: 10, 13, and 16 units. As may be seen in figure 4-95, three wires connected to the tower bridge were attached with clips to the respective insulators. On completing a test series,

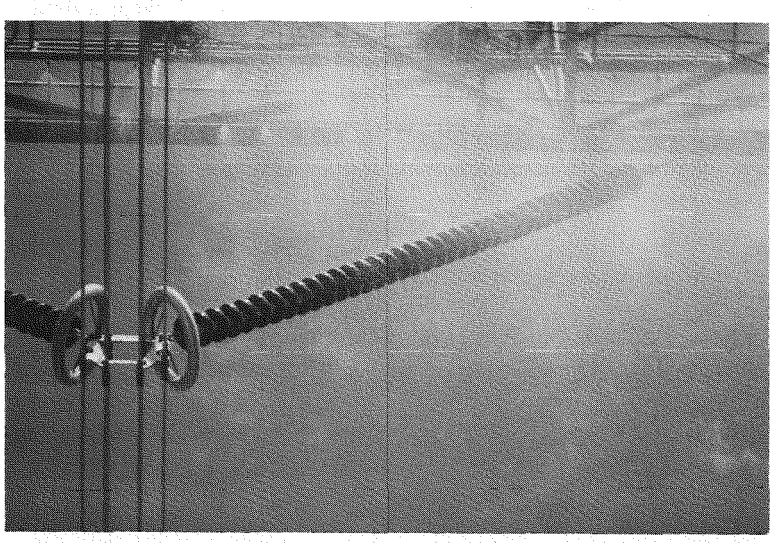


Figure 4-94. Rain Spray Produced by Artificial Rain System Above Center Phase on Tower 2. Note Water Dripping From Individual Units.

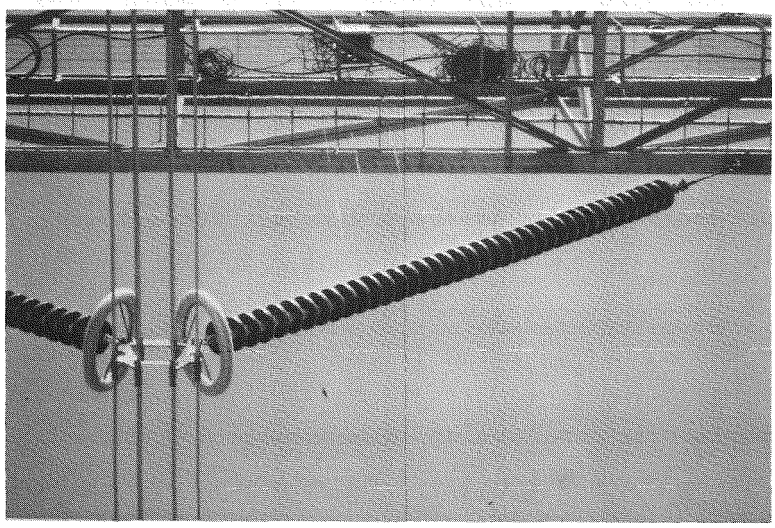


Figure 4-95. Center Phase Insulator String Showing Shorting Wires Used in Test Sequence to Change String Length in Clean Wet Tests.

with one string length, the wire was pulled from the bridge and the testing continued with the next length insulator string. The results are given in Table 4-28.

TABLE 4-28

FIFTY PERCENT FLASHOVER VOLTAGE AS A FUNCTION OF STRING LENGTH FOR 40,000 kg (90,000 lb) ANTI-FOG UNITS IN CLEAN, WET TESTS

String length (units)	V_{50} (kV ℓ-g)	V_{50}/unit
10	540	54.0
13	665	51.2
16	800	50.0

The data in Table 4-28 confirm that insulator string lengths to withstand power frequency voltages in clean conditions, at UHV levels, are much shorter than required by switching surge or contamination constraints.

Design Limits - Hangers, Switching Surges, Corona

As an estimate of the power frequency design limit for insulator strings in clean wet conditions, the data of Table 4-28 and an assumption of a 5% standard deviation of the flashover voltage will be made. For a 1200 kV system, designing for a withstand at the 3σ level, implies a fifty percent flashover voltage of $(1200/\sqrt{3}) \times 1.15 = 797$ kV. This would, according to Table 4-28, require only 16 units of that particular type of antifog insulator with a stress per unit of 43 kV. The physical length of the insulator string would be 3.5m (11.5 ft). Assuming a conductor bundle diameter of 1.07m (40 in), the minimum possible conductor-tower clearance would be 23m (7.6 ft). Typical requirements of switching surges at this voltage level would impose an air clearance of at least three times this distance, or 7.0m (22.6 ft)! The added clearance could be obtained with the use of a metal hanger to increase the conductor tower air clearance. However, these hangers also reduce the switching surge strength and this influence must be considered.

There are at least two advantages of using a smaller number of insulators and a long hanger. First, the total number of insulators to be installed is substantially reduced, resulting in some economic benefit. Second, the insulator strings will be much lighter and tower loading requirements may be reduced, leading again to some economic gain.

One disadvantage of using such a small number of units in a string is that the high stress per unit generates corona in both dry and wet conditions. Further research is required to determine the extent of these corona levels.

INSULATOR STRING HARDWARE

Introduction

The attachment of UHV insulator strings to conductor bundles requires complicated hardware. The nature of the attachment yoke plate may influence the contamination performance and definitely affects the level of corona generated on the string.

Before the three phase UHV test line was constructed, contamination and corona tests were performed in order to optimize the hardware. It should be noted, however, that the hardware used for the UHV test line is experimental in nature, with a major consideration being its flexibility for different conductor bundle and insulator string configurations. On an actual line, these parameters would be fixed and further improvements could be made. These modifications would be strongly influenced by such factors as the stringing techniques.

After the hardware for the three phase UHV line was selected, visual and photographic observations were made on the insulator strings and hardware, both in a single phase workup and on the line itself.

Effect of Attachment on Contamination Flashover

The basic suspension plate for the UHV test line is outlined in figure 4-96. In one insulator connection configuration which was tested, the attachment of the apex of the V-string was made on the top and just outside the bundle. This required an auxiliary section, shown dashed in figure 4-96, to be added to the main suspension plate. In the other configuration, the insulators were connected on the plate so that an imaginary apex of the V-string determined by extending a line along the insulators inside the bundle would be located just above the center of the conductor bundle. Both arrangements were tested with an 8-conductor bundle with conductors simulated by pipes about 6m (20 ft) in length; the suspension plate was located at the midpoint of this bundle.

The insulator configuration consisted of a single string of the antifog units shown in figure 4-10.

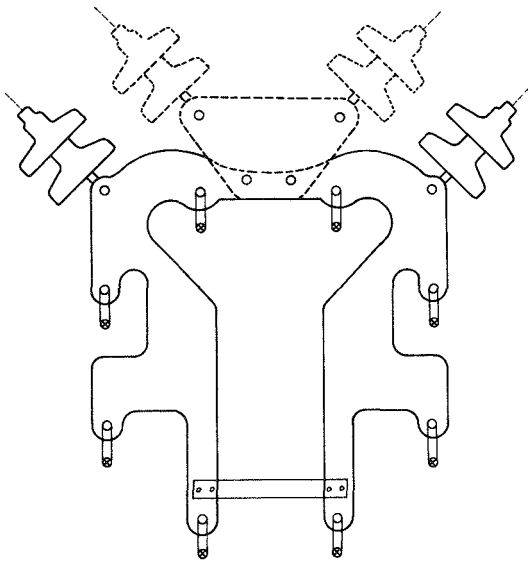


Figure 4-96. Suspension Plate Used for Testing of V-Strings.

Two contaminant mixtures were used to test the insulator/hardware arrangements in the UHV contamination chamber, one containing 40 g/ℓ kaolin and 80 g/ℓ NaCℓ, and the other 80 g/ℓ kaolin and 200 g/ℓ NaCℓ. For each test series, an "up-and-down" procedure was used to determine the critical or 50% flashover voltage (CFO), with constant voltage steps of approximately 10% of the CFO.

The mechanical support system in the UHV chamber did not allow sufficient loading to pull the string into a V with straight arms, as discussed earlier in this report. Consequently, the strings do not completely simulate the geometry which would apply to the full scale test line.

The basic results of the tests indicated that there was at most a 2.5% difference in flashover voltage for the two configurations, the case in which the apex of the V falls inside the bundle giving the higher flashover voltage. However, this difference is within the experimental accuracy of the tests and thus it was concluded that the performance of both types of hardware were the same.

Corona-Single Phase Tests

A test program on a single phase mockup was planned for the purpose of evaluating the corona performance of the suspension insulator hardware for the three phase test

line. Full scale tests were made to assess both visual corona and radio noise generation of the different configurations. Wet weather behavior was checked by making tests during natural and artificial rain. In many cases, the original hardware design led to such high levels of corona activity that modifications were required. These included changes in the attachment hardware itself and also a variety of grading electrodes in the shape of rings which were used mainly to suppress corona in the vicinity of the hardware. In addition, voltage distributions were obtained from measurements at low voltages for all the designs and their modifications in an attempt to correlate overall corona performance with the voltage distributions on insulator strings.

Table 4-29 provides a description of the six insulator strings which were planned for the initial installation of the three phase test line. The four configurations marked with an asterisk in Table 4-29 were chosen to be tested, since the basic attachment hardware of the remaining two is identical to that of the other strings, the only difference being the type of insulator unit.

TABLE 4-29

FIRST V-STRING CONFIGURATIONS FOR THREE PHASE TEST LINE

Type	Mech. Strength kg(lb)	Length (units)	Material
Single	40,000 (90,000)	39	Porcelain
*Single	55,000 (120,000)	38	Glass
Double	23,000 (50,000)	54	Porcelain
*Double	30,000 (66,000)	45	Glass
*Triple	18,000 (40,000)	50	Porcelain
*Quadruple	18,000 (40,000)	50	Porcelain

The tests were made by attaching the insulator strings, which were suspended from a pair of wood poles, to the single phase test line. The test setup is shown in figure 4-97 which illustrates the original hardware design for the single string configurations. The suspension plate in figure 4-96 was designed for the first three phase eight conductor bundle having a diameter of 1.07m (40 in). Since the single phase line at the time of these tests had a bundle diameter of 1.4m (56 in), special reducer spacers were installed 15m (50 ft) on either side of the suspension plate as shown in the figure. Although the first three phase conductor will have a 3.3cm (1.3 in) diameter, while the single phase test line conductor had 4.6cm (1.8 in) diameter, no significant difference is expected in hardware corona perfor-

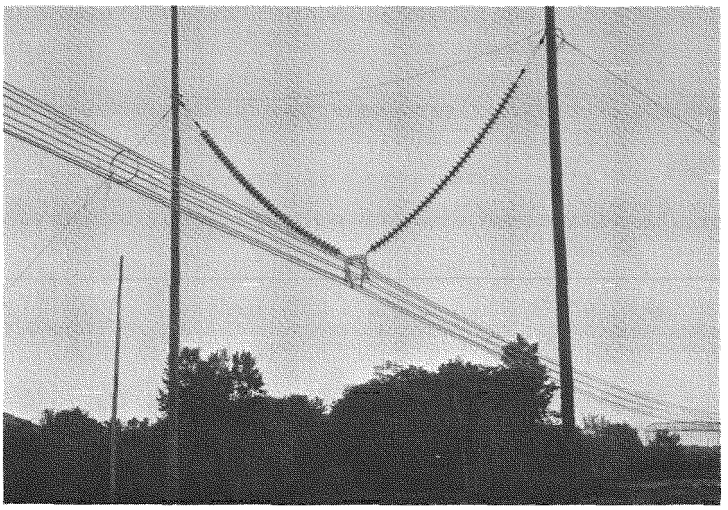


Figure 4-97. Test Setup for Corona Observations on Suspension Insulators and Hardware.

mance between these two cases, with the possible exception of the suspension shoes. Finally, it should be noted that the conductor height above ground (about 11.6m (38 ft) at the position of the string) and the tower simulation by the wood poles are not completely representative of the three phase line geometry. Since most corona activity occurs at the attachment hardware, it is assumed that these factors will not appreciably affect the corona performance.

Although the hardware used for the tests reported here is intended for a 1200 kV test line configuration, voltages ranging from 900 to 1500 kV (ℓ-ℓ) were applied in evaluating the corona activity. The data obtained over this voltage range allowed the determination of corona inception levels of the various designs. In addition, a description of performance at the higher voltages could be used for designing the necessary hardware appropriate to other voltage classes in excess of 1200 kV. Photographs of corona on the different configurations are given at 1400 kV (ℓ-ℓ), where activity is considerably higher than at 1200 kV (ℓ-ℓ). Nevertheless, at this voltage (1400 kV) a comparison may easily be made among configurations, and the effectiveness of design modifications in suppressing corona becomes quite evident.

The single and triple insulator strings make use of one attachment scheme to the suspension plate, whereas the double and quadruple strings share a second common set of hardware connections. As a result, it will be seen that those modifications which improved single string performance were also employed on the triple string, for example.

The 55,000 kV (120,000 lb) glass units were used to evaluate the single string hardware performance. A closeup of the original design of the attachment scheme is shown in figure 4-98. It should be noted in that figure that the two projecting pieces on the top part of the plate force the position of the first insulator to be quite distant from the conductor bundle. Consequently, it is not surprising that the corona activity, illustrated for 1400 kV (ℓ-ℓ) in figure 4-99, is intense on the hardware and the first several insulators. In figure 4-99, glow type corona can also be seen on the suspension shoes of the lower two subconductors.

Since the visual corona on the single insulator string was excessive, modifications in the form of shielding rings were added. The two shield designs which were examined are illustrated in figure 4-100. Both shields are composed of 7.6cm (3 in) diameter metal tubing formed into circles approximately .6m (2 ft) in diameter. As seen in figure 4-100, the shield on one side of the V-string consisted

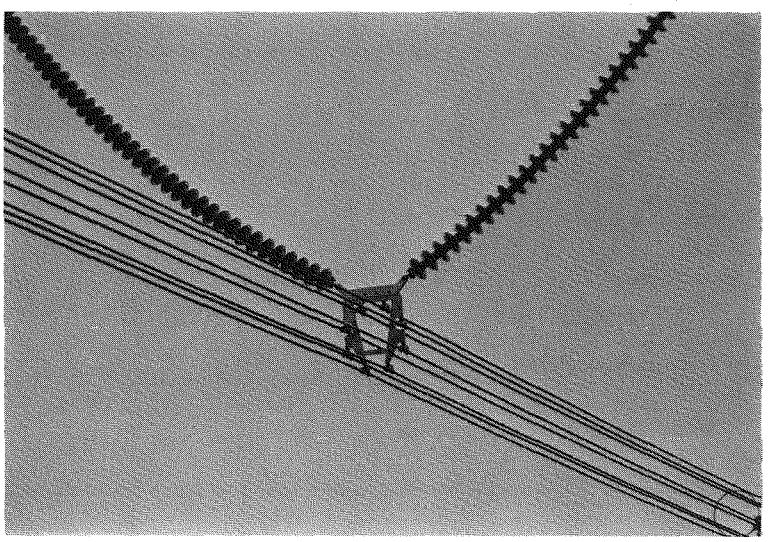


Figure 4-98. Original Hardware for Single V-String Illustrated With Sediver 120,000-lb. Units.

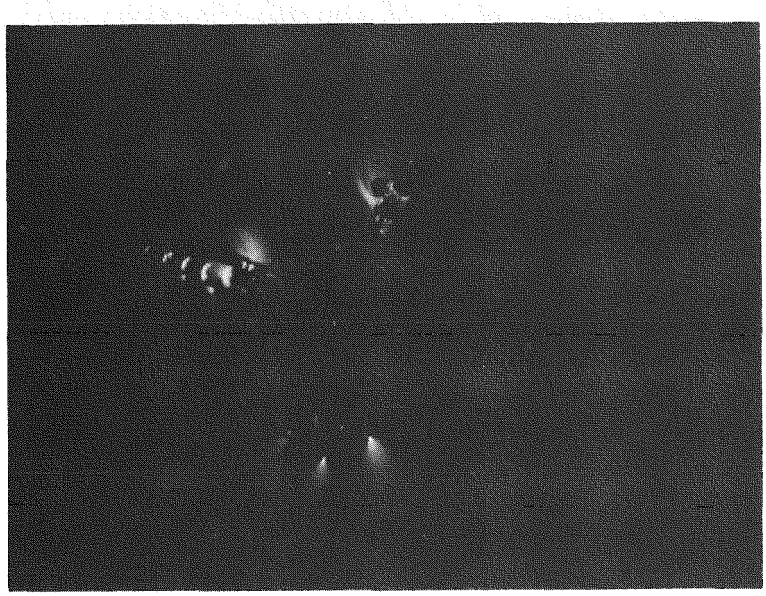


Figure 4-99. Corona on Hardware and Insulators of Original Design for Single V-String at 1400 kV.

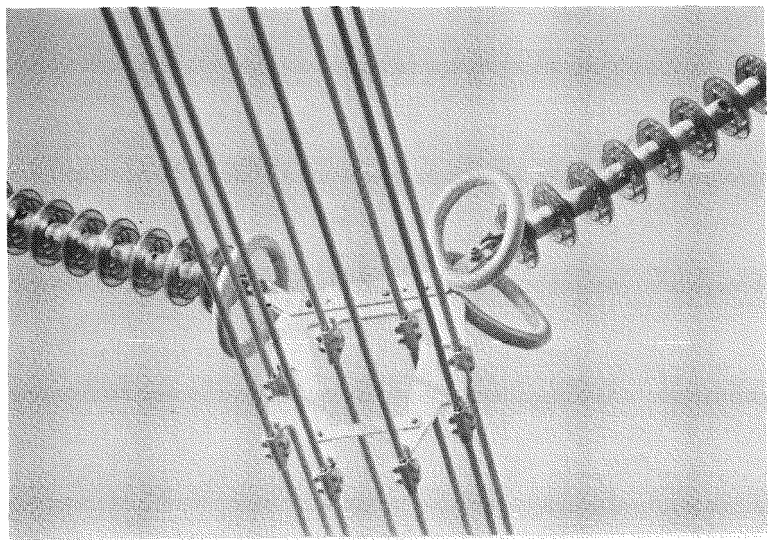


Figure 4-100. Two Shield Ring Designs Which were Employed for Suppressing Corona on Original Design for Single String. Single Ring on Left and "Butterfly" on Right all Composed of 3-in Tubing Formed into 2-ft Circle.

of a single ring encircling the string, whereas the other shield was made of two circular rings in a "butterfly" type arrangement. The corona activity on the single string with these two types of shields is shown in figure 4-101 at a voltage of 1400 kV (ℓ-ℓ). Two observations in figure 4-101 indicate that the single encircling ring is superior in suppressing corona. First, the insulator corona is confined to fewer units with the single ring when compared with the "butterfly" design. Second, corona plumes may be seen on the outermost portion of the "butterfly" shield ring itself. It was thus concluded that the single encircling ring is a more effective hardware and insulator corona shield.

It was mentioned above, the single and triple V-strings have the same basic connection to the bundle suspension plate, namely at the end of the projecting pieces shown in figure 4-98. It was decided that additional improvement of single string performance would be obtained if the attachment were made directly on the corner of the plate. A composite string with a triple configuration on one side and the single on the other was tested. As shown in figure 4-102, both insulator strings were connected directly to the suspension plate.

Another view of this arrangement is given in figure 4-103. The first corona tests on this composite single-triple string were made without any shielding rings.

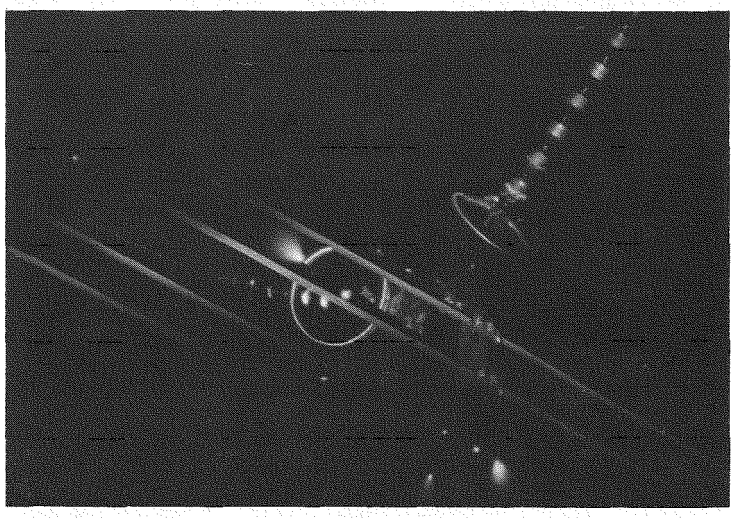


Figure 4-101. Corona Activity on Single String With Encircling and "Butterfly" Shields at 1400 kV.

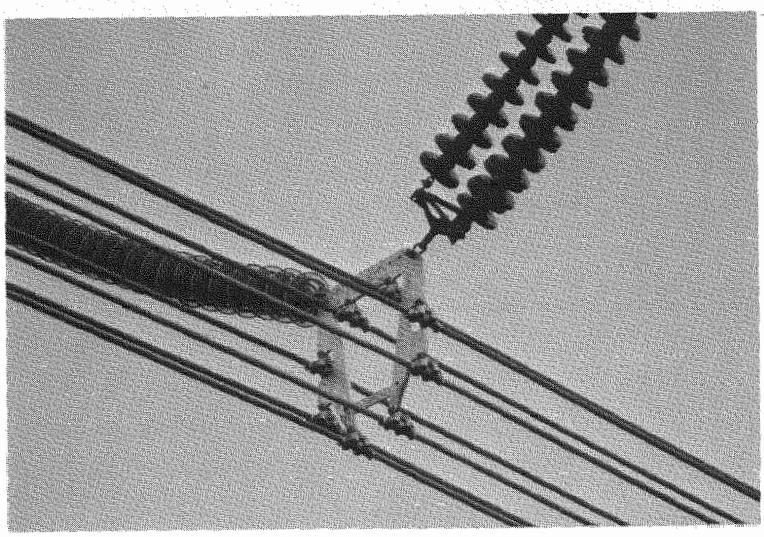


Figure 4-102. Single and Triple V-Strings Attached Directly to Suspension Plate.

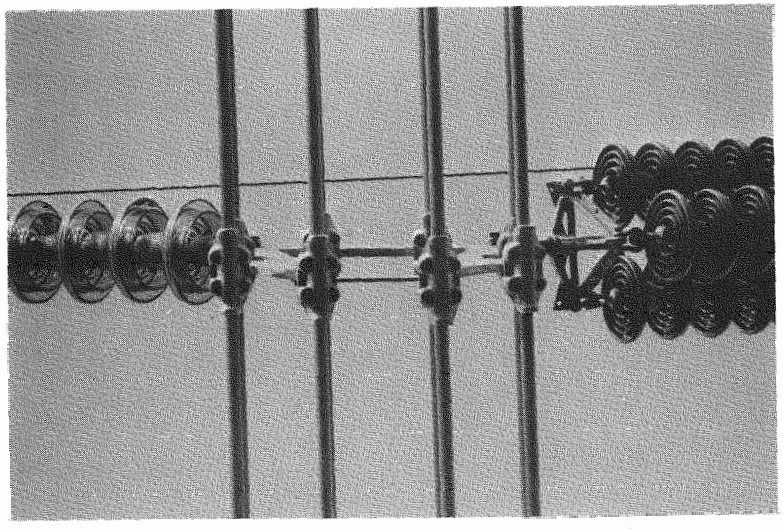


Figure 4-103. View of Composite Single/Triple String From Below.

Heavy corona activity, illustrated in figures 4-104 and 4-105 at 1000 kV (ℓ-ℓ) was present on several units of the single string and around the attachment hardware near the first units of the triple string. Initially, the composite string was tested again with the shield rings shown in figure 4-106.

Note that the shield on the single string was similar to that used before. A larger ring, composed of 15cm (6 in) diameter tubing formed into a .9m (3 ft) circle, was placed around the hardware of the triple string. Additional improvement in single string corona behavior was obtained by using the same large ring as was installed on the triple string. This final test configuration is shown in figure 4-107. The corona generation of the composite string at 1400 kV is given in figures 4-108 and 4-109. As a result of these observations, the visual corona performance of the single and triple strings attached to the suspension plate as shown in figure 4-106 and modified with the large shield rings of figure 4-107 is acceptable for use on a 1200 kV line.

The double V-string hardware was evaluated by using the glass 30,000 kg (66,000 lb) insulators. A view of the connection scheme from below the conductor bundle is shown in figure 4-110. The corona activity on the insulators and hardware is given

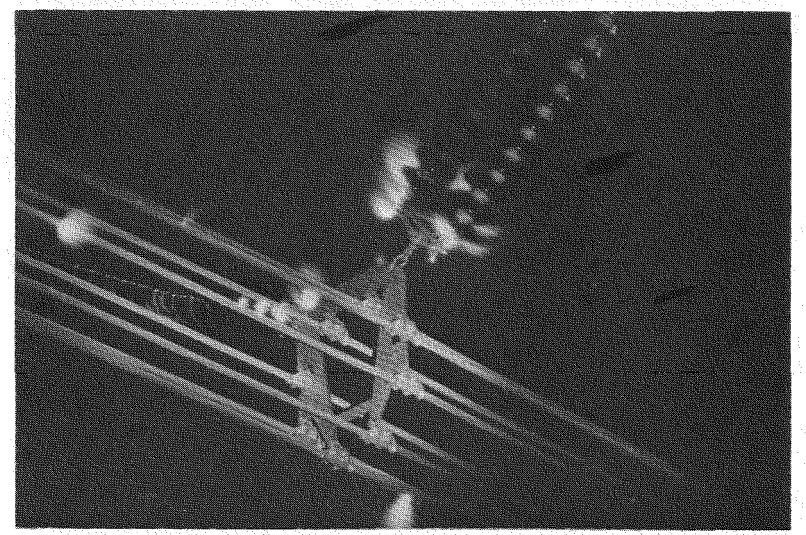


Figure 4-104. Corona on Composite Single/Triple String at 1400 kV Without Shield Rings.

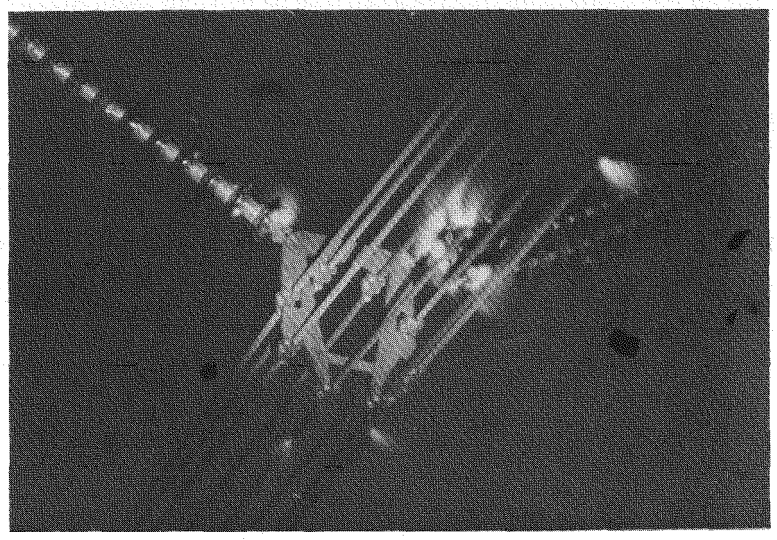


Figure 4-105. Alternate View of Corona on Composite Single/Triple String at 1400 kV Without Shield Rings.

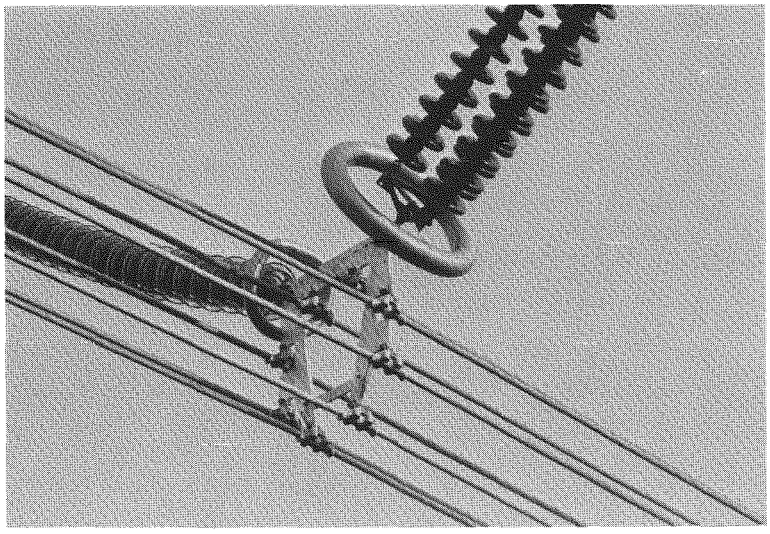


Figure 4-106. Composite Single/Triple With 2-ft Ring of 3-in Tubing on Single and 3-ft Ring of 6-in Tubing on Triple String.

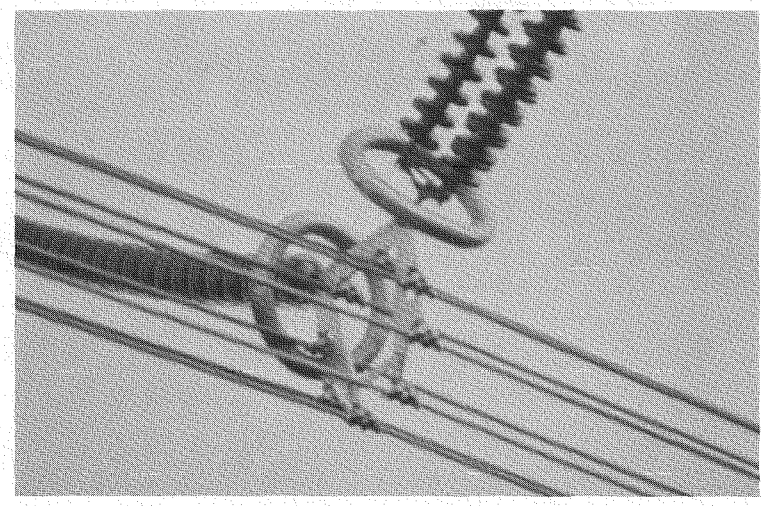


Figure 4-107. Composite Single/Triple with 3-ft Ring of 6-in Tubing on Both Single and Triple Strings.

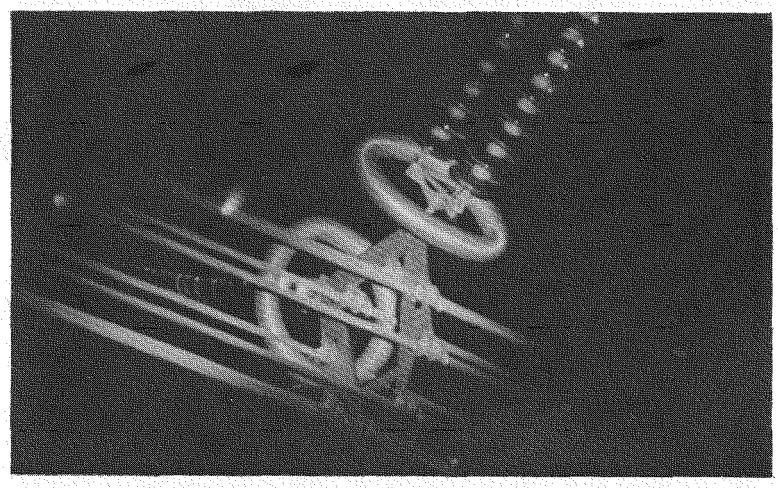


Figure 4-108. Corona Activity at 1400 kV on Composite Single/Triple with Shields Described in Figure 4-107.



Figure 4-109. Same as Figure 108, but in the Absence of Illumination in Order to Verify Corona Activity.

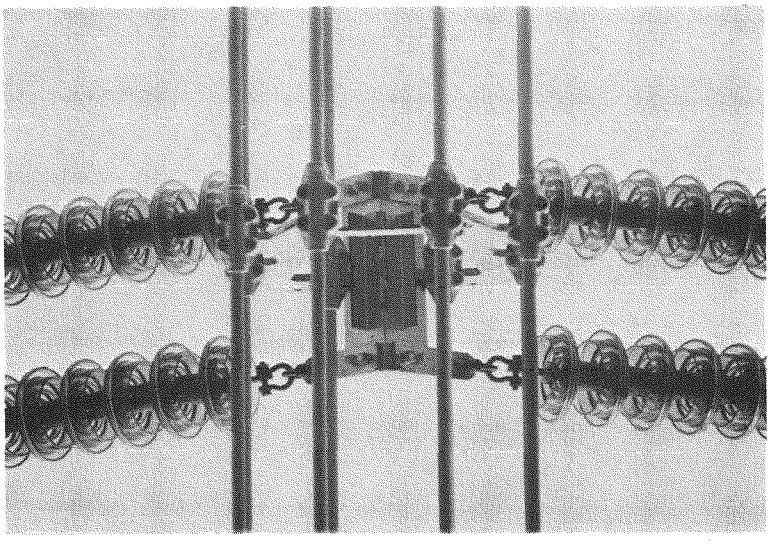


Figure 4-110. Attachment Hardware for Double Strings, Illustrated for Sediver 66,000-lb.Units.

in the absence of rings by figure 4-111 where another view of the attachment hardware may also be seen. In order to reduce the level of corona on the insulators and hardware, the rings shown in figure 4-112 were added. These rings are also composed of 15cm (6 in) tubing made into a circle of approximately .9m (3 ft) in diameter. As may be seen in figure 4-113, these shields were quite effective in substantially suppressing the corona and were selected for use on the three phase line.

The attachment of the quadruple V-string to the conductor bundle is accomplished by using some of the same basic hardware as the double string. Two views of the quadruple string are given in figures 4-114 and 4-115. The nylon ropes from the triangularly shaped plates to the conductor, which may be seen in those figures, were required in order to maintain the proper orientation of the two parallel double strings which comprise the quadruple.

The level of visual hardware corona on the quadruple string was quite low. At 1400 kV (ℓ-ℓ), the appearance of the area near the bundle is as shown in figure 4-116. It should be noted that the corona in 4-116 was of the glow type, and the apparent high intensity in the figure actually results from the fact that it is a time exposure.

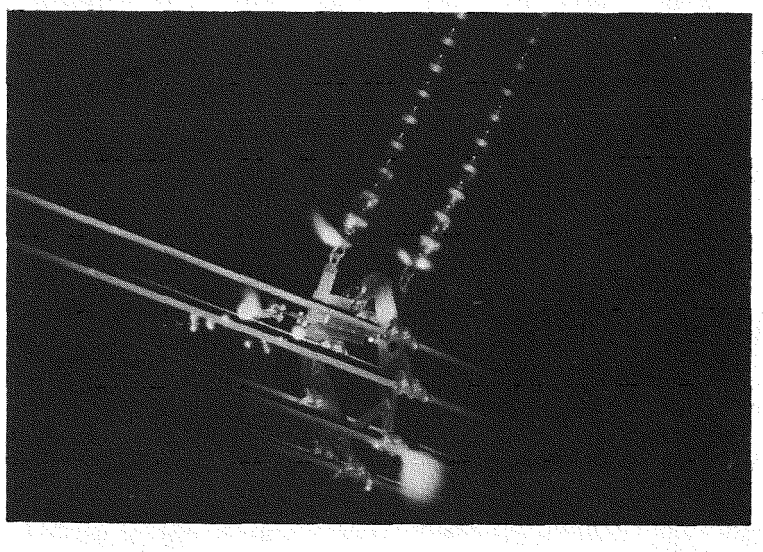


Figure 4-111. Corona on Double V-String at 1400 kV Without Shield Rings.

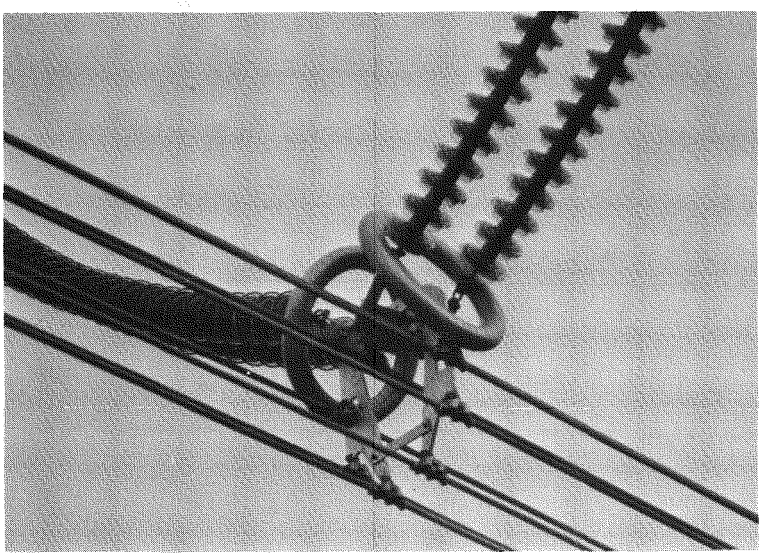


Figure 4-112. Shield Rings 3 Feet in Diameter (6-in Tubing) on Double V-String.

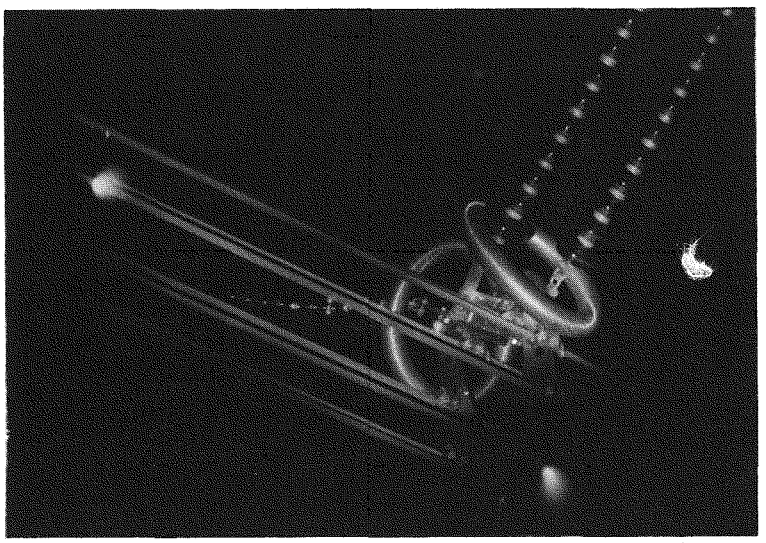


Figure 4-113. Corona Activity at 1400 kV on Double V-String with Shield Rings.

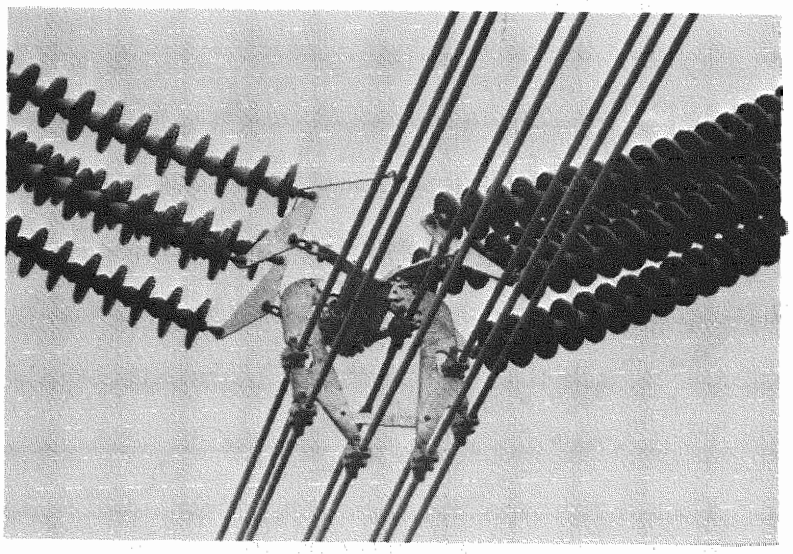


Figure 4-114. Attachment Hardware for Quadruple V-String of Locke 40,000-lb Insulators.

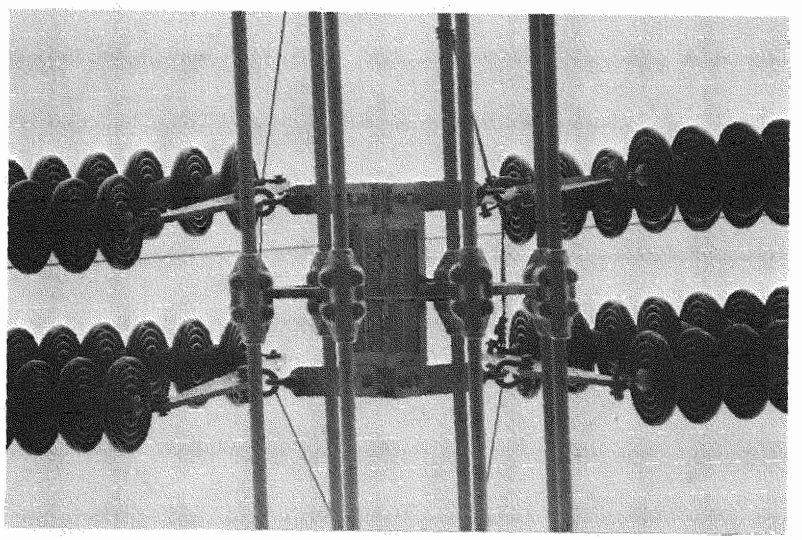


Figure 4-115. Alternate View of Quadruple String Hardware from Below.

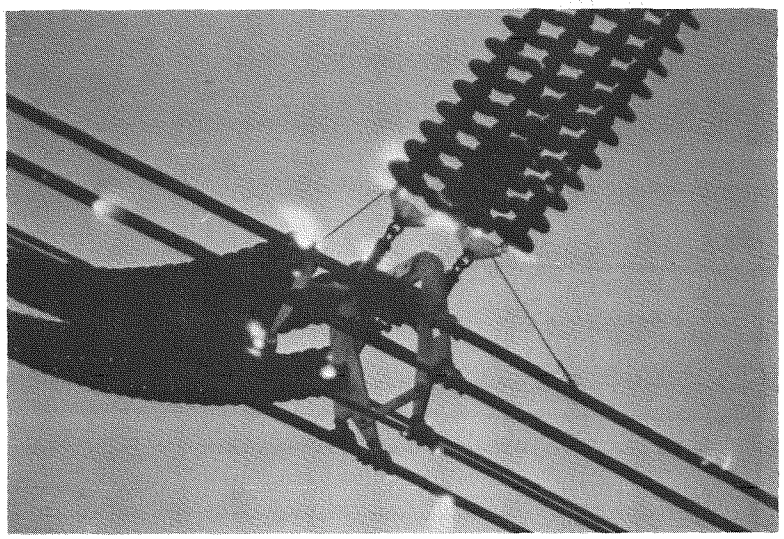


Figure 4-116. Corona on Quadruple V-String at 1400 kV.

A summary of the dry weather visual corona performance of the different configurations tested is given in figure 4-117. In that figure, the number of insulators in visual corona is shown as a function of applied voltage for all the hardware designs and their modifications discussed above. Of particular interest are the results for the single string which was subjected to the most extensive design alterations. A dramatic reduction in corona activity was achieved by the addition of the shielding rings and the modification of the point at which the insulator string is attached to the suspension plate.

A few tests were made during rain to determine whether a significant increase in hardware and insulator corona activity would occur in wet conditions. For the most part, artificial rain as supplied from a fire hose was used, although data were also obtained in one test with natural rain. Unfortunately, this period of natural rain did not persist long enough to saturate the hardware. This is illustrated in figure 4-118, which shows corona activity on the original single type insulator string at 1300 kV in natural rain. With artificial heavy rain, the corona on the same configuration and at the same voltage is given in figure 4-119. By comparing figures 4-118 and 4-119, it may be seen that during the artificial rain, the corona activity on the conductor bundle is intense, whereas in natural rain, no conductor corona is visible. This is due to the fact that the natural rain intensity was only

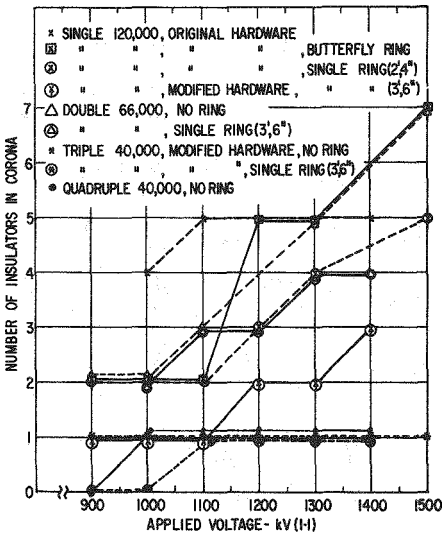


Figure 4-117.* Summary of Insulator String Corona Performance as Noted by Visual Observations for Different Voltage Levels.

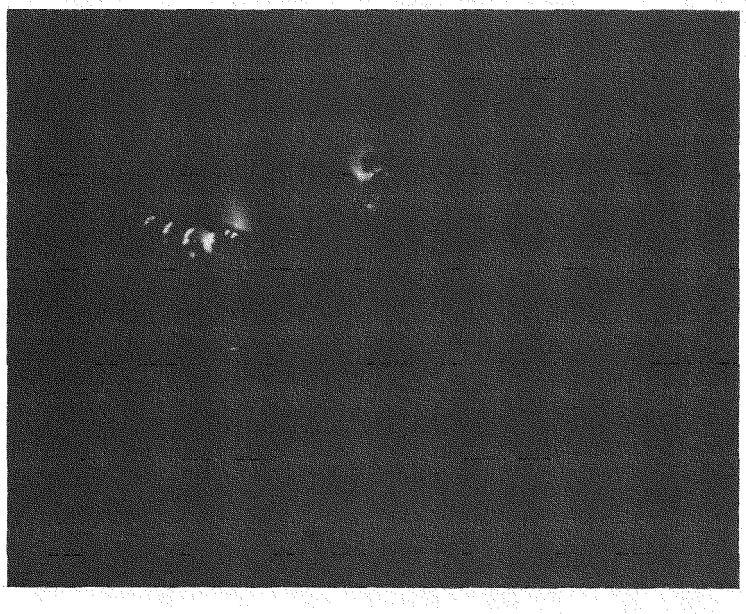


Figure 4-118. Corona Activity at 1300 kV on Single V-String in Natural Rain.

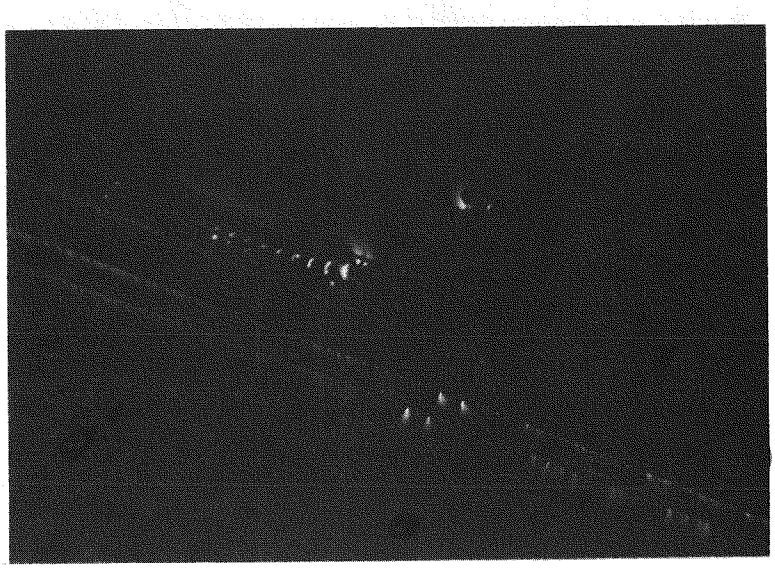


Figure 4-119. Corona at 1300 kV on Single String and Conductors in Heavy Artificial Rain.

moderate and stopped before the conductors and hardware were thoroughly wetted.

Corona on the double string arrangement in heavy artificial rain at 1400 kV (ℓ-ℓ) is shown in figure 4-120. Note that the conductors are in corona, but some activity may also be seen on the suspension shoes and on the top of the shielding rings.

On the basis of observations in the single phase tests such as those illustrated in figures 4-119 and 4-120, and comparing these results with tests in dry conditions, it is apparent that heavy rain will cause some increase in insulator and hardware corona. However, the corona on the conductor bundle itself is quite intense and will dominate over the insulator and hardware activity in both visual appearance and in the relative contribution to electrical interference.

Radio noise generated by the insulator strings under test was measured by recording the conducted RIV of the entire UHV single phase test span. The main concern in these experiments was the radio noise performance in dry conditions, since in foul weather it is expected that the contribution of insulator hardware to the overall RIV will be negligible compared with that due to conductor corona.

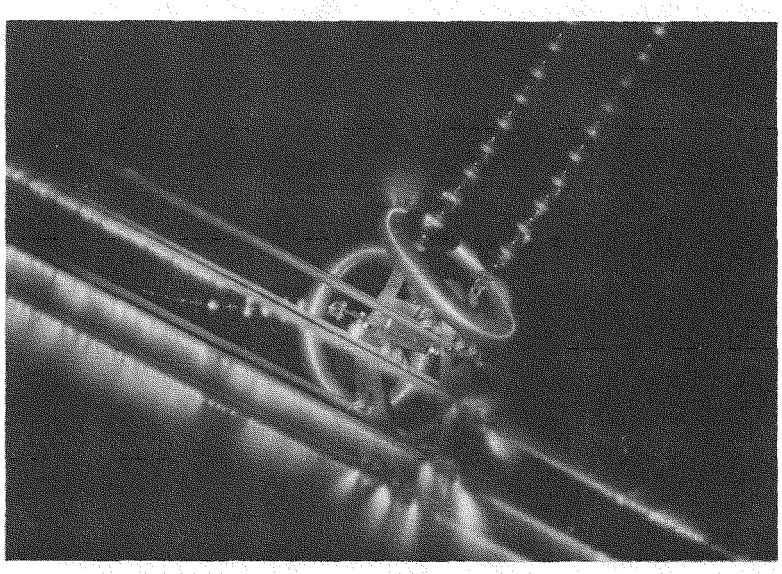


Figure 4-120. Corona Activity at 1400 kV on Double V-String in Heavy Artificial Rain.

Previous RIV data were obtained on a 8 x 4.6cm (1.8 in) conductor bundle in the absence of suspension insulator strings. [4-1] In those tests, the minimum line height was 12.4m (41.5 ft), as compared with 7.5m (25 ft) during the tests described in this report. As a result, considerably higher RIV levels than those obtained previously would be anticipated in the present experiments, even in the absence of suspension insulator strings. In order to determine whether the insulators and hardware cause a substantial increase in the conducted RIV, the radio noise generation of the bundle itself should first be estimated for this case of a lower height above ground. This was done by assuming that the radio noise for a given bundle is determined only by the maximum conductor surface gradient. It was found that the maximum surface gradient at 1500 kV in the previous tests would occur at 1300 kV in the present tests, using an average line height of 14.4m (48 ft) for the former test series and 9m (30 ft) for the present experiments. This implies that the level of conductor radio noise in the present tests at 1300 kV should be equal to that found previously at 1300 kV, where a minimum dry weather value of 31 dB above 1μV was obtained. The RIV data found in the tests reported here with the insulator strings in place was never higher than 33 dB at 1300 kV. Consequently, it was concluded that the hardware and insulators cause a negligible increase of the RIV above that due to the conductor bundle alone.

The distribution of voltage along the insulator strings was measured on each configuration and its various modifications. These measurements were made at low voltage using a 23 kV transformer and a series of neon bulb whose firing voltage was known.

An interesting comparison of the voltage distributions may be made for the different insulator strings and the design changes which were made for one string. For example, the data given in figure 4-121 show the effect of the hardware modifications and the addition of shield rings on the voltage distribution of the single insulator string, while similar data for the double string are shown in figure 4-122. The most dramatic change in the voltage distribution was noted for the triple string, presented in figure 4-123. As may be seen in that figure, the triple string also had the most nonuniform voltage distribution, even when shield rings were applied. The quadruple string without shield rings had a voltage distribution, as shown in figure 4-123, which was roughly equivalent to that of the triple string with rings.

Corona on Three-Phase Test Line Insulators

The observations of corona on all the insulator strings of the original three phase

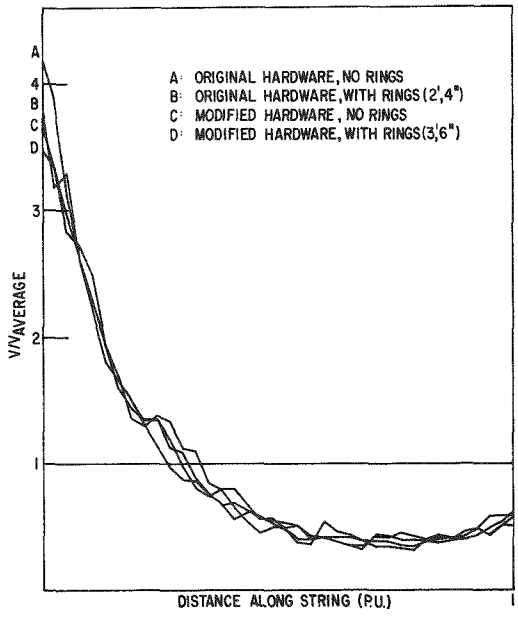


Figure 4-121. Voltage Distribution of Single Insulator String Showing Effects of Shield Rings and Hardware Modification.

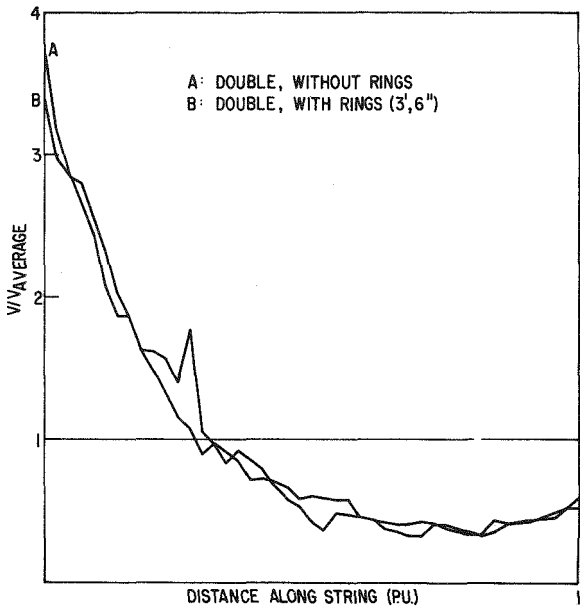


Figure 4-122. Voltage Distribution of Double Insulator String Showing Effects of Shield Rings.

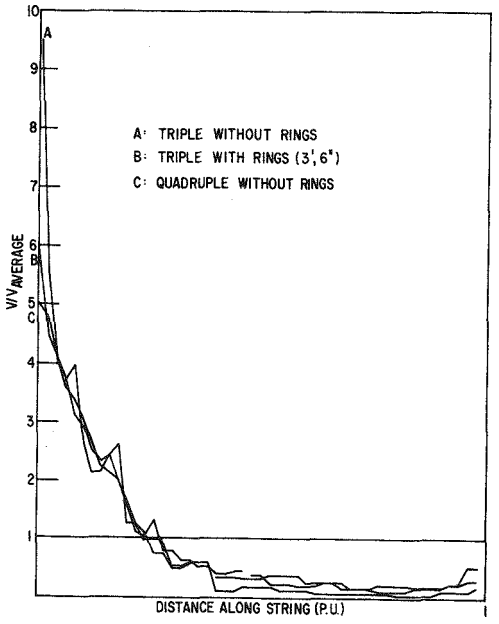


Figure 4-123. Voltage Distribution of Triple and Quadruple Strings.

line were made in dry conditions on two nights. Test voltages ranged from 1050 kV (ℓ-ℓ) to 1450 kV, in steps of 100 kV. A summary of the results is presented in Table 4-30, where corona activity as observed from the tower bridges is noted in the form of a visible glow seen with field glasses or audible noise from each of the six suspension insulator strings and their associated hardware. In the Table, it may be seen that the double, triple and quadruple porcelain strings were essentially free of corona discharges for voltages up to 1450 kV (ℓ-ℓ). At voltages above 1250 kV, there were some isolated spots of corona on the shield rings or other hardware. The corona activity on the rings was confined to the junction points of the flexible tubing or the hose clamps used to hold the tubing on the support ring braces. Examples of these corona discharges are shown in figures 4-124 and 4-125.

The two single insulator strings on the center phase and the double glass string had corona on the insulators themselves, even at the lowest test voltage of 1050 kV. On the double glass string, as many as seven insulators on the conductor end of the string were in corona at 1450 kV. This glow type corona, located mainly near the insulator pins, is illustrated in figure 4-126.

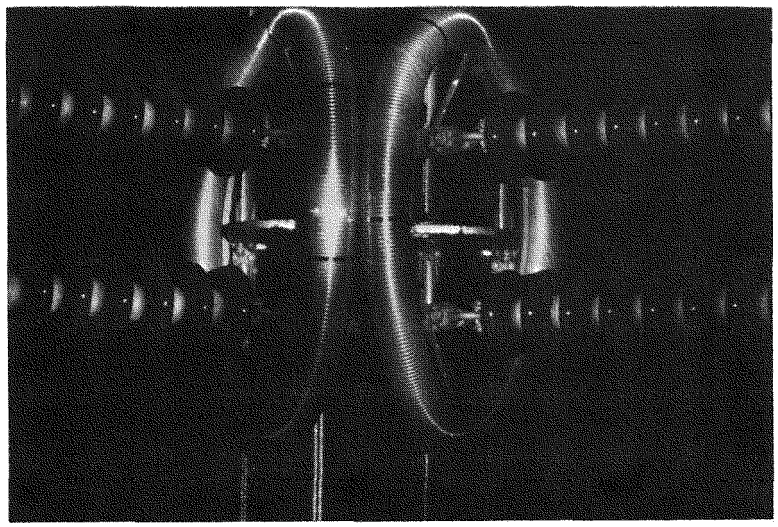


Figure 4-124. Corona on Shield Ring of Double Porcelain String seen from Tower Bridge.

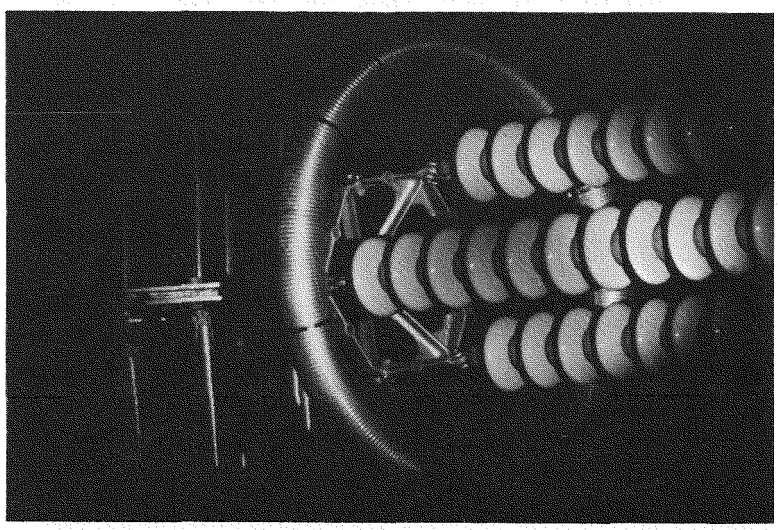


Figure 4-125. Corona on Shield Ring of Triple Porcelain String seen from Tower Bridge.

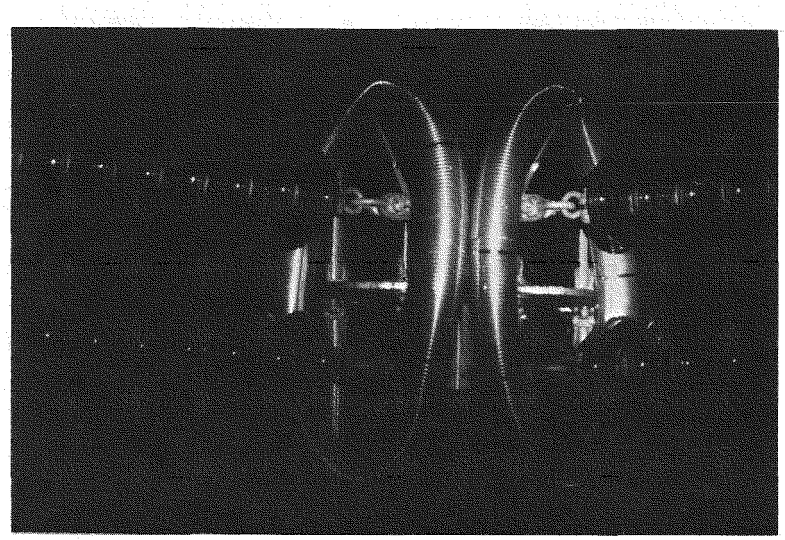


Figure 4-126. Corona on Units of Double Glass String seen from Tower Bridge.

TABLE 4-30

CORONA ACTIVITY OBSERVED ON SUSPENSION INSULATOR STRINGS FROM BRIDGES OF PORTAL TOWERS DURING DRY CONDITIONS. O DENOTES NO ACTIVITY.

Voltage (kV ℓ-ℓ)	1050	1150	1250	1350	1450
45 units Double glass 30,000 kg (66,000 lb)	buzzing 1st unit in corona	1st 3 units both sides in corona	1st 4 units in corona	1st 6 units in corona	1st 7 units; glow on gnd end hardware
39 units Single porcelain 40,000 kg (90,000 lb)	buzzing 1st unit; cap bases in corona	cap bases on 1st units in corona	cap bases on first 2 units in corona	cap bases on 2 units	cap bases on 2 units
50 units Double porcelain 23,000 kg (50,000 lb)	0	0	0	0	intermittent plume on ring
58 units Triple porcelain 23,000 kg (50,000 lb)	0	0	glow at one point of ring	more intense glow	intermittent plume on ring
38 units Single porcelain 55,000 kg (120,000 lb)	buzzing; 1st unit in glow corona	1st 3 units West leg, 2 units East leg in corona	1st 6 units West leg, 3 units East leg in corona	1st 6 on West, 3 on East; spot on gnd end hardware	1st 6 on W 3 on E; cap corona on units at gnd end
50 units Quadruple porcelain 18,000 kg (40,000 lb)	0	0	0	glow at one point of ring	light glow also on gnd end

An interesting observation was made on the single porcelain string in the three phase tests, due to the fact that the observer was located on the tower bridge above the insulators. Glow corona was seen at the base of the insulator caps adjacent to the porcelain surface, as shown in figure 4-127.

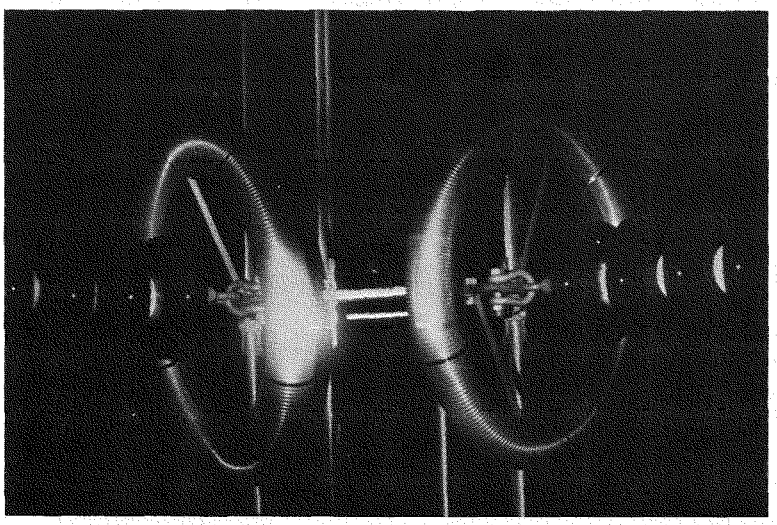


Figure 4-127. Corona at Base of Caps and on Shield Ring of Single Porcelain String.

On the single glass string, up to six insulators were in corona at the highest test voltage and an example is given in figure 4-128. The comparison of single and three phase corona tests on this set of insulators shown in figure 4-129 indicates that more units were in corona on the west leg of the V-string than on the east leg. However, the glow was only easily visible on the first few units.

One test was performed to evaluate the insulator string corona behavior in wet conditions, using the artificial rain spray apparatus above the single porcelain string. This rain spray system was described previously. At voltages below 1150 kV, only two or three units near the conductor had light corona activity. Above this voltage, some corona spots were seen at other points on the string. No streamers were observed on the hardware even at 1450 kV. The appearance of the conductor and insulator string during the wet test is shown in figure 4-130.

The visual observations of corona described here indicate that the suspension insulator strings on the original three phase test line are suitable for voltages up to 1500 kV, since the discharges are confined to only a few insulators and are of the glow type.

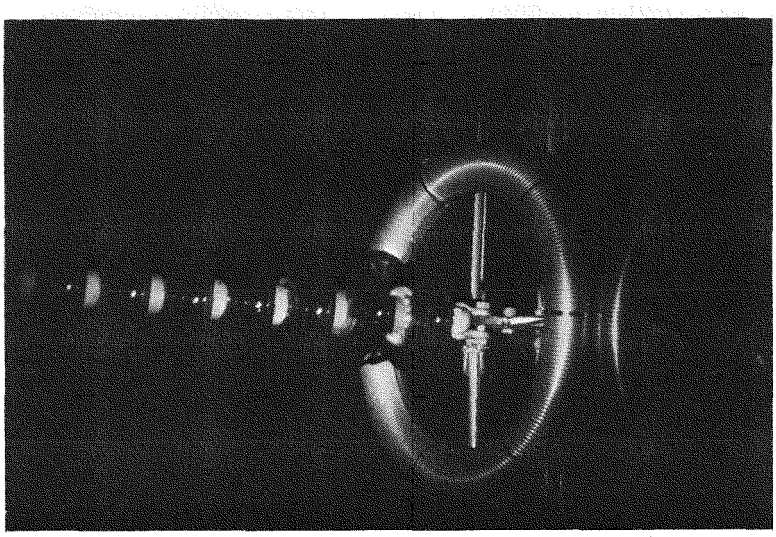


Figure 4-128. Corona on Single Glass V-String.

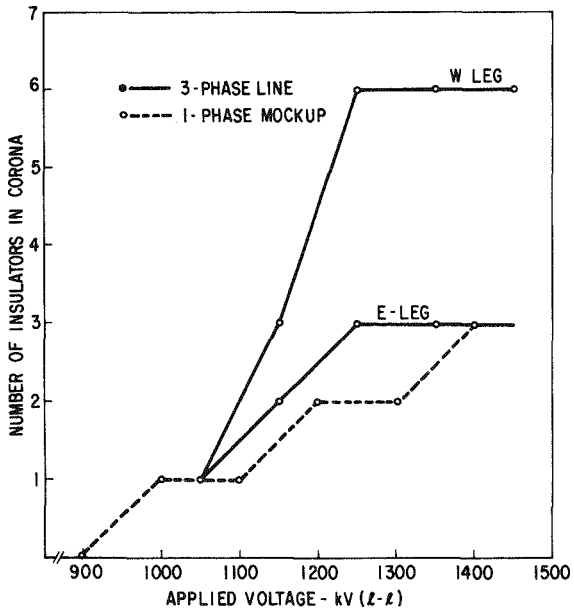


Figure 4-129. Comparison of Corona Performance of Single Glass Insulator V-String on One-Phase Mock-up with its Performance on the Three-Phase Line.

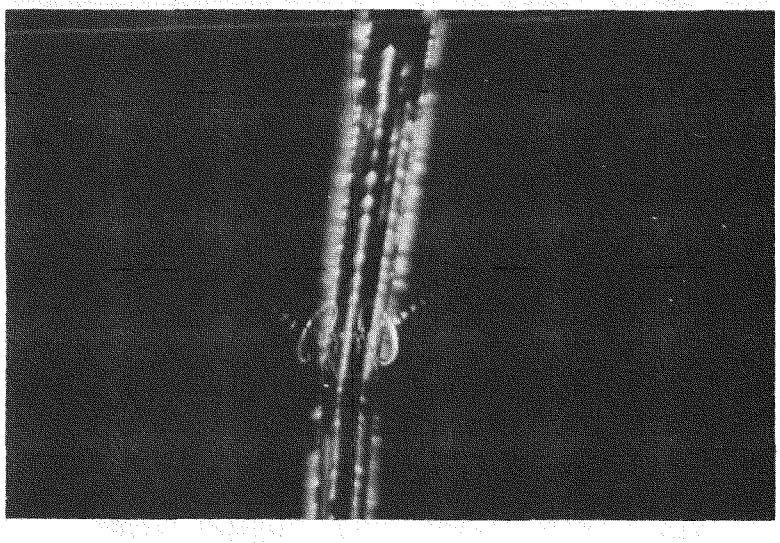


Figure 4-130. Corona Activity During Wet Test with Artificial Rain Spray System Above the Single Porcelain Center Phase String.

Two insulator string changes have been made since the initial configurations were installed. The double glass string and triple porcelain string on the east phase have been replaced with the Rosenthal and Ohio Brass plastic insulators respectively. The corona rings used were initially the same as those employed for the double and triple cap and pin strings which the plastic units replaced. The Rosenthal insulators also had a small factory installed ring (identical to the ones seen at the junction of the two sections) located on the high voltage and ground end hardware. An additional ring of 7.6cm (3 in) flexible tubing was added to this ring and a similar one was installed on the Ohio Brass units to suppress corona. Some corona still exists on these rings beginning at about 1300 kV in dry conditions.

REFERENCES

4-1. Electric Power Research Institute, Transmission Line Reference Book - 345 kV and Above, New York: Fred Weidner and Son Printers, Inc., 1975.

4-2. H. Fukui, K. Naito, T. Irie, and I. Kimoto, "A Practical Study on Application of Semiconducting Glaze Insulators to Transmission Lines," IEEE Transactions on Power Apparatus and Systems, Vol. PAS-93, September/October 1974, pp. 1430-1443.

4-3. J.H. Moran, "The Effect of 'Cold Switch-On' on Semiconducting Glazed Insulators," Paper C74-071-7, presented at IEEE PES Winter Meeting, New York, NY, January 27-February 1, 1974.

4-4. B. Macchiarole and F.J. Turner, "A New Contamination Test Method," IEEE Transactions on Power Apparatus and Systems, Vol. PAS-88, September 1969, pp. 1400-1411.

4-5. O. Nigol, J. Reichman, and G. Rosenblatt, "Development of New Semiconductive Glaze Insulators," IEEE Transactions on Power Apparatus and Systems, Vol. PAS-93, March/April 1974, pp. 614-622.

4-6. R. Cortina, "Influence of the Characteristics of the Source on the Withstand Salinity of Large Insulators - Test Voltage 84 kV rms," CIGRE SC 33-75 (WG 04) 12 IWD.

4-7. J.F. Hall, T. Hillesland, and S.R. Knudsen, "500 kV Station-Post Insulator Performance at PG and E's Outdoor Laboratory at Moss Landing," IEEE Transactions on Power Apparatus and Systems, Vol. PAS-95, January/February 1976, pp. 166-177.

4-8. D.W. Deno, "Transmission Line Fields," IEEE Transactions on Power Apparatus and Systems, Vol. PAS-95, September/October 1976, pp. 1600-1611.

4-9. M. Kawai, "AC Flashover Tests at Project UHV on Ice-Coated Insulators," IEEE Transactions on Power Apparatus and Systems, Vol. PAS-80, November/December 1970, pp. 1800-1804.

4-10. ANSI Standard C37.34, "Test Code for High Voltage Air Switches," 1971.

4-11. M. Kawai and C.W. Nicholls, "Full-Scale Contamination Tests on UHV Insulator Strings," Paper T74-072-5, presented at the PES Winter Meeting, January 27-February 1, 1974, New York, NY.